Niagara Mohawk

Richard B. Abbott
Vice President
Nuclear Engineering

Phone: 315.349.1812
Fax: 315.349.4417

March 8, 2001
NMP2L 2015

U. S. Nuclear Regulatory Commission
Attn: Document Control Desk
Washington, DC 20555

RE: Nine Mile Point Unit 2
Docket No. 50-410
NPF-69

Subject: ***10CFR50, Appendix H, Reactor Vessel Material Surveillance Program Requirements, Report of Test Results***

Gentlemen:

10CFR50, Appendix H, Reactor Vessel Material Surveillance Program Requirements, Section IV, Report of Test Results, requires that a summary technical report be submitted within one year of the date of capsule withdrawal. The report must include the data required by American Society for Testing and Materials (ASTM) E 185, as specified in paragraph III.B.1 of Appendix H, and the results of all fracture toughness tests conducted on the beltline materials in the irradiated and unirradiated conditions. If a change in the Technical Specifications is required, either in the pressure-temperature (P-T) limits or in the operating procedures required to meet the limits, the expected date for submittal of the revised Technical Specifications must be provided with the report. The purpose of this letter is to submit the attached summary technical report for the capsule that was withdrawn from the 3° azimuth location on March 12, 2000.

The current Nine Mile Point Unit 2 (NMP2) P-T curves, which were submitted and approved by the NRC as Amendment No. 26 to the Technical Specifications, were developed based on Regulatory Guide 1.99, Revision 2 (RG 1.99(2)). The current NMP2 P-T curves are based on a limiting beltline plate and are valid for up to 12.8 Effective Full Power Years (EFPY). The results from the Charpy data trends for the withdrawn capsule show that the neutron induced embrittlement of the limiting NMP2 vessel plate is low. At a fluence of 8.49E16 n/cm^2, the shift in the 30 ft-lb transition temperature for plate C3147 is only 20.2°F. The measured shift is within 1 sigma (17°F) of the RG 1.99(2) model prediction of 7.3°F. The measured upper-shelf energy (USE) for the plate was observed to increase by 11 ft-lb to 99.3 ft-lb.

The NMP2 surveillance program satisfies the 10CFR50, Appendix H requirements, except that the surveillance capsules have been positioned inside the vessel at locations that result in lead factors below 1.0. Therefore, in letters dated December 3, 1984 (NMP2L 0275) and December 17, 1985 (NMP2L 0562), Niagara Mohawk Power Corporation (NMPC) committed

A008

to supplement the surveillance data from NMP2 with data from LaSalle County Station Units 1 and 2 (LaSalle Units 1 and 2) and Washington Nuclear Plant No. 2 (WNP-2). The NMP2 plate surveillance data have been compared with the data from WNP-2 and LaSalle Units 1 and 2. In all cases, the measured data for NMP2 and the three comparison plants are within 2 sigma (34° F) of the RG 1.99(2) model prediction. Furthermore, the plate surveillance data for all four plants lie well within the trend for other Boiling Water Reactors (see Figure 7-1 of the attached technical report). Therefore, NMPC has concluded that the use of the RG 1.99(2) model is appropriate for NMP2.

The USE data for NMP2 have also been compared with WNP-2 and LaSalle Units 1 and 2. The NMP2 and WNP-2 USE levels after irradiation are slightly higher than the unirradiated values. This phenomenon has been observed in other plants. Conservatively assuming an end-of-license (EOL) fluence of up to 1.0E18 n/cm^2, the RG 1.99(2) predicted shelf drop for plate C3147-2 is less than 15% (i.e., EOL USE is greater than 75 ft-lb). Therefore, the 10CFR50, Appendix G requirement to maintain a 50 ft-lb USE throughout the plant operating period is satisfied for NMP2.

A fluence of 8.49E16 n/cm^2 has been calculated for the withdrawn capsule. Analysis of the dosimeter wires included in the capsule indicates good agreement between the dosimeters and the calculation. Average calculated-to-experimental (C/E) ratios of 0.95 for the copper dosimeters and 1.09 for the iron dosimeters have been obtained. The overall capsule average C/E ratio is 1.02. Thus, the capsule dosimetry results serve to validate the accuracy of the calculation for vessel fluence determination.

Based on analysis of the test results for the withdrawn capsule, NMPC has concluded that no change to the P-T curves specified in Technical Specification 3.4.11, "RCS Pressure and Temperature (P/T) Limits," is required at this time. Accordingly, the P-T curves will remain valid for 12.8 EFPY. It is estimated that 12.8 EFPY will be reached in the Spring of 2005. Therefore, a Technical Specification Amendment Application to revise the P-T curves is expected to be submitted by March 2004 to support implementation prior to March 2005.

Very truly yours,

Richard B Abbott

Richard B. Abbott
Vice President Nuclear Engineering

RBA/CDM/mlg
Attachment

xc: Mr. H. J. Miller, NRC Regional Administrator, Region I
Ms. M. K. Gamberoni, Section Chief PD-I, Section 1, NRR
Mr. G. K. Hunegs, NRC Senior Resident Inspector
Mr. P. S. Tam, Senior Project Manager, NRR
Mr. Tom Erwin
Energy Northwest
P.O. Box 968 (PEC M/D PE24)
Richland, WA 99352-0968
Mr. Greg Gezen
Exelon Nuclear
1400 Opus, Suite 400
Downers Grove, IL 60515
Records Management

Nine Mile Point Unit 2 3-Degree Pressure Vessel Surveillance Capsule Report

December, 2000

MPM
....SERVING CLIENT NEEDS
THROUGH ADVANCED TECHNOLOGY

Report Number MPM-1200676

Final Report

entitled

Nine Mile Point Unit 2 3-Degree Surveillance Capsule Report

prepared for

Niagara Mohawk Power Corporation
Nine Mile Point Unit 2
Lake Road
Lycoming, NY 13093

by

MPM Technologies, Inc.
2161 Sandy Drive
State College, PA 16803-2283

December, 2000

M C Manahan, Sr.
Preparer

2/14/01
Date

Checker

2/14/01
Date

M C Manahan, Sr.
MPM Approval

2/14/01
Date

Nuclear Quality Assurance Certification

This document certifies that MPM has performed all work under NMPC Purchase Order Number 00-30028 in accordance with the requirements of the Purchase Order. All work has been performed under the MPM Nuclear Quality Assurance Program.

M. P. Manahan, Sr.
President

2/14/01
Date

S. Clinger
QA Manager

2/14/01
Date

Executive Summary

The Nine Mile Point Unit 2 (NMP-2) 3-Degree surveillance capsule was irradiated from reactor start-up to the end of fuel cycle 7 (March 3, 2000) for a total exposure of 8.72 effective full power years (EFPY). Cycles 1 through 4 ran at 3323 MWth prior to the power uprate, and cycles 5 through 7 ran at 3467 MWth. The capsule contained a total of 36 Charpy impact specimens and 6 dosimeter wires. After performing the mechanical property tests, chemical measurements were made on one base metal and one weld metal Charpy specimen to verify that the surveillance materials used to fabricate the specimens were actually cut from the correct vessel plate and weld. It was verified that the base metal specimens were fabricated from plate C3147-2 material and the weld specimens were fabricated from weld heat 5P5657/lot 0931.

Neutron Transport Results

A fluence of 8.49×10^{16} n/cm^2 has been calculated for the capsule. At the end of cycle 7, the lead factor (capsule fluence divided by vessel maximum fluence) is calculated to be 0.43 (8.49E16/1.95E17). Analysis of the dosimeter wires indicates very good agreement between the dosimeters and the calculation. An average calculated-to-experimental (C/E) ratio of 0.95 for the Cu dosimeters and 1.09 for the Fe dosimeters has been obtained. The overall capsule average C/E ratio is 1.02. Thus, the transport calculation and dosimetry data are in very good agreement. The capsule dosimetry results serve to validate the accuracy of the calculation for vessel fluence determination. In accordance with draft guide DG-1053, the calculated fluence values are recommended for use in estimating vessel embrittlement and in calculating heatup and cooldown curves.

Charpy Test Results

The Charpy data trends show that the neutron induced embrittlement of the limiting NMP-2 vessel plate and weld are low. At a fluence of 8.49×10^{16} n/cm^2, the shift in the 30 ft-lb transition temperature for plate C3147 is only 20.2 F. The measured shift falls within 1σ of the Regulatory Guide (RG) 1.99(2) model prediction. The measured USE was observed to increase by 11 ft-lb to 99.3 ft-lb. Similarly, the surveillance weld embrittlement data trends were observed to be very low. At a fluence of 8.49×10^{16} n/cm^2, the shift in the 30 ft-lb transition temperature shift for weld Heat 5P5657 is 30.3 F. The USE for the weld increased by 10.2 ft-lb to 98.7 ft-lb.

Surveillance Data Credibility

RG1.99(2) requires assessment of surveillance data to determine whether the data are credible. Credibility is judged by five criteria given in the regulatory guide. The NMP-2 plate surveillance material satisfies the RG1.99(2) surveillance Criterion 1 because the surveillance plate material C3147-2 contains the limiting Cu/Ni content of the beltline plates and has the limiting ART. As shown in Section 6 of this report, the plots of Charpy energy versus

temperature have yielded valid upper shelf energies and 30 ft-lb transition temperatures. Therefore, Criterion 2 has been satisfied. Criterion 3 should be applied when there are two or more surveillance data points available. However, when only one data point is available, it is possible to compare the measured shift with the RG 1.99(2) calculated shift. As previously mentioned, the results of this evaluation show that the calculated and measured shift are within one standard deviation for base metal. Criterion 4 requires the irradiation temperature of the Charpy specimens in the capsule to match the vessel wall temperature at the cladding/base metal interface within ± 25 F. Since the capsule is located within 1 inch of the vessel clad surface, and the vessel clad nominal thickness is 0.1875 inches, Criterion 4 is satisfied for NMP-2. Since the 3-Degree capsule does not contain correlation monitor materials, Criterion 5 is not applicable to the 3-Degree capsule.

Integrated Surveillance Data Analysis

The NMP-2 surveillance capsule program was designed to the requirements of ASTM E185-73 (1973). The NMP-2 surveillance program satisfies the 10 CFR 50, Appendix H requirements, except that the surveillance capsules have been positioned inside the vessel at locations that result in lead factors (lag factors) below 1.0. Since the lead factor from the surveillance capsule to the peak 1/4T position is below 1.0, NMPC committed in the FSAR to review surveillance data from LaSalle Unit 1, LaSalle Unit 2, and WNP-2 in preparing future revisions to the P-T operating curves. In addition, the FSAR commits NMPC to pull and test the capsules to obtain valid dosimetry data.

The NMP-2 plate surveillance data have been compared with the WNP-2 data and the LaSalle Units 1 and 2 data. In all cases, the measured data for NMP-2 and the sister plants are within 2σ (34 F) of the RG 1.99(2) model prediction. Also, the plate data for the plants of interest lie well within the trend of BWR plate surveillance data. Therefore, it has been concluded that the use of the RG 1.99(2) model is appropriate for NMP-2.

10CFR50 Appendix H Analysis

10CFR50, Appendix H requires that the test results for a capsule withdrawal be reported within one year of the date of capsule withdrawal and that a determination be made as to whether a Technical Specification change is required. Based on analysis of the test results, it has been concluded that there is no requirement for a Technical Specification change and the current P-T limits are valid. However, the fluence reported here is significantly lower than the fluence used to calculate the current P-T limits and there would be significant reduction in the leak/hydro test temperature if the P-T limits were to be recalculated.

USE Analysis

The USE data for NMP-2 and the sister plants have been compared. The NMP-2 and WNP-2 USE levels after irradiation are slightly higher than the unirradiated values. This

phenomenon has been observed in other plants and may be related to low fluence improvement of the matrix material which results in more ductile ligament response during the ductile fracture process. Conservatively assuming an end-of-license (EOL) fluence of up to $1x10^{18}$ n/cm^2, the RG 1.99(2) predicted shelf drop for plate C3147-2 is less than 15%. Therefore, the 10CFR50, Appendix G requirement to maintain a 50 ft-lb USE throughout the plant operating period is satisfied for NMP-2.

Contents

1.0 Introduction

1.1 Neutron Embrittlement

Ferritic reactor pressure vessel (RPV) materials undergo a transition in fracture behavior from brittle to ductile as the test temperature of the material is increased. Charpy V-notch tests are conducted in the nuclear industry to monitor changes in the fracture behavior during irradiation. Neutron irradiation to fluences above about 5×10^{16} n/cm^2 causes an upward shift in the ductile-to-brittle transition temperature (DBTT) and a drop in the upper shelf energy (USE). The nuclear industry indexes the DBTT at 30 ft-lbs of absorbed energy and the shift in the DBTT is referred to in the literature as the ΔRT_{NDT} or the ΔT_{30} . This behavior is illustrated schematically in Figure 1-1. The initial nil-ductility reference temperature (RT_{NDT}) is measured in accordance with Section III of the American Society of Mechanical Engineers (ASME) Boiler & Pressure Vessel Code (the Code) and involves measurement of drop weight data and Charpy data at discrete test temperatures.

In order to ensure safe operation of a nuclear power plant during heatup, cooldown, and leakage/hydro test conditions, it is necessary to conservatively calculate allowable stress loadings for the ferritic RPV materials. These allowable loadings can be conveniently presented as a plot of measured coolant pressure versus measured coolant temperature (P-T curves). Appendix G to Title 10 of the Code of Federal Regulations (CFR) Part 50 (10CFR50) [1-1] and Appendix G to Section III of the American Society of Mechanical Engineers (ASME) Boiler and Pressure Vessel Code [1-2] presents a procedure for obtaining the allowable loadings for ferritic pressure-retaining materials in Class 1 components using linear elastic fracture mechanics (LEFM). The latest code year approved by NRC, which at present is the 1995 Edition and Addenda through 1996, must be used in P-T curve analysis.

Although the Code suggests that the lower bound toughness should be measured for the vessel materials of interest, Regulatory Guide 1.99, Revision 2 (RG 1.99(2)) [1-3] allows the use of the ASME reference stress intensity factor (K_{IR}) and requires that this curve be shifted by the Charpy shift to account for radiation effects. In particular, neutron damage within the RPV during plant operation is accounted for in the allowable pressure loading by calculating an adjusted nil-ductility reference temperature (ART_{NDT}). RG 1.99(2) defines the ART_{NDT} as the sum of the initial unirradiated nil-ductility reference temperature (RT_{NDT}), plus the RT_{NDT} irradiation induced shift (ΔRT_{NDT}), plus a margin term. Within the nuclear industry, the ΔRT_{NDT} is determined from the Charpy transition curve shift indexed at 30 ft-lbs of absorbed energy.

The requirement to conduct an RPV surveillance program is given in 10CFR50 Appendix H, and the detailed implementation is described in American Society for Testing and Materials (ASTM) standard E 185. For most boiling water reactor (BWR) plants in the US, three surveillance capsules were placed in the downcomer near the vessel inner diameter (ID) surface prior to initial startup. These capsules contain neutron dosimeters and tensile specimens in addition to Charpy specimens. Some capsules contain Charpy and tensile specimens which were

machined from an ASTM reference plate (referred to as correlation monitor material) and these specimens were included so that utilities could compare data from their surveillance program with a large industry data set to confirm the validity of their program. This could be accomplished by plotting the data on a graph of ΔT_{30} versus fluence. However, because of data traceability problems, ASTM has been slow to standardize a procedure and the correlation monitor data have not been widely used. However, it is prudent to test and report these data and thereby contribute to the national data base.

1.2 Surveillance Program Description

Three surveillance capsules were installed within the Nine Mile Point Unit 2 (NMP-2) downcomer region prior to initial operation. To date, one of the capsules have been removed for testing. The number and type of mechanical behavior specimens included in the original surveillance program as specified by GE, as well as the capsule identification and location within the vessel, are summarized in Table 1-1.

The NMP-2 surveillance capsule program was designed to the requirements of ASTM E 185-73. As stated in Reference [1-4], the NRC concluded that the NMP-2 surveillance program satisfies the 10 CFR 50, Appendix G requirements, except that the surveillance capsules have been positioned at locations that result in lead factors (lag factors) which are below 1.0. Since the lead factor from the surveillance capsule to the peak 1/4 T position is less than 1.0, NMPC committed in the FSAR to use data from LaSalle Unit 1, LaSalle Unit 2, and WNP-2 in preparing future revisions to the P-T operating curves. In addition, the FSAR commits NMPC to pull and test the capsules to obtain valid dosimetry data and to contribute to the national database. Further details concerning the NMP-2 integrated surveillance program are contained in References [1-5, 1-6].

1.3 3-Degree Capsule Opening

The surveillance capsule was shipped to MPM during September, 2000 and was opened on 9/28/00. The outside of the capsule had the following identification marking stamped on the stainless steel surface: GE131C8981 G00166. As expected, a total of 36 Charpy v-notch specimens were recovered along with two Fe and two Cu dosimeter wires. One end of each Charpy specimen was stamped with the number 66. The other end of the Charpy specimen was stamped with either a BF1 for base metal, a WF2 for weld metal, or an HF3 for heat-affected-zone (HAZ). Each specimen was placed in a plastic vial and MPM assigned the following numbering system to the specimens so that the identity of each specimen could be maintained in the future:

Base Metal Specimens	- BF1, BF1-2 through BF1-12
Weld Metal Specimens	- WF2, WF2-2 through WF2-12
HAZ Metal Specimens	- HF3, HF3-2 through HF3-12

1.4 Chapter 1 References

[1-1] Code of Federal Regulations, Title 10, Part 50, Appendix G.

[1-2] ASME Boiler and Pressure Vessel Code, Section III, Appendix G for Nuclear Power Plant Components, Division 1, "Protection Against Nonductile Failure", 1995 Edition and Addenda through 1996.

[1-3] U.S. NRC Regulatory Guide 1.99, "Radiation Embrittlement of Reactor Vessel Materials," Revision 2, May 1988.

[1-4] Safety Evaluation Report related to the operation of Nine Mile Point Nuclear Station, Unit No. 2, NUREG-1047, February, 1985.

[1-5] Safety Evaluation Report related to the operation of Nine Mile Point Nuclear Station, Unit No. 2, NUREG-1047, Supplement No. 3, July, 1986.

[1-6] Letter from C.V. Mangan (NMPC) to H. Denton (NRC), "Integrated Reactor Vessel Material Surveillance Program", September 30, 1985.

Table 1-1 Original NMP-2 Surveillance Program Mechanical Behavior Specimen Inventory.

Table 1-1
Surveillance Capsule Contents and Locations[1]

Capsule No.	Number of Transverse Charpy Specimens				Number of Flux Wires		With-drawal Sched.
	Azimuth	Base	HAZ	Weld	Fe	Cu	EFPY
1	3°	12	12	12	2*	2*	pulled 8.72
2	177°	12	12	12	2	2	~20
3	183°	12	12	12	2	2	spare

[1] The surveillance program does not include tensile specimens.
* Three Fe flux wires were also contained in a separate neutron dosimeter holder at the 3-deg location. The holder was lost, and therefore, these extra dosimeters were not analyzed.

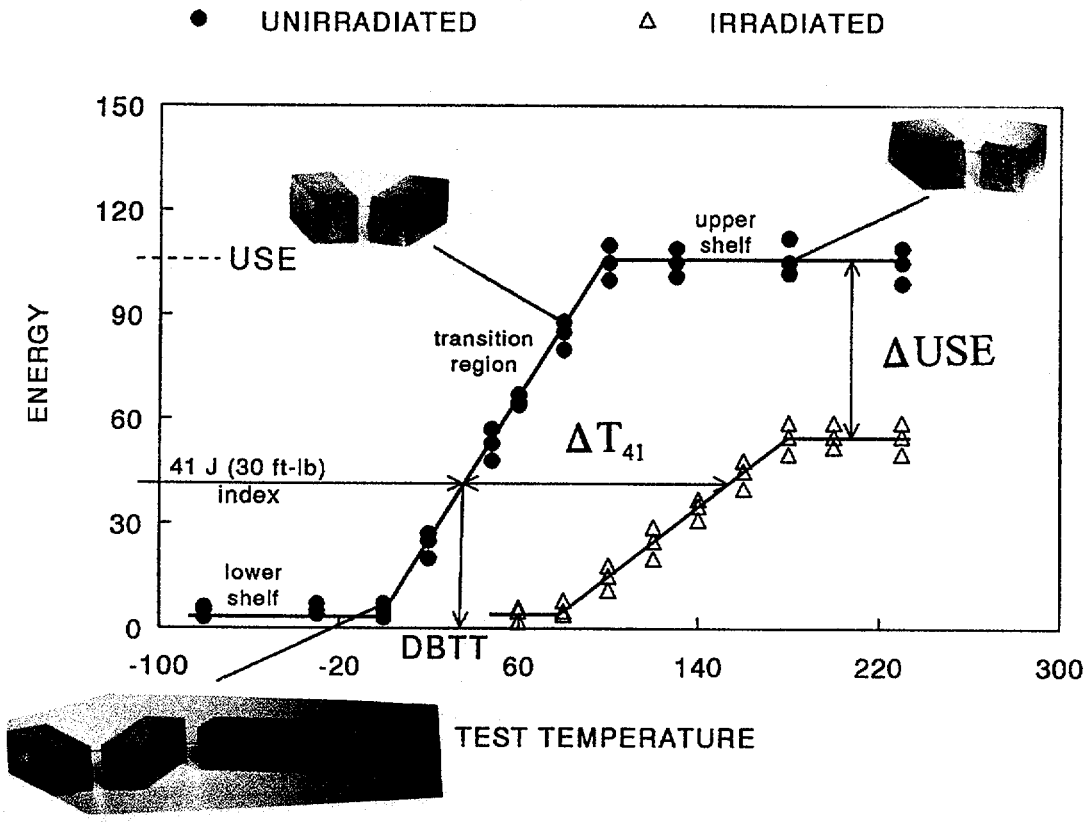

NOT ACTUAL DATA

Figure 1-1 **Schematic Illustration of Typical Charpy Curve and the Effect of Neutron Irradiation on the Curve. Ferritic Pressure Vessel Steels Exhibit a Transition in Fracture Behavior as the Notched Bar Impact Test Temperature is Increased: at Low Temperatures the Fracture is Predominantly Cleavage; at Intermediate Temperatures the Fracture is a Mixture of both Cleavage and Ductile; and Above the Transition Region the Fracture is Entirely Ductile.**

2.0 Neutron Dosimeter Measurements

This section of the report describes the measurements made to determine the specific radionuclide activity contained in the dosimeter materials. Information on the dosimeter materials, the measurement techniques, and the instruments and procedures used to make the measurements are described. The key results of the radiometric analysis are the specific activities of the dosimeter materials.

2.1 Dosimeter Material Description

The primary dosimeter materials are pure metal wires, which were located within the surveillance capsule. The wire types provided by GE for the NMP-2 surveillance program are copper and iron. Each wire is about three inches long. Upon receipt at the radiometric lab, the wires were removed from their plastic containers and visually inspected.

In addition to the pure metal wires, a section of a Charpy specimen composed of base metal was taken for radiometric analysis to provide additional neutron dosimetry. As discussed later in this report, the Charpy bar dosimetry material was used to resolve questions concerning the location of the dosimeter wires inside the capsule.

2.2 Dosimeter Cleaning and Mass Measurement

The dosimeter wires were cleaned with a lab wipe soaked in pure ethanol. Each wire was then sectioned into pieces about 0.75-inch long for subsequent coiling into an approximate point source geometry. The sectioned segments were then soaked in a bath of pure ethanol for at least 30 minutes. The cleaning was performed to remove any loose material and other removable deposits from the dosimeter wires prior to mass determination. The wire segments were allowed to completely dry in air at room temperature. The wires segments were then examined under low magnification. There appeared to be evidence of oxidation and some remaining surface contamination, indicating the need for further cleaning. This was accomplished by soaking the wire segments in a 4N solution of hydrochloric acid, followed by immersion in a 2N solution of nitric acid. The wires were then rinsed with distilled water, wiped once more with ethanol, and then allowed to dry in air at room temperature. The wires then exhibited a clean, shiny appearance. This was taken to indicate a good level of cleanness. The total mass of each wire was measured using a Mettler HL-52 digital balance. Table 2-1 lists the results of these measurements, as well as the identification assigned to each dosimeter.

The Charpy specimen was taken from the fracture surface side of one-half of a Charpy test specimen composed of base metal. The Charpy half was first cleaned in pure ethanol to remove and loose materials. The fracture surface of the specimen had been previously machined to remove metal chips for chemical analysis. This surface was taken to be the upper edge of the specimen. The Charpy specimen was marked to a depth of approximately 0.1 inches from the

fracture surface. A bandsaw equipped with a hardened steel blade was used to section a slice of the Charpy specimen approximately 0.1 inches thick, resulting in a piece of material approximately 0.1 inches thick and 0.4 inches on a side. This sample was then cleaned of loose materials and corrosion by wiping it with a clean cloth soaked in pure ethanol and visually inspecting it afterwards. The sample presented a clean, bright appearance. The specimen was then weighed using the same procedure as for the dosimeter wires.

2.3 Radiometric Analysis

Radiometric analysis was performed using high resolution gamma emission spectroscopy. In this method, gamma emissions from the dosimeter materials are detected and quantified using solid-state gamma ray detectors and computer-based signal processing and spectrum analysis. The specifications of the gamma ray spectrometer system (GRSS) are listed in Table 2-2. As shown in this table, there are two separate detectors in this system, one an older-style germanium-lithium, or Ge(Li) detector, and the other a newer, HyperPure germanium (HPGe) unit. Each detector is housed in a lead-copper shield (cave) to reduce background count rates.

System calibration was performed using a NIST-traceable quasi-point source supplied by Amersham Corporation. The analysis software was procured from Aptec Nuclear, Inc. and provides the capability for energy resolution, and efficiency calibration using specified standard source information. Calibration information is stored on magnetic disk for use by the spectrographic analysis software package.

Since detector efficiency depends on the source-detector geometry, a fixed, reproducible geometry/distance must be selected for the gamma spectrographic analysis of the dosimeter materials. For the dosimeter wires, the counting geometry was that of a quasi-point source (coiled 0.75 inch long wire) placed five inches vertically away from the top surface of the detector shell. In this way, extended sources up to 0.5-inch can be analyzed with a reasonable approximation to a point source. The coiled wires were well within the area needed to approximate a point source geometry. Both the Ge(Li) and HPGe detectors were calibrated for efficiency using the NIST traceable source.

Radiometric analysis of the Charpy specimen segment was performed using the HPGe detector, using a source-detector geometry that placed the source (Charpy specimen) eight inches away from the surface of the detector. Since the Charpy section was only 0.4 inches on a side and 0.1 inches thick, the small solid angle subtended by the source at the detector location allows the use of a quasi-point source efficiency calibration. As with the wire dosimeters, the HPGe detector efficiency for this geometry was calibrated with a NIST-traceable quasi-point source.

The accuracy of the efficiency calibration was tested using a gamma spectrographic analysis of a NIST traceable gamma source, separate from that used to perform the efficiency calibration, and supplied by a separate vendor. The isotope contained in this check source emits gamma rays, which span the energy response of the detector for the dosimeter materials. The results are summarized in Tables 2-3 and 2-4. They show that the efficiency calibration is providing a valid

estimate of source activity. The acceptance criteria for these measurements is that the software must yield a valid isotopic identification, and that the quantified activity of each correctly identified isotope must be within the uncertainty specified in the source certification.

Table 2-5 shows the counting schedule established for this work. Neutrons interact with the constituent nuclei of the dosimeter materials, producing radionuclides in varying amounts depending on total neutron fluence and its energy spectrum, and the nuclear properties of the dosimeter materials. Table 2-6 below lists the reactions of interest and their resultant radionuclide products for each element contained in the dosimeters. Some of these are threshold reactions involving an n-p or n-α interaction.

Finally, Table 2-7 presents the primary results of interest for flux determination. The activity units are in dps/mg, which normalizes the activity to dosimeter mass. The activities are specified for both the time of the analysis, and a reference date/time, which in this case is the NMP-2 shutdown date and time. This was specified as March 3, 2000, at 14:17 EST.

Table 2-1 Dosimeter Material Descriptions.

Dosimeter Composition	Dosimeter Mass (milligrams)	Dosimeter ID
Copper	226.51	Cu-1
Iron	125.86	Fe-1
Copper	201.04	Cu-2
Iron	120.82	Fe-2
Base Metal	1696.82	Charpy
(BF1-8)		

Table 2-2 GRSS Specifications.

System Component	Description and/or Specifications
Detectors	One Ge(Li), PGT Model LGC14, One HPGe, Canberra Model GC1420
Energy Resolution	Ge(Li): 1.78 @ 1332.5 KeV HPGe: 1.77 @ 1332.5 KeV
Detector Efficiency (Relative to 3-inch x 3-inch NaI)	Ge(Li): 12.9% @ 1332.5 KeV HPGe: 14.0% @ 1332.5 KeV
Amplifiers	Two Aptec Nuclear Inc. Model 6300 Low-Noise Spectroscopy Amplifiers
ADC	Two Aptec Nuclear Inc. Model S4008 PC-ISA Cards, 8192 Channels, 6 μsec. fixed conversion time, successive approximation conversion method
Computer System	120 MHZ Pentium-Based PC, 16 MB Main Memory, 1.1 GB Hard Disk, 17-inch Monitor, Laserjet 4M Printer
Software	Aptec Nuclear, Inc. OSQ/Professional, Version 6.10
Bias Supplies	Two Mech-Tronics Model 258 HV Supplies

Table 2-3 Performance Check of the Ge(Li) Detector and OSQ Software.

Isotope ID	Specified Activity in (μCi)	Specified Uncertainty (%)	Measured Activity in (μCi)	Measured Uncertainty (%)	Acceptance Criteria Met?
^{57}Co	3.483	3.0	3.395	2.3	Yes
^{60}Co	0.9583	3.1	0.9828	3.7	Yes

Table 2-4 Performance Check of the HPGe Detector and OSQ Software.

Isotope ID	Specified Activity in (μCi)	Specified Uncertainty (%)	Measured Activity in (μCi)	Measured Uncertainty (%)	Acceptance Criteria Met?
^{57}Co	3.483	3.0	3.468	2.5	Yes
^{60}Co	0.9583	3.1	0.9644	4.6	Yes

Table 2-5 Dosimeter Counting Schedule.

Dosimeter ID	Count Start Date	Count Start Time (EDT)	Count Duration (Live Time Seconds)
Cu-1	10/6/00	15:22	225934
Fe-1	10/17/00	16:58	145350
Cu-2	10/13/00	17:25	237659
Fe-2	10/6/00	11:20	250050
Charpy	12/18/00	16:24	235605
(BF1-8)			

Table 2-6 Reactions of Interest.

Dosimeter Element	Neutron-Induced Reactions	Reaction Product Isotope
Copper	n-α	Co-60
Iron	n-p	Mn-54
	n-α	Fe-59
Nickel	n-p	Co-58
Cobalt	n-α	Co-60

Table 2-7 Results of the Radiometric Analysis.

Dosimeter ID	Isotope ID	Activity At Count Date/Time[a] (dps/mg)	Activity At Reference Date/Time[b] (dps/mg)	Activity Uncertainty (%)
Cu-1	^{60}Co	4.60	4.97	3.65
Fe-1	^{54}Mn	16.78	27.84	1.09
	^{59}Fe	0.27	8.83	9.01
	^{60}Co	4.87	5.28	1.07
Cu-2	^{60}Co	4.26	4.62	0.86
Fe-2	^{54}Mn	17.60	28.49	1.06
	^{59}Fe	0.31	8.71	6.36
	^{60}Co	4.82	5.21	0.93
Charpy	^{54}Mn	16.44	30.62	1.19
(BF1-8)	^{59}Fe	0.1270	9.403	8.03
	^{58}Co	0.1911	2.968	3.67
	^{60}Co	11.32	12.52	0.92

[a] See Table 2-5

[b] This was specified as March 3, 2000, at 14:17 EST.

3.0 Neutron Fluence Calculation

3.1 Introduction

The neutron exposure of reactor structures is determined by a neutron transport calculation, or a combination of neutron transport calculations, to represent the distribution of neutron flux in three dimensions. The calculation determines the distribution of neutrons of all energies from their source from fission in the core region to their eventual absorption or leakage from the system. The calculation uses a model of the reactor geometry that includes the significant structures and geometrical details necessary to define the neutron environment at locations of interest.

A previous set of calculations was carried out for NMP-2 to determine the shroud exposure [3-1]. These calculations also included the surveillance capsule and vessel. The shroud fluence estimates were based on neutron transport calculations performed using fuel power and void fraction distributions taken at the midpoint of cycles 3, 4, and 7. In this report, determination of the fluence for the NMP-2 capsule at the end of cycle 7 was carried out using the previous results for cycles 3 and 4, and new calculations were performed using fuel power and void fraction distributions at the middle of each of cycles 1, 2, 5, and 6, and at five representative times during cycle 7. The detailed evaluation of the variation in flux level due to changes in fission distributions and void fraction distributions during cycle 7 was made to allow for accurate determination of dosimeter activities from the surveillance capsule that was withdrawn at the end of this cycle. It also provides an indication of the variation in flux level that occurs during a fuel cycle.

During reactor operation, the neutron flux level at any point in the shroud or vessel will vary due to changes in fuel composition, power distributions within the core, and water void fraction. These changes occur between fuel cycles due to changes in fuel loading and fuel design, and within a fuel cycle due to fuel burnup and resultant changes in power shape, control rod position, fission contributions by nuclide, and void fraction vs. axial height in each fuel bundle. In order to ensure that the fuel cycle data input to the model was representative, NMPC performed an analysis of the axial power shapes. For cycles 1 through 6, the core average axial power shape was plotted versus cycle exposure. An exposure-weighted cycle average power shape was calculated based on all of the individual power shapes. Power shapes close to the middle of cycle (MOC) were compared with the cycle average shape to determine which shape was representative of the entire cycle.

For cycle 7, NMPC once again examined the core average axial power shapes and the shapes were plotted throughout the cycle. Five cases were selected: beginning-of-cycle (boc); before middle-of-cycle (bmoc); middle-of-cycle (moc); after middle-of-cycle (amoc); and near the end-of-cycle (neoc). An axial shape which was most representative of each regime was chosen to represent that segment of cycle exposure.

The NMPC approach for selecting power shape inputs is not all that sophisticated but it does result in power shapes that are representative of the fuel cycle (or fuel cycle segment). Power shape

throughout a typical cycle's worth of operation has similar characteristics from cycle to cycle. Power starts out being preferentially produced in the bottom of the core via rod pattern manipulation, causing a spectral shift and enhanced Pu production. The Pu produced in the early part of the cycle is beneficial for "squeezing" extra energy out of the core toward the EOC when control blades are not available for power shaping. During MOC, the axial segments of the core burned harder in the early cycle cause the power shape to flatten. As the cycle comes to a close, and rods are nearly fully withdrawn, the power shifts to the top of the core and the reactor is subsequently shut down for refueling as EOC is achieved. These cycle characteristics are repeatable for all cycles which allows one to choose a MOC shape as representative of the average over the entire cycle.

3.2 Neutron Transport Model

The transport calculations for NMP-2 were carried out in R-θ and R-Z geometry using the DORT two-dimensional discrete ordinates code [3-2] and the BUGLE-96 cross-section library [3-3]. The DORT code is an update of the DOT code which has been in use for this type of problem for many years. The BUGLE-96 library is a 47 energy group ENDF/B-VI based data set produced specifically for light water reactor applications (an update of the earlier SAILOR library). The energy group boundaries for the 47 groups are given in Table 3-1. This library contains cross-sections collapsed using a BWR core spectrum which were used for the core region. Outside the core region, cross sections collapsed using PWR downcomer and PWR vessel spectra were used. The difference between BWR and PWR collapsing in these regions is not significant. In these analyses, anisotropic scattering was treated with a P3 expansion of the scattering cross-sections, and the angular discretization was modeled with an S8 order of angular quadrature. These procedures are in accordance with ASTM Standard E-482 [3-4].

The computer codes were obtained from the Radiation Safety Information Computational Center (RSICC) at Oak Ridge National Laboratory. Each code was then compiled on the computer used by MPM for the calculations and a series of test cases were run to verify the code performance. The test cases all agreed within allowable tolerance with established results. This verification was conducted under the MPM Nuclear Quality Assurance Program. The calculational procedures meet standards specified by the NRC and ASTM as appropriate. In particular, the analysis (including all modeling details and cross-sections) is consistent with draft guide DG-1053. The calculations have been benchmarked to measured plant specific BWR data as described in Section 3.4. However, the calculational benchmarks specified in DG-1053 have not been calculated since they have not yet been issued. This is planned to be carried out when the benchmarks are issued as additional methods verification.

R-θ Calculations

The R-θ layout is shown in Figure 3-1. Dimensions for the various structures are given in Table 3-2 [3-5]. In this figure, all structures outside the core were modeled with a cylindrical symmetry except for the inclusion of a surveillance capsule centered at 3° and jet pump structures

located in the downcomer region. The latter are not to scale in the figure. The jet pumps are only approximate models of two pumps with a central pipe (riser) in between. These structures were modeled as 2 slabs of stainless steel each centered at a radius of approximately 112.28 inches [3-5]. The slabs representing the pumps are at about 22 and 36.5 degrees, and the riser is at about 29.3 degrees. The slabs extend over approximately 3.85 degrees and have a thickness of 0.477 inches. The pipe slab extends over about 4.25 degrees and is 0.523 inches thick.

The R-θ model included 186 mesh points in the radial direction covering the range from the center of the core to ten inches into the biological shield. This large number of mesh points was used to accurately calculate the neutron flux transport from the core edge to the outside of the vessel. In the azimuthal direction, 48 mesh points were used to model a single octant of the reactor. Inspection of the fuel loading patterns indicated that only minor deviations from an octant symmetry were present and these were ignored. The 48 points provided good definition of the variation of the core edge with angle and defined the azimuthal flux variation. In the discussion below, all angles are referred to in the first octant (i.e. relative to the nearest cardinal axis) and thus welds at both 45° and 225° are referred to as a 45° location. It should be noted that the azimuthal flux shape between 45° and 90° is the mirror image of that between 0° and 45° (i.e. an angle of 50° corresponds to 40° in the first octant).

The core region used a homogenized material distribution which includes the fuel, fuel cladding, and the water. The water region in the fuel contains both liquid water and steam. The fraction occupied by steam is known as the void fraction and varies by assembly and axial position within the fuel. Values of void fraction for each cycle at the middle of the cycle (moc), and at the additional times during the cycle for cycle 7, were supplied by NMPC for each assembly at 25 axial nodes [3-6, 3-7, 3-8]. Inspection of these values indicated that while some assemblies exhibit significant variation in the void fraction, some groups of neighboring assemblies had close to the same void fraction. To model the void fraction variation in the R-θ model, the outer rows of assemblies were divided into seven regions of approximately uniform water material density, and the average water density for the assemblies in each of these regions was calculated by multiplying the base water density (0.7365 g/cc) by 1.0 minus the void fraction. The inner assemblies were assigned to an eighth region and the core average void fraction was used for this region. The assemblies in each of these regions are indicated by the region numbers defined in Figure 3-1. Each one of these regions had a void fraction assigned as the average midplane void fraction value for the assemblies in the region. These average void fraction values were different for each case analyzed. Values for the average axial midplane void fractions by region for each case are given in Table 3-3.

Water density in the bypass region was varied between 0.7585 g/cc at the inlet and 0.7394 g/cc at the outlet [3-5]. The value at midplane was taken to be an average of these values. The downcomer water density was calculated for a temperature of 534 °F and a pressure of 1037 psia.

The DOTSOR code (available as part of the LEPRICON code package [3-9]), was used to convert the cycle power distributions from x,y to R,θ coordinates and to place the source in each mesh cell. The source per group was defined by an average fission spectrum calculated for a fission

breakdown by isotope determined for the average burnup of the outer assemblies for each case. The main isotopes that contribute to the fission spectrum are U-235 and Pu-239, but contributions from U-238, Pu-240, and Pu-241 were also included. This is a good approximation to the fission spectrum because the outer assemblies were all burned assemblies with similar burnup, and the fission spectrum only slowly varies with burnup. Almost all of the neutrons that reach the capsule and vessel originate in the outer rows of fuel bundles.

The source calculations used the appropriate power distribution for all the fuel bundles in the first octant together with pin power distributions for the outer rows of bundles. The pin power distributions were used to model the spatial variation of the source within the bundles and took into account the gaps between bundles and water rods in the center. Equal pin power weighting was used for interior fuel bundles. In the calculations, the variation in relative pin power distributions within similar bundles between cycles was determined to be small [3-1] and so the cycle 7 9x9 moc pin power distributions were used in the calculations for all the cases.

The calculation of the fuel fission parameters was handled differently from the previous calculations. The ORIGEN 2.1 code [3-10] was used to calculate the effects of burnup on the neutron source. This was carried out using an ORIGEN BWR cross section library appropriate for high burnup fuel. The results were validated by comparison to NMP-2 calculated fuel compositions as a function of fuel burnup [3-11].

For the ORIGEN calculations, the initial fuel composition for each cycle was taken to be the average initial composition for the outer assemblies. The effects of the varying axial initial enrichment, burnup, and void fraction were ignored in this calculation and are assumed to have negligible impact because the effects of the change in parameters are minor. The ORIGEN code calculated the fission fraction by isotope and the average energy deposited in the reactor per fission (κ). The isotopic fission fractions were used to determine the fission spectrum and the average number of neutrons per fission (ν). The normalization of the neutron source in the DORT calculations is directly proportional to ν/κ which slowly varies with burnup.

Since the average burnup of the outer assemblies was used for the source normalization, this is an updated method compared to [3-1] where the average core burnup was used. The present assumption more accurately represents the neutrons that escape from the core. This effect is small enough that it was ignored for the cycle 3 and 4 cases.

R-Z Calculations

A second set of transport calculations were performed for each case in R-Z geometry. For this calculation, the core was divided into 3 radial regions. Two of these regions consisted of each of the outer two rows of assemblies averaged over the octant. The third region consisted of the inner part of the core. The neutron source in each of these regions was calculated using a radial source averaged over the octant (calculated by DOTSOR as for the R,θ case) together with an average axial power shape for each region. The axial power distribution was supplied for each assembly in 25

nodes, each representing 6 inches of core height. Neutron source outside the equivalent core radius was eliminated.

Each radial region was also divided into axial regions according to variation in void fraction. The void fraction was also given for each assembly in 25 axial nodes. Except for nodes near the bottom of the core which had zero void fraction, each node was modeled as a separate region for the calculation. This resulted in a total of 70 regions in the core, each with a distinct cross section set. In addition, the GE11 fuel bundles contain 8 part length fuel pins that end at 96 inches above the bottom of the active fuel (BAF). The volume of these pins was replaced with water at axial meshes above the 96 inch level. The bypass region was also modeled with a varying axial water density. The bypass region was divided into 12 subregions within the core height, each with a different water density.

For the R-Z model, the core radius was taken to be that which gave the equivalent core volume. Regions above and below the core were not modeled exactly but consisted of a one-foot high water reflector with vacuum boundaries at the top and bottom of the model. The model had 186 mesh points in the radial direction as in the R-θ model except with slightly different boundaries near the core edge. In the axial direction, the model had 68 mesh points with 38 in the core region.

Flux Synthesis

As indicated above, the calculations were carried out in 2 dimensions. In order to estimate the fluence rate in the 3 dimensional geometry, the following equation was used to evaluate the flux, ϕ, for each cycle case:

$$\phi(R,\theta,Z) = \phi(R,\theta) * \phi(R,Z) / \phi(R) .$$

In this equation, $\phi(R,\theta)$ is taken from the DORT R, θ calculation (normalized to the power at midplane in the model region), and $\phi(R,Z)$ is from the R,Z calculation normalized to the power in the entire core. A third calculation determined $\phi(R)$ using a one-dimensional cylindrical model normalized at core midplane. The model for the one-dimensional calculation used the same radial geometry as the R,Z calculation.

3.3 Capsule Fluence Results

The calculated fluxes for each case for the 3-Degree surveillance capsule are given in Table 3-4. These values are for the midpoint of the capsule at the axial midplane. The five cases for cycle 7 are averaged to get an average value for this cycle. The average of the flux values for the seven cycles is also calculated (this is a straight average, not a weighted average) and the fractional standard deviation is given in Table 3-4. It is seen that variation between the cycles gives a standard deviation of 19%. For the five cycle 7 cases, the standard deviation is about 16%.

Table 3-5 gives fluence values for the capsule for each of the 7 cycles and the total fluence

at the end of cycle 7. The fluence (E > 1 MeV) at the center of the capsule is slightly higher than that previously calculated [3-1]. The difference (about 6%) is due to a combination of the changes in model assumptions discussed in Section 3-2 , the more detailed evaluation of the cycle 7 flux variation, and the inclusion of the calculations of cycles 1,2, 5, and 6.

Values for the flux may also be compared to previous calculations. In reference [3-12], several results of other calculations are given, and the calculation by GE [3-13] was recommended. This calculation obtained a value for the capsule of 2.70 E8 n/cm^2/s for the flux E>1 MeV at the uprated power for cycle 5. The comparable value in the present calculation is 2.53E8 n/cm^2/s which is a difference of 7%. This is considered very good agreement considering all the differences between the calculations, including differences in the fuel power distribution used, different models, and different cross section data (including the changes in the iron cross section that occurred with the change to the BUGLE-96 library). In reference [3-13] a lead factor for the vessel ID (ratio of capsule to maximum flux at the vessel surface) was calculated to be 0.30. The value in the present calculation for cycle 5 is 0.41. This difference can be partly explained by the omission of the jet pumps from the model used in the reference [3-13] calculation. A calculation with the jet pumps omitted indicated a flux increase at the maximum vessel point of about 10% [3-1]. The jet pump modeling does not affect the capsule flux.

For the fluence at the end of cycle 7, the lead factor (capsule over vessel maximum) is calculated to be 0.43 (8.49E16/1.95E17) using the vessel maximum fluence results given in Section 3-5.

Uncertainty in the evaluation of the capsule fluence is evaluated in Section 3-6.

3.4 Capsule Measurement Results

The capsule removed at the end of cycle 7 was irradiated from initial reactor start-up to March 3, 2000 for a total of 8.72 effective full power years (EFPY). The power history was supplied as the thermal generation per month over this period. The use of monthly power history data is not expected to introduce any significant error in the evaluation of the dosimetry results since the half-lives of both Mn-54 and Co-60 are significantly longer than one month.

The capsule dosimetry consisted of two sets of Cu and Fe wires. This dosimetry was counted to determine the fast neutron reactions shown in Table 3-6. This table also gives the nuclear constants used to determine the reaction rates. These data are taken from the appropriate ASTM standards [3-14, 3-15, 3-16].

The dosimetry results that relate to fast fluence are given in Table 3-7 (taken from Table 2-7). The dosimeter measurements are presented in units of disintegrations per second per milligram (dps/mg), adjusted to the end-of-irradiation (March 3, 2000 at 14:17 EST). Using the power history and the reaction rates for Fe and Cu determined by the DORT calculation for each cycle and the five cycle 7 cases, the activity at the end of the irradiation was calculated for a point at the geometrical

center of the capsule. The results were obtained by multiplying the reaction rate for the two reactions obtained from the synthesis procedure for each calculation by the effective full power seconds (EFPS) for each monthly time interval and then accounting for radioactive decay during the interval and to the end-of-irradiation time. The number of activation product atoms per target atom is converted to dps/mg using the parameters in Table 3-6.

The C/E ratios for each dosimeter measurement and the average is tabulated in Table 3-7. The average C/E ratio (1.07) indicates very good agreement between the calculation and the measurement. The Fe and Cu dosimetry results do show a consistent difference, however. It should be noted that 95% of the iron response is from the last two irradiation cycles, while 48% of the copper response is from earlier cycles. In addition, copper has a much higher reaction threshold and so only responds to a small fraction of the fast neutrons while the iron responds to a larger fraction. In addition, the copper cross section is not as well known as the iron cross section. Taking all these factors into account, an average of the two monitors probably produces the best indication of the adequacy of the calculation to estimate the integrated fluence.

The location of the dosimeters in the capsule is somewhat uncertain. The initial location was thought to be near the front top of the capsule at the right side as viewed from the core. This would place the dosimeters at about 0.48 cm towards the core from the capsule radial center and about 6 inches above core midplane. The radial correction would increase the calculated activity by 4.6% for copper and 7.4% for iron. The axial correction varies during the fuel cycle and between cycles, but the activities 6 inches above midplane average about 4% higher. The azimuthal difference is small, but the activity to the right (higher angles in the first octant) increases by about 1% from that at the center of the capsule. If all these factors are included, the calculated copper activity at the indicated dosimeter position is higher by about 10% compared to the capsule center and the iron by 13%. This results in average C/E ratios of 1.02 for copper and 1.37 for iron with an average C/E of 1.19.

However, it may also be postulated that the copper dosimeter is positioned towards the core side of the capsule, while the iron is positioned towards the vessel side. If this assumption is made, then the iron average C/E ratio is 1.19 and the average of the two dosimeter types is 1.11. It is also possible to assume that the dosimeter wires dropped to the bottom of the capsule. This would lower the calculated activity by 4% compared to the capsule axial midplane (instead of increasing it as noted above for the correction to the top of the capsule). The average C/E ratio would then be about 1.02.

To test the hypothesis regarding the dosimeter location, a sample was cut from a Charpy bar as previously described. The sample was a complete slice across the specimen taken just below the fracture surface, and thus is radially centered and located very near the azimuthal center of the capsule. By counting with the 0.4 inch x 0.4 inch surface facing the detector, the Charpy bar dosimeter sample gives an average of the center of the capsule. Unfortunately, the axial location of the Charpy bar within the capsule is not known. Further discussion of the uncertainty is given below.

The measured result for the Charpy bar dosimeter, adjusted to the reference time, is 30.62 dps/mg (refer to Table 2-7). The Charpy bar material is not pure iron, but has been determined to have an iron fraction of 0.9694. Using this value, the dps/mg of iron is then 31.59. The Charpy bar data is summarized in Table 3-7. This Charpy bar yielded a C/E ratio of 1.08 which shows very good agreement between the calculated bar activity and the measured activity. Further, this result is 12% higher than the result from the Fe dosimeter wires. Thus it is likely that the iron dosimeters were actually located towards the rear of the capsule and also probably at the bottom. The C/E ratio results using this assumption are shown in the last column of Table 3-7. The average C/E for copper is 0.95 and for iron is 1.09, for an overall average of 1.02.

Uncertainty in the activity measurements are given in Table 2-7. These values are regarded as precision estimates. The measurements also contain a bias (due primarily to calibration uncertainty) that is typically about 3% [3-14,3-15]. The uncertainty in the C/E ratio also contains the contribution from the dosimeter position uncertainty, dosimeter cross section uncertainty, and the flux history uncertainty. As discussed above, the dosimeter position uncertainty can be as large as 10-13%. However, using the Charpy measurement which has a better known position, reduces this uncertainty to about 5%. The dosimeter cross section uncertainty is limited by correlation with benchmark measurements. It can be assumed that typical iron and copper reaction integral cross sections are known to within 3% [3-18]. The flux history uncertainty will vary with the half-life, but can be conservatively assumed to be less than 8% (see discussion in Section 3-6). The total uncertainty in the measurement is then about 10%. The uncertainty in the calculated values may be taken from the calculated fluence uncertainty evaluated in Section 3-6 to be 15.3%.

It is seen that the best estimate C/E value of 1.02 is well within both the measurement uncertainty and the calculation uncertainty. It is concluded that the measurement provides an excellent validation of the adequacy of the calculation. Additional verification is provided by comparisons to dosimetry measurements from the Nine Mile Point Unit 1 reactor as described in Reference [3-19] which was calculated using identical methodology. The Unit 1 measurements included both dosimetry from a surveillance capsule, and measurements of samples removed from the reactor shroud. These BWR measurements provide specific validation of BWR calculations in contrast to most measurements which are in PWRs or simulations of PWR geometry. In accordance with draft guide DG-1053, the calculated fluence values are recommended for use in estimating vessel embrittlement and in P-T curves.

3.5 Vessel Fluence Results

The fluence to the reactor vessel was also determined from the calculations for each cycle using the flux synthesis. The flux shape was found to vary somewhat from cycle to cycle due to the differences in fuel loading pattern and due to differences in axial power shape and void fraction. Inspection of the azimuthal variation of the fast flux indicated that the maximum flux in the vessel occurs at approximately 26°. This is shown in Figure 3-2 which is a plot of the fluence (E > 1 MeV) at the end of cycle 7 at core midplane. The fluence is shown for the clad-base metal interface (the vessel inner radius (IR)), at 1/4 of the distance into the vessel (1/4 T), and at 3/4 of the distance

through the vessel (3/4 T).

The peak fluence point varies axially, both during cycles and between cycles. Therefore, the maximum fluence point must be determined by integrating the flux at several axial heights to find the peak value. The maximum fluence point at the end of cycle 7 is at about 30 inches above midplane. This is shown in Figure 3-3 which plots the fluence (E > 1 MeV) at the end of cycle 7 versus axial distance from core midplane for the IR, 1/4 T, and 3/4 T positions. The fluence in this figure is at the maximum azimuth.

Values for the calculated maximum vessel fluence E > 1 Mev, fluence E > 0.1 MeV, and dpa are given in Table 3-8 for the inner radius of the vessel clad (wetted surface), the vessel base metal IR, the 1/4 T position, and the 3/4 T position calculated at the end of cycle 7 (8.72 EFPY). Exposure values extrapolated to 22 EFPY are also given in Table 3-8. The 22 EFPY exposure was calculated in support of a planned revision to the P-T curves. The data in Table 3-8 have been extrapolated using cycle 7 average flux and dpa/s values since future cycles are projected to be similar to cycle 7. Since the maximum flux point for cycle 7 is slightly closer to axial midplane, the maximum vessel fluence at 22 EFPY was determined by integrating the flux at various axial points and taking the maximum value which was found to occur at 24 inches above midplane. The difference between the maximum value at 24 inches above midplane and 30 inches above midplane at 22 EFPY is only a small fraction of a percent (about 0.3% for fluence (E > 1 MeV)), and this difference is not deemed to be significant. The values in Table 3-8 are the calculated maxima and thus the axial position of the fluence values in this table for 8.72 and 22 EFPY are not the same.

Radiation embrittlement effects are usually correlated with fluence E > 1 MeV. However, it is generally thought that dpa might be a better correlation parameter and, if this is correct, the use of the fluence E > 1 MeV values within the vessel are non-conservative. Accordingly, a dpa attenuation factor is used for fluence through the vessel. This can be done using calculated dpa attenuation from Table 3-8 or using a formulation specified in the RG 1.99(2). The fluence values using both these attenuation methods are given in Table 3-9 for 8.72 and 22 EFPY.

The dpa values in this report are calculated from the ASTM E693-94 Standard dpa cross-section [3-17]. This evaluation of the dpa cross section is based on the ENDF-IV cross-section file. A new dpa cross-section evaluation based on ENDF-VI (consistent with the cross-sections in BUGLE-96) is expected to be used as the standard in the future. This change is not expected to have any significant impact on the results reported here.

3.6 Uncertainty Estimation

A detailed uncertainty analysis was performed to estimate each source of uncertainty in the calculated fluence values. This analysis made use of defined uncertainties and tolerances where possible, but some of the uncertainty estimates had to be based on estimates derived from data variation, such as the detailed power distribution and void fraction variations within a single cycle. The geometry uncertainty assignments are from Reference [3-5] and are the same as those used for

the previous calculation [3-1]. The uncertainty estimates based on data variation are similar to those in Reference [3-1] except for increasing the power history uncertainty as a result of the variations in capsule flux level by cycle. Discussion of each uncertainty assumption is given below. Based on these uncertainty values, detailed uncertainty evaluations were performed for the surveillance capsule and reactor vessel. The uncertainty evaluations for reactor beltline locations are summarized in Table 3-10.

In the uncertainty evaluations, uncertainties were treated as normally distributed and all uncertainties were valued in terms of 1 standard deviation (1σ). The individual uncertainties were assumed to be randomly distributed and independent (except where correlations occur such as increases in steel thickness which result in a decreased water thickness). The total uncertainty is then determined by quadrature (square root of the sum of the squares of the contributing uncertainty components given as 1σ values).

3.6.1 Uncertainty Assumptions

Nuclear Data

Nuclear data input to the transport calculations includes the multigroup cross sections and neutron spectrum. Uncertainties in the cross sections are complicated because of the large number of cross section values and the correlations between these values. Although the uncertainties in individual cross section values may be relatively large, the total effect of cross section uncertainties is limited by adjustments made by cross section evaluators to agree with benchmark data. The approach taken here is to limit the cross section uncertainty effects to just the total cross section and to evaluate this by varying the material densities (see below).

Uncertainty in the multigroup fission source arises from uncertainty in the fission spectra for each fissioning isotope, the distribution of fission among the fissioning isotopes, the energy release per fission (κ), and the number of neutrons produced per fission (υ). Uncertainty in the fission spectrum is mainly at the higher energies, which has little effect on the fluence above 1 MeV except for very deep penetrations. The uncertainty was represented as an uncertainty in burnup, which was taken as 10,000 MWd/MTU (megawatt days per metric ton of uranium). The uncertainty is assumed to be fairly large to encompass the use of average burnup of the outer fuel bundles rather than including explicitly the detailed radial and axial burnup variation. A 1-D calculation was performed [3-19] to determine the spectral effect and it was found to vary between 0.2% in the core to 1.8% at the outside of the vessel.

The parameters υ and κ both increase with burnup, but the source normalization is proportional to the ratio υ / κ. Thus, the variation with burnup is small. For an uncertainty of 10,000 MWd/MTU, the normalization uncertainty is 1.1%. Since this is in the same direction as the spectrum uncertainty, it is added to the spectrum contribution to give the values in Table 3-10.

Normalization

In addition to the normalization uncertainty due to υ / κ, there is an overall normalization uncertainty in reactor power as measured by the heat balance. This uncertainty is estimated by the plant to be 2%.

Geometry

Geometric uncertainties are taken from Reference [3-5]. The vessel inner radius uncertainty was taken to be a typical value [3-19]. The uncertainty in the shroud inner radius was based on as-built measurements of the inner diameter. These measurements indicate a range of 203.062 to 203.250 inches. The radius will then have a maximum to minimum range of 101.531 to 101.625 inches (a range of 0.094 inches). The important distance is, however, the distance from the core edge to the shroud, and if the shroud is slightly off-center, then this uncertainty could be larger. To be conservative, an uncertainty of 0.188 inches was used and assumed to be 1 standard deviation. The shroud radius used in the calculation was actually not the center of the range, but was the design radius 101.56 inches which is only 0.029 inches from the minimum as-built value. The tolerance on the shroud thickness of 0.042 is a conservative value taken from [3-19].

Jet Pumps

The jet pumps could not be exactly modeled in the calculations due to the complex geometry of the jet pumps. The steel from the jet pumps was approximately included as slabs of steel placed appropriately in the downcomer region in the R,θ calculation. The jet pumps were not included in the R,Z calculation. To estimate the uncertainty introduced by the crude model, a separate R,θ calculation was made with the jet pumps omitted. This had no effect on the surveillance capsule fluence, but the maximum fluence at the vessel inner radius increased up to 16.4%. For fluence at the maximum fluence points, a reasonable estimate of uncertainty from the imperfect modeling of the jet pumps is 25% of this value, or 4.1%.

Material Densities

The material density uncertainty was treated differently for the water density and the steel density. The water density in the core decreases with height as the void fraction increases. Based on the variation in the void fraction in Nine Mile Point Unit 1 [3-19], a comparison of the Unit 2 data for the various cycles, and on the necessity for the heat generation in the core to produce a certain rate of steam, the void fraction uncertainty was estimated to be 5%. The bypass water is not thought to have any void volume, but the temperature may vary from the value that was assumed. The uncertainty was estimated by taking one half of the difference between the estimated bypass water density at the bottom and top. This indicates an uncertainty of 1.3%. This is consistent with the value of 1.4% in Reference [3-19] which was estimated using a slightly different method. The slightly higher value of 1.4% was adopted. The uncertainty in the downcomer water density was calculated from a temperature uncertainty of 5 °F [3-19].

The effect of each of the water density uncertainties on the fluence was calculated separately. Because of the relatively large azimuthal variation in vessel fluence, the effect of the core water density uncertainty and the bypass water density uncertainty were calculated using 2-dimensional R,θ calculations [3-1]. The azimuthal variation of the bypass water is particularly pronounced and is lowest at the highest flux point where the distance from the core to the vessel is the smallest. The uncertainty due to the downcomer water density was determined by a 1-dimensional calculation [3-1].

The uncertainty in steel density is less than about 1%. However, as noted above, the cross section uncertainty was included as an addition to the steel density uncertainty. An estimate for this uncertainty was derived by considering vessel mockup benchmark results [3-20], comparisons of reactor cavity and surveillance capsule measurements [3-21, 3-22, 3-23, 3-24], and comparisons of cross section evaluations [3-25]. It was concluded that uncertainties due to the iron cross section contribute a 10% effect on fluence through a reactor vessel. This translates into a cross section uncertainty of 3.5%. This value was adopted as the density variation and uncertainties were calculated based on this uncertainty estimate. In addition, the core cross sections for the fuel and cladding were also assumed to have this uncertainty. This estimate includes effects due to the core homogenization.

Source Uncertainty

Source uncertainties were estimated in [3-19] based on the variation of the calculated power distributions at points within a single cycle. This produced estimated uncertainties of 6% radially and 3.7% axially. Larger differences were observed between cycles and these uncertainties were included in the flux history uncertainty (see below). These estimates were compared with differences between the Unit 2 cycle 4 and cycle 7 power distributions and it was felt that the cycle differences were bounded by these uncertainty estimates.

Methods Uncertainty

The neutron transport was calculated using a model of the reactor and S_N code. This is only an approximation to the solution of the Boltzmann transport equation and thus also contributes uncertainty. Two components of this uncertainty were considered. First, the uncertainty of the fuel model was considered. From the VENUS benchmark measurements, it was found that a typical range of C/E results was about 10% [3-26]. Thus, the standard deviation was about 5% and this value was used here. The second component was the adequacy of the S_8 calculation. To test this, S_{16} calculations were performed to indicate the accuracy [3-19]. Differences of 1.4% were observed in the shroud and as high as 3% at the outside of the vessel. The differences were added in quadrature to the 5% from the first modeling effect.

Additional uncertainty is introduced by the 3-D synthesis procedure in regions near the edge of the core where the modeling is less precise. Effects due to the fact that the capsule and jet pumps do not extend through the entire core height are also not taken into account. Uncertainty

contributions due to these effects only are significant for fluences well below the maxima. In particular, the synthesis uncertainty in the capsule and at the maximum fluence point in the vessel is considered to already be included in the 5% modeling uncertainty. Significant deviations in the accuracy of the synthesis would be expected above the top of the jet pumps (about four feet above core centerline) at angles behind the pump locations. Although the maximum vessel fluence occurs behind a jet pump, it is a sufficient distance below the top of the jet pumps so that the effect of neutrons reaching the vessel at the maximum point by streaming over the top of the pumps is negligible. Uncertainty in vessel fluence near the top and bottom of the fueled regions would be larger than that determined for the higher fluence region.

Flux History

In Reference [3-19] an estimate of the impact of flux history uncertainty on the fluence was made. It was estimated that a conservative value for this uncertainty contributor was 7% based on cycle-to-cycle variation. For the present series of calculations, it was found that the flux at the surveillance capsule had a standard deviation of about 19% over the seven cycles and about 16% within cycle 7. Moreover, while the cycle 7 moc calculation fell near the middle, it was about 6% different at the capsule compared to a cycle average over the 5 calculated points in time. Most of the effects of the cycle variation are included in the moc representations, but this variation within the cycle remains as an uncertainty. This uncertainty was estimated by taking one-half of the 16% cycle standard deviation to provide a reasonable estimate of the moc variation from the cycle average. Thus, this uncertainty contribution was increased from 7% to 8%.

3.6.2 Uncertainty Evaluation

The results for the uncertainty evaluation are summarized in Table 3-10, which is applicable to the vessel in the beltline region and the surveillance capsule. In this table, some of the uncertainty results are given as ranges that are derived from the 2-dimensional calculations. The uncertainty contribution due to the bypass water density uncertainty is a minimum at the vessel maximum point and the jet pump uncertainty is a maximum at this point.

A total uncertainty was derived by combining the independent individual contributors in quadrature. This gave an uncertainty for the maximum vessel fluence of 15.5% (using 1.6% for the bypass water uncertainty and 4.1% for the jet pump uncertainty), and an uncertainty for the capsule fluence of 15.3%. The vessel fluence uncertainty is evaluated at the maximum fluence point, but the variation in vessel uncertainty with position is relatively small.

The uncertainty in the surveillance capsule fluence is similar to that for the reactor vessel inner radius with only minor differences. The assumption is made that the accuracy of the capsule location is the same as the accuracy of the vessel IR. The jet pumps are not near the capsule so no error is contributed from the jet pump model. It may also be assumed that the axial and azimuthal location of the capsule is well known. For a 1 inch error in axial height, the fluence uncertainty is 0.8% and for a 1 degree uncertainty in azimuth, the uncertainty is 2.4%. The total uncertainty in

capsule fluence (summing in quadrature all the components from Table 3-10) is 15.3%.

The C/E ratio for the capsule dosimetry measurements will have contributions from the uncertainty in calculated fluence at the center of the capsule, the uncertainty in dosimetry position, the uncertainty in dosimeter cross section, and the uncertainty in the activity measurement. The most significant contributor is the calculated fluence uncertainty. The effect of the dosimetry position uncertainty within the capsule is discussed in Section 3.4 where it is shown that the average C/E falls between 1.03 and 1.15. The total C/E uncertainty is likely to be about 17% assuming dosimetry position uncertainty of 6% (half of the C/E range). Thus it is clear that the C/E value falls within the expected uncertainty range.

3.7 Chapter 3 References

[3-1] "Nine Mile Point Unit 2 Shroud Neutron Transport and Uncertainty Analysis," Report MPM-200623, MPM Technologies, Inc., 2161 Sandy Drive, State College, PA 16803-2283, February 2000.

[3-2] RSICC Computer Code Collection, CCC-543, TORT-DORT-PC, Two- and Three-Dimensional Discrete Ordinates Transport Version 2.7.3, available from the Radiation Safety Information Computational Center, Oak Ridge National Laboratory, Oak Ridge, TN, June 1996.

[3-3] RSICC Data Library Collection, DLC-185, BUGLE-96, Coupled 47 Neutron, 20 Gamma Ray Group Cross Section Library Derived from ENDF/B-VI for LWR Shielding and Pressure Vessel Dosimetry Applications, available from the Radiation Safety Information Computational Center, Oak Ridge National Laboratory, Oak Ridge, TN, March 1996.

[3-4] ASTM Designation E482-89, *Standard Guide for Application of Neutron Transport Methods for Reactor Vessel Surveillance*, in ASTM Standards, Section 12, American Society for Testing and Materials, Philadelphia, PA, 2000.

[3-5] Letter, Shashi K. Dhar to M. P. Manahan, "Input Data for NMP-2 Fluence/Transport Calculations - Final," File Code ESB3-M99058, October 26, 1999.

[3-6] Winkelbleck, J., Email with attached files, entitled, "NMP-2 Cycles 4, 5, & 7 Core Neutronics Data", From J. Winklebleck to M. P. Manahan, Sr., August 4, 1999.

[3-7] Winklebleck, J., Email with attached files, entitled, "NMP-2 Cycles 3 Core Neutronics Data", From J. Winklebleck to M. P. Manahan, Sr., January 13, 2000.

[3-8] Email from J. Winkelbleck to M. P. Manahan, Sr.: Power and Void Fraction, casematrix.xls - 9/20/00, nmp2flue.zip - 9/27/00; Cycle 7 Power History, cycle7_pow.xls - 10/2/00, cycle7thermal.xls - 10/11/00; Cycle 1

Power and Void Fraction, c1mocmap_rev01.txt - 11/15/00.

[3-9] RSICC Peripheral Shielding Routine Code Collection, PSR-277, LEPRICON, PWR Pressure Vessel Surveillance Dosimetry Analysis System, available from the Radiation Safety Information Computational Center, Oak Ridge National Laboratory, Oak Ridge, TN, June 1995.

[3-10] RSICC Computer Code Collection, CCC-371, "ORIGEN 2.1, Isotope Generation and Depletion Code Matrix Exponential Method," available from the Radiation Safety Information Computational Center, Oak Ridge National Laboratory, Oak Ridge, TN, May 1999.

[3-11] Letter, Shashi K. Dhar to M. P. Manahan, File Code ESB2-M99-043, July 29, 1999.

[3-12] "Nine Mile Point Unit 2 Reactor Pressure Vessel Surveillance Capsule Withdrawal Schedule Analysis", MPM-1197409, November, 1997.

[3-13] GE letter NMP2-95-21, D. R. Pankratz to A. D. Sassini, "RPV Fluence Lead Factor Analysis for NMP-2 Power Uprate (Cycle 5), May 8, 1995.

[3-14] ASTM Designation E263-00, Standard Test Method for Measuring Fast-Neutron Reaction Rates by Radioactivation of Iron, in ASTM Standards, Section 12, American Society for Testing and Materials, Philadelphia, PA, 2000.

[3-15] ASTM Designation E523-92, *Standard Test Method for Measuring Fast-Neutron Reaction Rates by Radioactivation of Copper*, in ASTM Standards, Section 12, American Society for Testing and Materials, Philadelphia, PA, 2000.

[3-16] ASTM Designation E1005-97, *Standard Test Method for Application and Analysis of Radiometric Monitors for Reactor Vessel Surveillance, E706(IIIA)*, in ASTM Standards, Section 12, American Society for Testing and Materials, Philadelphia, PA, 2000.

[3-17] ASTM Designation E693-94, *Standard Practice for Characterizing Neutron Exposures in Iron and Low Alloy Steels in Terms of Displacements Per Atom (DPA), E706(ID)*, in ASTM Standards, Section 12, American Society for Testing and Materials, Philadelphia, PA, 2000.

[3-18] ASTM Designation E261-94, *Standard Practice for Determining Neutron Fluence, Fluence Rate, and Spectra by Radioactivation Techniques*, in ASTM Standards, Section 12, American Society for Testing and Materials, Philadelphia, PA, 2000.

[3-19] "Nine Mile Point Unit 1 Shroud Neutron Transport and Uncertainty Analysis," Report Number MPM-108679, MPM Technologies, Inc, 2161 Sandy Drive, State College, PA 16803-2283, October, 1998.

[3-20] McElroy, W.N., Ed., "LWR-PV-SDIP: PCA Experiments and Blind Test", NUREG/CR-1861, 1981.

[3-21] Lippincott, E.P., "Consumers Power Company Palisades Nuclear Plant Reactor Vessel Fluence Analysis", WCAP-13348, May 1992.

[3-22] Maerker, R.E., et.al., "Application of LEPRICON Methodology to LWR Pressure Vessel Dosimetry", Reactor Dosimetry: Methods, Applications, and Standardization, ASTM STP 1001, 1989, pp 405-414.

[3-23] Anderson, S.L., "Westinghouse Fast Neutron Exposure Methodology for Pressure Vessel Fluence Determination and Dosimetry Evaluation", WCAP-13362, May 1992.

[3-24] Lippincott, E.P., et.al., "Evaluation of Surveillance Capsule and Reactor Cavity Dosimetry from H. B. Robinson Unit 2, Cycle 9", WCAP-11104, NUREG/CR-4576, February 1987.

[3-25] Haghighat, A. and Veerasingam, "Comparison of the Different Cross Section Libraries used for Reactor Pressure Vessel Fluence Calculations", Trans. Amer. Nuclear Society, 64, p. 357, 1991.

[3-26] Fero, A.H., "Neutron and Gamma Ray Flux Calculations for the Venus PWR Engineering Mockup," NUREG/CR-4827 (WCAP-11173), January, 1987.

Table 3-1 Neutron Energy Group Structure – 47 Groups.

Energy Group	Upper Energy (MeV)	Energy Group	Upper Energy (MeV)
1	1.733E+01	25	2.972E-01
2	1.419E+01	26	1.832E-01
3	1.221E+01	27	1.111E-01
4	1.000E+01	28	6.738E-02
5	8.607E+00	29	4.087E-02
6	7.408E+00	30	3.183E-02
7	6.065E+00	31	2.606E-02
8	4.966E+00	32	2.418E-02
9	3.679E+00	33	2.188E-02
10	3.012E+00	34	1.503E-02
11	2.725E+00	35	7.102E-03
12	2.466E+00	36	3.355E-03
13	2.365E+00	37	1.585E-03
14	2.346E+00	38	4.540E-04
15	2.231E+00	39	2.145E-04
16	1.920E+00	40	1.013E-04
17	1.653E+00	41	3.727E-05
18	1.353E+00	42	1.068E-05
19	1.003E+00	43	5.044E-06
20	8.208E-01	44	1.855E-06
21	7.427E-01	45	8.764E-07
22	6.081E-01	46	4.140E-07
23	4.979E-01	47	1.000E-07
24	3.688E-01		1.000E-11

Table 3-2 Nine Mile Point Unit 2 Radial Dimensions.

Component	Dimension (in)	Dimension (cm)	Reference
Fuel Bundle Size	6.000	15.240	DB-0003.04
Core edge at 0 degrees	89.759	227.988	15 times fuel bundle size minus outside water gap of 0.241 inches (DB-0003.04)
Shroud IR	101.56	257.962	105E1347A
Shroud OR	103.56	263.042	105E1347A
Vessel Clad IR	126.5	321.310	VPF#3516-213-2 and VPF#3516-214-4
Vessel Base Metal IR	126.6875	321.786	
Vessel OR	133.l25	338.138	
Bio Shield Iron IR	168.75	428.625	USAR Section 3.8.3.1.3
Bio Shield Concrete IR	170.25	432.435	
Capsule IR	125.60	319.024	105D5036, 105D5017, 112D1065 and VPF3516-304-3
Capsule OR	126.14	320.396	

Table 3-3 Fuel Region Void Fractions at Midplane for Each R-θ Calculation.

Case	Void Fraction by Region							
	1	2	3	4	5	6	7	8
Cycle 1	0.363	0.521	0.239	0.333	0.074	0.362	0.425	0.530
Cycle 2	0.183	0.150	0.010	0.072	0.014	0.145	0.119	0.417
Cycle 3	0.368	0.432	0.275	0.258	0.083	0.317	0.171	0.486
Cycle 4	0.169	0.293	0.068	0.184	0.030	0.272	0.271	0.470
Cycle 5	0.264	0.257	0.055	0.232	0.136	0.381	0.288	0.509
Cycle 6	0.310	0.341	0.080	0.203	0.057	0.283	0.266	0.530
Cycle 7 boc	0.464	0.500	0.373	0.451	0.226	0.415	0.345	0.562
Cycle 7 bmoc	0.313	0.352	0.259	0.363	0.147	0.343	0.268	0.534
Cycle 7 moc	0.320	0.368	0.199	0.300	0.086	0.283	0.216	0.500
Cycle 7 amoc	0.286	0.337	0.193	0.302	0.087	0.295	0.212	0.522
Cycle 7 neoc	0.224	0.279	0.118	0.229	0.041	0.228	0.147	0.450

Table 3-4 Surveillance Capsule Flux and dpa/s Results.

Case	Flux (E > 1 MeV) n/cm^2 /s	Flux (E > 0.1 MeV) n/cm^2 /s	dpa/s
Cycle 1	3.45E+08	5.90E+08	5.43E-13
Cycle 2	2.41E+08	4.12E+08	3.80E-13
Cycle 3	4.23E+08	7.28E+08	6.67E-13
Cycle 4	2.62E+08	4.52E+08	4.15E-13
Cycle 5	2.53E+08	4.34E+08	4.00E-13
Cycle 6	3.36E+08	5.73E+08	5.29E-13
Cycle 7 boc	4.20E+08	7.22E+08	6.62E-13
Cycle 7 bmoc	3.19E+08	5.49E+08	5.04E-13
Cycle 7 moc	3.48E+08	5.96E+08	5.49E-13
Cycle 7 amoc	2.78E+08	4.77E+08	4.39E-13
Cycle 7 neoc	3.10E+08	5.32E+08	4.89E-13
Cycle 7 average	3.28E+08	5.63E+08	5.18E-13
Average (all cycles)	3.13E+08	5.36E+08	4.93E-13
fractional std. dev.	0.192	0.193	0.191

Note: For comparison purposes, all the values in the above table are normalized to a full power of 3467 MWth. Cycles 1 through 4 actually operated at 3323 MWth.

Table 3-5 Surveillance Capsule Fluence and dpa Results.

Cycle	Effective Full-Power Seconds	Fluence (E > 1 MeV) n/cm^2	Fluence (E > 0.1 MeV) n/cm^2	dpa
1	4.41E+07	1.46E+16	2.49E+16	2.29E-05
2	2.69E+07	6.20E+15	1.06E+16	9.78E-06
3	3.64E+07	1.48E+16	2.54E+16	2.33E-05
4	3.87E+07	9.73E+15	1.68E+16	1.54E-05
5	3.95E+07	1.00E+16	1.72E+16	1.58E-05
6	4.24E+07	1.42E+16	2.43E+16	2.24E-05
7	4.69E+07	1.54E+16	2.64E+16	2.43E-05
Total	5.86E+08	8.49E+16	1.46E+17	1.34E-04

Note: The effective full-power seconds are calculated using a full power of 3323 MWth for cycles 1 to 4 and 3467 MWth for cycles 5 to 7. The flux values in Table 3-4 were adjusted down by 3323/3467 before multiplying by the efps in this table to get the correct fluence.

Table 3-6 Nuclear Parameters Used in the Evaluation of Neutron Sensors.

Monitor Material	Reaction of Interest	Isotopic Fraction	Approximate Response Threshold	Product Half-Life
Copper	$Cu^{63}(n,\alpha)Co^{60}$	0.6917	5 MeV	1925.5 days
Iron	$Fe^{54}(n,p)Mn^{54}$	0.05845	2 MeV	312.3 days

Table 3-7 Tabulation of Dosimetry Results.

Dosimeter	Measured Activity (dps/mg)	Calculated Activity (dps/mg) [a]	Ratio (C/E) [a]	Ratio (C/E) [b]
Cu-1	4.97	4.50	0.91	0.92
Cu-2	4.62	4.50	0.97	0.99
Avg Cu	4.80	4.50	0.94	0.95
Fe-1	27.84	34.10	1.22	1.10
Fe-2	28.49	34.10	1.20	1.08
Avg Fe	28.16	34.10	1.21	1.09
Capsule Average			1.07	1.02
Charpy Bar	31.59[c]	34.10	1.08	N/A

Note: a. Assuming dosimetry at capsule center.
b. Assuming dosimetry at best estimate positions.
c. Corrected for iron composition.

Table 3-8 Calculated Maximum Vessel Fluence and dpa at End of Cycle 7 (8.72 EFPY) and at 22 EFPY.

Position	Fluence (E > 1 MeV) n/cm^2	Fluence (E > 0.1 MeV) n/cm^2	dpa
End of Cycle 7 (8.72 EFPY)			
Clad IR	1.98E+17	3.60E+17	3.09E-04
Vessel IR	1.95E+17	3.67E+17	3.04E-04
Vessel 1/4 T	1.31E+17	3.24E+17	2.12E-04
Vessel 3/4 T	4.34E+16	1.72E+17	8.34E-05
After 22 EFPY[a]			
Clad IR	5.71E+17	1.03E+18	8.90E-04
Vessel IR	5.62E+17	1.06E+18	8.74E-04
Vessel 1/4 T	3.76E+17	9.29E+17	6.08E-04
Vessel 3/4 T	1.25E+17	4.86E+17	2.37E-04

Note: a. The values at 22 EFPY were calculated at the maximum flux point in the vessel. The extrapolated data was obtained using time averaged cycle 7 values. Cycle 7 average values of flux (E > 1 MeV), flux (E > 0.1 MeV), and dpa/s at the vessel IR are 8.78E8 n/cm^2/s, 1.64E9 n/cm^2/s, and 1.36E-12 s^{-1}, respectively. Note that due to a slight shift in the axial position of the maximum flux point, the difference in maximum fluence values between 8.72 and 22 EFPY is not directly proportional to these maximum values but the differences are a small fraction of a percent.

Table 3-9 Maximum Vessel Fluence (E > 1 MeV) (n/cm^2) at End of Cycle 7 (8.72 EFPY) and at 22 EFPY Using Alternate Schemes for Attenuation through the Vessel.

Position	Calculated Fluence (E > 1 MeV) n/cm^2	Attenuation using Calculated dpa [a] n/cm^2	Attenuation using RG1.99(Rev 2) [b] n/cm^2
End of Cycle 7 (8.72 EFPY)			
Vessel IR	1.95E+17	1.95E+17	1.90E+17
1/4 T	1.31E+17	1.36E+17	1.29E+17
3/4 T	4.34E+16	5.35E+16	5.95E+16
After 22 EFPY			
Vessel IR	5.62E+17	5.61E+17	5.46E+17
1/4 T	3.76E+17	3.90E+17	3.71E+17
3/4 T	1.25E+17	1.52E+17	1.71E+17

Note: a. Calculated fluence at the vessel inner wetted surface (clad IR) times the ratio of dpa at the vessel interior points to the dpa at the inner wetter surface.

b. Calculated fluence at the vessel inner wetted surface (clad IR) times exp(-0.24*x) where x is the distance into the vessel in inches.

Table 3-10 Nine Mile Point Unit 2 Fluence Calculational Uncertainty.

Uncertainty Contributor	Assigned Uncertainty	Vessel IR Fluence Uncertainty % (1σ)	Capsule Fluence Uncertainty % (1σ)
Fission Spectrum and nu/kappa	10000 MWd/MTU	2.9	2.9
Heat Balance	2%	2.0	2.0
Shroud IR	0.188 inches	0.0	0.0
Shroud Thickness	0.042 inches	1.0	1.0
Vessel IR	0.125 inches	3.2	3.2
Core Void Fractions	5%	4.4	4.4
Bypass Water Density	1.4%	1.6 - 3.2	2.9
Downcomer Water Temperature	5 °F	3.9	3.9
Steel Density (total cross section)	3.5%	2.3	2.3
Core Fuel Density	3.5%	3.0	3.0
Radial Source Dist.	6.0%	6.0	6.0
Axial Source Dist.	3.7%	3.7	3.7
Methods Uncertainty	5%	5.8	5.8
Flux History	7.0%	8.0	8.0
Jet Pump Model	25% of steel	0.0 - 4.1	0.0
Capsule Location	1 inch, 1 degree	0.0	2.6
Total		15.5	15.3

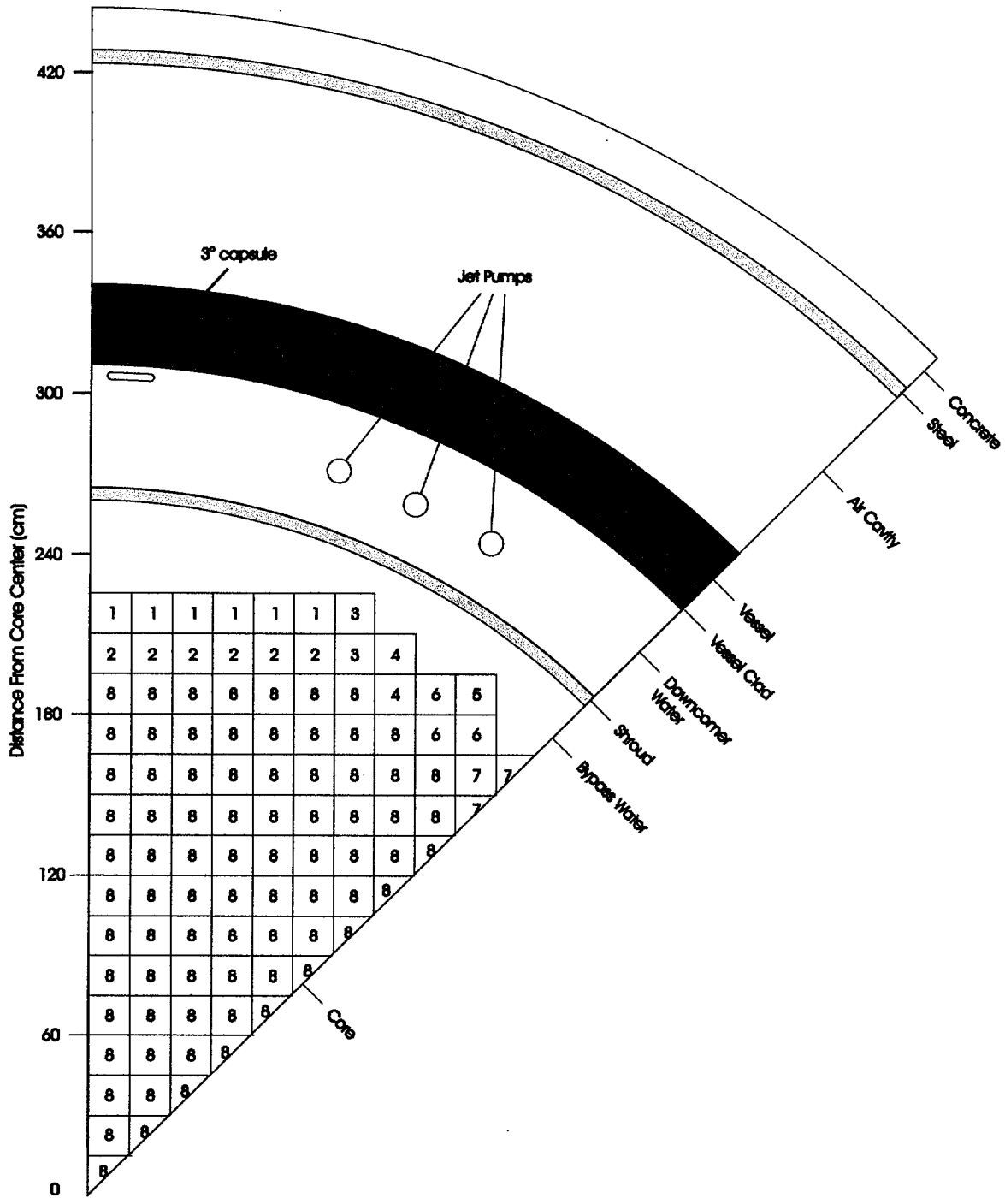

Figure 3-1 Nine Mile Point Unit 2 R-θ Geometry Used in the DORT Calculations.
(Note: jet pumps and capsule are not drawn to scale)

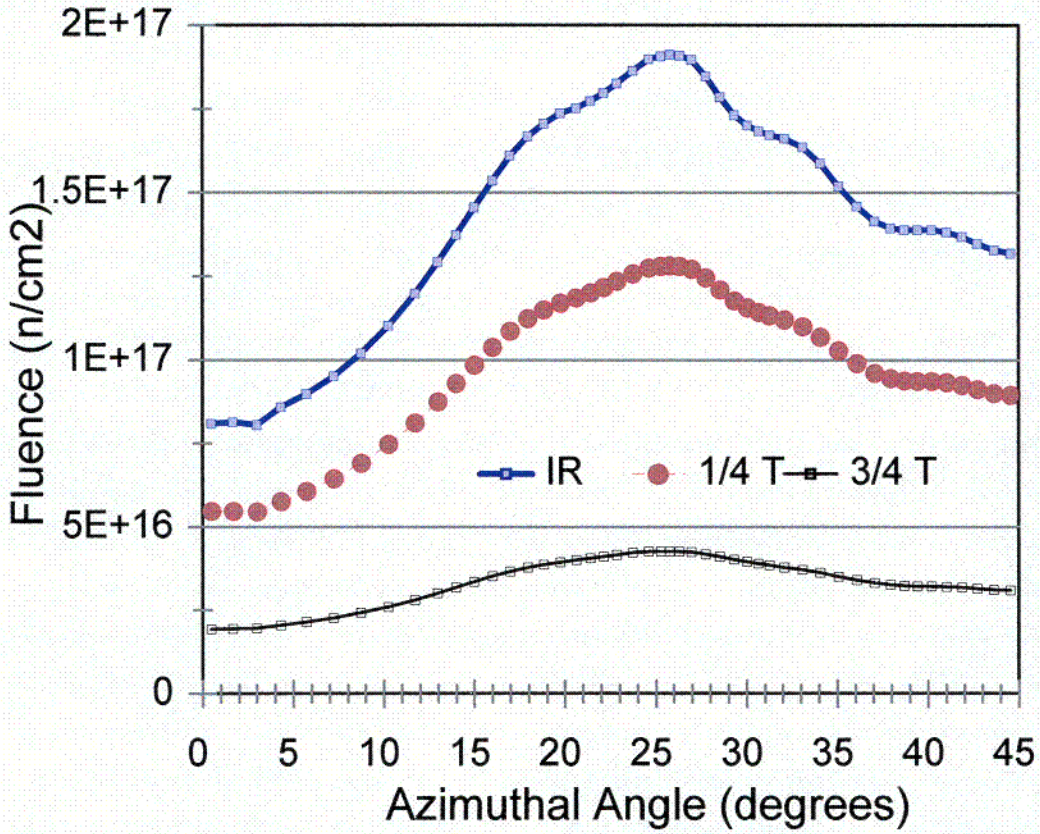

Figure 3-2 Reactor Vessel Fluence at the End of Cycle 7 at Core Midplane.

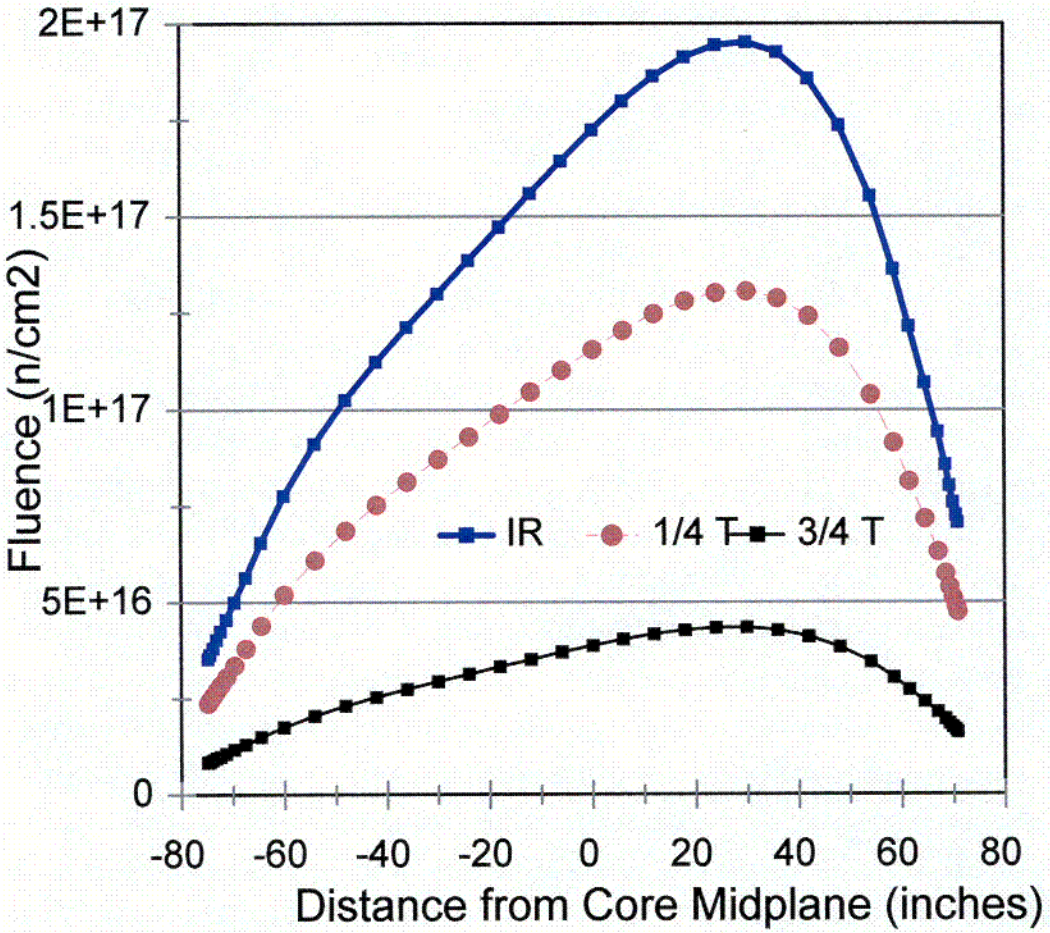

Figure 3-3 Reactor Vessel Fluence at the End of Cycle 7 at Azimuthal Maximum.

C-2

4.0 Test Specimen Chemical Analysis

NMPC has specified that chemical composition measurements be performed on selected Charpy specimens to confirm the material composition. These measurements were made using inductively coupled plasma mass spectrometry (ICP-MS).

4.1 Specimen Selection and Machining of Samples

A Charpy specimen composed of base metal and another of weld metal were used for chemical analysis after Charpy testing was completed. The samples were machined using a clean end mill to ensure that no contamination of the sample occurred. The chemical analysis samples were machined from the fracture surface ends of the Charpy specimens. A NIST-traceable sample of steel was also analyzed as a check on the analysis method.

4.2 Preparation of Samples for Analysis

The chemistry samples were placed in marked plastic vials. Table 4-1 lists the sample identifications and their corresponding descriptions. Prior to analysis via ICP-MS, the samples were cleaned by immersion in a bath of 100% ethyl alcohol to remove any surface contaminants.

4.3 ICP Measurements

The ICP-MS system used in this work was manufactured by Perkin-Elmer and is designated as the Sciex ELAN 6000 system. It was calibrated using traceable ICP standard solutions. The specimens taken for analysis were dissolved in an acid solution in preparation for introduction to the ICP-MS system. ICP data were accumulated to show well-defined peaks for the elements of interest. Tables 4-2 and 4-3 list the elements of interest and the results obtained from the ICP-MS analysis. It should be noted that iron is assumed to be the matrix element and is not quantified.

Review of the base metal results in Table 4-2 confirms that the capsule base metal specimens were fabricated from plate C3147 as expected. Similarly, Table 4-3 shows that the weld metal specimen was fabricated from heat 5P5657 (tandem wire process).

Table 4-1 Sample Identifications and Descriptions.

Sample ID	Material Description
B (BF1-8)	Charpy Base Metal
W (WF2)	Charpy Weld Metal
STD	NIST SRM 1262A (AISI 94B17)

Table 4-2 Results of the ICP-MS Analysis for the Base Metal.

Element	Sample B	Baseline Data*
	(wt %)	(wt %)
Cu	0.095	0.11
Mn	1.305	1.28
Mo	0.560	0.56
Ni	0.646	0.63
P	0.012	0.012
Si	0.241	0.24

* plate C3147

Table 4-3 Results of the ICP-MS Analysis for the Weld Metal.

Element	Sample W	Baseline Data Single Wire*	Baseline Data Tandem Wire**
	(wt %)	(wt %)	(wt %)
Cu	0.037	0.07	0.04
Mn	1.390	1.47	1.45
Mo	0.484	0.42	0.50
Ni	0.880	0.71	0.89
P	0.011	0.015	0.016
Si	0.421	0.42	0.44

* weld heat 5P5657 single wire submerged arc process

** weld heat 5P5657 tandem wire submerged arc process

Table 4-4 Comparison of Measured and Reported Values for the Standard Sample.

Element Symbol	Sample STD	Reported
P	0.033	0.044
Cu	0.524	0.51
Mo	0.069	0.07
Ni	0.613	0.60
Mn	1.092	1.05
Si	0.423	0.40

5.0 Charpy Test Data

5.1 Charpy Test Procedure

Charpy impact tests were conducted in accordance with ASTM Standard Practice E 185-82. A drawing showing the Charpy test specimen geometry is given in Figure 5-1. The 1982 version of E185 has been reviewed and approved by NRC for surveillance capsule testing applications. This standard references ASTM E23. The tests were conducted using a Tinius Olsen Testing Machine Company, Inc. Model 84 impact test machine with a 300 ft-lb range. The MPM Model 84 is equipped with a dial gage as well as an optical encoder for accurate absorbed energy measurement. In all cases, the optical encoder measured energy was reported as the impact energy. The impact energy was corrected for windage and friction for each test performed. The velocity of the striker at impact was 17.94 ft/s. Calibration of the machine was verified as specified in E-23 and verification specimens were provided by NIST.

Impact tests were conducted using an instrumented striker system fabricated by MPM. A standard is currently being developed by ASTM for instrumented testing but is not yet available for use in testing. The guidance provided in the draft standard was followed in the testing, however, the instrumented data provided should not be considered as nuclear quality assurance data at the present time. Figure 5-2 illustrates the raw data recorded by the instrumented system software. The voltage-time signal is converted to a force time signal through calibration of the striker as shown in Figure 5-3. The force-time curve is integrated to produce the velocity-time curve, which in turn is integrated to yield the striker displacement-time curve. Figure 5-4 shows a typical force-displacement curve along with the critical load points. This curve is the key result from instrumented testing. The instrumented data, as shown in Figure 5-4, can be used in materials embrittlement research and for development of fracture toughness correlations.

The E23 procedures for specimen temperature control using an in-situ heating and cooling system was followed. The advantage of using in-situ heating/cooling is that each specimen is thermally conditioned right up to the instant of impact. Thermal losses, such as those associated with liquid bath system, are completely eliminated. Each specimen was held at the desired test temperature for at least 10 minutes prior to testing and the fracture process zone temperature was held to within ± 1 C up to the instant of strike. Precision calibrated tongs were used for specimen transfer.

Lateral expansion was determined from measurements made with a lateral expansion gage. The lateral expansion gage was calibrated using precision gage blocks which are traceable to NIST. The percentage of shear fracture area was determined by integrating the ductile and brittle fracture areas using the MPM image analysis system. The percent shear fracture area determined by integration was checked using the E23 comparison method.

The number of Charpy specimens for measurement of the transition region and upper shelf was limited. Therefore, the choice of test temperatures was very important. Prior to

testing, the Charpy energy-temperature curve was predicted using embrittlement models and previous data. The first test was then conducted near the middle of the transition region and test temperature decisions were then made based on the test results. Overall, the goal was to perform four tests on the upper shelf and to use the remaining eight specimens to characterize the 30 ft-lb index. This approach was successful as illustrated in the next chapter.

5.2 Charpy Test Data

Twelve irradiated base metal, weld, and HAZ specimens were tested over the transition region temperature range and on the upper shelf. The data are summarized in Tables 5-1 through 5-3. The C3147-2 base metal surveillance specimens have a T-L orientation. In addition to the energy absorbed by the specimen during impact, the measured lateral expansion values and the percentage shear fracture area for each test specimen are listed in the tables. The Charpy energy was read from the Tinius Olsen optical encoder and has been corrected for windage and friction in accordance with ASTM E23. The impact energy is the energy required to initiate and propagate a crack. The optical encoder and the dial cannot correct for tossing energy and therefore this small amount of additional energy, if present, may be included in the data for some tests. The instrumented striker data is provided in Appendix A. As discussed earlier, these data were not obtained under the quality assurance program because there is not yet an ASTM test procedure available. However, since research is currently being conducted to extract fracture toughness from instrumented Charpy data, it was considered prudent to perform the tests with an instrumented test system. The instrumented integrated energy is typically different from the dial measured energy because a windage/friction correction is not needed for the instrumented striker and the tossing energy can be quantified and removed from the energy. Other causes for differences between the dial and instrumented striker energies are discussed in Reference [5-1]. Since the dial/optical encoder is the method used to establish the US embrittlement database, the instrumented striker data has been normalized to agree with the encoder energy.

The lateral expansion is a measure of the transverse plastic deformation produced by the striking edge of the striker during the impact event. Lateral expansion is determined by measuring the maximum change of specimen thickness along the sides of the specimen. Lateral expansion is a measure of the ductility of the specimen. The nuclear industry tracks the embrittlement shift using the 35 mil lateral expansion index.

The percentage of shear fracture area is a direct quantification of the transition in the fracture modes as the temperature increases. All metals with a body centered cubic lattice structure, such as ferritic pressure vessel materials, undergo a transition in fracture modes. At low test temperatures, a crack propagates in a brittle manner and cleaves across the grains. As the temperature increases, the percentage of shear (or ductile) fracture increases. This temperature range is referred to as the transition region and the fracture process is mixed mode. As the temperature increases further, the fracture process is eventually completely ductile (ie., no brittle component) and this temperature range is referred to as the upper shelf region.

Preparation of pressure-temperature (P-T) operating curves requires the determination of the Charpy 30 ft-lb transition temperature shift. This index is determined by fitting the energy-temperature data to find the mean curve. It is also necessary to estimate the upper shelf energy to ensure that the shelf has not dropped below the 10CFR50, Append G, 50 ft-lb screening criterion. The Charpy data analysis results are provided in the next section of this report. 10CFR50, Appendix H requires that the unirradiated data be included in the surveillance report. Therefore, the base and weld unirradiated data are given in Tables 5-4 through 5-6. The NMP-2 FSAR Appendix 5A is the source of the unirradiated Charpy impact energy, fracture appearance, and lateral expansion data for the beltline materials. Unirradiated HAZ data was not developed for this plant.

5.3 Chapter 5 Reference

[5-1] Manahan, M. P., Sr., and Stonesifer, R. B., "The Difference Between Total Absorbed Energy Measured Using An Instrumented Striker and That Obtained Using and Optical Encoder", Pendulum Impact Testing: A Century of Progress, ASTM STP 1380, T. A. Siewert and M. P. Manahan, Sr., Eds., American Society for Testing and Materials, West Conshohocken, PA, 1999.

Table 5-1 Charpy V-Notch T-L Impact Test Results for Irradiated C3147-2 Base Metal Specimens from the Nine Mile Point Unit 2 3-Degree Surveillance Capsule.

Specimen Identification	Test Temperature (°F)	Impact Energy (ft-lb)	Fracture Appearance (% Shear Area)	Lateral Expansion (mils)
BF1-8	-90.4	7.9	5.3	5.5
BF1-2	-90.4	4.6	2.0	2.5
BF1-5	-36.4	9.8	10.3	a
BF1	-31.0	23.1	17.2	18.8
BF1-4	17.6	37.2	30.3	29.0
BF1-6	19.4	33.2	34.9	27.5
BF1-10	66.2	53.3	52.0	43.0
BF1-12	66.2	60.7	53.0	a
BF1-7	145.4	107.1	100.0	a
BF1-11	145.4	97.0	100.0	67.5
BF1-3	251.6	97.9	100.0	67.5
BF1-9	260.6	95.2	100.0	69.0

a In accordance with ASTM E23, these values are not reported due to limitations on the partial break.

Table 5-2 Charpy V-Notch Impact Test Results for Irradiated Weld Metal Specimens (heat 5P5657) from the Nine Mile Point Unit 2 3-Degree Surveillance Capsule.

Specimen Identification	Test Temperature (°F)	Impact Energy (ft-lb)	Fracture Appearance (% Shear Area)	Lateral Expansion (mils)
WF2	-128.2	5.1	7.3	2.0
WF2-9	-115.6	5.7	19.9	4.0
WF2-12	-54.4	27.0	30.0	23.0
WF2-10	-50.8	26.8	29.3	25.0
WF2-2	-0.4	49.0	52.8	40.0
WF2-6	3.2	37.5	37.9	33.5
WF2-4	64.4	70.5	84.5	53.8
WF2-5	66.2	73.6	79.9	50.6
WF2-3	145.4	96.4	100.0	75.0
WF2-7	147.2	95.5	100.0	72.5
WF2-11	249.8	102.4	100.0	72.8
WF2-8	251.6	100.4	100.0	70.3

Table 5-3 Charpy V-Notch Impact Test Results for Irradiated HAZ Metal Specimens from the Nine Mile Point Unit 2 3-Degree Surveillance Capsule.

Specimen Identification	Test Temperature (°F)	Impact Energy (ft-lb)	Fracture Appearance (% Shear Area)	Lateral Expansion (mils)
HF3-11	-99.4	16.3	12.3	10.5
HF3-10	-92.2	9.9	14.0	6.0
HF3-6	-56.2	18.5	21.3	12.5
HF3	-54.4	39.8	24.2	30.5
HF3-5	-29.2	47.3	55.8	a
HF3-7	-29.2	64.7	42.6	43.0
HF3-2	-0.4	36.2	53.0	30.0
HF3-9	1.4	103.6	78.7	a
HF3-4	59.0	109.9	100.0	73.2
HF3-8	66.2	117.7	100.0	73.5
HF3-12	206.6	94.8	100.0	73.0
HF3-3	212.0	96.2	100.0	74.0

a In accordance with ASTM E23, these values are not reported due to limitations on the partial break.

Table 5-4 Charpy V-Notch T-L Impact Test Results for Unirradiated C3147-2 Base Metal Specimens from the Nine Mile Point Unit 2 Surveillance Program.

Test Temperature (°F)	Impact Energy (ft-lb)	Fracture Appearance (% Shear Area)	Lateral Expansion (mils)	Test Temperature (°F)	Impact Energy (ft-lb)	Fracture Appearance (% Shear Area)	Lateral Expansion (mils)
-150	5	1	2	40	91	70	70
-150	4	1	3	40	96	70	65
-150	6	1	2	40	96	70	68
-20	31	20	21	50	47	50	40
-20	23	20	21	50	56	50	42
-20	31	20	16	50	40	50	36
0	34	30	31	50	54	50	48
0	35	30	33	50	56	50	40
0	32	30	32	50	50	50	45
30	51	60	48	60	52	60	48
30	56	60	51	60	50	60	44
30	51	60	48	60	50	60	44
30	70	90	65	100	78	90	64
30	80	90	74	100	78	90	71
30	90	90	80	100	80	90	66
40	50	40	36	212	93	99	85
40	51	40	38	212	86	99	79
40	41	40	41	212	86	99	81

Table 5-5 Charpy V-Notch Impact Test Results for Unirradiated Single Wire Weld Metal Specimens (heat 5P5657) from the Nine Mile Point Unit 2 Surveillance Program.

Test Temperature (°F)	Impact Energy (ft-lb)	Fracture Appearance (% Shear Area)	Lateral Expansion (mils)
-80	39	5	27
-80	39	5	37
-80	29	5	32
-60	19	10	18
-60	20	10	22
-60	32	10	28
0	51	30	50
0	55	30	50
0	68	55	63
10	69	50	61
10	69	50	65
10	66	40	59
10	62	60	60
10	57	40	63
40	77	70	73
40	76	80	72
212	88	100	86
212	91	100	75
212	85	100	83

Table 5-6 Charpy V-Notch Impact Test Results for Unirradiated Tandem Wire Weld Metal Specimens (heat 5P5657) from the Nine Mile Point Unit 2 Surveillance Program.

Test Temperature (°F)	Impact Energy (ft-lb)	Fracture Appearance (% Shear Area)	Lateral Expansion (mils)
-80	14	5	15
-80	23	5	22
-80	20	5	19
-20	42	20	41
-20	45	15	43
-20	47	20	44
-10	48	15	44
-10	46	20	42
-10	39	20	40
0	51	20	50
0	57	30	54
0	55	20	40
10	58	55	58
10	61	40	54
10	65	55	59
10	55	45	50
10	63	75	60
40	69	75	64
40	76	80	74
212	88	100	75
212	88	100	84
212	91	100	74

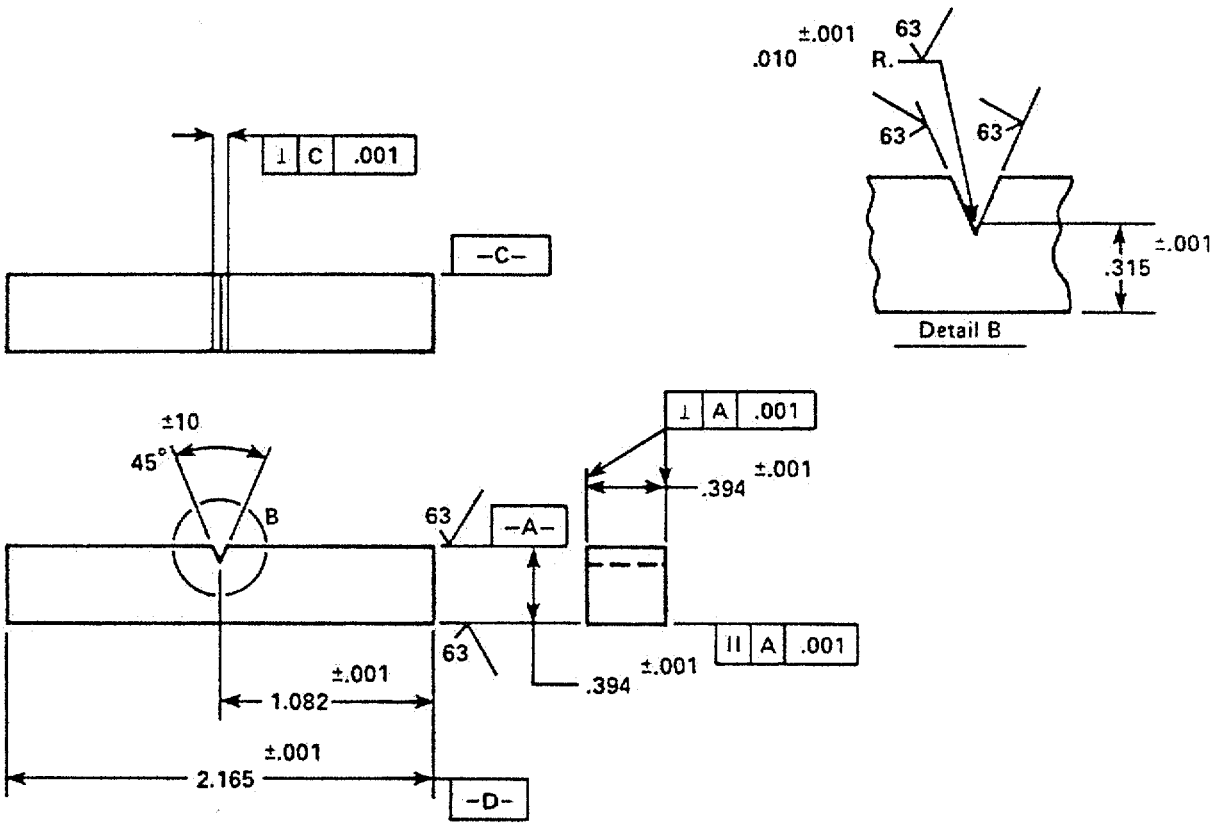

Figure 5-1 Drawing Showing Charpy Test Specimen Geometry.

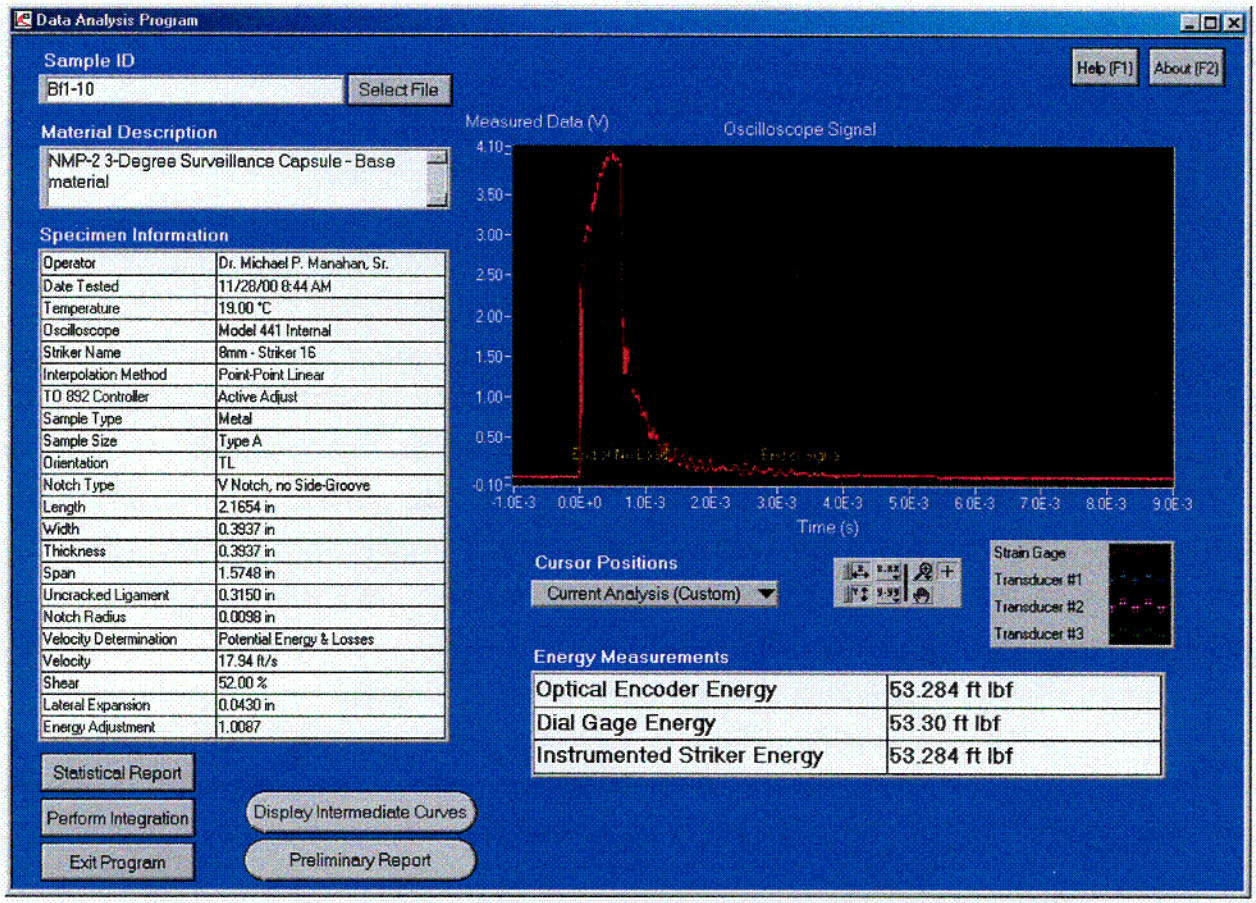

Figure 5-2 Typical Instrumented Striker Raw Data Signal.

C-3

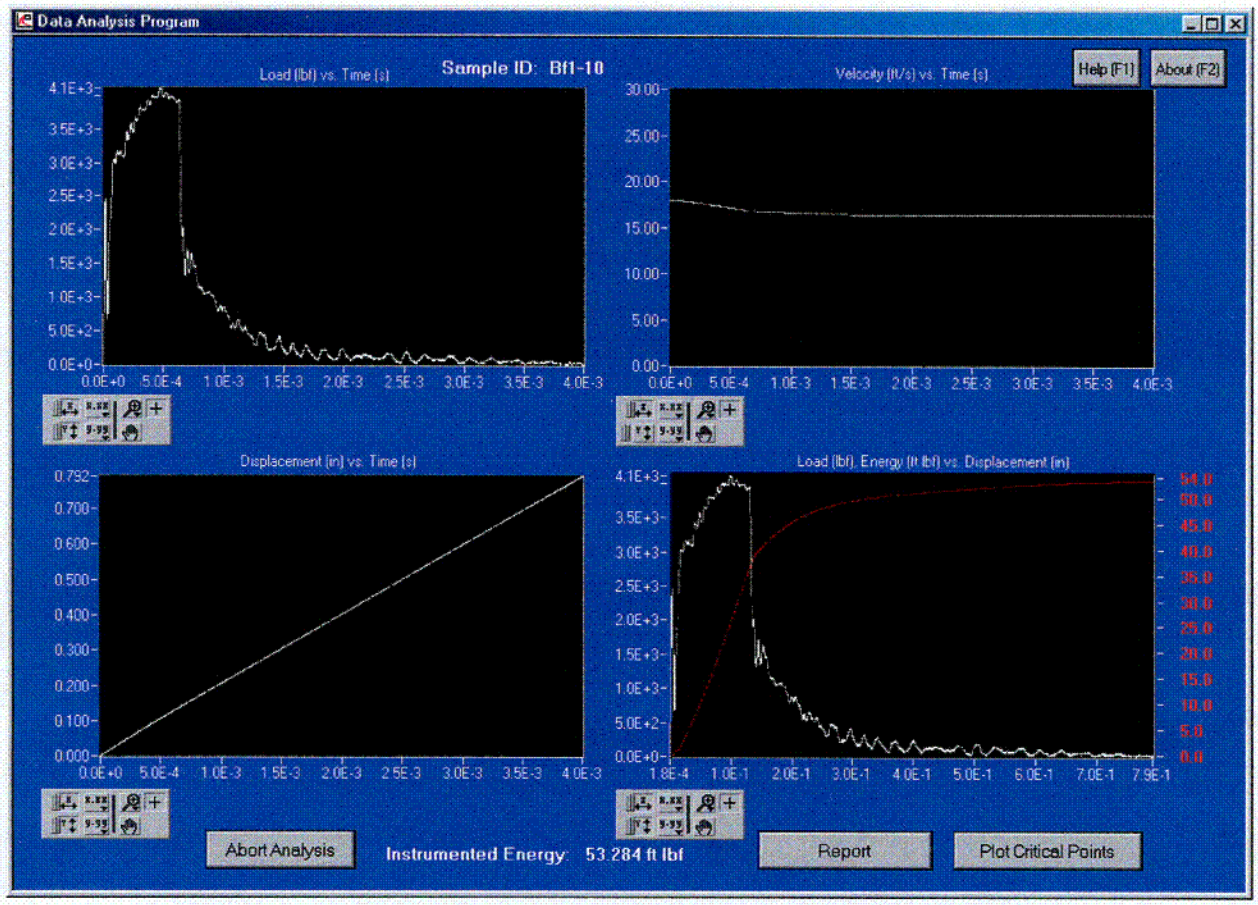

Figure 5-3 Example Plots Showing Integrations Performed to Obtain Load-Deflection Curve.

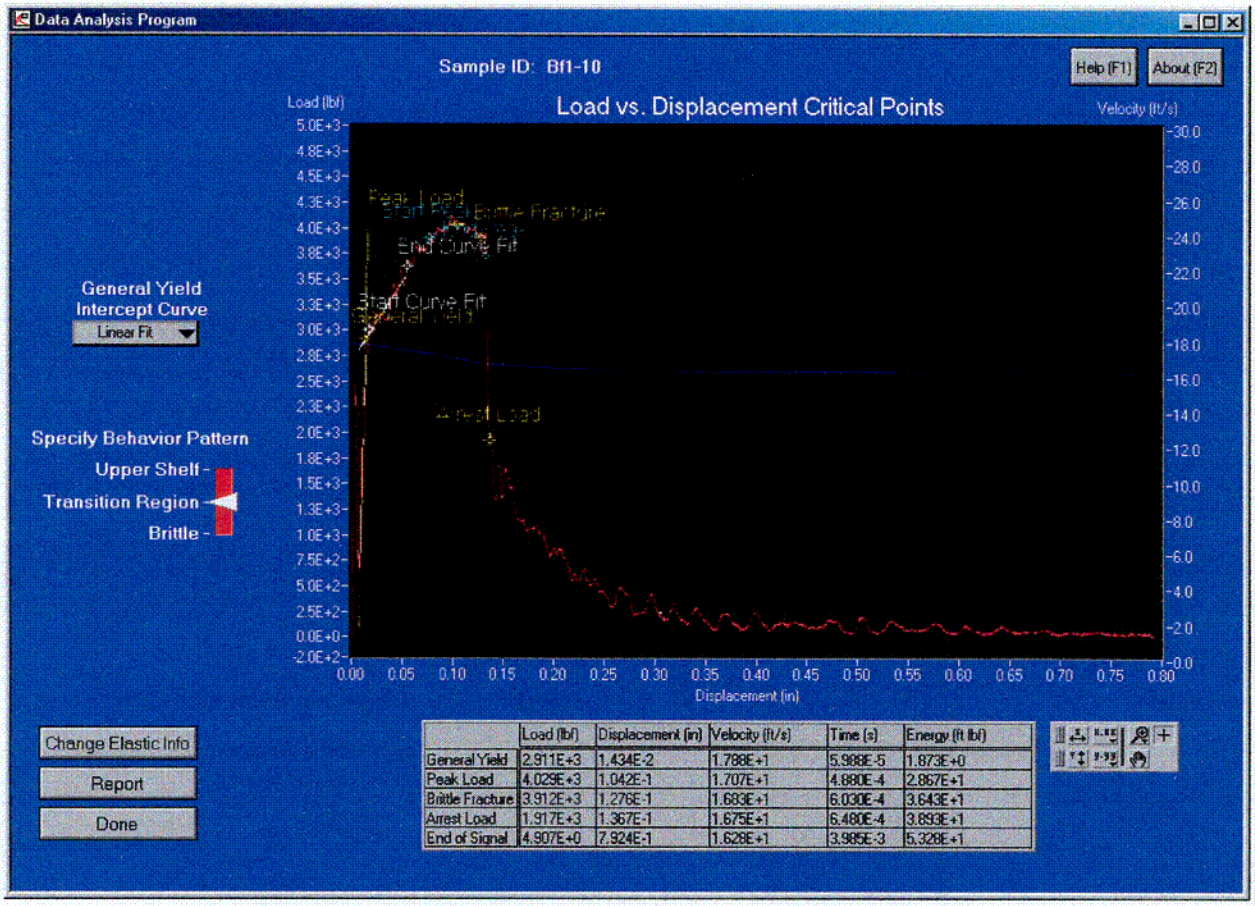

	Load (lbf)	Displacement (in)	Velocity (ft/s)	Time (s)	Energy (ft lbf)
General Yield	2.911E+3	1.434E-2	1.788E+1	5.988E-5	1.873E+0
Peak Load	4.029E+3	1.042E-1	1.707E+1	4.880E-4	2.867E+1
Brittle Fracture	3.912E+3	1.276E-1	1.683E+1	6.030E-4	3.643E+1
Arrest Load	1.917E+3	1.367E-1	1.675E+1	6.480E-4	3.893E+1
End of Signal	4.907E+0	7.924E-1	1.628E+1	3.985E-3	5.328E+1

Figure 5-4 Typical Load-Deflection Curve Showing Critical Load Points.

6.0 Charpy Curve Fitting

Charpy curve fitting for pressure vessel surveillance applications is a challenging task because, for most capsules, there are relatively few data points. In the current 3-Degree Capsule analysis, there are twelve data points available to characterize the entire transition region and upper shelf. MPM has addressed this challenge by developing an advanced Charpy curve fitting software package (Reference [6-1]). The Charpy Fit 1.0 software has been QA validated and verified.

The curve fitting results are given in terms of plots of Charpy energy, lateral expansion, and fracture appearance (percent shear) as functions of temperature. These plots show the data points as well as the best fit trends. Data from prior testing of unirradiated specimens have also been fit and plotted to characterize the radiation damage trends.

Four definitions of transition temperature are applied to the fitted data and the results are summarized in tabular form. The four transition temperature definitions, referred to as the Charpy indices, are:

- 30 ft-lb Charpy energy
- 50 ft-lb Charpy energy
- 35 mil lateral expansion
- fracture appearance (50% shear)

Upper shelf Charpy energy and upper shelf lateral expansion are also tabulated.

6.1 Fitting Procedure

The Charpy Fit software allows data to be fit as a function of temperature using either of two functions. One function is the hyperbolic tangent function. The other is a second order polynomial. For each function, the user has the option of fitting a median trend for the data or fitting both a median trend and a statistical distribution trend. The statistical distribution is a three parameter Weibull type distribution for both functions. If a Weibull statistical fit is specified, then the variance from the Weibull fit is used as a weight function in the least squares fitting of the median trend. If a "median only" fit is specified, the least squares weighting of the data points assumes that the variance is proportional to the magnitude of the median at that temperature. This default weighting for a "median only" fit can be circumvented by doing a "median and Weibull" fit while fully (or partially) specifying the Weibull distribution parameters. The accuracy of the fitting algorithm was verified for each of the two fitting functions. Also, each fitting function was verified in both the "median only" and the "median and Weibull" modes.

The fitting done in the current calculation used only the hyperbolic tangent function. The "median and Weibull" mode was used in all cases with two (b_1, and b_3) out of the three Weibull parameters preselected and the remaining Weibull parameter (b_2) determined by the fitting of each subject data set. The first preselected Weibull parameter, denoted b_1, sets the lower bound of the fitted data in the lower shelf regime and this was assigned a value of zero in all cases. The

other preselected parameter, denoted b_3, is the temperature dependent Weibull distribution shape parameter. The parameter b_2 , which was determined by the fit algorithm for each data set, has the physical meaning of the asymptotic absolute lower bound of the quantity being fit in the upper shelf regime.

A study was undertaken to determine if the b_3 that results from the current fitting algorithm can be expected to converge to the actual b_3. In this study, random data sets were generated based on selected sets of median and Weibull parameters. The random data sets were then fit to see if the parameters resulting from the fits were equal to the parameters used to generate the random data. Ideally, as the number of generated data points increases toward infinity, the parameters from the fit should approach the parameters used to generate the data. The approach was to generate ten different random data sets with each set having 1000 data points. Each set was fit using the Charpy Fit software and then the mean and standard deviation of the resulting fit b_3 values were computed. This process was repeated for four values of b_3. The chosen values of b_3 were 2.0, 3.25, 3.7, and 5. This range was expected to bound the range of values to be found in real Charpy data. Recall that the Weibull distribution becomes nearly symmetric in the range of 3.25 to 3.75. A bias was found to exist in the fit b_3 values. When the b_3 used to generate the data was less than about 3.3, the fit b_3 was found to be larger than the actual b_3. When the actual b_3 was larger than about 3.3, the fit b_3 was smaller than the actual value. It was concluded that the Charpy Fit software algorithm tends to find best fit values of b_3 that result in a more normal (i.e., symmetrical) variation than was used to generate the data. The b_3 bias is essentially zero at a b_3 of about 3.3. The bias increases as the actual value of b_3 becomes increasing different from 3.3. The amount of bias that was found is not considered to be excessive, but is significant.

Reliably obtaining b_3 by fitting requires many data points (on the order 100). The data points must also be well distributed over the entire brittle to ductile transition region. In the current calculation, there are not enough data points per data set , typically 12, to reliably fit b_3. Therefore b_3 was set to a selected value based on a fit to Charpy energy data of a similar material (unirradiated NMP-1 plate G-8-3 and G-8-4 material [6-2]) for which a large number of data points (97) are available. Figure 6-1 shows the results of fitting the 97 unirradiated data points. Note that a significant portion of the upper shelf is included in the data being fit. The value of b_3 from the fitting procedure was in this case 2.5. It is concluded that after correcting for bias, the actual best fit b_3 would be about 2.2. For the 1000 point data sets used to generate the bias correction, the uncertainty in the 0.3 correction is about ± 0.1. The uncertainty for a 97 point set would be larger and could perhaps be as great or even greater than the 0.3 bias correction. The plot of Figure 6-2 shows the result when only the data points between -80 F and +60 F were fit. Comparing with Figure 6-1, it can be seen that the median trend is closer to the 1% probability trend in Figure 6-2. This is consistent with the fact that the transition region data of Figure 6-2 produced a smaller b_3. When most of the upper shelf data was eliminated from the fit, the b_3 that resulted from the fitting was 1.8. After correcting for bias, the best estimate of b_3 became 1.5. Based on the results of Figure 6-1 and Figure 6-2, an intermediate value of b_3 equal to 1.8 was selected for use in all fitting of this report.

6.2 3-Degree Surveillance Capsule Fitting Results

Since the reason for testing irradiated material is to determine the extent to which the irradiation has embrittled the material, it is necessary to compare the irradiated material test results to the test results of the same material in the unirradiated condition. Data for the unirradiated condition was obtained from Reference [6-3]. The data in Reference [6-3] was reviewed and verified to be in agreement with the data listed in FSAR Appendix 5A. Charpy energies, lateral expansions, and fracture appearances for the Heat C3147 slab 2 (C3147-2) base metal were included in Reference [6-3] from the Lukens Steel Company test certificate. Charpy energies, lateral expansions, and fracture appearances for single wire and tandem wire welds (Raco 1NMM heat 5P5657) were included in Reference [6-3]. No test data was available for unirradiated HAZ material. All of the available unirradiated base and weld material data was reviewed and fit as a part of the current analysis.

Figure 6-3, 6-4, and 6-5 compare unirradiated Charpy energy, lateral expansion, and fracture appearance data (respectively) for the C3147-2 base material with testing done in the TL (transverse) and LT (longitudinal) material orientations. As expected, it can be seen that the TL orientation is the more limiting material orientation. All of the 3-Degree Capsule specimens are in the TL orientation and all comparisons made between irradiated and unirradiated data in this report include only TL data.

Figure 6-6, 6-7, and 6-8 compare unirradiated Charpy energy, lateral expansion, and fracture appearance data (respectively) for the Heat 5P5657 weld metal. Some of the welds were done using a single wire method and some were made using a tandem wire method. It can be seen from these figures that there is no significant difference between the single wire and tandem wire data. Therefore, all comparisons between unirradiated and irradiated weld data in this report use the combined single and tandem wire unirradiated data.

6.2.1 Charpy Energy Data Fitting

The procedures for fitting the energy data were as follows. The Weibull b_3 parameter was set to 1.8 based on the analyses described previously. The Weibull b_1 parameter was set to zero. The b_2 parameter was left to be determined by the fit. The Weibull parameters define the statistical variation in the data as a function of temperature. The Weibull parameters affected the best fit median behavior only in terms of the weight factors that were applied to the data points in the least squares fitting algorithm. The weighting procedure used the Weibull variation to give more weight to data points at temperatures that produce less data variation (generally lower temperatures) and less weight to data points at temperatures that produce greater variation (generally higher temperatures).

Since the lower shelf temperature regime had few if any data points, the asymptotic lower shelf median trend energy parameter a_1 was set to 6 ft-lb for all fitting of energy data. The asymptotic upper shelf median trend energy parameter a_2 was calculated for each data set prior to fitting and then input to the fitting procedure. This USE value was calculated by averaging the energies of all data points considered to be representative of upper shelf behavior. The sole

basis for being included in the upper shelf energy calculation was the specimen's fracture appearance. If the fracture appearance was greater than or equal to 99% shear, the data was included in the upper shelf energy calculation.

6.2.1.1 Charpy Energy Data and Curve Fitting for C3147-2 Base Metal

The above fitting procedures were applied to the irradiated C3147-2 base metal data from the 3-Degree capsule specimens as well as the unirradiated base metal data compiled in [6-3]. There are 30 unirradiated data points and 12 irradiated data points. The data points and the resulting best fit trends are shown in Figure 6-9. Figure 6-9 shows a temperature shift of the Charpy energy transition region to higher temperatures due to the irradiation. The data also show an increase in the USE due to irradiation. The 30 and 50 ft-lb transition temperatures and the USE are summarized in Table 6-1. At the 30 ft-lb level, the temperature shift is +20.2 degrees F. At the 50 ft-lb level, the temperature shift is +5.6 degrees F. The USE increased by 11 ft-lbs. This phenomenon has been observed in other plants and may be related to low fluence improvement of the matrix material which results in more ductile ligament response during the ductile fracture process. Conservatively assuming an EOL fluence of up to $1x10^{18}$ n/cm^2, the RG 1.99(2) predicted shelf drop for plate C3147-2 is less than 15%. Therefore, the 10CFR50, Appendix G requirement to maintain a 50 ft-lb USE throughout the plant operating period is satisfied for NMP-2.

6.2.1.2 Charpy Energy Data and Curve Fitting for Weld Metal

The above fitting procedures were applied to the irradiated weld metal from the capsule specimens as well as the previous weld metal data compiled in [6-3]. There are 41 unirradiated data points and 12 irradiated data points. The data points and the resulting best fit trends are shown in Figure 6-10. The transition region shift and the USE change were found to be qualitatively similar to those found for the base metal. Figure 6-10 shows a temperature shift of the Charpy energy transition region to higher temperatures due to the irradiation and an increase in the USE due to irradiation. The 30 and 50 ft-lb transition temperatures and the USE are summarized in Table 6-2. At the 30 ft-lb level, the temperature shift is +30.3 degrees F. At the 50 ft-lb level, the temperature shift is +26.6 degrees F. The USE increased by 10.2 ft-lbs.

6.2.1.3 Charpy Energy Data and Curve Fitting for HAZ Metal

The fitting procedures were applied to the irradiated HAZ metal from the capsule specimens. No unirradiated HAZ data was available for fitting. The 30 and 50 ft-lb transition temperatures and the USE are summarized for the HAZ material in Table 6-3. The Charpy energy test data points and the resulting best fit trends are shown in Figure 6-11. The best fit trends of the irradiated base metal and weld metal from Figures 6-9 and 6-10 are included for the sake of comparison. It can be seen that the transition temperature for the HAZ material is significantly below that for the weld and base metal. The base metal mean energy trend is more conservative than the weld and HAZ trends in the transition regions of the curves (i.e., the base metal Charpy energy is lower at a given temperature). At the upper shelf, the base and weld metal have essentially identical USE and both are about 5 ft-lb below the USE of the HAZ material. Comparing Figures 6-9 through 6-11, it can be seen that the HAZ material showed

significantly more scatter than either the weld or the base metal.

6.2.2 Lateral Expansion Data Fitting

The procedures for fitting the lateral expansion data were as follows. The Weibull b_3 parameter was set to 1.8. By using this value, it was inherently assumed that the statistical behavior of lateral expansion data is the same as for the Charpy energy data. This was deemed the most reasonable assumption since a large data set of lateral expansion data, similar to that used to establish b_3 for the Charpy energy data, was not available. The Weibull b_1 parameter was set to zero. The b_2 parameter was left to be determined by the fitting algorithm. Since there were no data points on the lower shelf, an asymptotic lower shelf lateral expansion of 1 mil was assumed and input to the fitting algorithm as the a_1 hyperbolic tangent curve fit parameter. An upper shelf lateral expansion (USLE) was computed for each data set based on the average of the upper shelf data points. These USLE values were input to the fitting algorithm as the a_2 hyperbolic tangent curve fit parameter. The upper shelf data points were identified based on their fracture appearance so that the same data points used to calculate the USE were used to calculate the upper shelf lateral expansion.

6.2.2.1 Lateral Expansion Data and Curve Fitting for C3147-2 Base Metal

The above lateral expansion fitting procedures were applied to the irradiated C3147-2 base metal specimens from the 3-Degree Capsule and to the unirradiated base metal data compiled in [6-3]. The data points and the resulting best fit trends are shown in Figure 6-12. It can be seen in Figure 6-12 that lateral expansions were decreased as a result of the irradiation for both the transition region and the upper shelf region. The relatively small +9.4 degrees F temperature shift at 35 mils lateral expansion is on the order of the scatter in the data. The decrease in the USLE is 13.7 mils. The 35 mil lateral expansion and the USLE for the base metal are summarized in Table 6-4.

6.2.2.2 Lateral Expansion Data and Curve Fitting for Weld Metal

The lateral expansion fitting procedures were applied to the irradiated weld metal data from the capsule specimens and to the unirradiated weld metal data compiled in [6-3]. The data points and the resulting best fit trends are shown in Figure 6-13. It can be seen in Figure 6-13 that lateral expansions were decreased as a result of the irradiation for both the transition region and the upper shelf region. This is similar to the behavior seen for the base metal data. The temperature shift at 35 mils lateral expansion is +28.3 degrees F, and is therefore larger than the +9.4 F found for the base metal. The decrease in the USLE, at 6.8 mils, is half of the decrease found for the base metal. The 35 mil lateral expansion and the USLE for the weld metal are summarized in Table 6-5.

6.2.2.3 Lateral Expansion Data and Curve Fitting for HAZ Metal

The fitting procedures were applied to the irradiated HAZ metal from the capsule specimens. No unirradiated HAZ data was available for fitting. The 35 mil transition temperature and the USLE are summarized for the HAZ material in Table 6-6. The Charpy

specimen lateral expansion data and the resulting best fit trend are shown in Figure 6-14. The best fit trends of the irradiated base metal and weld metal from Figures 6-12 and 6-13 are included for comparison. It can be seen that the 35 mil transition temperature for the HAZ material is slightly less than that for the weld material but is significantly less than that for the base metal. The base metal mean lateral expansion curve is to the right of the weld and HAZ curves in the transition and upper shelf regions of the curves and therefore the base metal is more limiting than the HAZ and weld metals. Comparing Figures 6-12 through 6-14, it can be seen that the HAZ material showed significantly more scatter than either the weld or the base metal which is the same behavior as observed above for the Charpy energy data.

6.2.3 Fracture Appearance Data Fitting

The procedures for fitting the fracture appearance (percent shear) data were as follows. The Weibull b_3 parameter was set to 1.8. By using this value, it was inherently assumed that the statistical behavior of fracture appearance data is the same as Charpy energy data. This was deemed the most reasonable assumption since a large data set of fracture appearance data, similar to that used to establish b_3 for the Charpy energy data, was not available. The Weibull b_1 parameter was set to zero. The b_2 parameter was left to be determined by the fit. Since there were no data points on the lower shelf, an asymptotic lower shelf percent shear of 1% was assumed and input to the fitting algorithm as the a_1 hyperbolic tangent curve fit parameter. An upper shelf percent shear of 100% was input to the fitting algorithm as the a_2 hyperbolic tangent curve fit parameter.

6.2.3.1 Fracture Appearance Data and Curve Fitting for C3147-2 Base Metal

The above fracture appearance fitting procedures were applied to the irradiated C3147-2 base metal specimens from the 3-Degree Capsule as well as the unirradiated base metal data compiled in [6-3]. The data points and the resulting best fit trends are shown in Figure 6-15. It can be seen in Figure 6-15 that percent shear in the transition region was slightly decreased as a result of the irradiation. The relatively small +11.4 degrees F temperature shift at 50% shear is on the order of the scatter in the data. The 50% shear transition temperatures are summarized in Table 6-7.

6.2.3.2 Fracture Appearance Data and Curve Fitting for Weld Metal

The fracture appearance fitting procedures were applied to the irradiated weld metal specimens from the 3-Degree Capsule as well as the unirradiated weld metal data compiled in [6-3]. The data points and the resulting best fit trends are shown in Figure 6-16. It can be seen in Figure 6-16 that the irradiated data points fall within the scatter band of the unirradiated data except for the four data points in the lower transition region. These four data points have unexpectedly high percent shear. The fracture appearance data for these specimens were rechecked and found to be accurate. This elevation in percent shear at the low end of the transition region significantly affects the best fit trend throughout the transition region. Due to the higher percent shear of the irradiated data in the lower transition region, the 50% shear transition temperature from the best fit trends is -20.3 degrees F. The 50% shear transition temperatures are summarized in Table 6-8. As discussed earlier, MPM integrates areas of brittle

and ductile fracture on the fracture surface to obtain very accurate percent shear results. In most cases, older Charpy percent shear estimates were determined by the photograph comparison method of ASTM E23. This approach has an uncertainty of at least ±10% shear. It is expected that a re-analysis of the unirradiated data using the area integration method would result in the unirradiated data falling within the scatter band of the irradiated data.

6.2.3.3 Fracture Appearance Data and Curve Fitting for HAZ Metal

The fracture appearance fitting procedures were applied to the irradiated HAZ metal from the capsule specimens. No unirradiated HAZ data was available for fitting. The 50% shear transition temperature for the HAZ material is given in Table 6-9. The Charpy specimen fracture appearance data and the resulting best fit trend are shown in Figure 6-17. The best fit trends of the irradiated base and weld metals from Figures 6-15 and 6-16 are included for comparison. It can be seen that the 50% shear transition temperature for the HAZ material is slightly less than for the weld material but is significantly less than that for the base metal. The base metal mean percent shear trend is more conservative than that of the weld and HAZ metals.

6.3 Chapter 6 References

[6-1] MPM Technologies, Inc., "Charpy Fit Version 1.0 Software", February, 1998

[6-2] Manahan, M.P., "Nine Mile Point Unit 1 Surveillance Capsule Program", NMEL-90001, dated January 4, 1991

[6-3] Pepper, R., "Surveillance Test Specimen Documentation for General Electric Corporation P. O. #205-AE026, CBIN Contract #72-C102", January 2, 1980.

Table 6-1 Base Metal (heat C3147-2) Charpy Impact Properties (TL Orientation).

Fluence (E>1.0 Mev) (n/cm^2)	30 ft-lb Transition Temperature (F)	50 ft-lb Transition Temperature (F)	Upper Shelf Energy (ft-lb)
0	-9.5	41.1	88.3[1]
8.49×10^{16}	10.7	46.7	99.3[2]

[1]Based on the average of three upper shelf data points.
[2]Based on the average of four upper shelf data points.

Table 6-2 Weld Metal (heat 5P5657) Charpy Impact Properties.

Fluence (E>1.0 Mev) (n/cm^2)	30 ft-lb Transition Temperature (F)	50 ft-lb Transition Temperature (F)	Upper Shelf Energy (ft-lb)
0	-61.7	-13.5	88.5[1]
8.49×10^{16}	-31.4	13.1	98.7[2]

[1]Based on the average of six upper shelf data points.
[2]Based on the average of four upper shelf data points.

Table 6-3 HAZ Metal Charpy Impact Properties.

Fluence (E>1.0 Mev) (n/cm^2)	30 ft-lb Transition Temperature (F)	50 ft-lb Transition Temperature (F)	Upper Shelf Energy (ft-lb)
0	not available	not available	not available
8.49×10^{16}	-55.8	-30.7	104.7[1]

[1]Based on the average of four upper shelf data points.

Table 6-4 Base Metal (heat C3147-2) Charpy Lateral Expansion (TL Orientation).

Fluence (E>1.0 Mev) (n/cm^2)	35 mil Lateral Expansion Transition Temperature (F)	Upper Shelf Lateral Expansion (mils)
0	20.4	81.7[(1)]
8.49×10^{16}	29.8	68.0[(1)]

[(1)]Based on the average of three upper shelf data points.

Table 6-5 Weld Metal (heat 5P5657) Charpy Lateral Expansion Behavior.

Fluence (E>1.0 Mev) (n/cm^2)	35 mil Lateral Expansion Transition Temperature (F)	Upper Shelf Lateral Expansion (mils)
0	-45.5	79.5[(1)]
8.49×10^{16}	-17.2	72.7[(2)]

[(1)]Based on the average of six upper shelf data points.
[(2)]Based on the average of four upper shelf data points.

Table 6-6 HAZ Metal Charpy Lateral Expansion Behavior.

Fluence (E>1.0 Mev) (n/cm^2)	35 mil Lateral Expansion Transition Temperature (F)	Upper Shelf Lateral Expansion (mils)
0	not available	not available
8.49×10^{16}	-25.8	73.4[(1)]

[(1)]Based on the average of four upper shelf data points.

Table 6-7 Base Metal (heat C3147-2) Charpy Fracture Appearance (TL Orientation).

Fluence (E>1.0 Mev) (n/cm^2)	50% Shear Transition Temperature (F)
0	38.3
8.49×10^{16}	49.7

Table 6-8 Weld Metal (heat 5P5657) Charpy Fracture Appearance.

Fluence (E>1.0 Mev) (n/cm^2)	50% Shear Transition Temperature (F)
0	18.2
8.49×10^{16}	-2.1

Table 6-9 HAZ Metal Charpy Fracture Appearance.

Fluence (E>1.0 Mev) (n/cm^2)	50% Shear Transition Temperature (F)
0	not available
8.49×10^{16}	-21.8

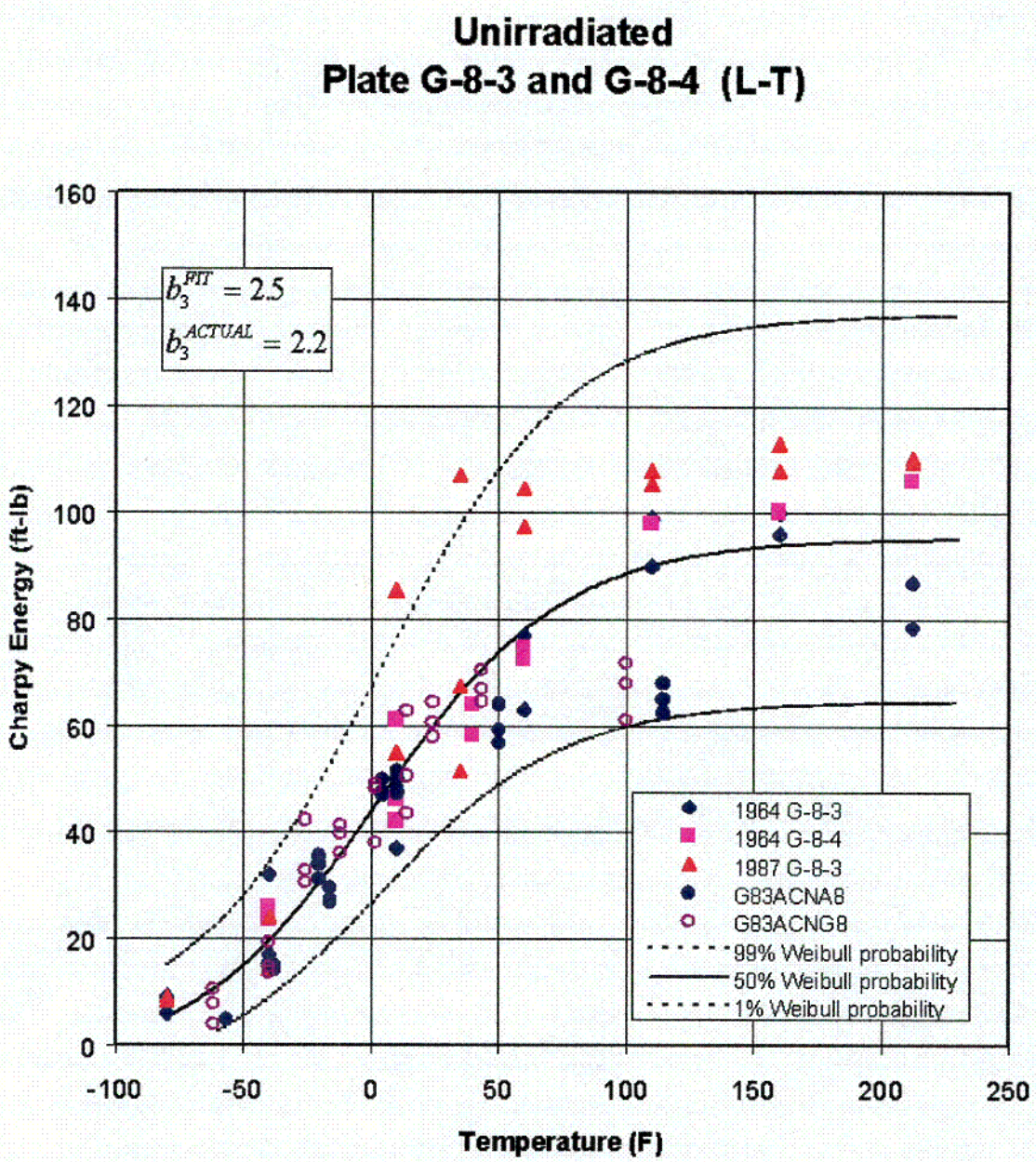

Figure 6-1 **Determination of b_3 by Fitting of a Large Data Set for Unirradiated Material that Includes Upper Shelf Data.**

C-6

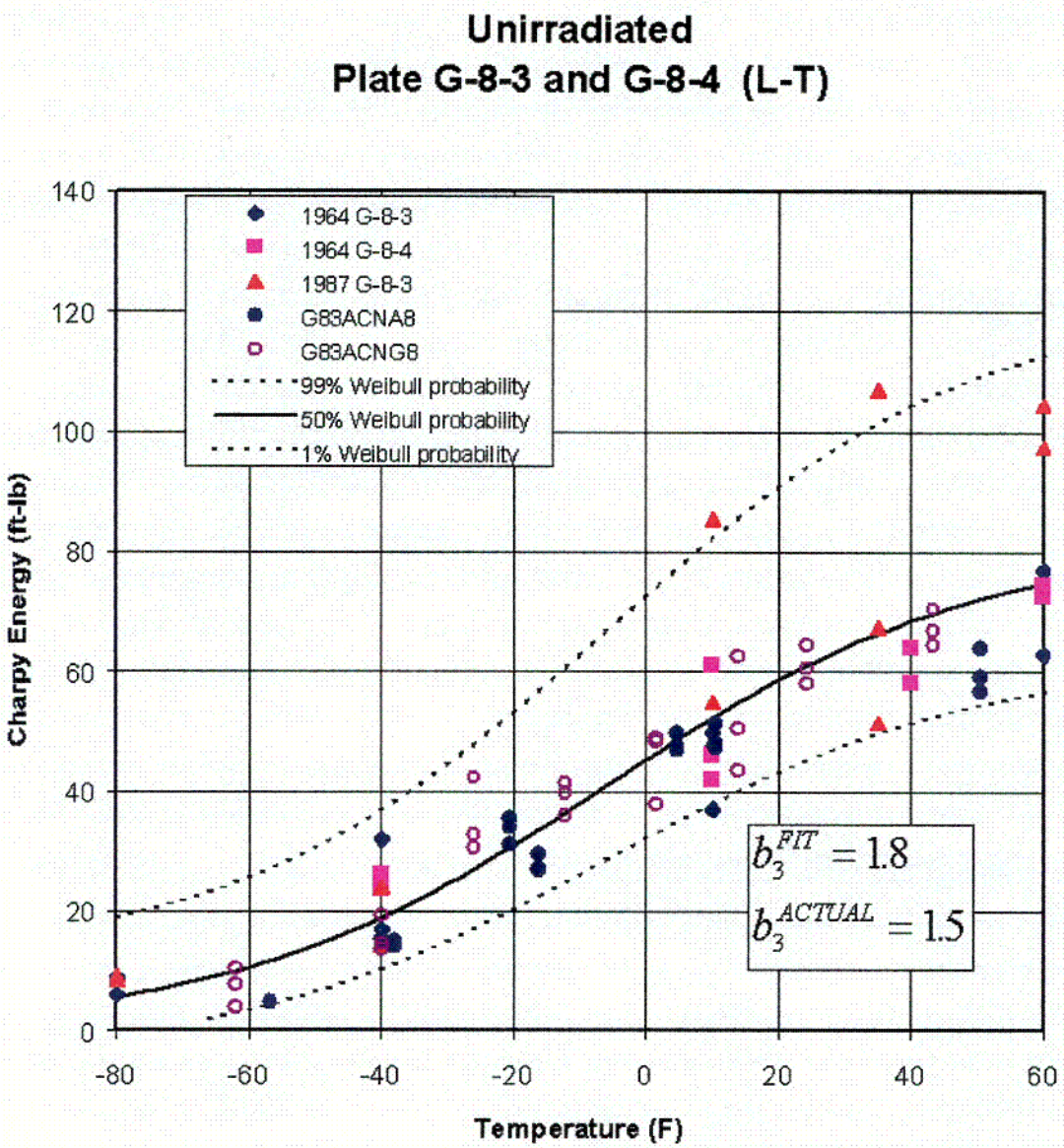

Figure 6-2 **Determination of b_3 by Fitting of a Large Data Set for Unirradiated Material that Includes Only Transition Temperature Range Data.**

C-7

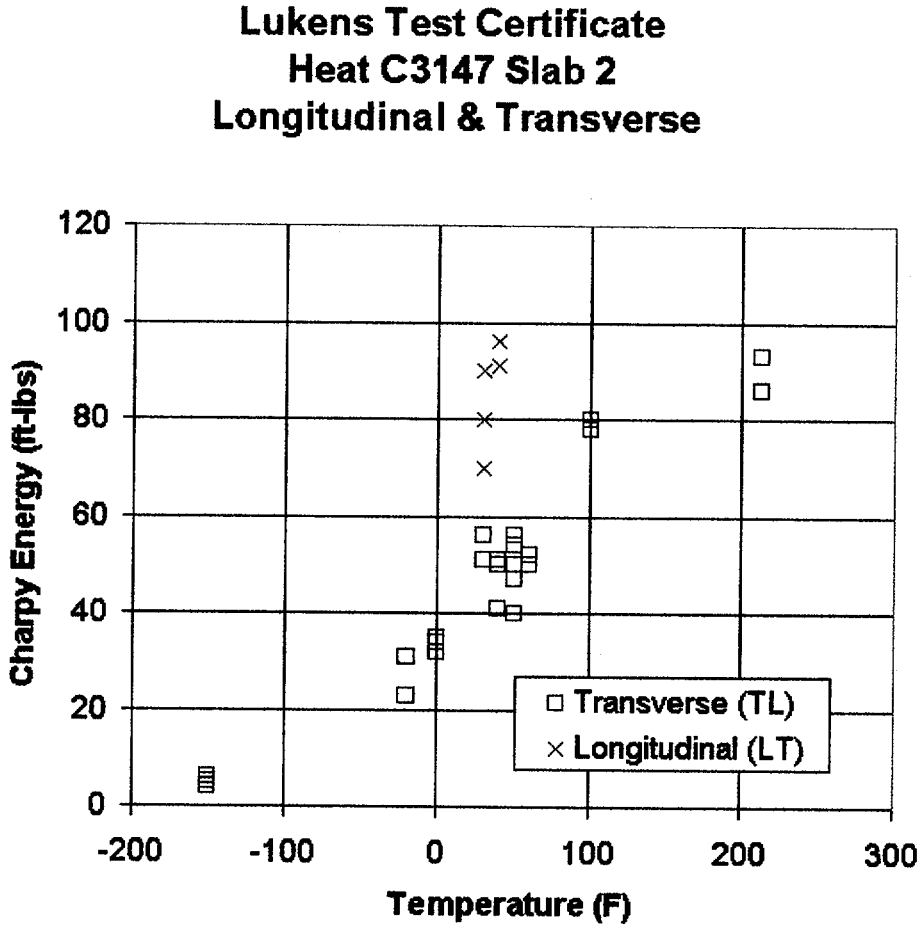

Figure 6-3 **Comparison of TL (transverse) and LT (longitudinal) Charpy Energy Data for the Unirradiated C3147-2 Base Metal.**

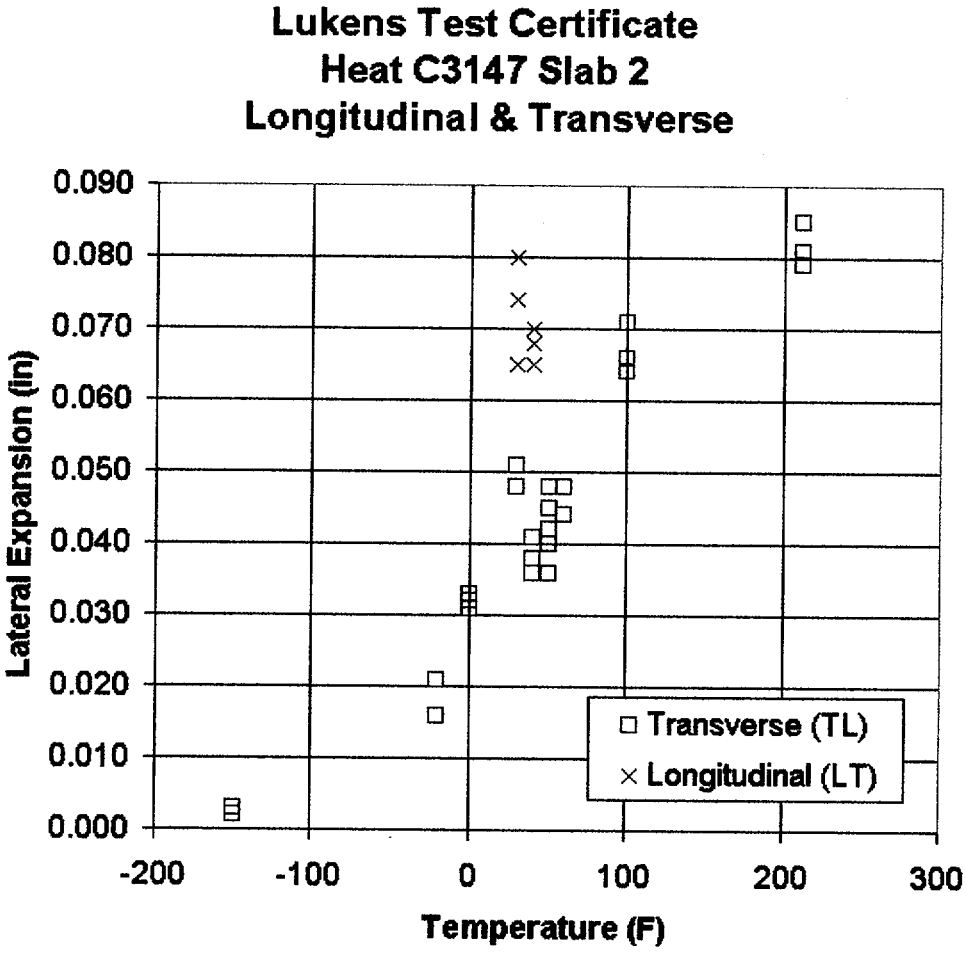

Figure 6-4 **Comparison of TL (transverse) and LT (longitudinal) Charpy Lateral Expansion Data for the Unirradiated C3147-2 Base Metal.**

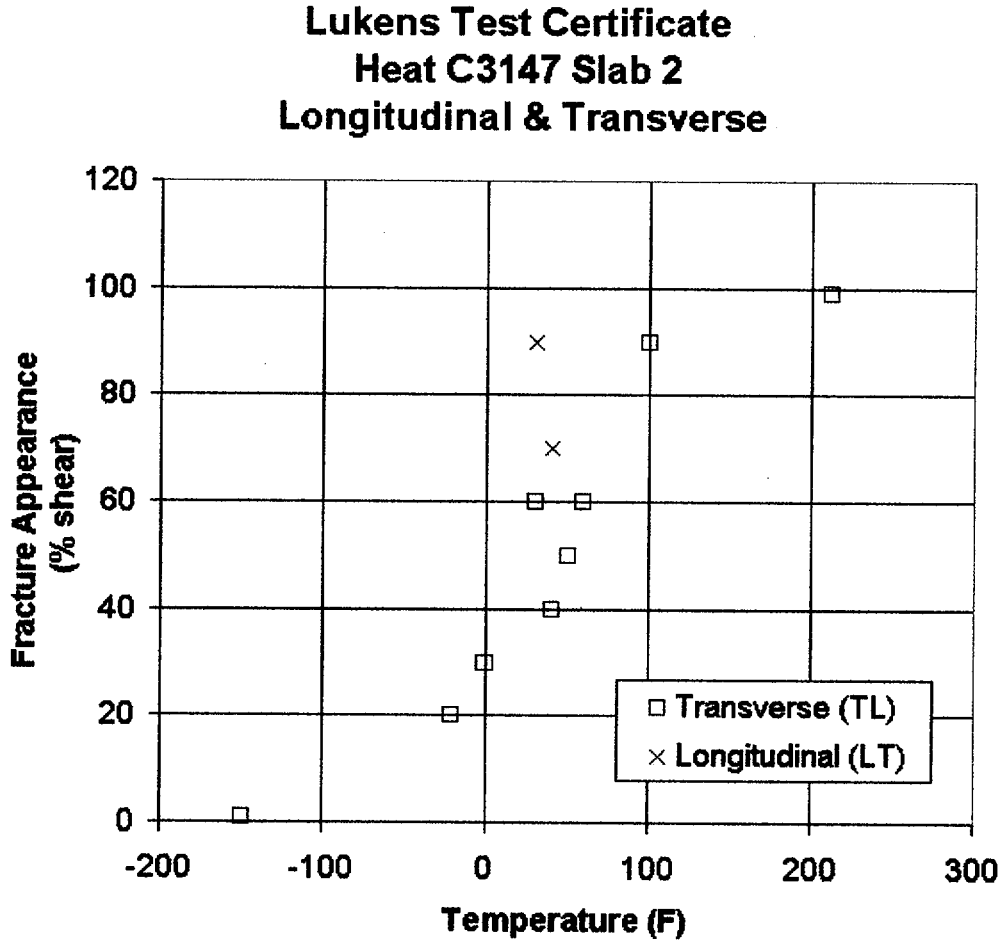

Figure 6-5 **Comparison of TL (transverse) and LT (longitudinal) Charpy Fracture Appearance Data for the Unirradiated C3147-2 Base Metal.**

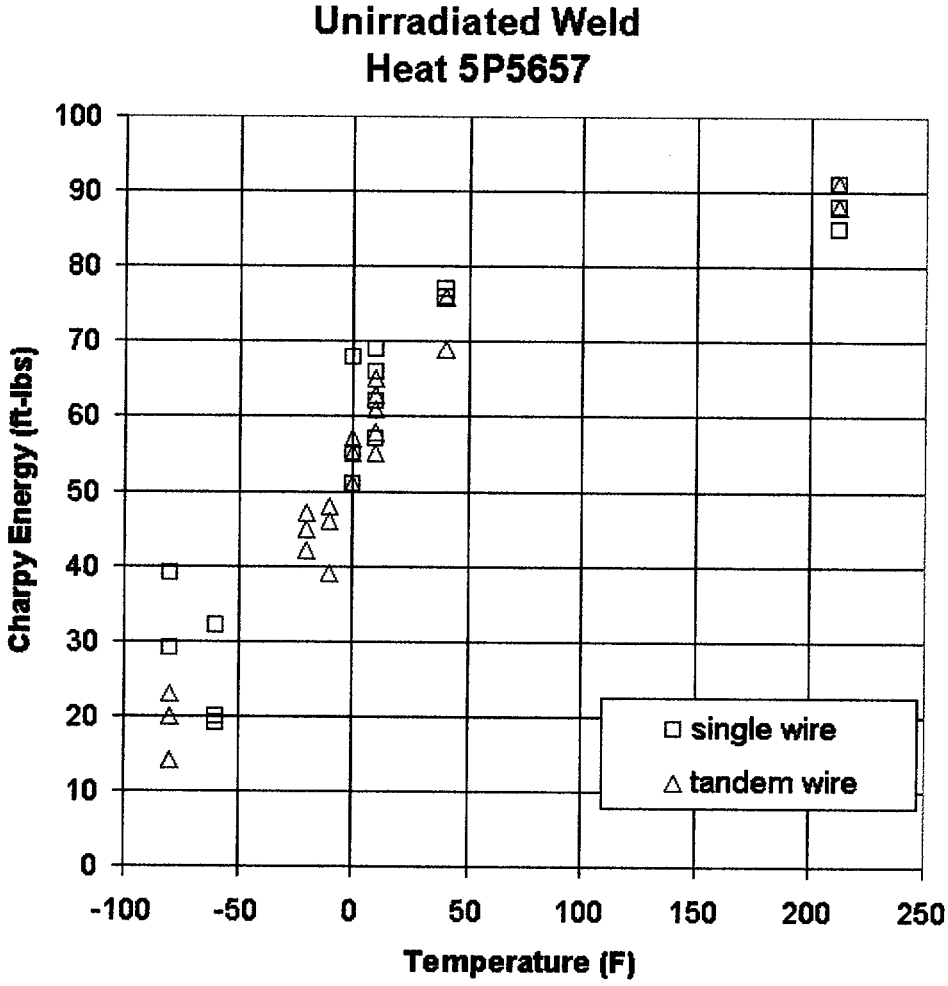

Figure 6-6 **Comparison of Single Wire and Tandem Wire Weld Charpy Energy Data for the Unirradiated Weld Metal (heat 5P5657).**

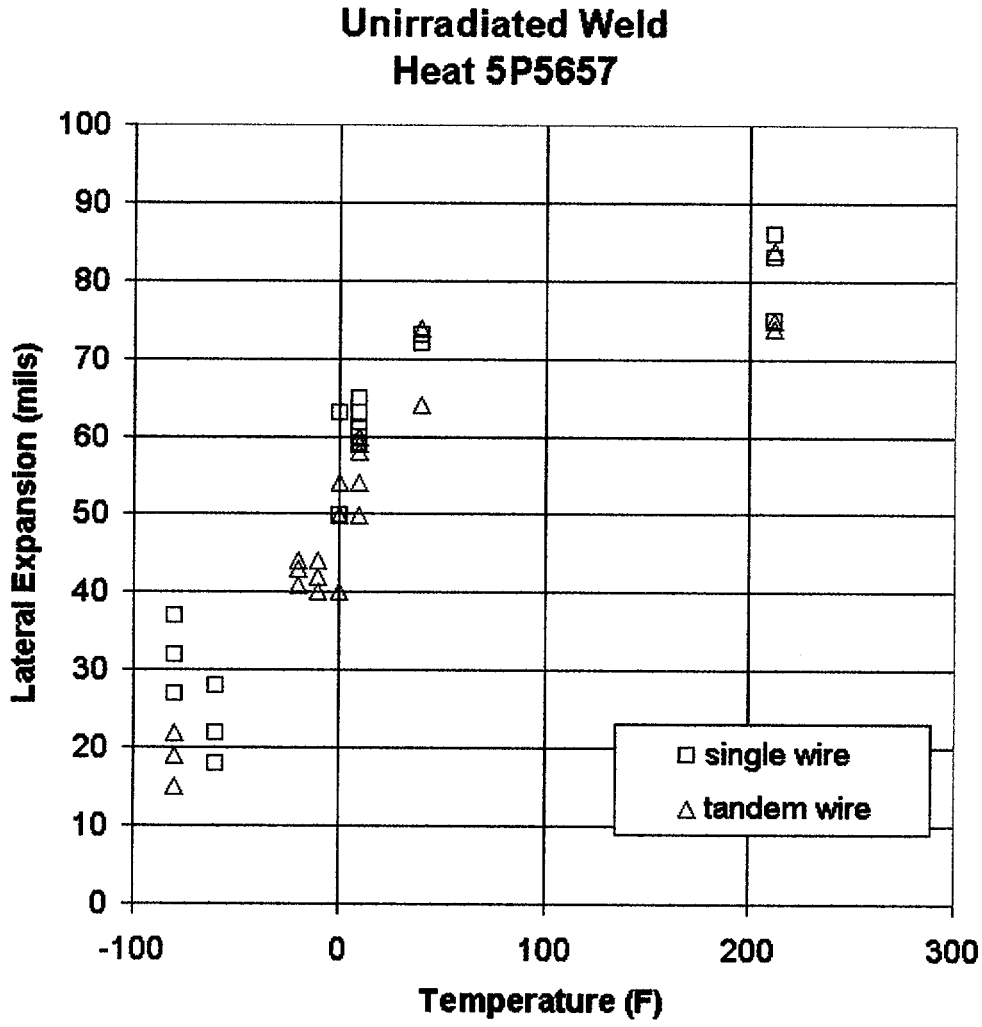

Figure 6-7 **Comparison of Single Wire and Tandem Wire Weld Charpy Lateral Expansion Data for the Unirradiated Weld Metal (heat 5P5657).**

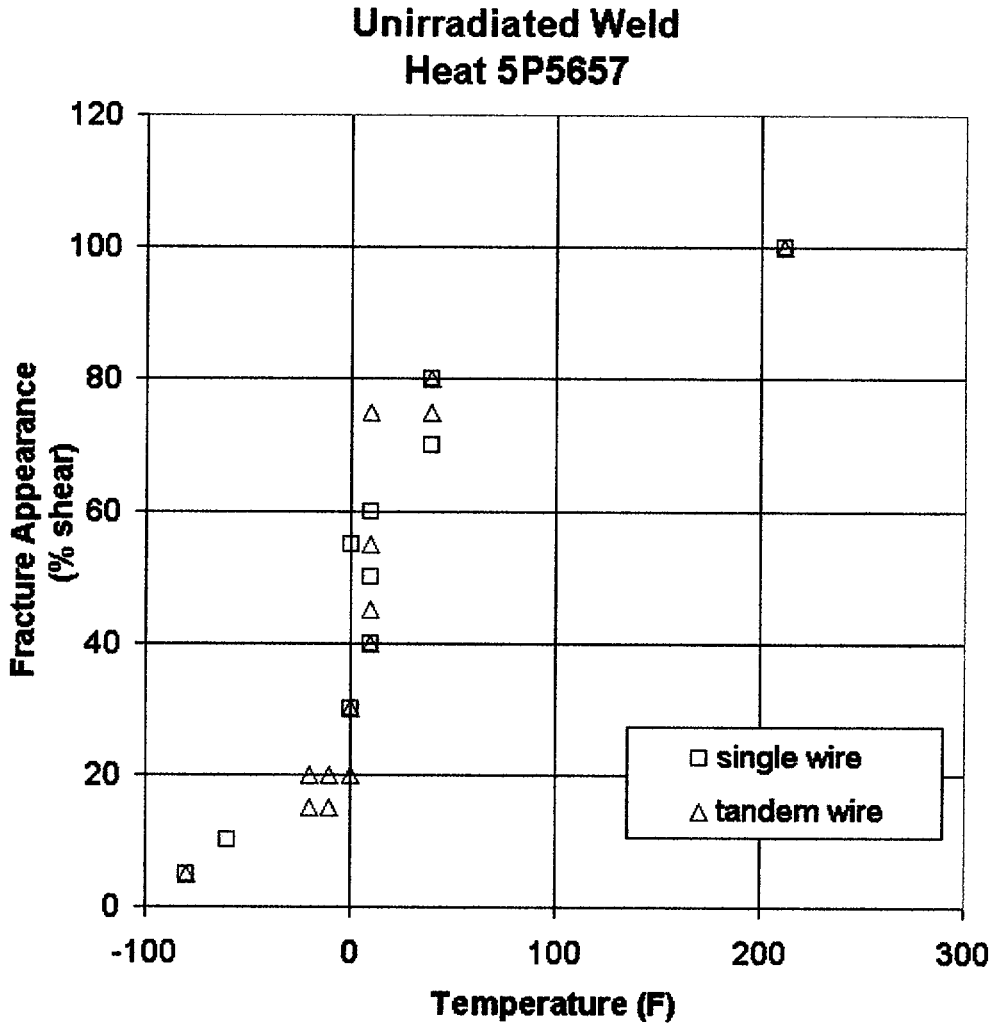

Figure 6-8 **Comparison of Single Wire and Tandem Wire Weld Charpy Fracture Appearance Data for the Unirradiated Weld Metal (heat 5P5657).**

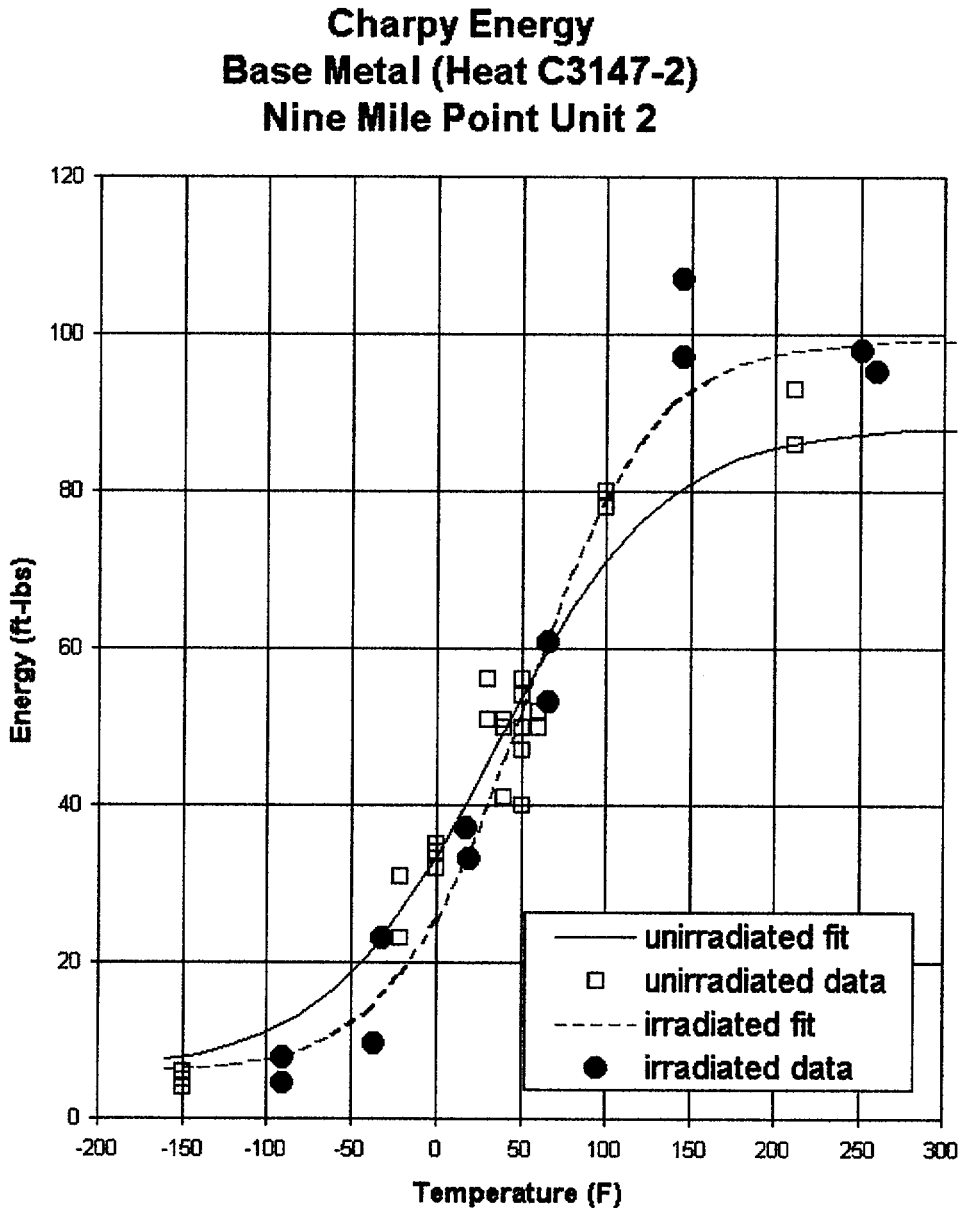

Figure 6-9 **Charpy Energy Data and Curve Fits for C3147-2 Base Metal in the Unirradiated and Irradiated (8.49×10^{16} n/cm^2 ;E>1.0 Mev) Conditions (TL Orientation).**

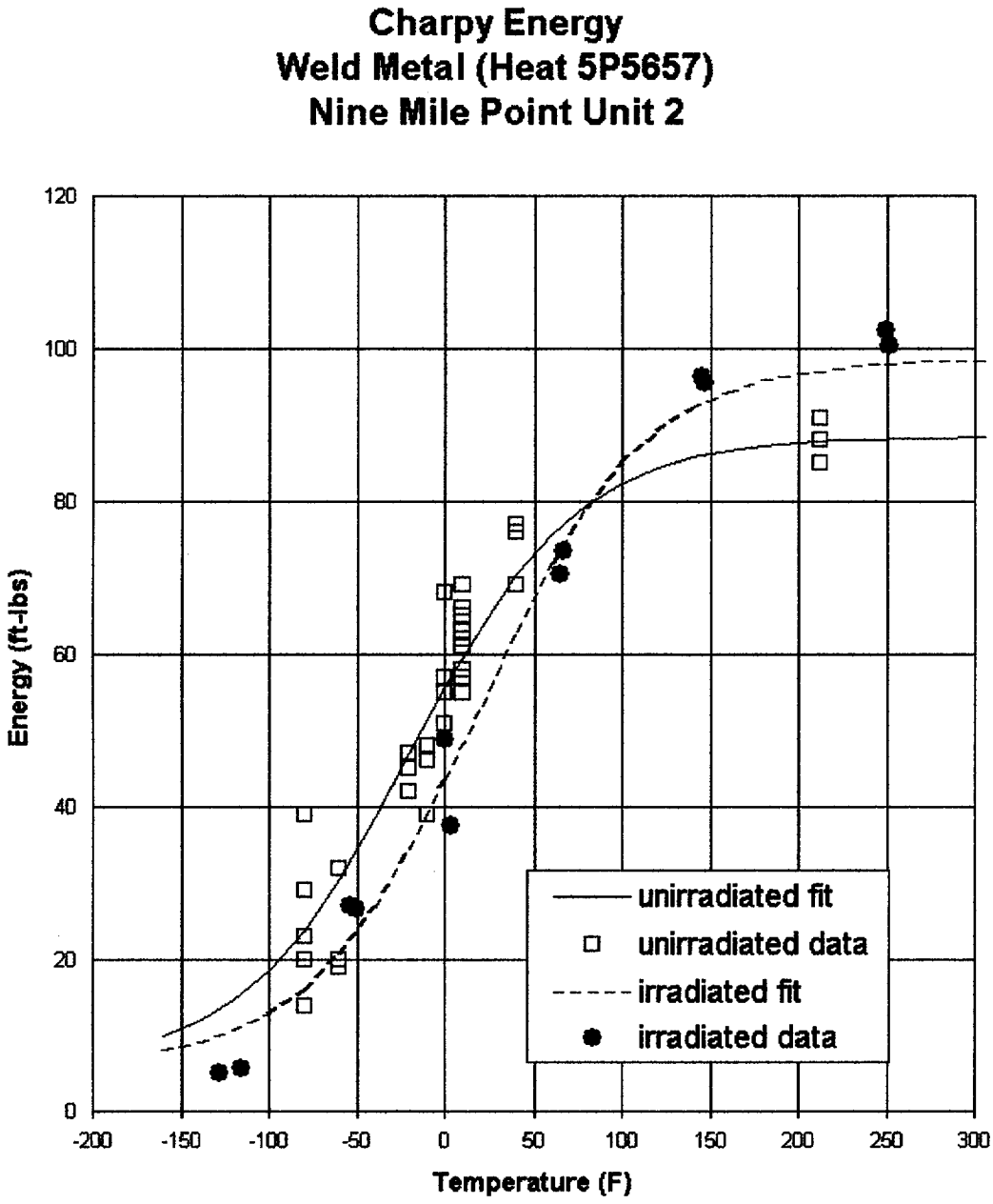

Figure 6-10 Charpy Energy Data and Curve Fits for Weld Metal (heat 5P5657) in the Irradiated (8.49×10^{16} n/cm^2 ;E>1.0 Mev) and Unirradiated Conditions.

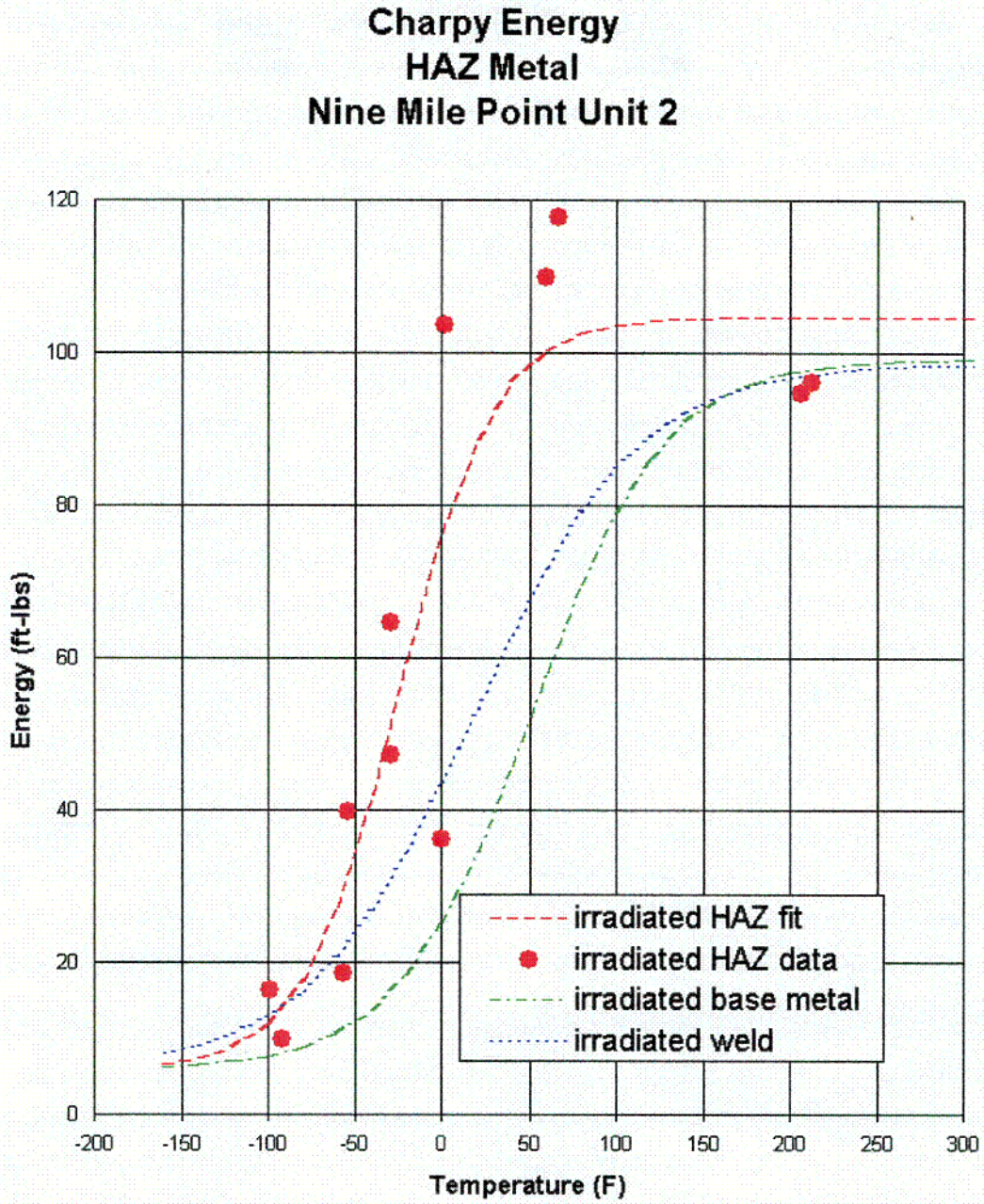

Figure 6-11 **Charpy Energy Data and Curve Fits for Irradiated (8.49×10^{16} n/cm^2 ;E>1.0 Mev) HAZ Metal with Irradiated Base and Weld Metal Curves for Comparison.**

C-8

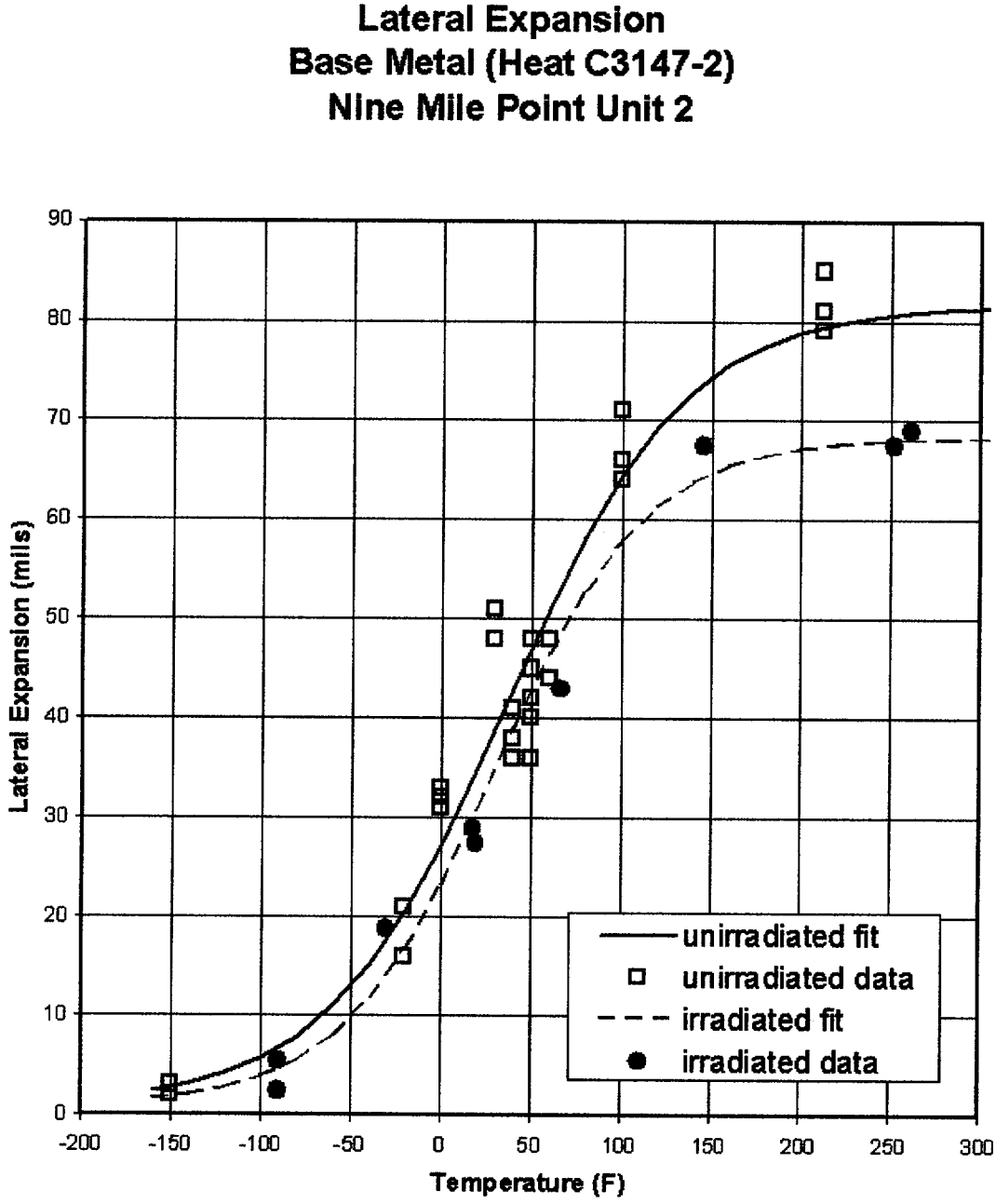

Figure 6-12 **Charpy Lateral Expansion Data and Curve Fits for C3147-2 Base Metal in the Unirradiated and Irradiated (8.49×10^{16} n/cm^2 ;E>1.0 Mev) Conditions (TL Orientation).**

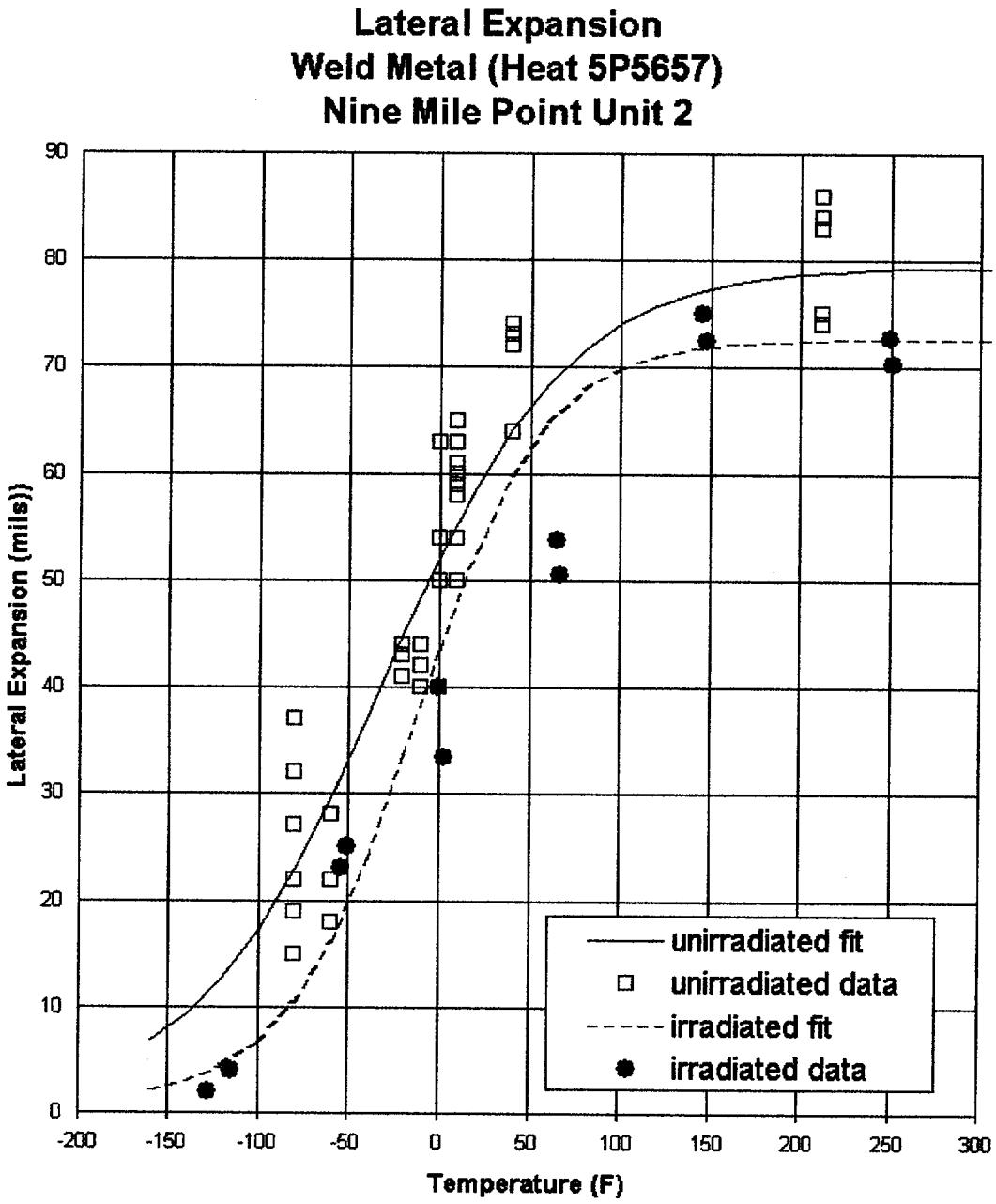

Figure 6-13 **Charpy Lateral Expansion Data and Curve Fits for Weld Metal (heat 5P5657) in the Irradiated (8.49×10^{16} n/cm^2 ;E>1.0 Mev) and Unirradiated Conditions.**

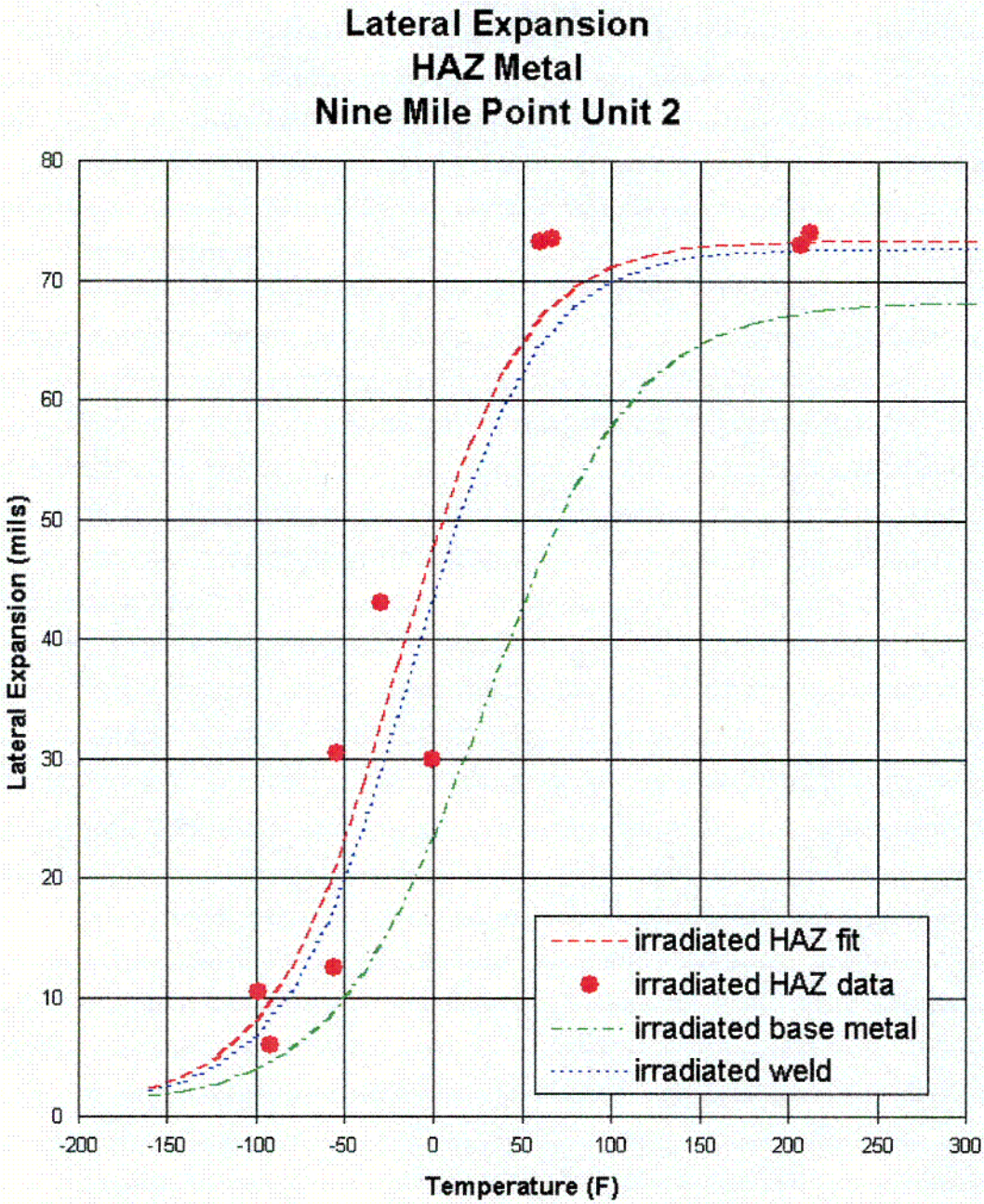

Figure 6-14 **Charpy Lateral Expansion Data and Curve Fits for Irradiated (8.49×10^{16} n/cm^2 ;E>1.0 Mev) HAZ Metal with Irradiated Base and Weld Metal Curves for Comparison.**

L-9

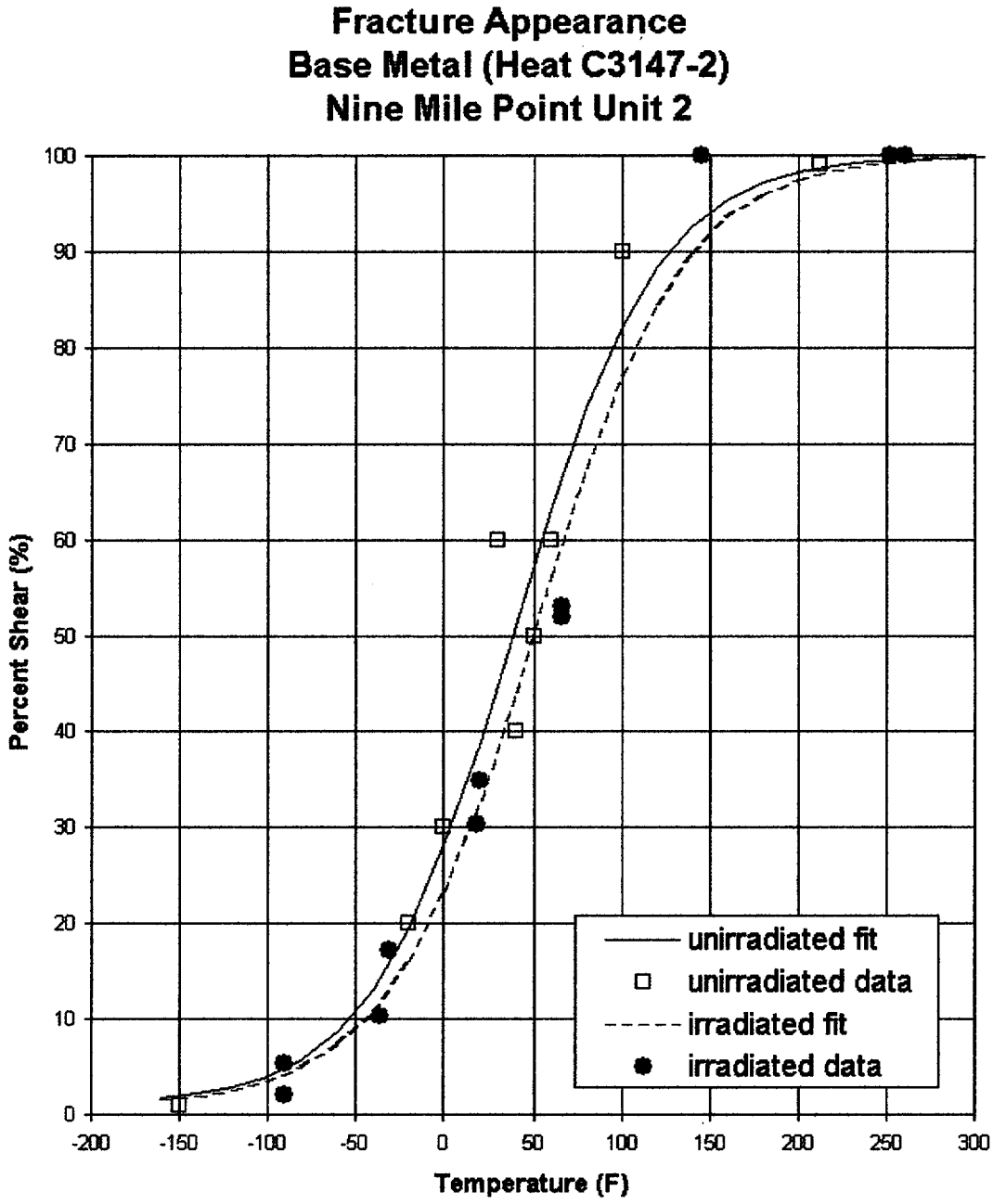

Figure 6-15 Charpy Fracture Appearance Data and Curve Fits for C3147-2 Base Metal in the Unirradiated and Irradiated (8.49×10^{16} n/cm^2 ;E>1.0 Mev) Conditions (TL Orientation).

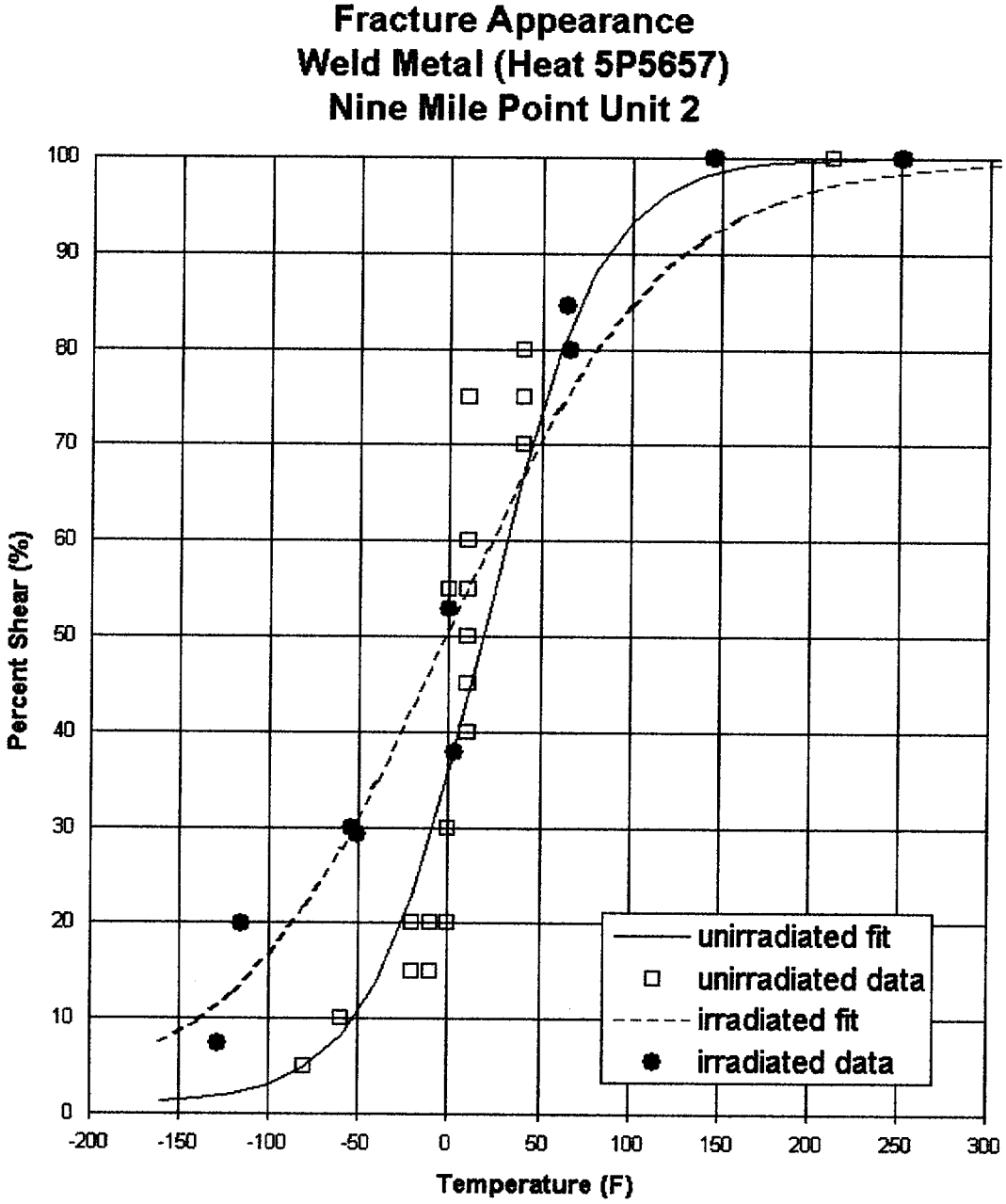

Figure 6-16 **Charpy Fracture Appearance Data and Curve Fits for Weld Metal (heat 5P5657) in the Irradiated (8.49×10^{16} n/cm^2 ;E>1.0 Mev) and Unirradiated Conditions.**

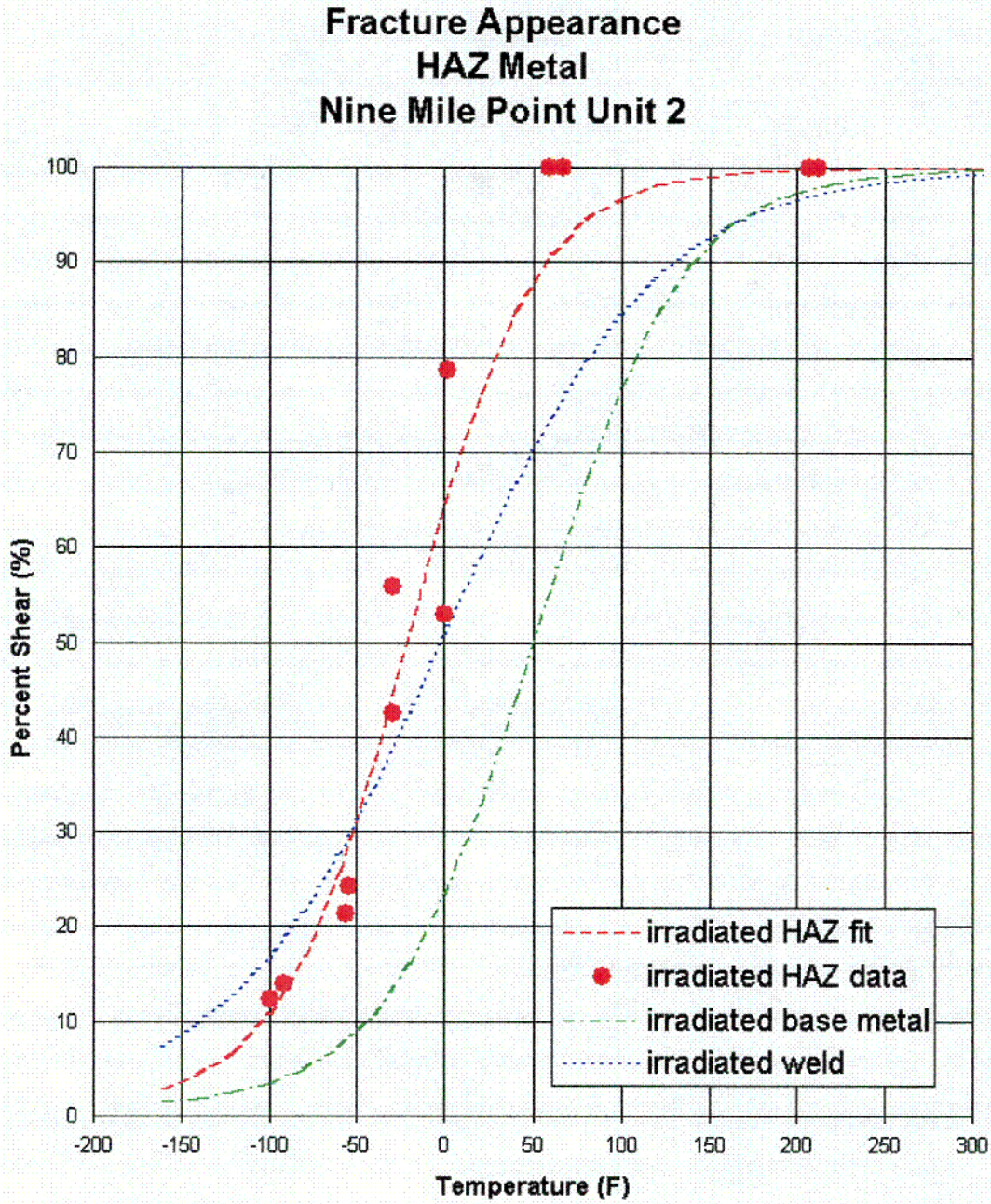

Figure 6-17 **Charpy Fracture Appearance Data and Curve Fits for Irradiated (8.49×10^{16} n/cm^2 ;E>1.0 Mev) HAZ Metal with Irradiated Base and Weld Metal Curves for Comparison.**

7.0 Charpy Data Analysis

7.1 Surveillance Data Credibility

RG1.99(2) requires assessment of surveillance data to determine whether the data are credible. Credibility is judged by five criteria given in the regulatory guide. As shown in Table 7-1, the NMP-2 plate surveillance material satisfies the RG1.99(2) surveillance Criterion 1 because the surveillance plate material C3147-2 contains the limiting Cu/Ni content of the beltline plates and has the limiting ART. As shown in Section 6 of this report, the plots of Charpy energy versus temperature have yielded valid upper shelf energies and 30 ft-lb transition temperatures. Therefore, Criterion 2 has been satisfied.

Criterion 3 should be applied when there are two or more surveillance data point available. However, when only one data point is available, it is possible to compare the measured shift with the RG 1.99(2) calculated shift. Table 7-2 summarizes the results of this evaluation. As shown in the table, the calculated and measured shift are within one standard deviation (17 F) for base metal.

Criterion 4 requires the irradiation temperature of the Charpy specimens in the capsule to match the vessel wall temperature at the cladding/base metal interface within ± 25 F. Since the capsule is located within 1 inch of the vessel clad surface, and the vessel clad nominal thickness is 0.1875 inches, Criterion 4 is satisfied for NMP-2. Since the 3-Degree capsule does not contain correlation monitor materials, Criterion 5 is not applicable to the 3-Degree capsule.

7.2 Integrated Surveillance Data Analysis

The NMP-2 surveillance capsule program was designed to the requirements of ASTM E185-73 (1973). As stated in Reference [7-1], the NRC concluded that the NMP-2 surveillance program satisfies the 10 CFR 50, Appendix H requirements, except that the surveillance capsules have been positioned inside the vessel at locations that result in lead factors (lag factors) below 1.0. Since the lead factor from the surveillance capsule to the peak 1/4T position is below 1.0, NMPC committed in the FSAR to review surveillance data from LaSalle Unit 1, LaSalle Unit 2, and WNP-2 in preparing future revisions to the P-T operating curves. In addition, the FSAR commits NMPC to pull and test the capsules to obtain valid dosimetry data. Further details concerning the NMP-2 integrated surveillance program are contained in References [7-2, 7-3].

Tables 7-3 through 7-6 contain data from the NRC Reactor Vessel Structural Integrity Database (RVID) for WNP-2 and Lasalle Units 1 and 2. The RVID was developed by NRC using industry data following NRC staff review of licensee responses to Generic Letter (GL) 92-01, Revision 1, "Reactor Vessel Structural Integrity". The database was designed to summarize the current status of reactor pressure vessel integrity for all of the US plants. Some of the data categories represent inputs of docketed information while other data categories are representative of computed values that may not have been docketed. The calculations in the database follow the methodology in RG 1.99 (2). The RVID was recently updated with new data based on the NRC's review of the responses to GL 92-01, Revision 1, Supplement 1. The NRC

released the updated database in June 1999 as RVID Version 2 (RVID 2).

The NMP-2 plate surveillance data are compared with the WNP-2 data and Lasalle Units 1 and 2 data in Table 7-6. In all cases, the measured data are within 2σ (34 F) of the RG 1.99(2) model prediction. Also, as shown in Figure 7-1, the plate data for the plants of interest lies within the trend of BWR plate surveillance data. Therefore, it has been concluded that the use of the RG 1.99(2) model is appropriate for NMP-2.

7.3 10CFR50 Appendix H Analysis

10CFR50, Appendix H requires that the test results for a capsule withdrawal be reported within one year of the date of capsule withdrawal and that a determination be made as to whether a Technical Specification change is required. Based on analysis of the test results, it has been concluded that there is no requirement for a Technical Specification change and the current P-T limits are valid. However, the fluence reported here is significantly lower than the fluence used to calculate the current P-T limits and there would be significant reduction in the leak/hydro test temperature if the P-T limits were to be recalculated.

7.4 USE Analysis

The USE data for NMP-2 and for WNP-2 and Lasalle Units 1 and 2 are summarized in Table 7-7. The NMP-2 and WNP-2 USE levels after irradiation are slightly higher than the unirradiated values. This phenomenon has been observed in other plants and may be related to low fluence inprovement of the matrix material which results in more ductile ligament response during the ductile fracture process.

Conservatively assuming an EOL fluence of up to $1x10^{18}$ n/cm^2, the RG 1.99(2) predicted shelf drop for plate C3147-2 is less than 15%. Therefore, the 10CFR50, Appendix G requirement to maintain a 50 ft-lb USE throughout the plant operating period is satisfied for NMP-2.

7.5 Chapter 7 References

[7-1] Safety Evaluation Report related to the operation of Nine Mile Point Nuclear Station, Unit No. 2, NUREG-1047, February, 1985

[7-2] Safety Evaluation Report related to the operation of Nine Mile Point Nuclear Station, Unit No. 2, NUREG-1047, Supplement No. 3, July, 1986

[7-3] Letter from C. V. Mangan (NMPC) to Harold Denton (NRC), "Integrated Reactor Vessel Material Surveillance Program", September 30, 1985.

Table 7-1 Analysis of NMP-2 Beltline Materials at 22 EFPY to Identify Limiting ART.

Material ID	Wetted Surface Fluence (n/cm^2)	RG1.99 Fluence Factor (FF)	Cu Content (wt %)	Ni Content (wt %)	RG 1.99 Chemistry Factor (CF) (F)	RG 1.99 Source of CF	Initial RT_{NDT} (TL) (F)	ΔRT_{NDT} (F)	Margin (F)	ART (F)
Plate C3065-1	5.71×10^{17}	0.314	0.06	0.63	37.0	Table	-10	11.6	31.2	32.9
Plate C3121-2	5.71×10^{17}	0.314	0.09	0.65	58.0	Table	0	18.2	34.3	52.5
Plate C3147-1	5.71×10^{17}	0.314	0.11	0.63	74.5	Table	0	23.4	37.3	60.7
Plate C3147-2 (1)	5.71×10^{17}	0.314	0.11	0.63	74.5	Table	0	23.4	37.3	60.7
Plate C3066-2	5.71×10^{17}	0.314	0.07	0.64	44.0	Table	-20	13.8	32.1	26.0
Plate C3065-2	5.71×10^{17}	0.314	0.06	0.63	37.0	Table	10	11.6	31.2	52.9
Weld 5P5657/0931 (1,2)	5.71×10^{17}	0.314	0.07	0.71	95.0	Table	-60	29.9	41.6	11.5
Weld 5P5657/0931 (1,3)	5.71×10^{17}	0.314	0.04	0.89	54.0	Table	-60	17.0	33.6	-9.4
Weld 5P6214B/0331(2)	5.71×10^{17}	0.314	0.02	0.82	27.0	Table	-50	8.5	30.2	-11.3
Weld 5P6214B/0331(3)	5.71×10^{17}	0.314	0.014	0.70	22.8	Table	-40	7.2	29.9	-3.0
Weld 4P7465/0751 (2)	5.71×10^{17}	0.314	0.02	0.82	27.0	Table	-60	8.5	30.2	-21.3
Weld 4P7465/0751 (3)	5.71×10^{17}	0.314	0.02	0.80	27.0	Table	-60	8.5	30.2	-21.3
Weld 4P7216/0751 (2)	5.71×10^{17}	0.314	0.06	0.85	82.0	Table	-50	25.8	38.8	14.6
Weld 4P7216/0751 (3)	5.71×10^{17}	0.314	0.04	0.83	54.0	Table	-80	17.0	33.6	-29.4

(1) These materials are also in the surveillance program.
(2) Single wire submerged arc process.
(3) Tandem wire submerged arc process.

Table 7-2 Surveillance Data Credibility Assessment for Plate C3147-2.

Capsule Identification	Fluence (n/cm^2)	Fluence Factor (FF)	Measured ΔRT_{NDT} (F)	RG 1.99(2) Predicted ΔRT_{NDT} (F)	Measured ΔRT_{NDT} Minus Predicted ΔRT_{NDT} (F)
3°	8.49×10^{16}	0.09798	20.2	7.3	12.9

Table 7-3 RVID Surveillance Data Summary for WNP-2.

NRC - Reactor Vessel Integrity Database

Surveillance Data Summary

WNP-2

Printed 12/9/2000 11:55:14
Page 1

Docket No: 50-397
EOL Date: 12/20/2023

Type Direction	Heat ID Capsule, Lead Factor	Neutron Fluence	Fluence Factor	Group CF	Used in CF Calcs	Predicted ΔRTndt	Measured ΔRTndt	Predicted - Measured ΔRTndt	Credible RG1.99 Scatter	cpof Pred-Meas ΔRTndt	Unir USE	Meas USE	% Drop in USE	% Drop in USE Line Offset	Cu %	Ni %	P %	S %
PLATE	B5301-1	0.02	0.15		YES		-1.0				150.2	154.8	0.00	-3.57352	0.110	0.490	0.014	0.000
UNKNOWN	300, 0.95																	
WELD	3P4966	0.02	0.15		YES		-4.9				102.5	114.6	0.00	-3.57206	0.030	0.890	0.100	0.000
N/A	300, 0.95																	

Table 7-4 RVID Surveillance Data Summary for Lasalle Unit 1.

NRC - Reactor Vessel Integrity Database

Surveillance Data Summary

LASALLE 1

Printed 12/9/2000 11:58:17
Page 1

Docket No: 50-373
EOL Date: 05/17/2022

Type Direction	Heat ID Capsule, Lead Factor	Neutron Fluence	Fluence Factor	Group CF	Used in CF Calcs	Predicted ΔRTndt	Measured ΔRTndt	Predicted - Measured ΔRTndt	Credible RG1.99 Scatter	cpof Pred-Meas ΔRTndt	Unir USE	Meas USE	% Drop in USE	% Drop in USE Line Offset	Cu %	Ni %	P %	S %
PLATE	C6345-1	0.01	0.10		YES		28.4				153.3	140.5	8.35	1.39918	0.140	0.540	0.015	
LONGITUDINAL	300, 0.98																	
WELD	1P3571	0.01	0.10		YES		34.9				119.2	107.2	10.07	1.47146	0.210	0.780	0.016	
N/A	300, 0.98																	

Table 7-5 RVID Surveillance Data Summary for Lasalle Unit 2.

NRC - Reactor Vessel Integrity Database

Surveillance Data Summary

LASALLE 2

Printed 12/9/2000 12:00:07
Page 1

Docket No: 50-374
EOL Date: 12/16/2023

Type Direction	Heat ID Capsule, Lead Factor	Neutron Fluence	Fluence Factor	Group CF	Used in CF Calcs	Predicted ΔRTndt	Measured ΔRTndt	Predicted - Measured ΔRTndt	Credible RG1.99 Scatter	σof Pred-Meas ΔRTndt	Unir USE	Meas USE	% Drop in USE	% Drop in USE Line Offset	Cu %	Ni %	P %	S %
PLATE	C9481-1	0.01	0.12		NO							124.8	0.00		0.010	0.480	0.003	0.023
LONGITUDINAL	120 / 0.98																	
WELD	SP7397	0.01	0.12		YES		18.6				83.3	86.9	0.00	-3.54140	0.040	0.890	0.014	0.015
N/A	120 / 0.98																	

Table 7-6 Comparison of NMP-2 Plate Charpy Shift Data with Similar Data from WNP-2 and Lasalle Units 1 and 2.

Capsule Identification	Plate Identification	Fluence (n/cm^2)	RG1.99 Fluence Factor (FF)	RG1.99 Chem Factor (CF)	Measured ΔRT_{NDT} (F)	RG 1.99(2) Predicted ΔRT_{NDT} (F)	Measured ΔRT_{NDT} Minus Predicted ΔRT_{NDT} (F)
NMP-2 3°	C3147-2	8.49×10^{16}	0.09798	74.5	20.2	7.3	12.9
WNP-2 300°	B5301-1	1.55×10^{17}	0.14649	72.9	-1	10.7	11.7
Lasalle-1 300°	C6345-1	8.97×10^{16}	0.10178	97.3	28.4	9.9	18.5
Lasalle-2 300°	C9481-1	1.15×10^{17}	0.12048	20	a	2.4	a

a Unirradiated data not available

Table 7-7 Comparison of NMP-2 Plate Upper Shelf Energy Data with Similar Data from WNP-2 and Lasalle Units 1 and 2.

Capsule Identification	Plate Identification	Fluence (n/cm^2)	Measured USE (ft-lb)	Measured USE Change (ft-lb)
NMP-2 3°	C3147-2	8.49×10^{16}	99.3	+11.0
WNP-2 300°	B5301-1	1.55×10^{17}	154.8	+4.6
Lasalle-1 300°	C6345-1	8.97×10^{16}	140.5	-12.8
Lasalle-2 300°	C9481-1	1.15×10^{17}	124.8	a

a Unirradiated data not available

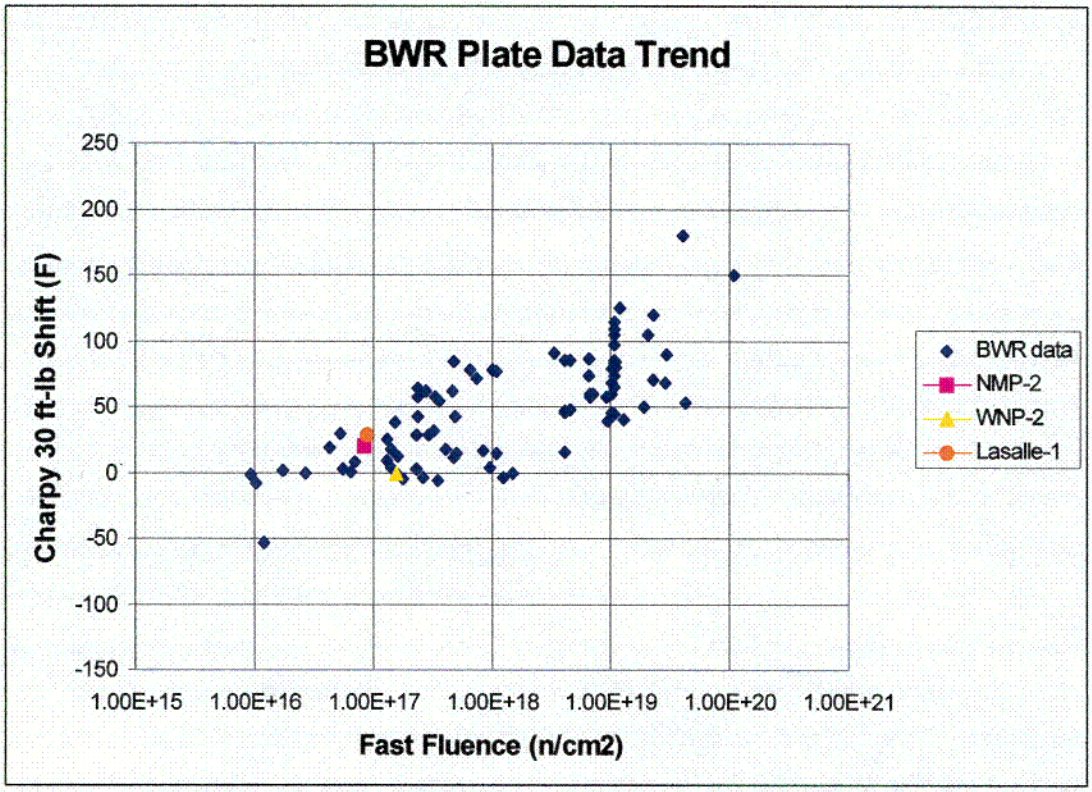

Figure 7-1 **Plot of the BWR Plate Surveillance Data Showing the NMP-2, WNP-2, and Lasalle Units 1 and 2 are Well within the Data Trend.**

8.0 Summary and Conclusions

Testing of the NMP-2 3-Degree surveillance capsule and evaluation of the data has led to the following conclusions:

- The neutron induced plate C3147-2 embrittlement is low and the Charpy shift is within the expected range as prediceted by RG 1.99(2). At a fluence of 8.49 x 10^{16} n/cm^2, the 3-Degree capsule measured shift in the 30 ft-lb transition temperature is 20.2 F. The measured change in USE is +11.0 ft-lb.

- Similarly, low surveillance weld embrittlement results were obtained. The 3-Degree capsule measured weld metal shift in the 30 ft-lb transition temperature at a fluence of 8.49 x 10^{16} n/cm^2 is 30.3 F. The measured change in the weld USE is +10.2 ft-lbs. Since there are no unirradiated HAZ data available, it is not possible to report the shift or shelf drop for the HAZ material.

- A fluence of 8.49 x 10^{16} n/cm^2 has been estimated for the 3-Degree capsule exposure. Analysis of the dosimetry data has resulted in an average C/E ratio of 0.95 for the Cu dosimeter and 1.09 for the Fe dosimeter. The overall capsule average C/E ratio is 1.02. Overall, the transport calculation and dosimetry are in very good agreement.

- Chemical measurements made on the capsule Charpy specimens have verified that the base metal specimens were fabricated from plate C3147 material. The capsule weld specimens were prepared from heat 5P5657 using both single and tandem wire processes. The weld metal specimen analyzed was fabricated from heat 5P5657 (tandem wire process). Overall, the chemical analyses performed confirm that the surveillance specimen chemical compositions are in agreement with the plant records.

- RG1.99(2) requires assessment of surveillance data to determine whether the data are credible. Credibility is judged by five criteria given in the regulatory guide. Analysis of the data has led to the conclusion that the NMP-2 data are credible.

- At the end of cycle 7, the lead factor (capsule fluence divided by vessel maximum fluence) is calculated to be 0.43 (8.49E16/1.95E17).

- Since the lead factor from the surveillance capsule to the peak 1/4T position is below 1.0, NMPC committed in the FSAR to review surveillance data from LaSalle Unit 1, LaSalle Unit 2, and WNP-2 in preparing future revisions to the P-T operating curves. Analysis of the sister plant data has shown that the measured data for all three plants are within 2σ (34 F) of the RG 1.99(2) model prediction. Also, plotting the NMP-2 and sister plant data with the BWR surveillance data, shows that the plate data for the plants of interest lies within the trend of BWR plate surveillance data. Therefore, it has been concluded that the

use of the RG 1.99(2) model is appropriate for NMP-2.

- 10CFR50, Appendix H requires that the test results for a capsule withdrawal be reported within one year of the date of capsule withdrawal and that a determination be made as to whether a Technical Specification change is required. Based on analysis of the test results, it has been concluded that there is no requirement for a Technical Specification change and the current P-T limits are valid. However, the fluence reported here is significantly lower than the fluence used to calculate the current P-T limits and there would be significant reduction in the leak/hydro test temperature if the P-T limits were to be recalculated.

- The NMP-2 and WNP-2 USE levels after irradiation are slightly higher than the unirradiated values. This phenomenon has been observed in other plants and may be related to low fluence improvement of the matrix material which results in more ductile ligament response during the ductile fracture process. Conservatively assuming an EOL fluence of up to $1x10^{18}$ n/cm^2, the RG 1.99(2) predicted shelf drop for plate C3147-2 is less than 15%. Therefore, the 10CFR50, Appendix G requirement to maintain a 50 ft-lb USE throughout the plant operating period is satisfied for NMP-2.

9.0 Nomenclature

ASME	-	American Society of Mechanical Engineers
ASTM	-	American Society for Testing and Materials
ART_{NDT}	-	Adjusted Nil-Ductility Reference Temperature
BAF	-	Bottom of Active Fuel
BWR	-	Boiling Water Reactor
DBTT	-	Ductile-Brittle Transition Temperature
CF	-	Chemistry Factor Specified in RG 1.99(2)
CFR	-	Code of Federal Regulations
EFPY	-	Effective Full Power Years
EFPS	-	Effective Full Power Seconds
EOL	-	End-of-License
F,°F	-	Degrees Farenheit
Ge(Li)	-	Germanium-Lithium gamma ray detector
GRSS	-	Gamma Ray Spectrometer System
HPGe	-	HyperPure Germanium gamma ray detector
ICP-MS	-	Inductively-Coupled Plasma - Mass Spectrometer
ID	-	Inner Diameter
KeV	-	Kiloelectron Volt (unit of gamma ray emission energy)
LT	-	Longitudinal-Transverse
LEFM	-	Linear-Elastic Fracture Mechanics
LWR	-	Light Water Reactor
MeV	-	Million Electron Volt (unit of gamma ray emission energy)
NMP-2	-	Nine Mile Point Unit 2
NMPC	-	Niagara Mohawk Power Corporation
NRC	-	Nuclear Regulatory Commission
NIST	-	National Institute of Standards and Technology
OSQ	-	On-Screen Quantification software package
P-T	-	Pressure-Temperature
PWR	-	Pressurized Water Reactor
PSU	-	Pennsylvania State University
RG1.99(2)	-	Regulatory Guide 1.99 (Revision 2)
RPV	-	Reactor Pressure Vessel
RT_{NDT}	-	Nil-Ductility Reference Temperature
$\Delta RT_{NDT}, \Delta T_{30}$	-	Neutron Induced Shift in Nil-Ductility Reference Temperature Indexed at 30 ft-lbs of absorbed energy
T	-	Vessel Wall Thickness
TL	-	Transverse-Longitudinal
USE	-	Upper Shelf Energy
ΔUSE	-	Charpy Upper Shelf Energy Drop
USE_o	-	Unirradiated USE

Appendix A 3-Degree Capsule Instrumented Impact Data

Appendix A-1 Base Metal Plate C3147-2 Data

The base metal Charpy data are summarized below. The instrumented data provided on the pages which follow are given in the order shown in the table. There are three instrumented data plots for each specimen tested.

Summary of Charpy V-Notch T-L Impact Test Results for Irradiated C3147-2 Base Metal Specimens from the Nine Mile Point Unit 2 3-Degree Surveillance Capsule.

Specimen Identification	Test Temperature (°F)	Impact Energy (ft-lb)	Fracture Appearance (% Shear Area)	Lateral Expansion (mils)
BF1-8	-90.4	7.9	5.3	5.5
BF1-2	-90.4	4.6	2.0	2.5
BF1-5	-36.4	9.8	10.3	a
BF1	-31.0	23.1	17.2	18.8
BF1-4	17.6	37.2	30.3	29.0
BF1-6	19.4	33.2	34.9	27.5
BF1-10	66.2	53.3	52.0	43.0
BF1-12	66.2	60.7	53.0	a
BF1-7	145.4	107.1	100.0	a
BF1-11	145.4	97.0	100.0	67.5
BF1-3	251.6	97.9	100.0	67.5
BF1-9	260.6	95.2	100.0	69.0

a In accordance with ASTM E23, these values are not reported due to limitations on the partial break.

Impact V2.1

Summary Report

Sample ID

BF1-8

Material Description

NMP-2 3-Degree Surveillance Capsule - Base material

Test Parameter	Value
Operator	Dr. Michael P. Manahan, Sr.
Date Tested	11/28/00 4:03 PM
Temperature	-68.00 °C
Oscilloscope	Model 441 Internal
Striker Name	8mm - Striker 16
Interpolation Method	Point-Point Linear
TO 892 Controller	Active Adjust
Sample Type	Metal
Sample Size	Type A
Orientation	TL
Notch Type	V Notch, no Side-Groove
Length	2.1654 in
Width	0.3937 in
Thickness	0.3937 in
Span	1.5748 in
Uncracked Ligament	0.3150 in
Notch Radius	0.0098 in
Velocity Determination	Potential Energy & Losses
Velocity	17.94 ft/s
Shear	5.30 %
Lateral Expansion	0.0055 in
Energy Adjustment	1.0812

Measured Data (V)

Oscilloscope Signal

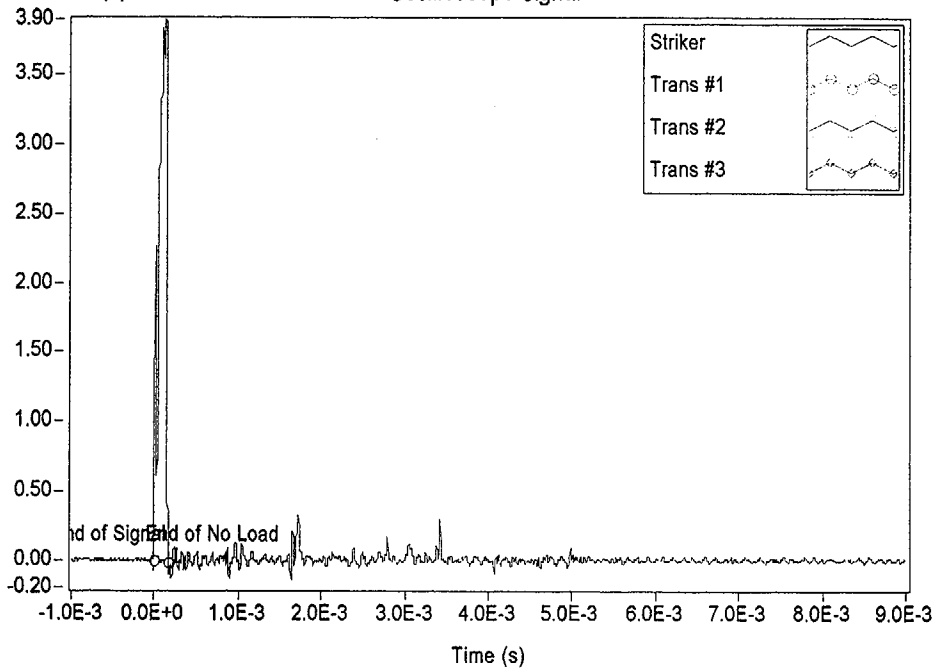

Result	Value
Optical Encoder Energy	7.8614 ft lbf
Dial Gage Energy	7.900 ft lbf
Instrumented Striker Energy	7.8614 ft lbf

Impact V2.1

Integration Report

Signal Source: 8mm - Striker 16 Striker

Load (lbf) vs. Time (s)

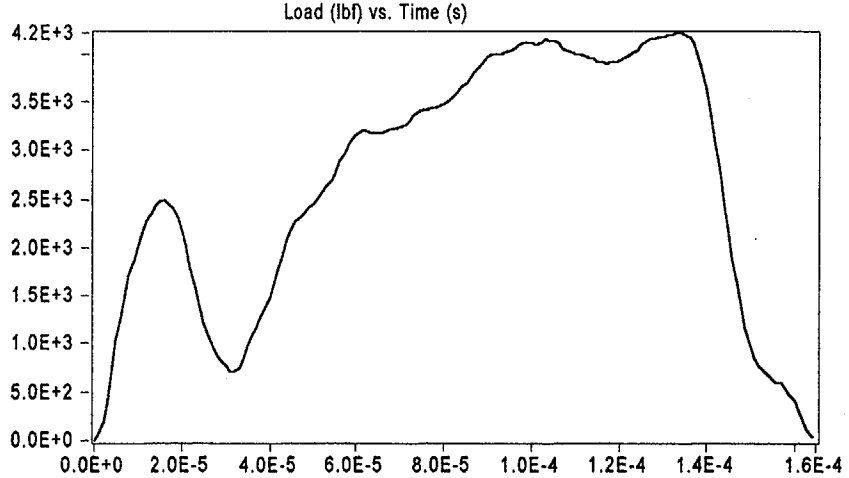

Velocity (ft/s) vs. Time (s)

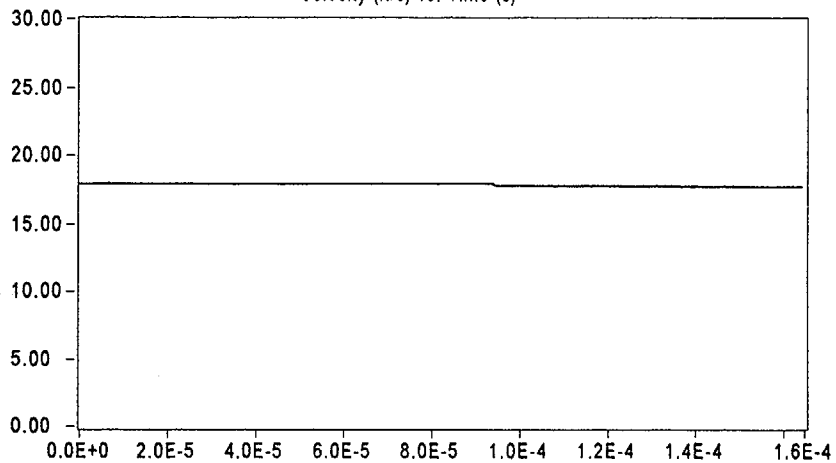

Displacement (in) vs. Time (s)

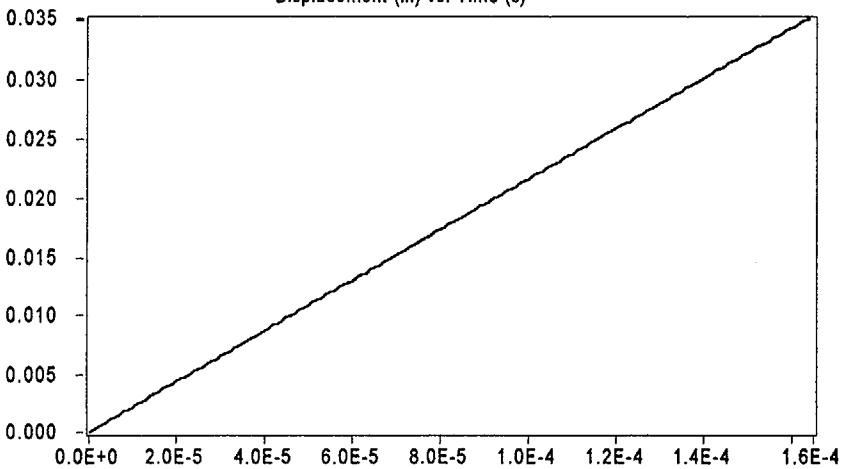

Load (lbf), Energy (ft lbf) vs. Displacement (in)

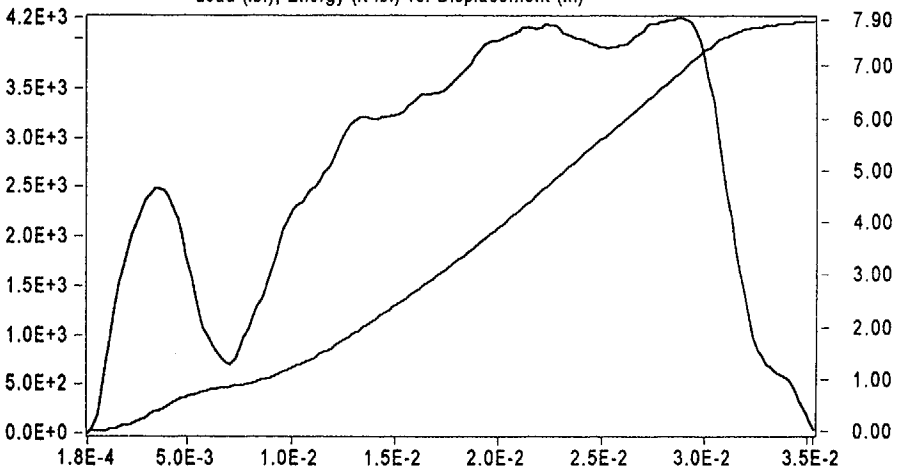

Sample Name: Bf1-8

Instrumented Striker Energy: 7.8614 ft lbf

Impact V2.1

Load vs. Displacement Critical Points

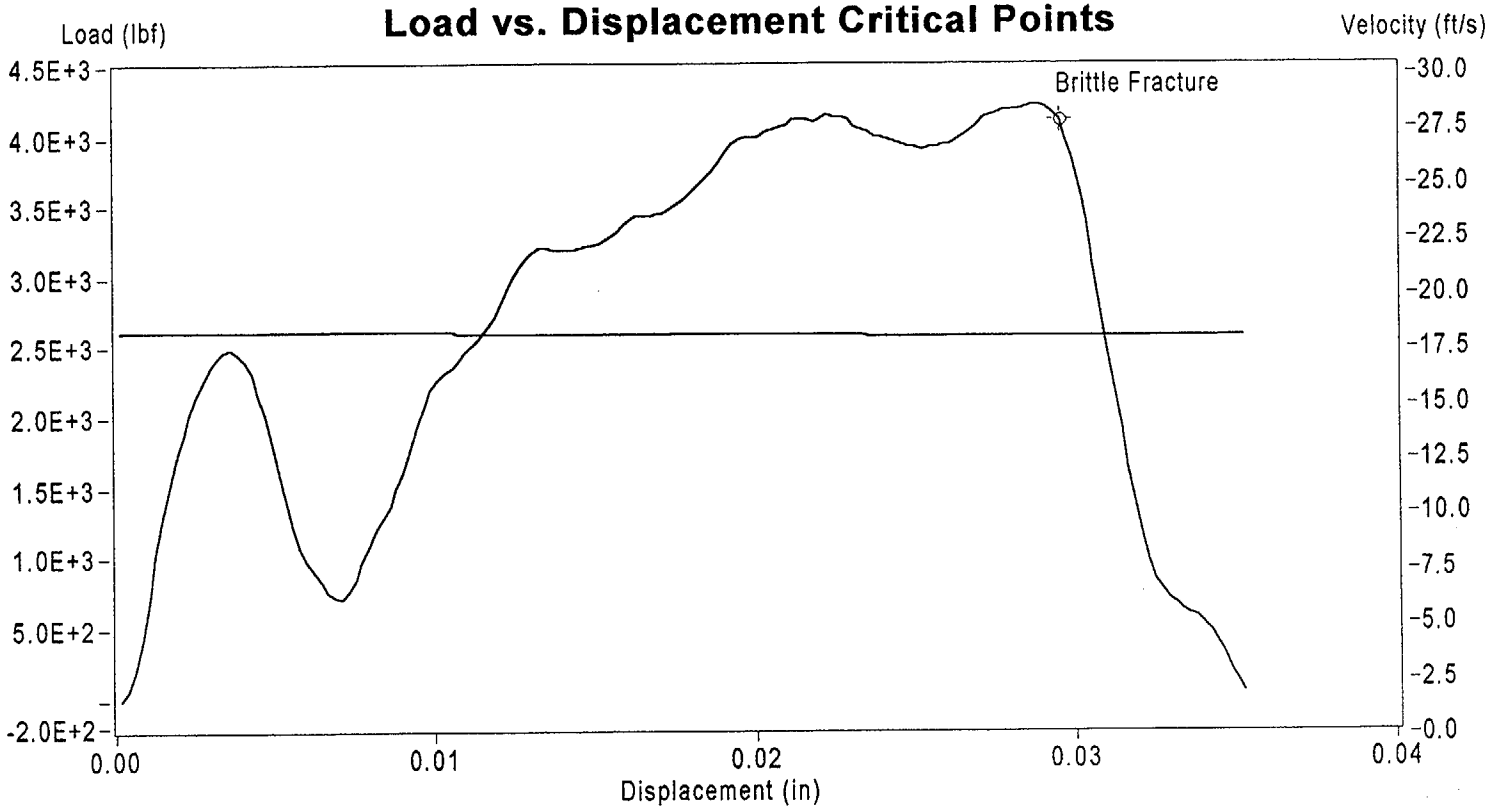

	Load (lbf)	Displacement (in)	Velocity (ft/s)	Time (s)	Energy (ft lbf)
Brittle Fracture	4.108E+3	2.953E-2	1.773E+1	1.320E-4	7.164E+0
End of Signal	4.152E+1	3.523E-2	1.770E+1	1.590E-4	7.861E+0

Sample ID: Bf1-8

Impact V2.1

Summary Report

Sample ID

BF1-2

Material Description

NMP-2 3-Degree Surveillance Capsule - Base material

Test Parameter	Value
Operator	Dr. Michael P. Manahan, Sr.
Date Tested	11/28/00 4:52 PM
Temperature	-68.00 °C
Oscilloscope	Model 441 Internal
Striker Name	8mm - Striker 16
Interpolation Method	Point-Point Linear
TO 892 Controller	Active Adjust
Sample Type	Metal
Sample Size	Type A
Orientation	TL
Notch Type	V Notch, no Side-Groove
Length	2.1654 in
Width	0.3937 in
Thickness	0.3937 in
Span	1.5748 in
Uncracked Ligament	0.3150 in
Notch Radius	0.0098 in
Velocity Determination	Potential Energy & Losses
Velocity	17.94 ft/s
Shear	2.00 %
Lateral Expansion	0.0025 in
Energy Adjustment	1.0533

Measured Data (V)

Oscilloscope Signal

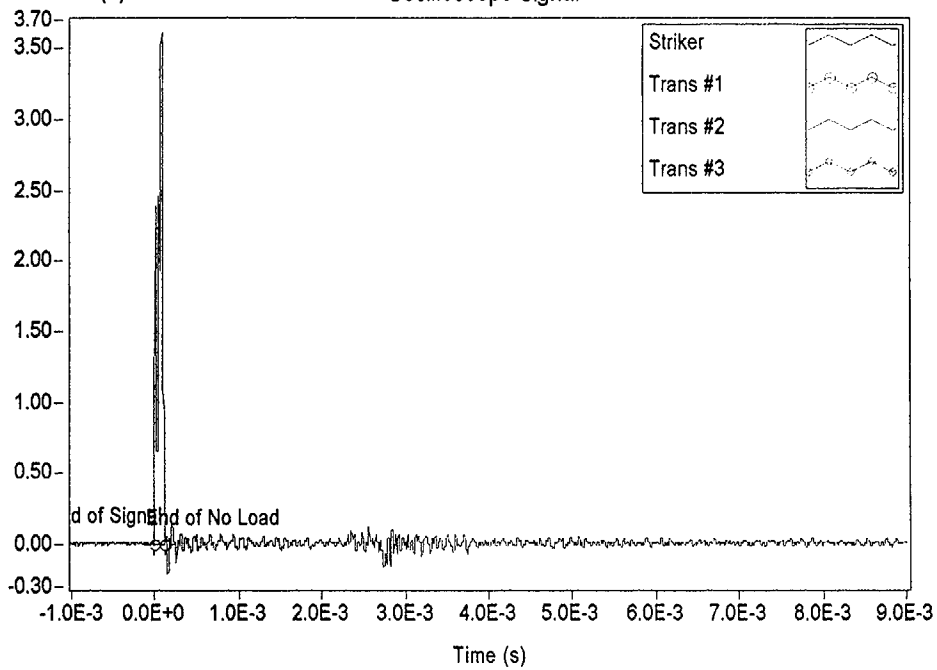

Result	Value
Optical Encoder Energy	**4.5620 ft lbf**
Dial Gage Energy	**4.800 ft lbf**
Instrumented Striker Energy	**4.5620 ft lbf**

Impact V2.1

Integration Report

Signal Source: 8mm - Striker 16 Striker

Load (lbf) vs. Time (s)

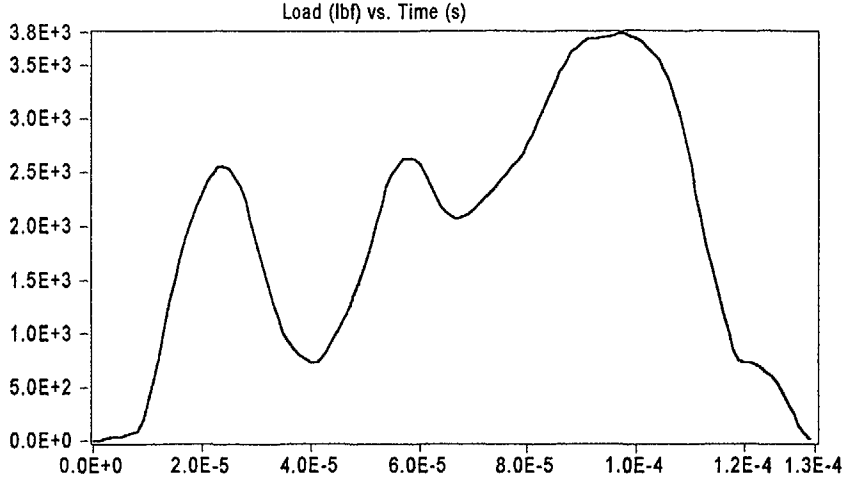

Velocity (ft/s) vs. Time (s)

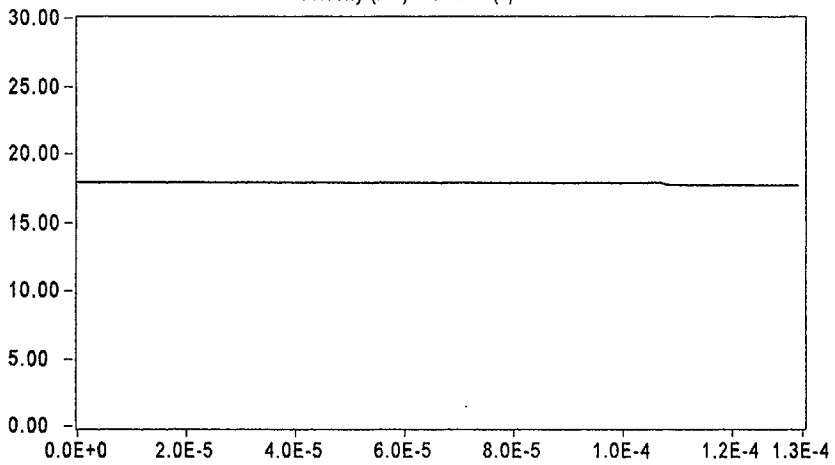

Displacement (in) vs. Time (s)

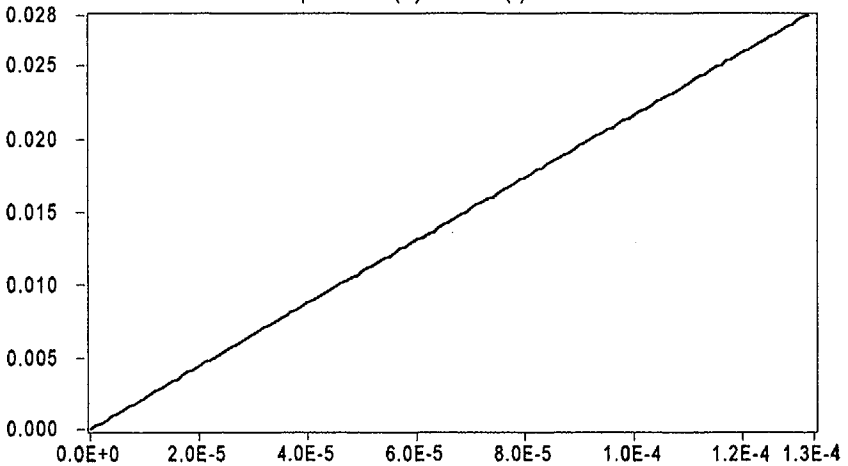

Load (lbf), Energy (ft lbf) vs. Displacement (in)

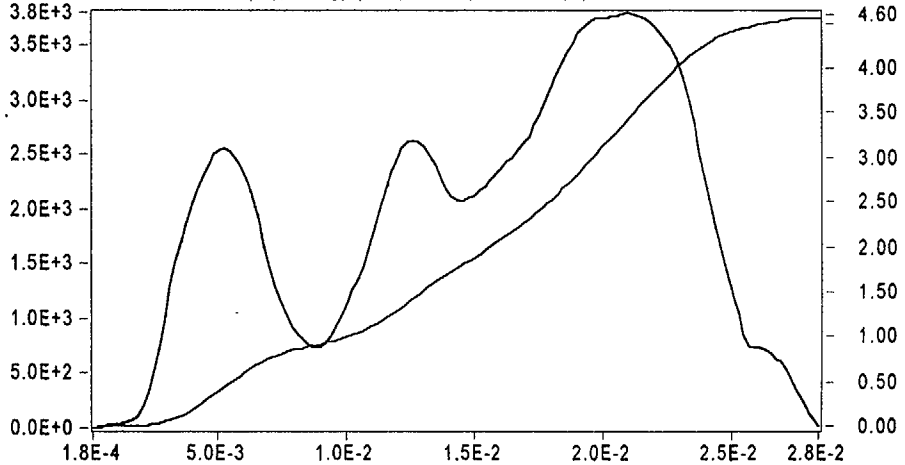

Sample Name: Bf1-2

Instrumented Striker Energy: 4.5620 ft lbf

Impact V2.1

Load vs. Displacement Critical Points

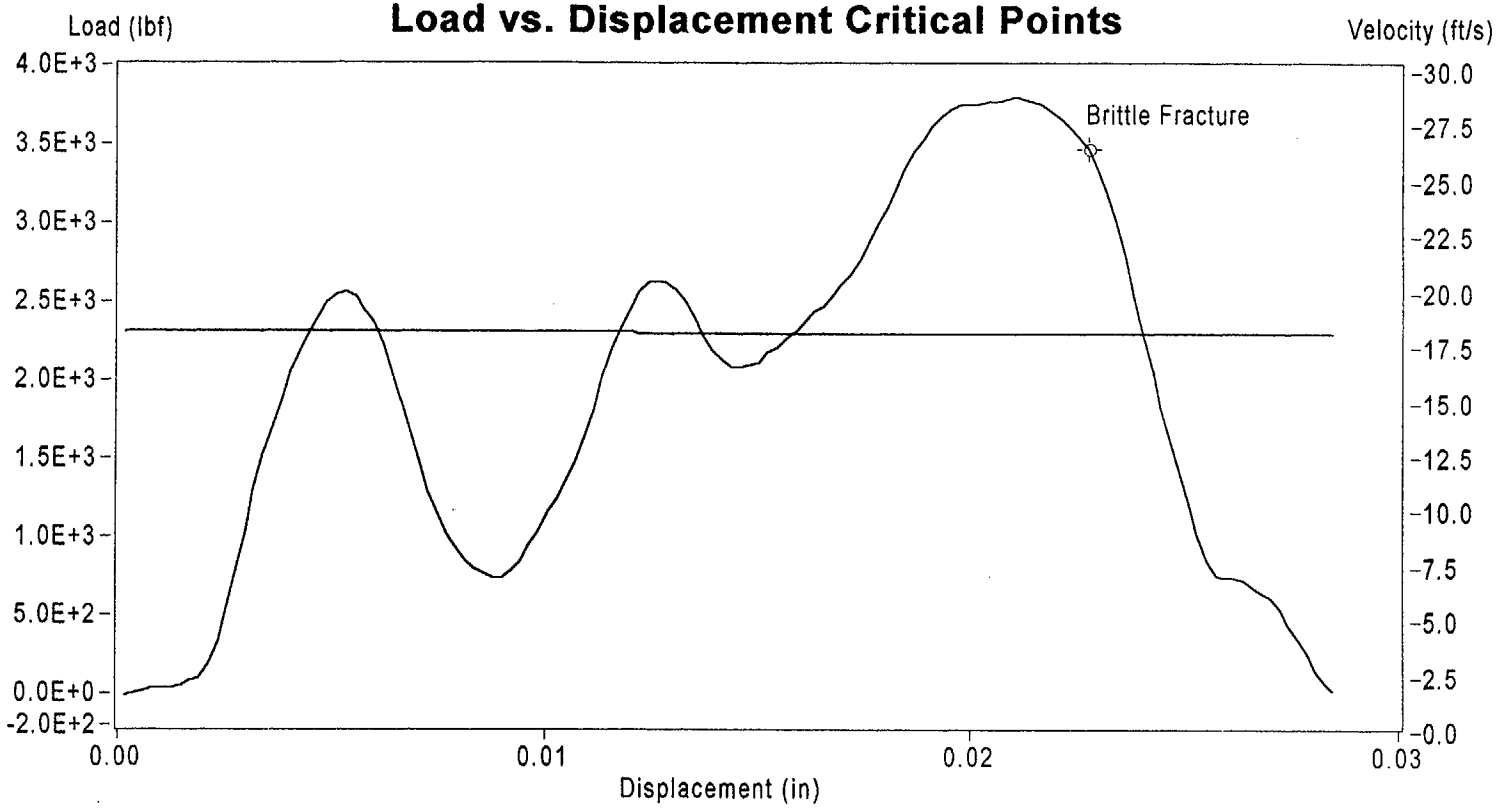

	Load (lbf)	Displacement (in)	Velocity (ft/s)	Time (s)	Energy (ft lbf)
Brittle Fracture	3.462E+3	2.273E-2	1.782E+1	9.300E-5	3.959E+0
End of Signal	1.670E+1	2.846E-2	1.780E+1	1.200E-4	4.562E+0

Sample ID: Bf1-2

Impact V2.1

Summary Report

Sample ID

BF1-5

Material Description

NMP-2 3-Degree Surveillance Capsule - Base material

Test Parameter	Value
Operator	Dr. Michael P. Manahan, Sr.
Date Tested	11/28/00 2:58 PM
Temperature	-38.00 °C
Oscilloscope	Model 441 Internal
Striker Name	8mm - Striker 16
Interpolation Method	Point-Point Linear
TO 892 Controller	Active Adjust
Sample Type	Metal
Sample Size	Type A
Orientation	TL
Notch Type	V Notch, no Side-Groove
Length	2.1654 in
Width	0.3937 in
Thickness	0.3937 in
Span	1.5748 in
Uncracked Ligament	0.3150 in
Notch Radius	0.0098 in
Velocity Determination	Potential Energy & Losses
Velocity	17.94 ft/s
Shear	10.30 %
Lateral Expansion	NaN in
Energy Adjustment	1.2821

Measured Data (V)

Oscilloscope Signal

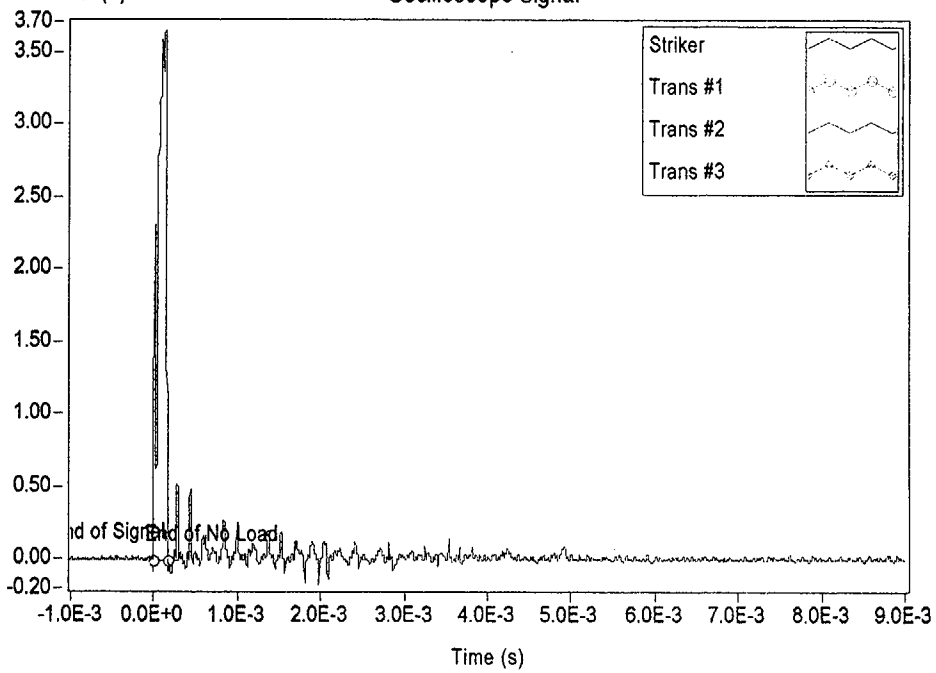

Result	Value
Optical Encoder Energy	9.7543 ft lbf
Dial Gage Energy	9.900 ft lbf
Instrumented Striker Energy	9.7543 ft lbf

Impact V2.1

Integration Report

Signal Source: 8mm - Striker 16 Striker

Load (lbf) vs. Time (s)

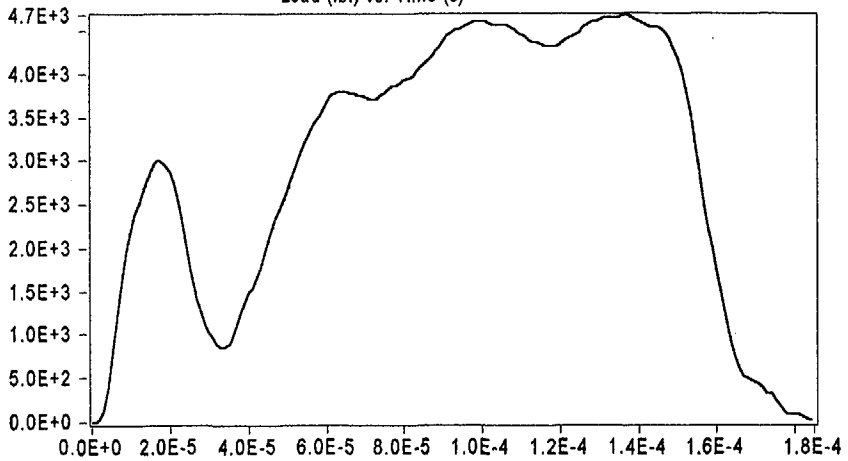

Velocity (ft/s) vs. Time (s)

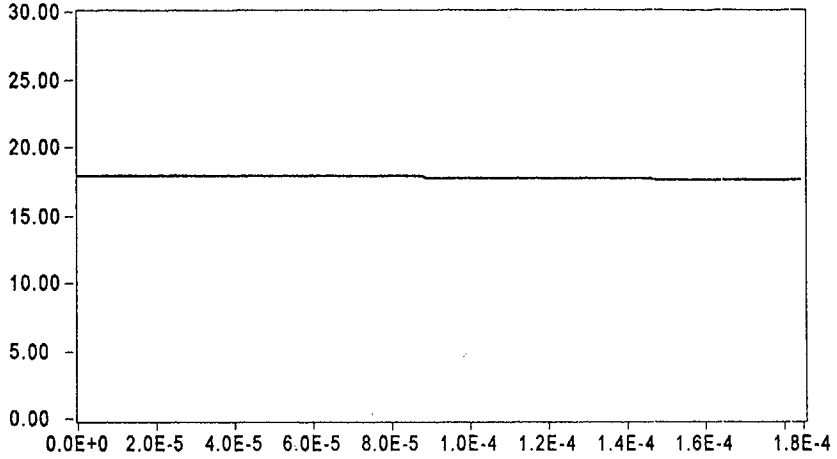

Displacement (in) vs. Time (s)

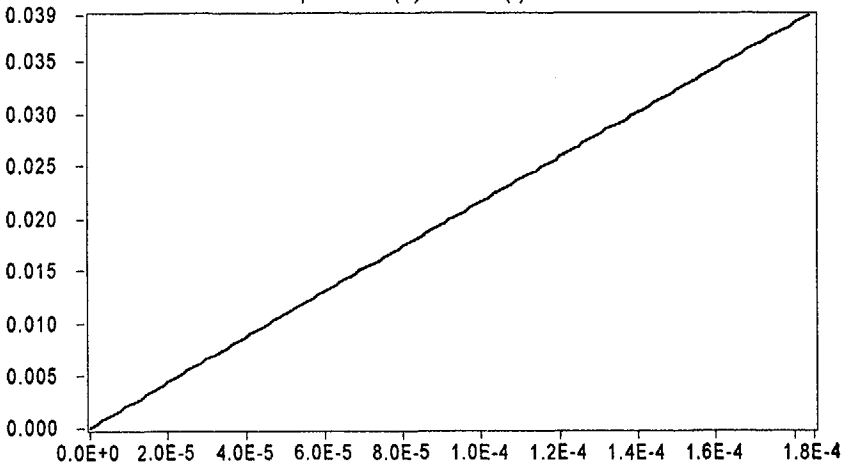

Load (lbf), Energy (ft lbf) vs. Displacement (in)

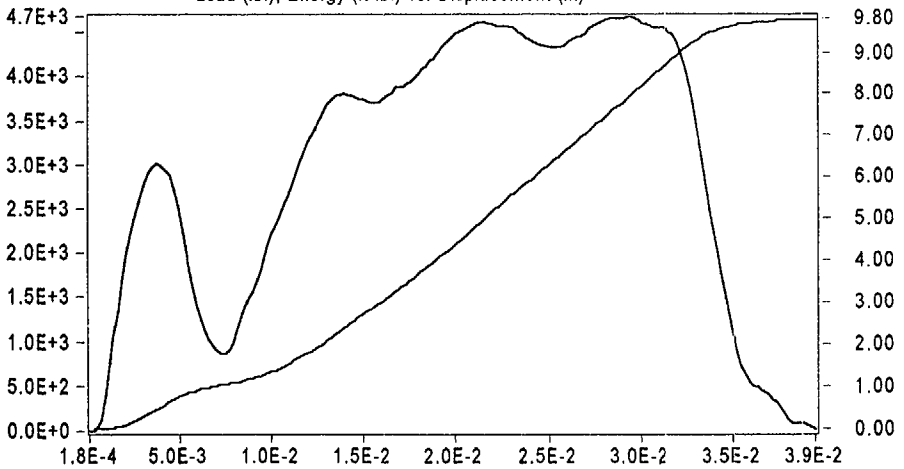

Sample Name: Bf1-5

Instrumented Striker Energy: 9.7543 ft lbf

Impact V2.1

Load vs. Displacement Critical Points

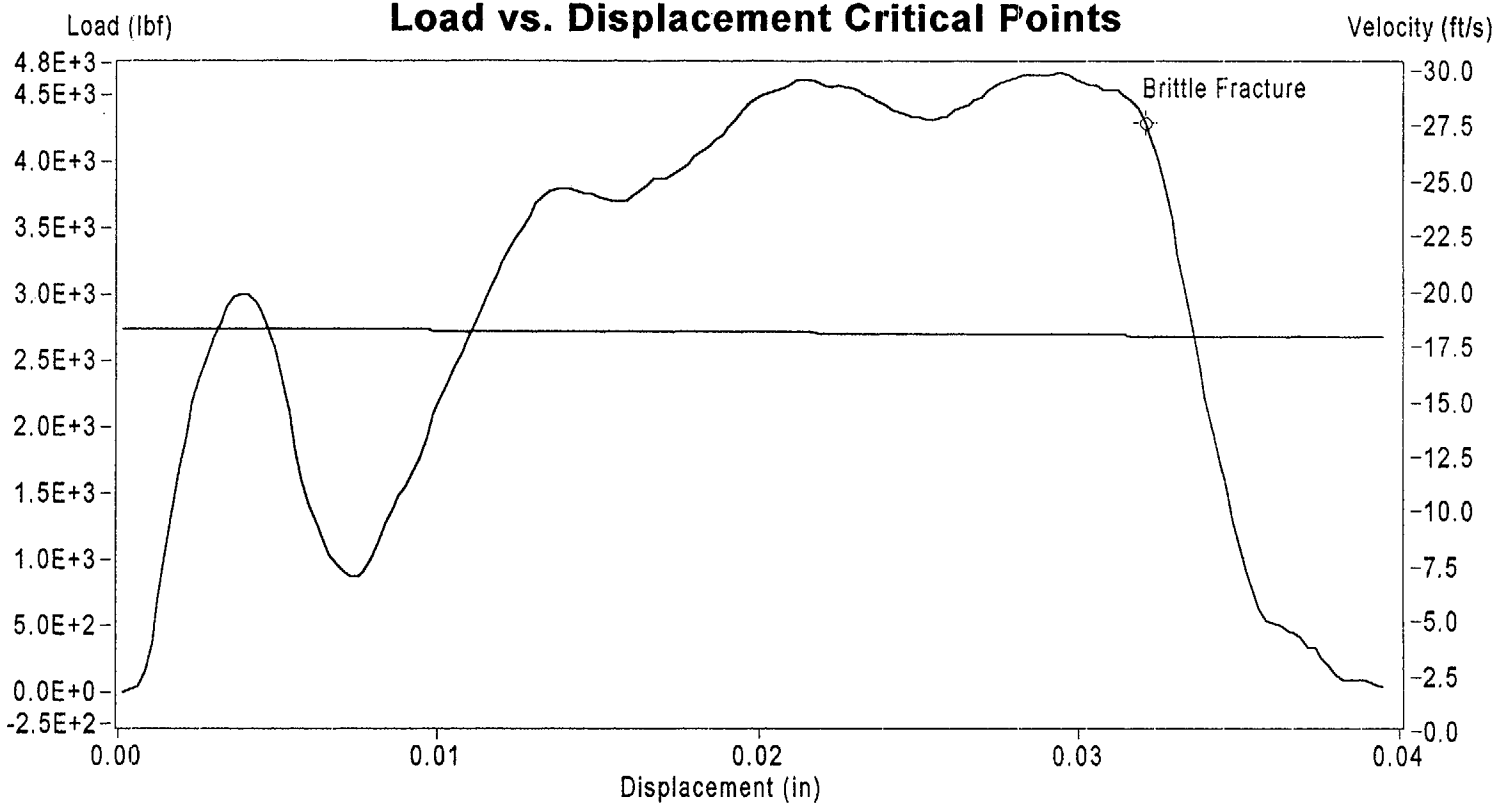

	Load (lbf)	Displacement (in)	Velocity (ft/s)	Time (s)	Energy (ft lbf)
Brittle Fracture	4.312E+3	3.206E-2	1.767E+1	1.430E-4	8.979E+0
End of Signal	2.308E+1	3.944E-2	1.765E+1	1.780E-4	9.754E+0

Sample ID: Bf1-5

Impact V2.1

Summary Report

Sample ID

BF1

Material Description

NMP-2 3-Degree Surveillance Capsule - Base material

Test Parameter	Value
Operator	Dr. Michael P. Manahan, Sr.
Date Tested	11/28/00 2:39 PM
Temperature	-35.00 °C
Oscilloscope	Model 441 Internal
Striker Name	8mm - Striker 16
Interpolation Method	Point-Point Linear
TO 892 Controller	Active Adjust
Sample Type	Metal
Sample Size	Type A
Orientation	TL
Notch Type	V Notch, no Side-Groove
Length	2.1654 in
Width	0.3937 in
Thickness	0.3937 in
Span	1.5748 in
Uncracked Ligament	0.3150 in
Notch Radius	0.0098 in
Velocity Determination	Potential Energy & Losses
Velocity	17.94 ft/s
Shear	17.20 %
Lateral Expansion	0.0188 in
Energy Adjustment	1.0421

Measured Data (V)

Oscilloscope Signal

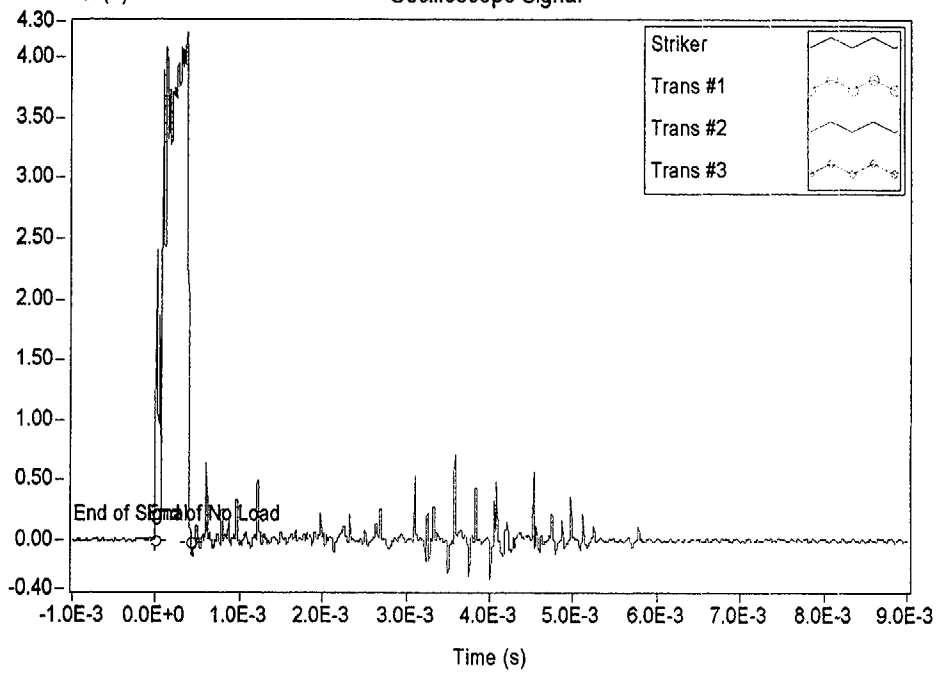

Result	Value
Optical Encoder Energy	**23.116 ft lbf**
Dial Gage Energy	**23.30 ft lbf**
Instrumented Striker Energy	**23.116 ft lbf**

Impact V2.1

Integration Report

Signal Source: 8mm - Striker 16 Striker

Load (lbf) vs. Time (s)

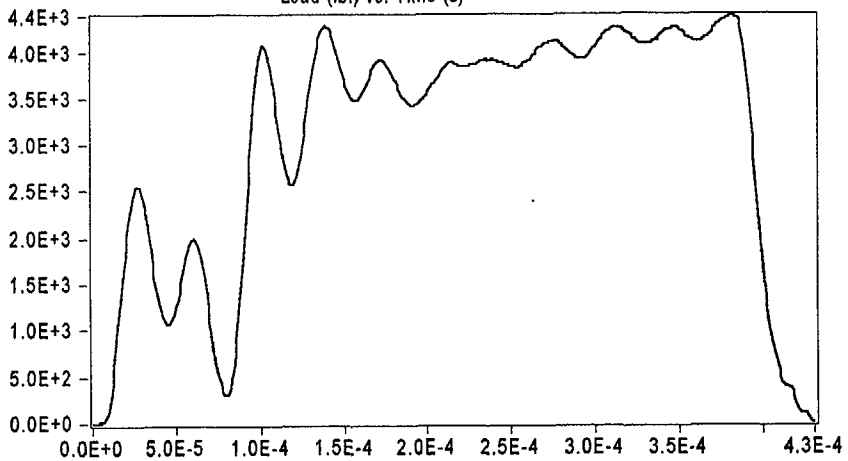

Velocity (ft/s) vs. Time (s)

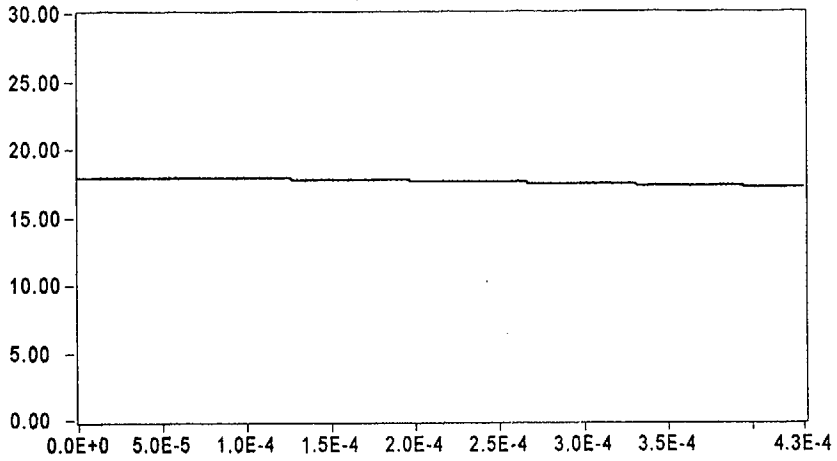

Displacement (in) vs. Time (s)

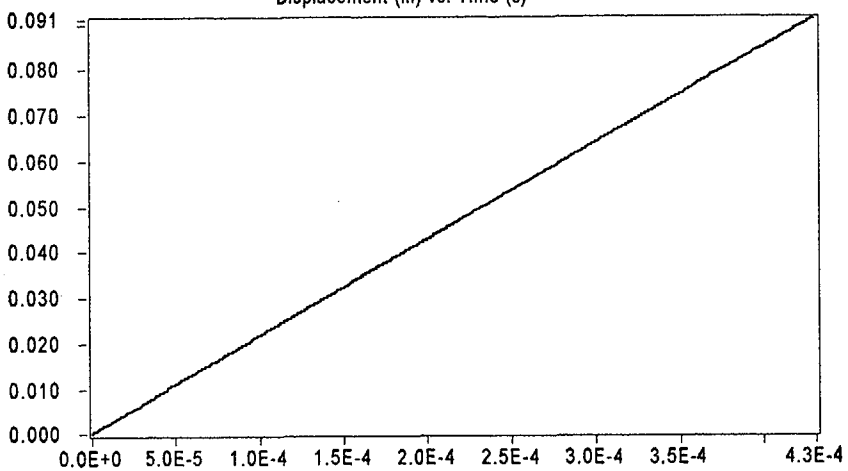

Load (lbf), Energy (ft lbf) vs. Displacement (in)

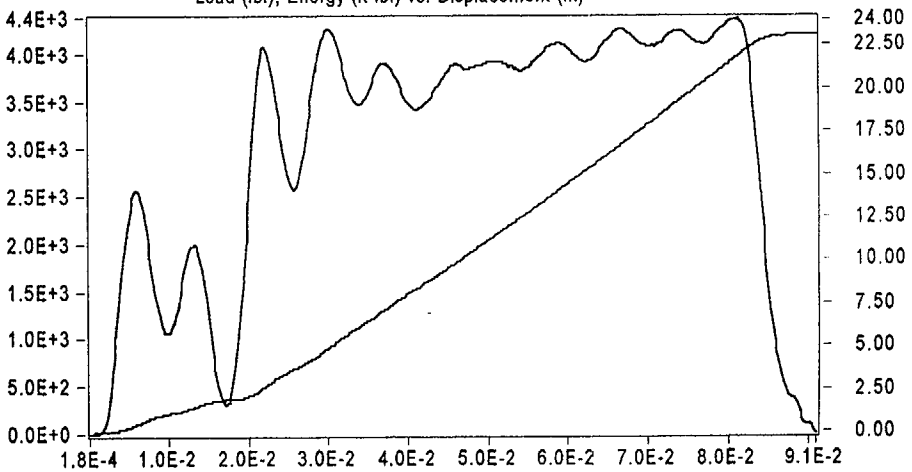

Sample Name: Bf1

Instrumented Striker Energy: 23.116 ft lbf

Impact V2.1

Load vs. Displacement Critical Points

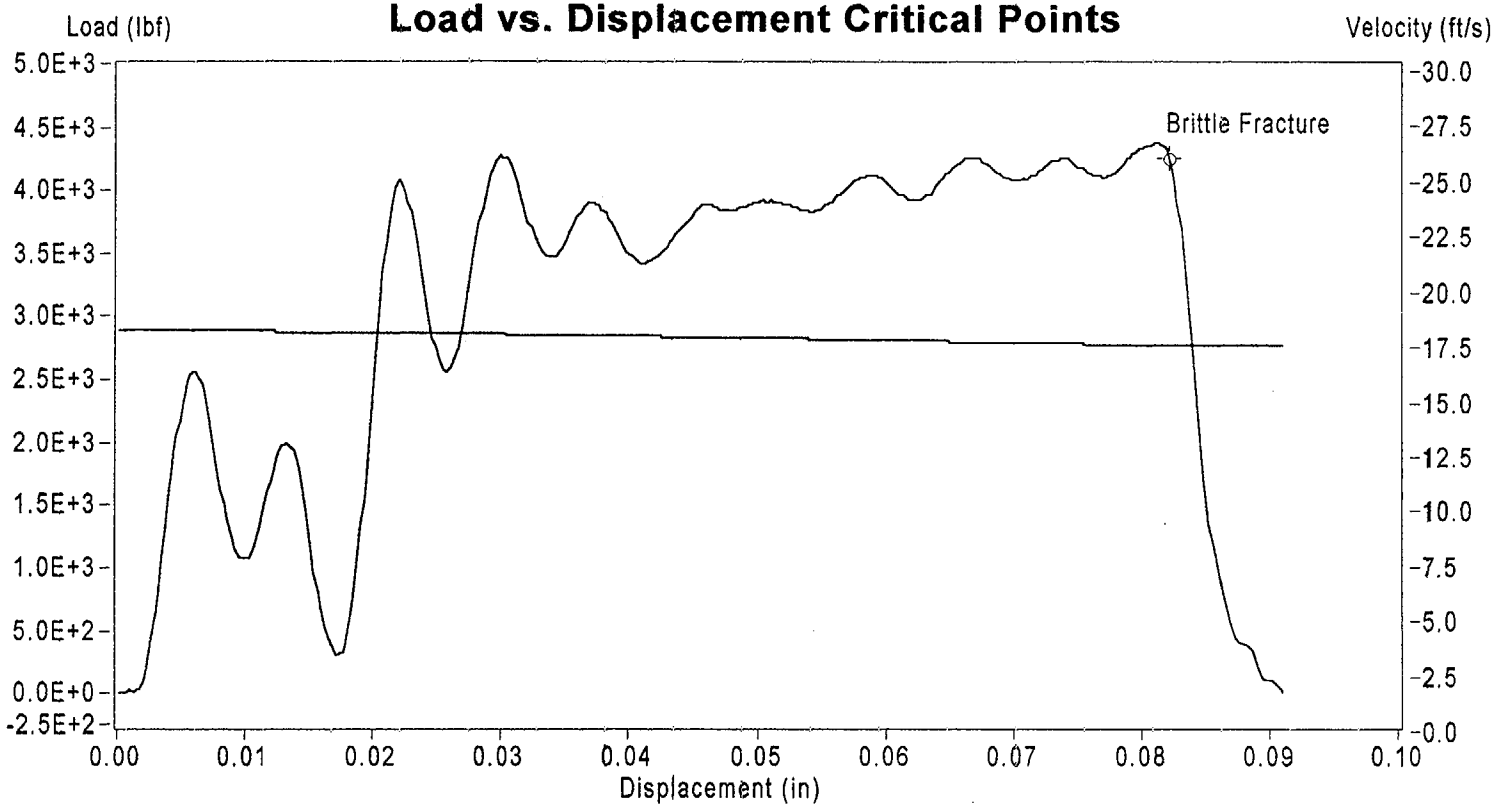

	Load (lbf)	Displacement (in)	Velocity (ft/s)	Time (s)	Energy (ft lbf)
Brittle Fracture	4.260E+3	8.220E-2	1.727E+1	3.730E-4	2.219E+1
End of Signal	7.250E+0	9.106E-2	1.724E+1	4.160E-4	2.312E+1

Sample ID: Bf1

Impact V2.1

Summary Report

Sample ID

BF1-4

Material Description

NMP-2 3-Degree Surveillance Capsule - Base material

Test Parameter	Value
Operator	Dr. Michael P. Manahan, Sr.
Date Tested	11/28/00 2:04 PM
Temperature	-8.00 °C
Oscilloscope	Model 441 Internal
Striker Name	8mm - Striker 16
Interpolation Method	Point-Point Linear
TO 892 Controller	Active Adjust
Sample Type	Metal
Sample Size	Type A
Orientation	TL
Notch Type	V Notch, no Side-Groove
Length	2.1654 in
Width	0.3937 in
Thickness	0.3937 in
Span	1.5748 in
Uncracked Ligament	0.3150 in
Notch Radius	0.0098 in
Velocity Determination	Potential Energy & Losses
Velocity	17.94 ft/s
Shear	30.30 %
Lateral Expansion	0.0290 in
Energy Adjustment	1.1272

Measured Data (V)

Oscilloscope Signal

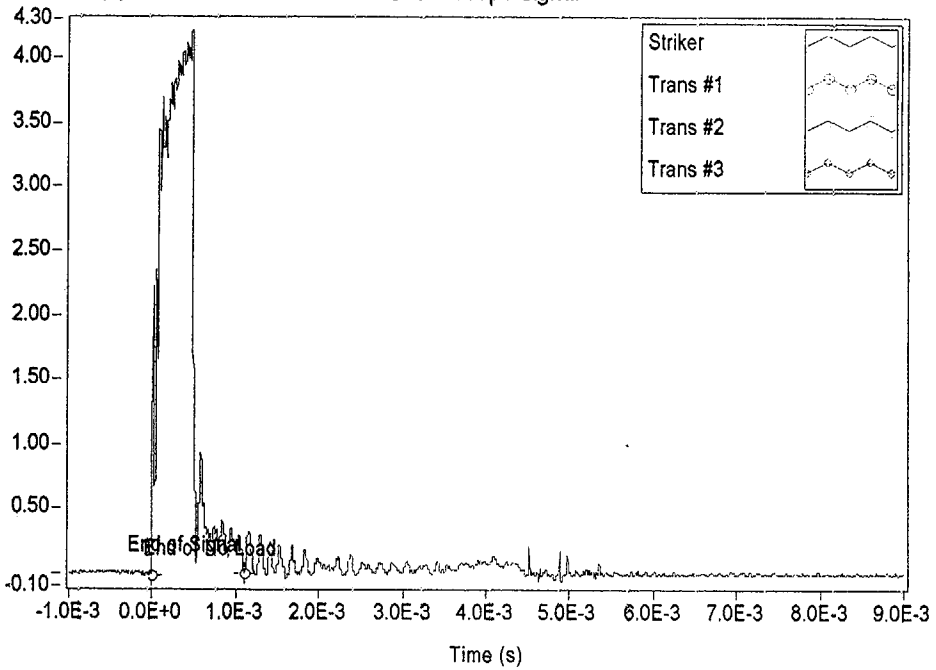

Result	Value
Optical Encoder Energy	37.159 ft lbf
Dial Gage Energy	37.20 ft lbf
Instrumented Striker Energy	37.159 ft lbf

Impact V2.1

Integration Report

Signal Source: 8mm - Striker 16 Striker

Load (lbf) vs. Time (s)

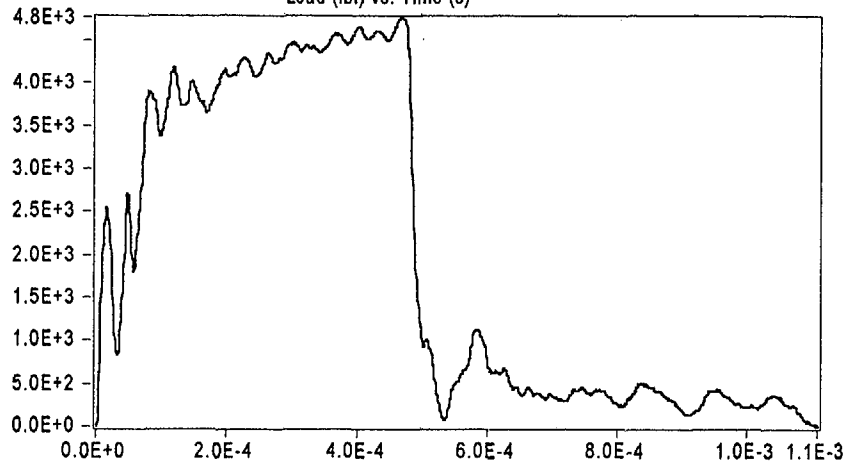

Velocity (ft/s) vs. Time (s)

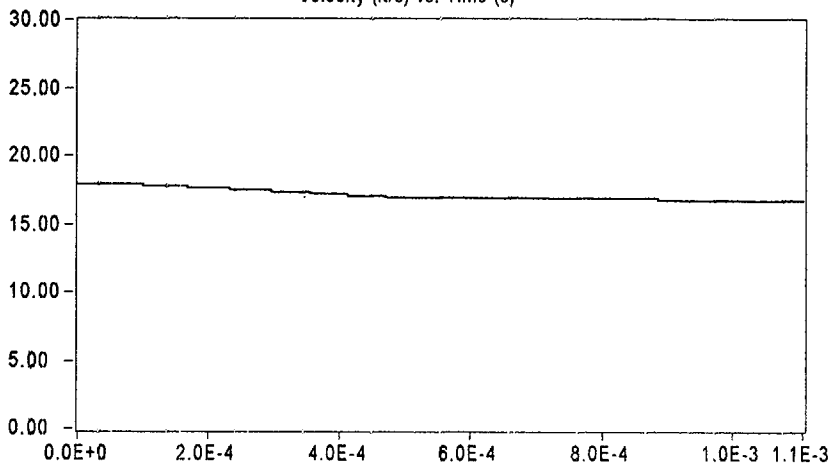

Displacement (in) vs. Time (s)

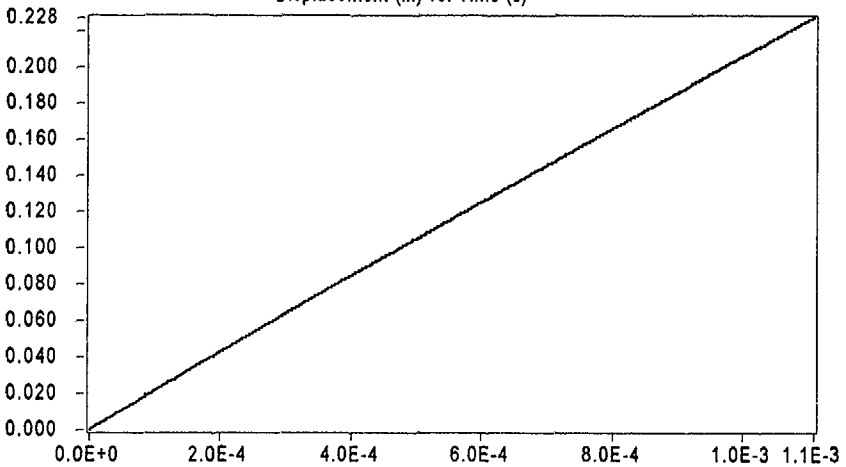

Load (lbf), Energy (ft lbf) vs. Displacement (in)

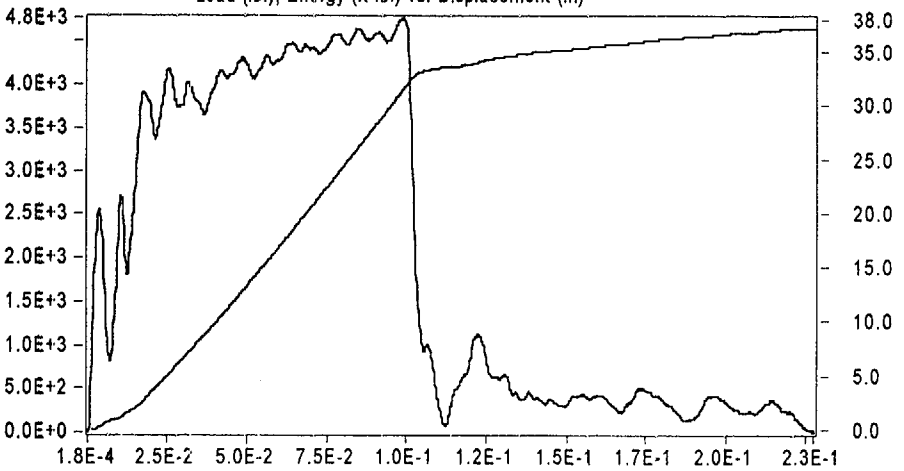

Sample Name: Bf1-4

Instrumented Striker Energy: 37.159 ft lbf

Impact V2.1

Load vs. Displacement Critical Points

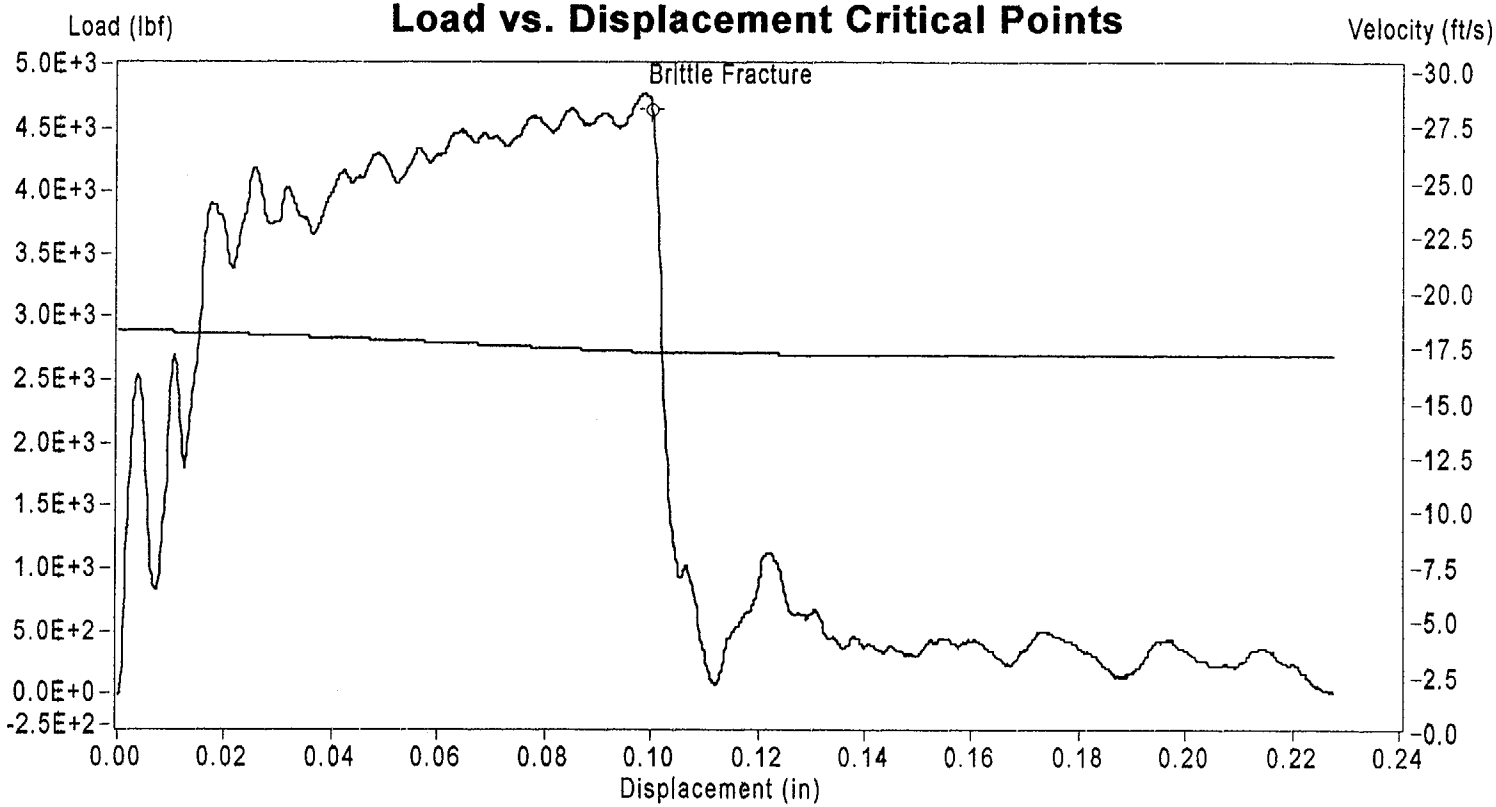

	Load (lbf)	Displacement (in)	Velocity (ft/s)	Time (s)	Energy (ft lbf)
Brittle Fracture	4.650E+3	1.002E-1	1.696E+1	4.710E-4	3.221E+1
End of Signal	2.521E+0	2.276E-1	1.680E+1	1.101E-3	3.716E+1

Sample ID: Bf1-4

Impact V2.1

Summary Report

Sample ID

BF1-6

Material Description

NMP-2 3-Degree Surveillance Capsule - Base material

Test Parameter	Value
Operator	Dr. Michael P. Manahan, Sr.
Date Tested	11/28/00 2:13 PM
Temperature	-7.00 °C
Oscilloscope	Model 441 Internal
Striker Name	8mm - Striker 16
Interpolation Method	Point-Point Linear
TO 892 Controller	Active Adjust
Sample Type	Metal
Sample Size	Type A
Orientation	TL
Notch Type	V Notch, no Side-Groove
Length	2.1654 in
Width	0.3937 in
Thickness	0.3937 in
Span	1.5748 in
Uncracked Ligament	0.3150 in
Notch Radius	0.0098 in
Velocity Determination	Potential Energy & Losses
Velocity	17.94 ft/s
Shear	34.90 %
Lateral Expansion	0.0275 in
Energy Adjustment	1.0642

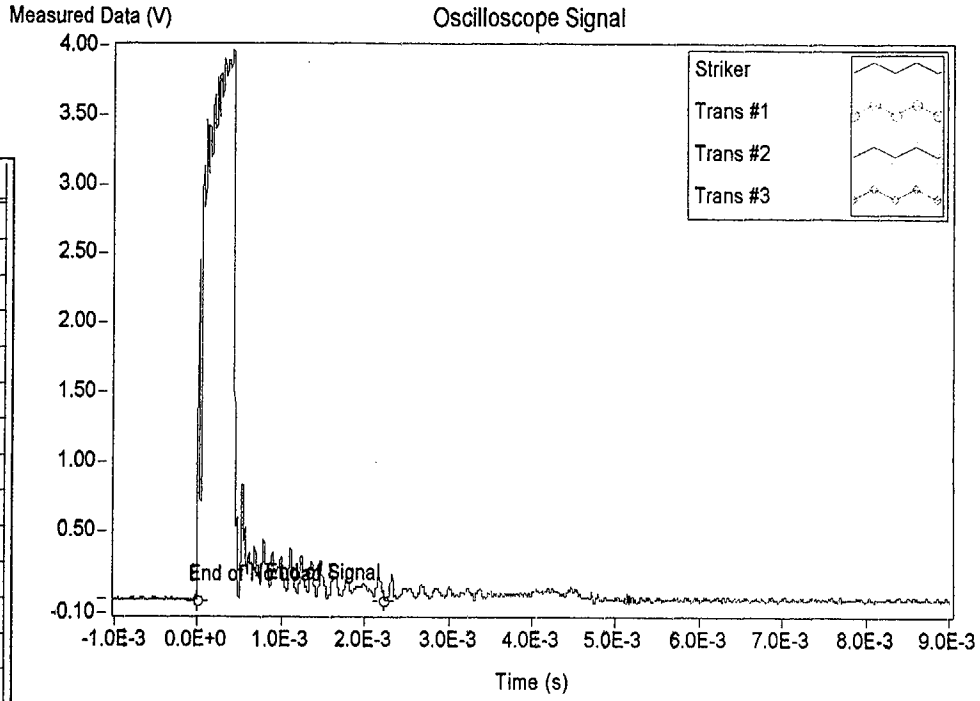

Result	Value
Optical Encoder Energy	33.180 ft lbf
Dial Gage Energy	33.40 ft lbf
Instrumented Striker Energy	33.180 ft lbf

Impact V2.1

Integration Report

Signal Source: 8mm - Striker 16 Striker

Load (lbf) vs. Time (s)

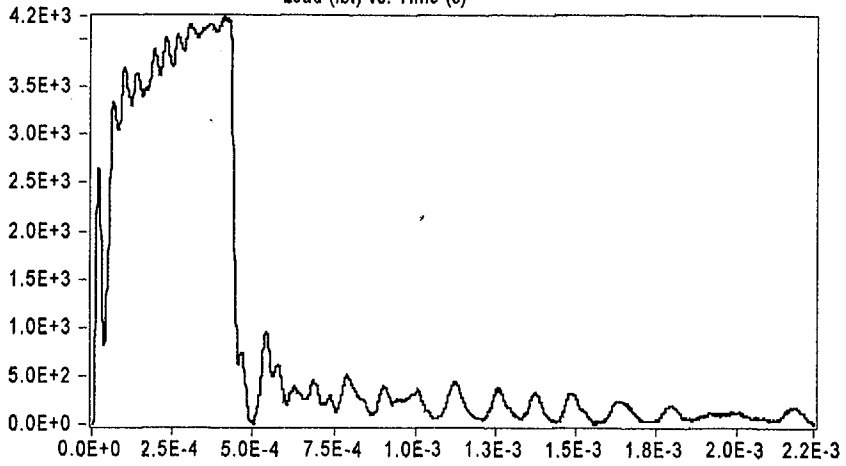

Velocity (ft/s) vs. Time (s)

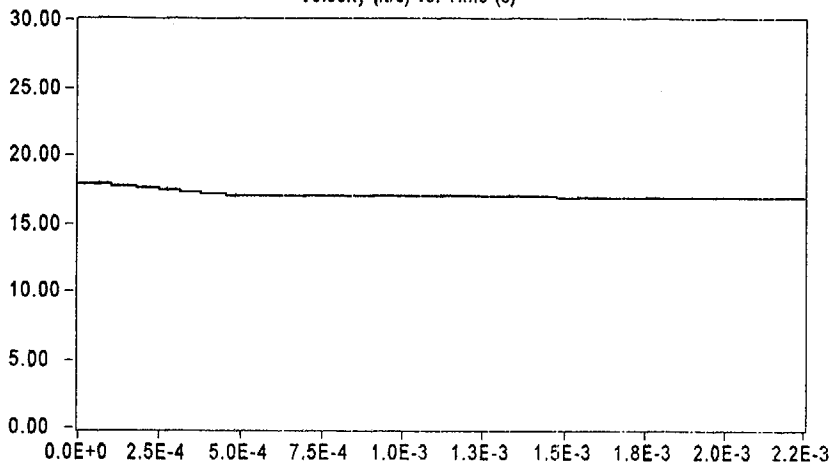

Displacement (in) vs. Time (s)

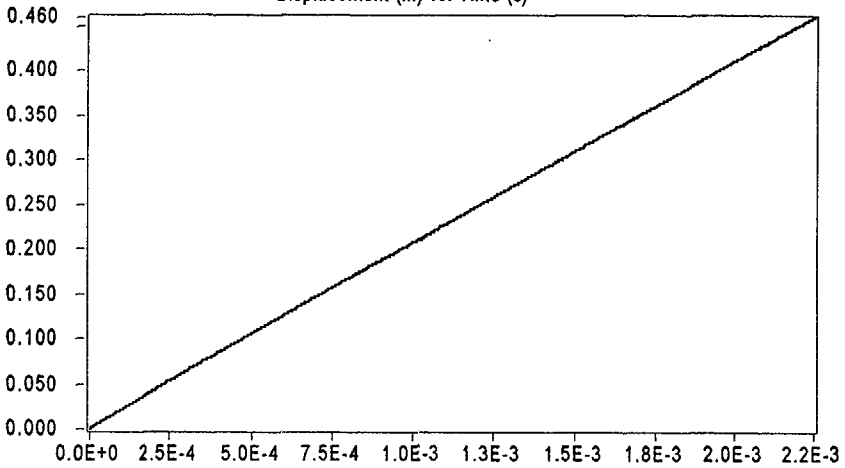

Load (lbf), Energy (ft lbf) vs. Displacement (in)

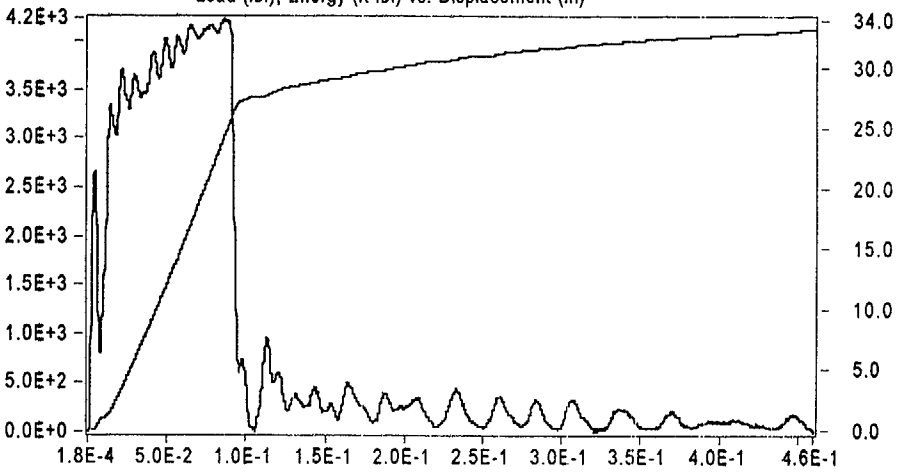

Sample Name: Bf1-6

Instrumented Striker Energy: 33.180 ft lbf

Impact V2.1

Load vs. Displacement Critical Points

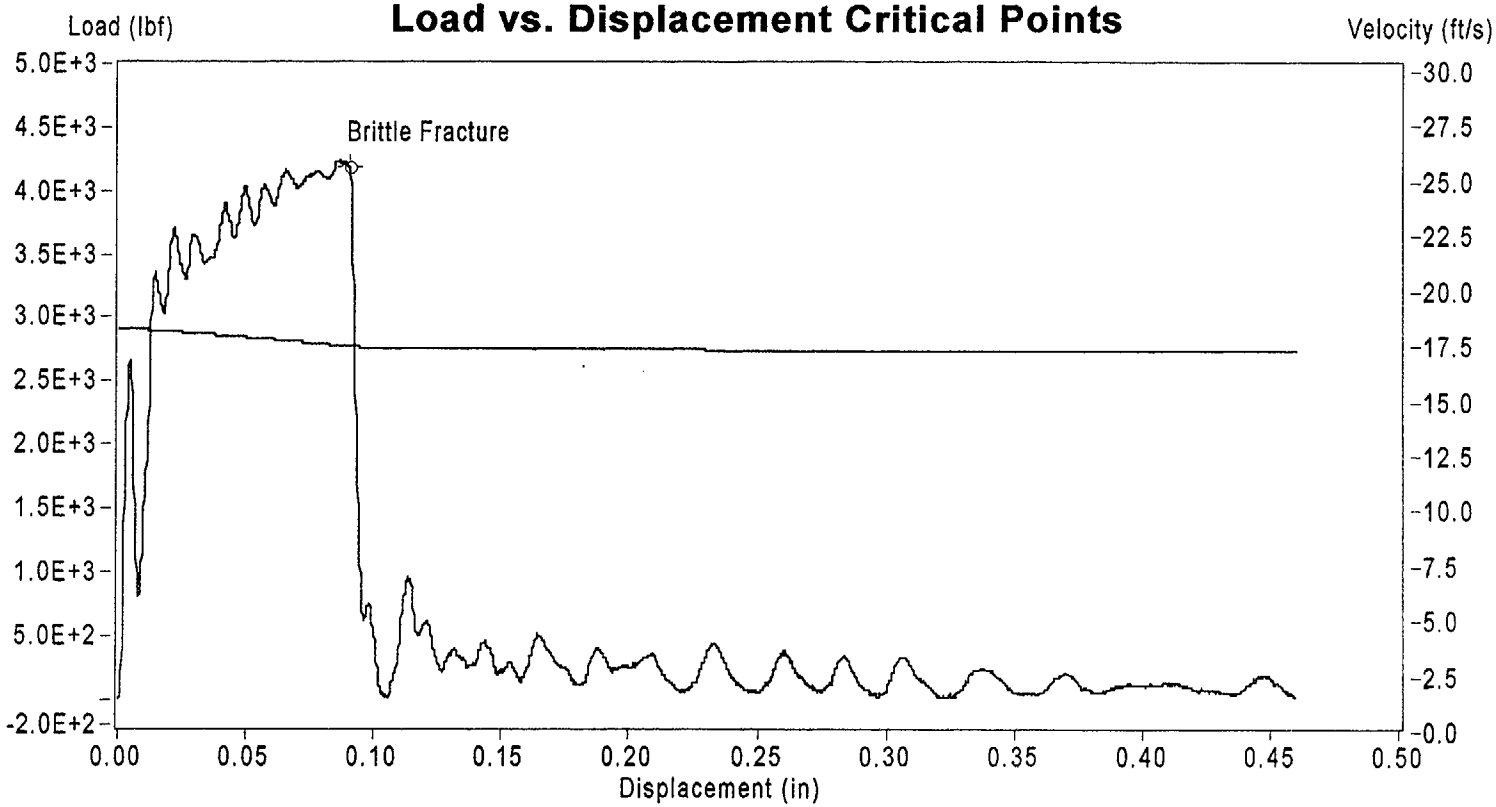

	Load (lbf)	Displacement (in)	Velocity (ft/s)	Time (s)	Energy (ft lbf)
Brittle Fracture	4.187E+3	8.988E-2	1.715E+1	4.170E-4	2.611E+1
End of Signal	1.877E+1	4.598E-1	1.693E+1	2.231E-3	3.318E+1

Sample ID: Bf1-6

Impact V2.1

Summary Report

Sample ID

BF1-10

Material Description

NMP-2 3-Degree Surveillance Capsule - Base material

Test Parameter	Value
Operator	Dr. Michael P. Manahan, Sr.
Date Tested	11/28/00 8:44 AM
Temperature	19.00 °C
Oscilloscope	Model 441 Internal
Striker Name	8mm - Striker 16
Interpolation Method	Point-Point Linear
TO 892 Controller	Active Adjust
Sample Type	Metal
Sample Size	Type A
Orientation	TL
Notch Type	V Notch, no Side-Groove
Length	2.1654 in
Width	0.3937 in
Thickness	0.3937 in
Span	1.5748 in
Uncracked Ligament	0.3150 in
Notch Radius	0.0098 in
Velocity Determination	Potential Energy & Losses
Velocity	17.94 ft/s
Shear	52.00 %
Lateral Expansion	0.0430 in
Energy Adjustment	1.0087

Measured Data (V)

Oscilloscope Signal

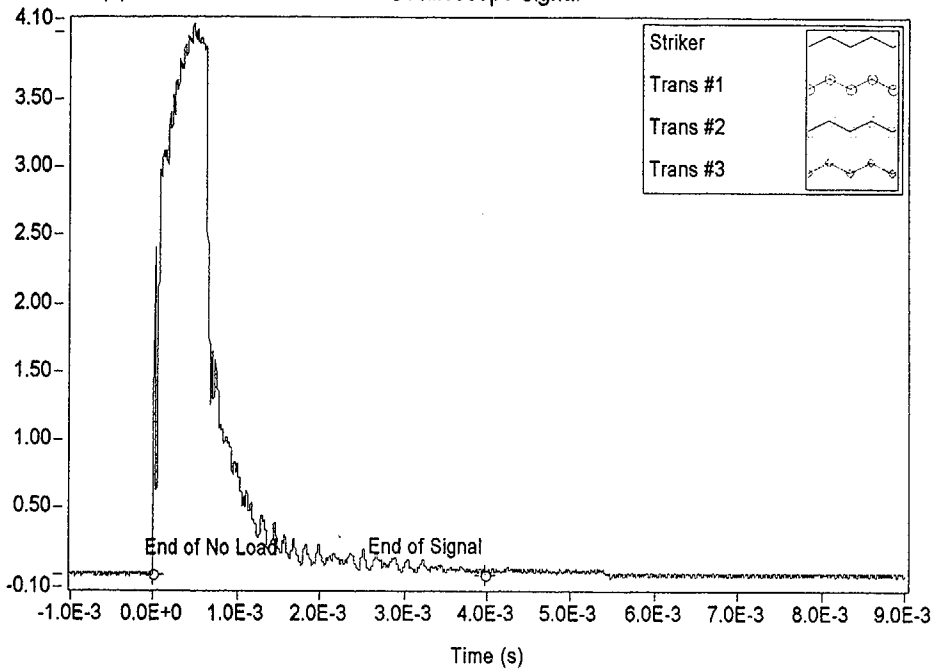

Result	Value
Optical Encoder Energy	**53.284 ft lbf**
Dial Gage Energy	**53.30 ft lbf**
Instrumented Striker Energy	**53.284 ft lbf**

Impact V2.1

Integration Report

Signal Source: 8mm - Striker 16 Striker

Load (lbf) vs. Time (s)

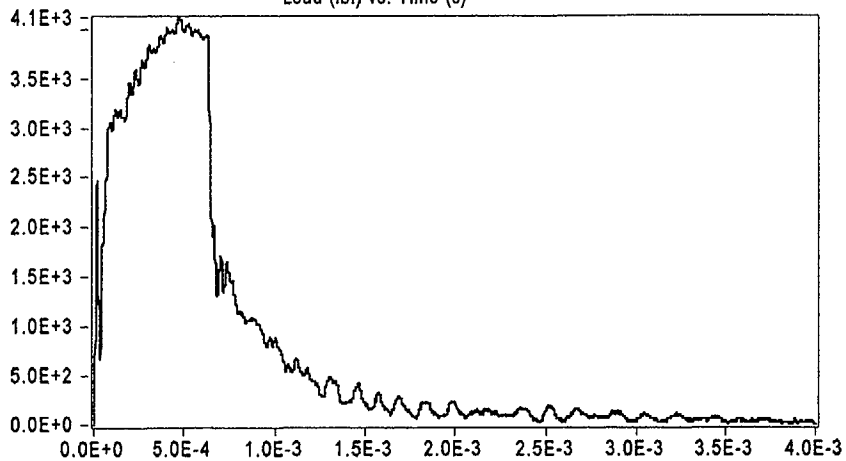

Velocity (ft/s) vs. Time (s)

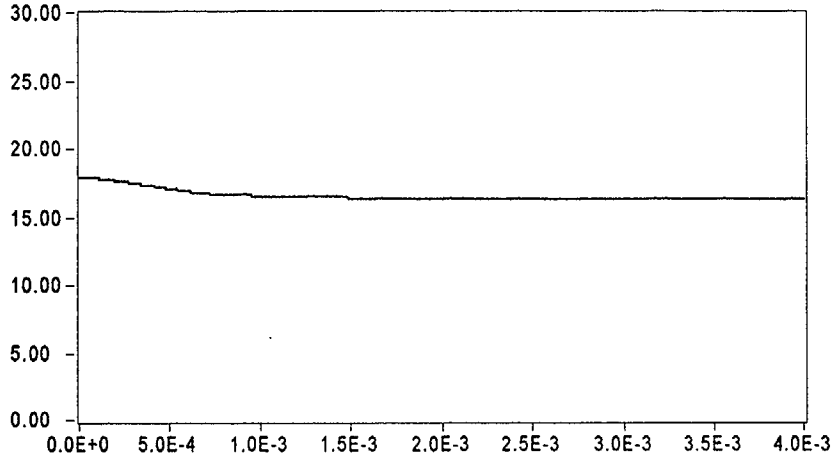

Displacement (in) vs. Time (s)

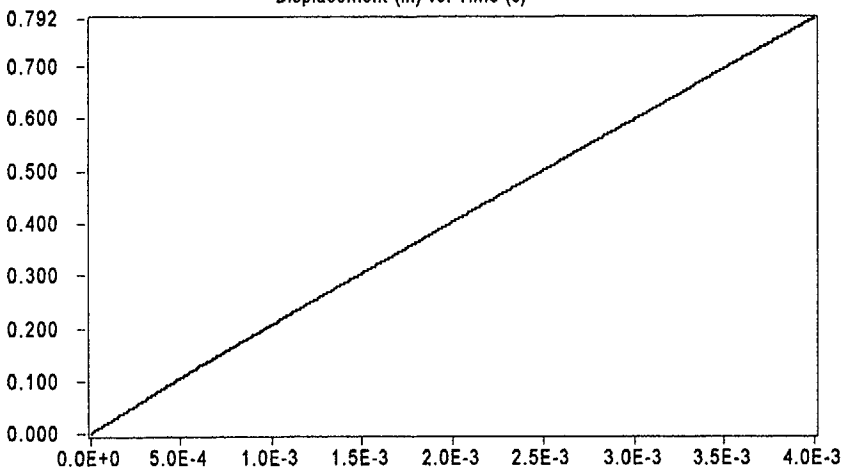

Load (lbf), Energy (ft lbf) vs. Displacement (in)

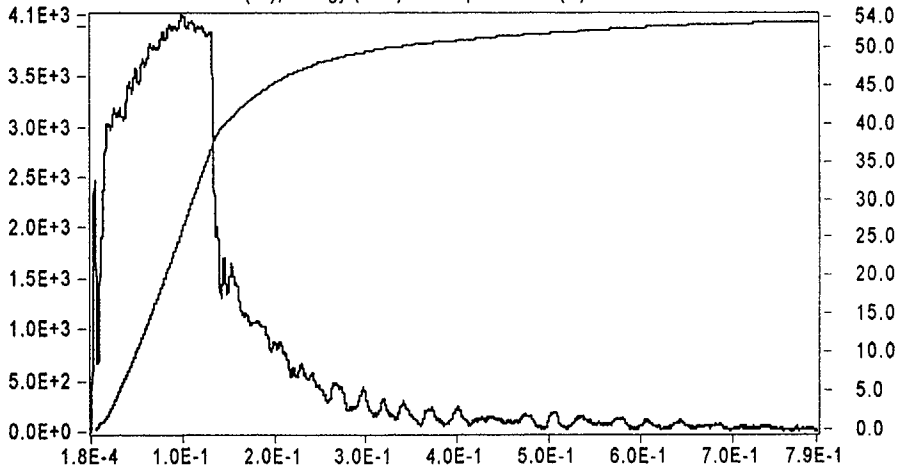

Sample Name: Bf1-10

Instrumented Striker Energy: 53.284 ft lbf

Impact V2.1

Load vs. Displacement Critical Points

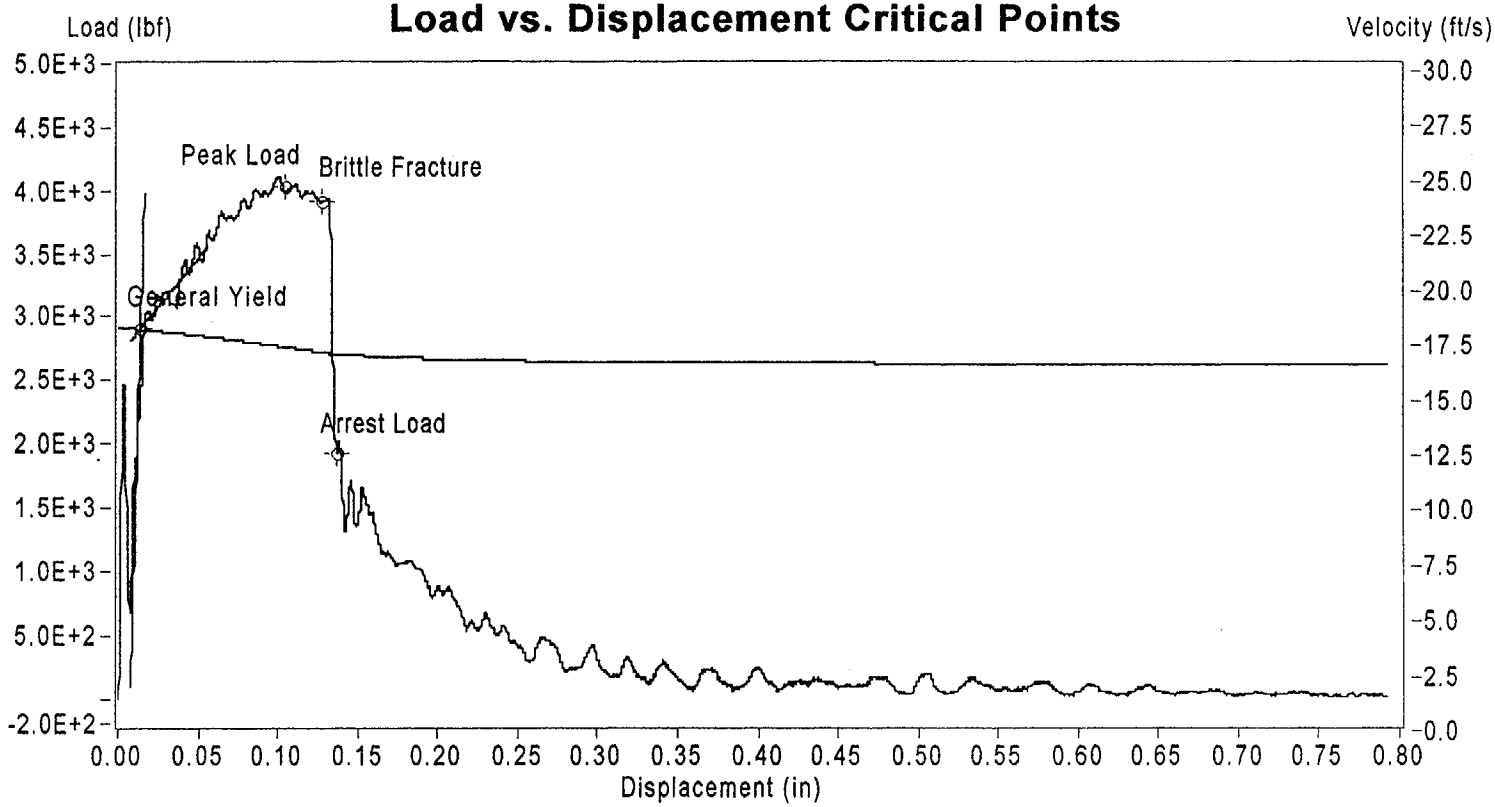

	Load (lbf)	Displacement (in)	Velocity (ft/s)	Time (s)	Energy (ft lbf)
General Yield	2.911E+3	1.434E-2	1.788E+1	5.988E-5	1.873E+0
Peak Load	4.029E+3	1.042E-1	1.707E+1	4.880E-4	2.867E+1
Brittle Fracture	3.912E+3	1.276E-1	1.683E+1	6.030E-4	3.643E+1
Arrest Load	1.917E+3	1.367E-1	1.675E+1	6.480E-4	3.893E+1
End of Signal	4.907E+0	7.924E-1	1.628E+1	3.985E-3	5.328E+1

Sample ID: Bf1-10

Impact V2.1

Summary Report

Sample ID

BF1-12

Material Description

NMP-2 3-Degree Surveillance Capsule - Base material

Test Parameter	Value
Operator	Dr. Michael P. Manahan, Sr.
Date Tested	11/28/00 8:53 AM
Temperature	19.00 °C
Oscilloscope	Model 441 Internal
Striker Name	8mm - Striker 16
Interpolation Method	Point-Point Linear
TO 892 Controller	Active Adjust
Sample Type	Metal
Sample Size	Type A
Orientation	TL
Notch Type	V Notch, no Side-Groove
Length	2.1654 in
Width	0.3937 in
Thickness	0.3937 in
Span	1.5748 in
Uncracked Ligament	0.3150 in
Notch Radius	0.0098 in
Velocity Determination	Potential Energy & Losses
Velocity	17.94 ft/s
Shear	53.00 %
Lateral Expansion	NaN in
Energy Adjustment	1.0071

Measured Data (V)

Oscilloscope Signal

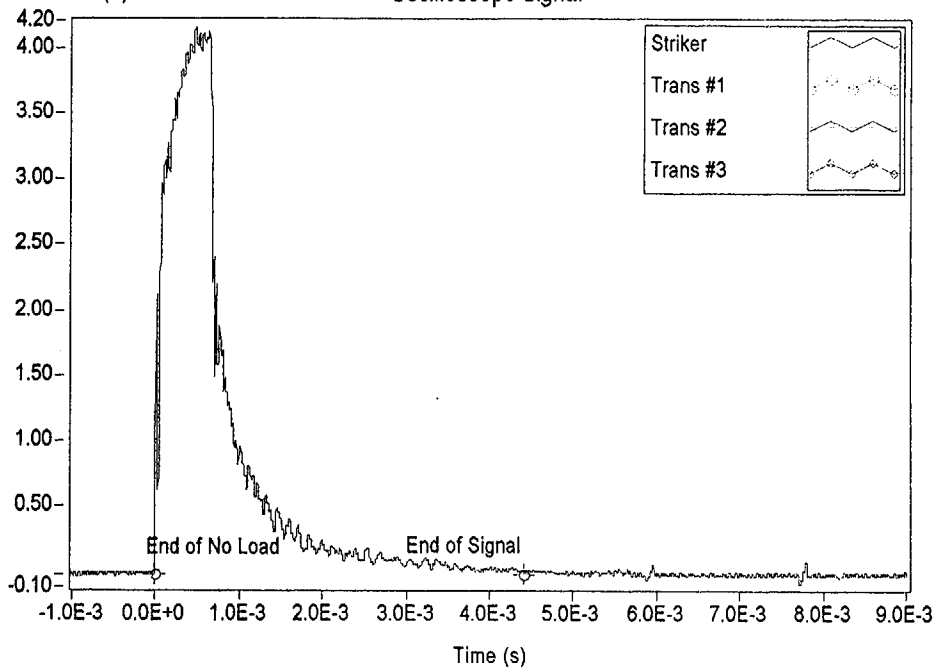

Result	Value
Optical Encoder Energy	60.729 ft lbf
Dial Gage Energy	60.90 ft lbf
Instrumented Striker Energy	60.729 ft lbf

Impact V2.1

Integration Report

Signal Source: 8mm - Striker 16 Striker

Load (lbf) vs. Time (s)

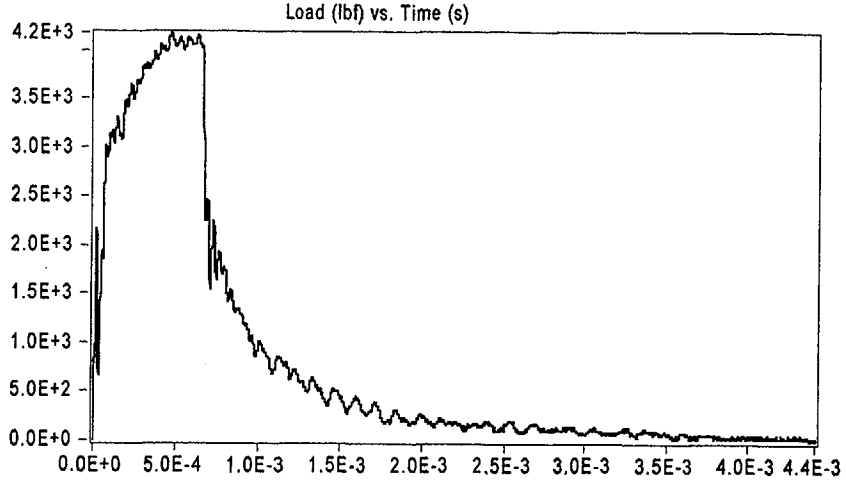

Velocity (ft/s) vs. Time (s)

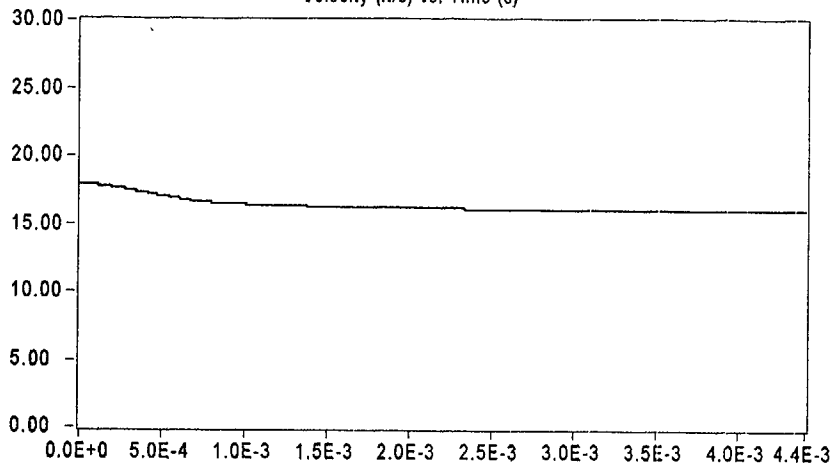

Displacement (in) vs. Time (s)

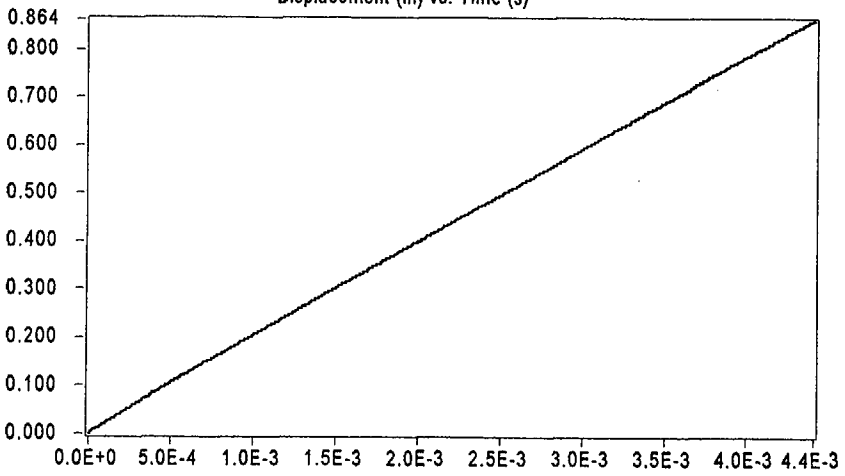

Load (lbf), Energy (ft lbf) vs. Displacement (in)

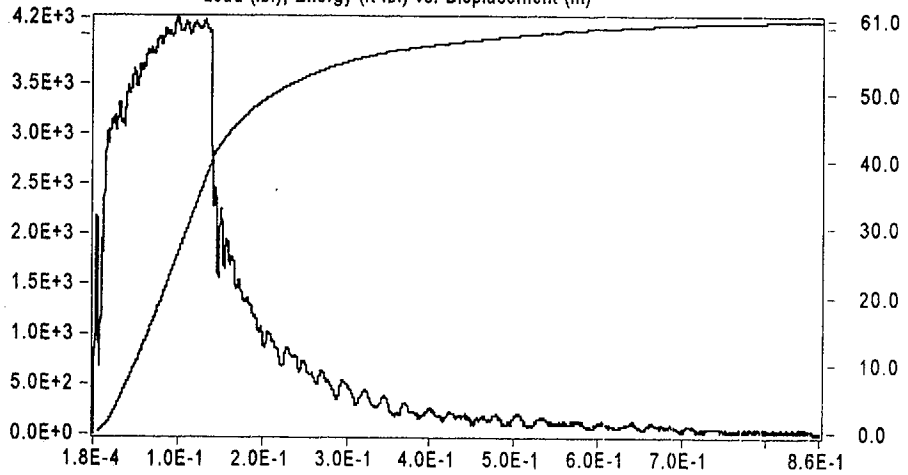

Sample Name: Bf1-12

Instrumented Striker Energy: 60.729 ft lbf

Impact V2.1

Load vs. Displacement Critical Points

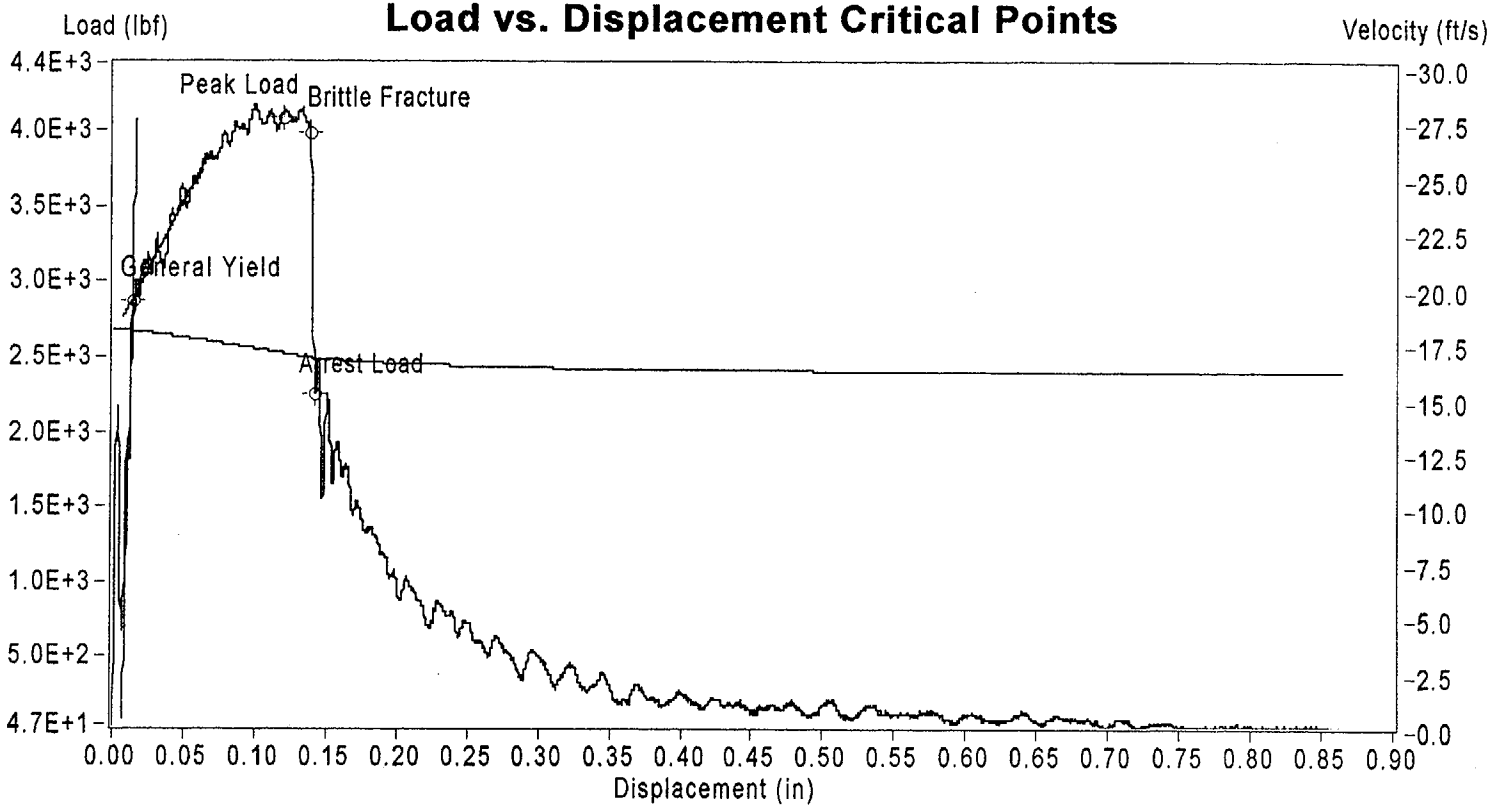

	Load (lbf)	Displacement (in)	Velocity (ft/s)	Time (s)	Energy (ft lbf)
General Yield	2.876E+3	1.327E-2	1.789E+1	5.587E-5	1.642E+0
Peak Load	4.093E+3	1.193E-1	1.690E+1	5.630E-4	3.416E+1
Brittle Fracture	3.986E+3	1.386E-1	1.669E+1	6.590E-4	4.074E+1
Arrest Load	2.260E+3	1.418E-1	1.666E+1	6.750E-4	4.153E+1
End of Signal	5.757E+0	8.641E-1	1.604E+1	4.399E-3	6.073E+1

Sample ID: Bf1-12

Impact V2.1

Summary Report

Sample ID

BF1-7

Material Description

NMP-2 3-Degree Surveillance Capsule - Base material

Test Parameter	Value
Operator	Dr. Michael P. Manahan, Sr.
Date Tested	11/28/00 9:52 AM
Temperature	63.00 °C
Oscilloscope	Model 441 Internal
Striker Name	8mm - Striker 16
Interpolation Method	Point-Point Linear
TO 892 Controller	Active Adjust
Sample Type	Metal
Sample Size	Type A
Orientation	TL
Notch Type	V Notch, no Side-Groove
Length	2.1654 in
Width	0.3937 in
Thickness	0.3937 in
Span	1.5748 in
Uncracked Ligament	0.3150 in
Notch Radius	0.0098 in
Velocity Determination	Potential Energy & Losses
Velocity	17.94 ft/s
Shear	100.00 %
Lateral Expansion	NaN in
Energy Adjustment	1.0219

Measured Data (V)

Oscilloscope Signal

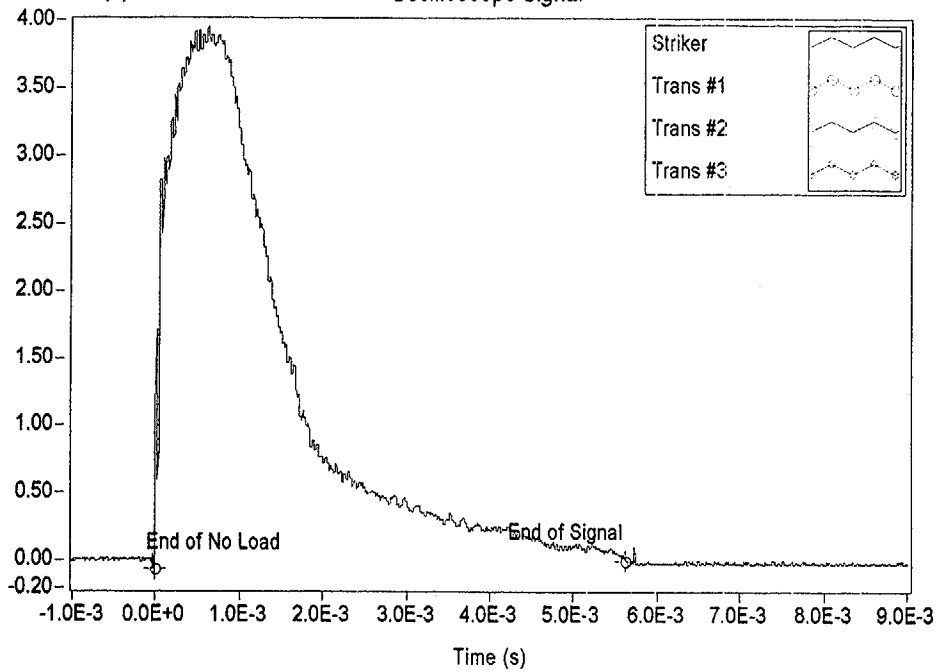

Result	Value
Optical Encoder Energy	107.07 ft lbf
Dial Gage Energy	107.1 ft lbf
Instrumented Striker Energy	107.07 ft lbf

Impact V2.1

Integration Report

Signal Source: 8mm - Striker 16 Striker

Load (lbf) vs. Time (s)

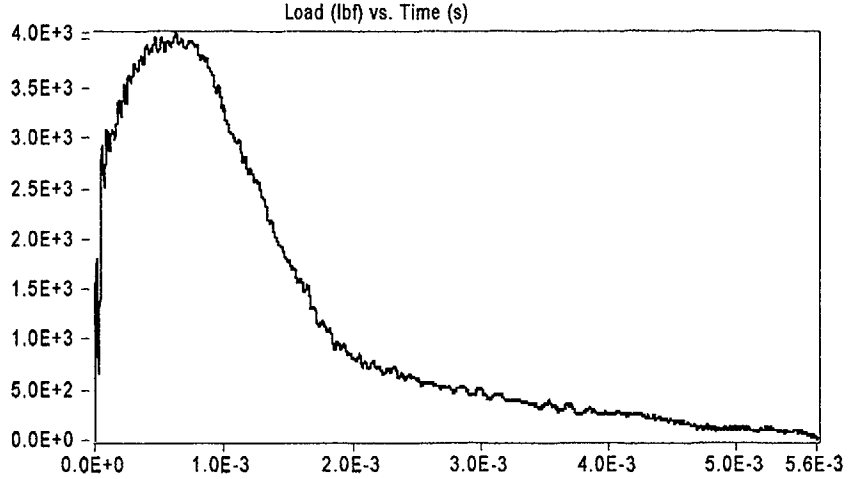

Velocity (ft/s) vs. Time (s)

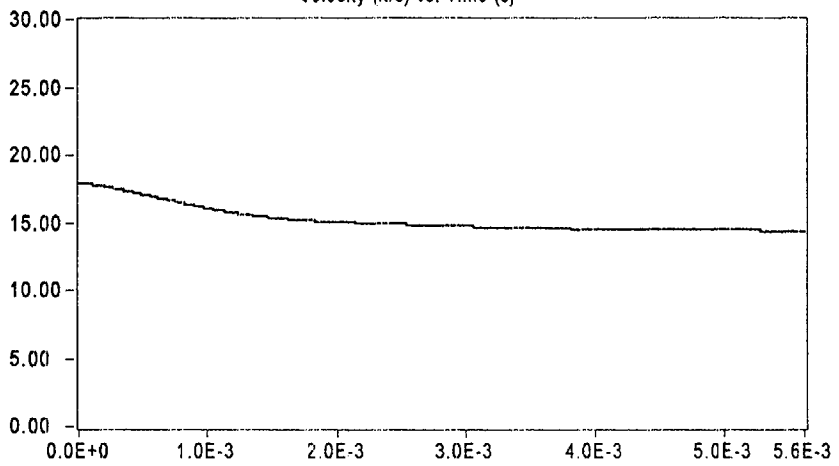

Displacement (in) vs. Time (s)

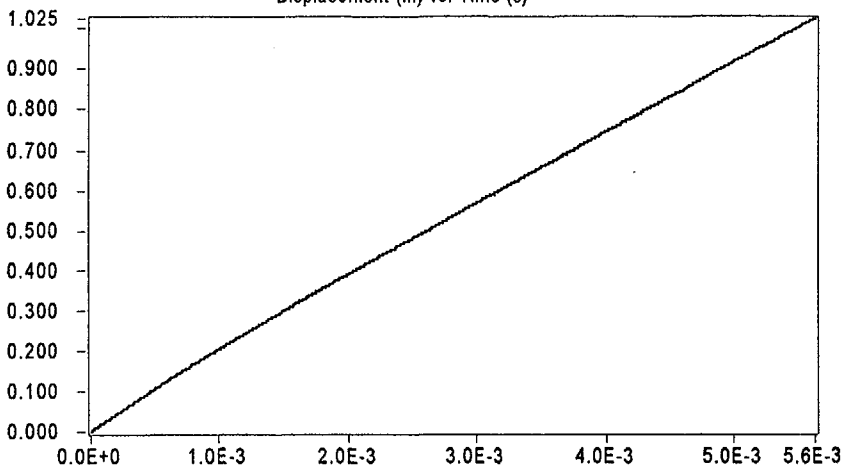

Load (lbf), Energy (ft lbf) vs. Displacement (in)

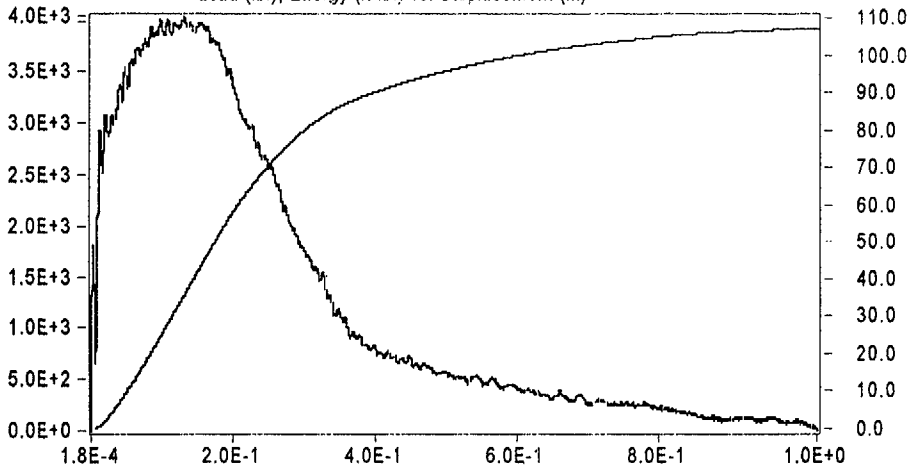

Sample Name: Bf1-7

Instrumented Striker Energy: 107.07 ft lbf

Impact V2.1

Load vs. Displacement Critical Points

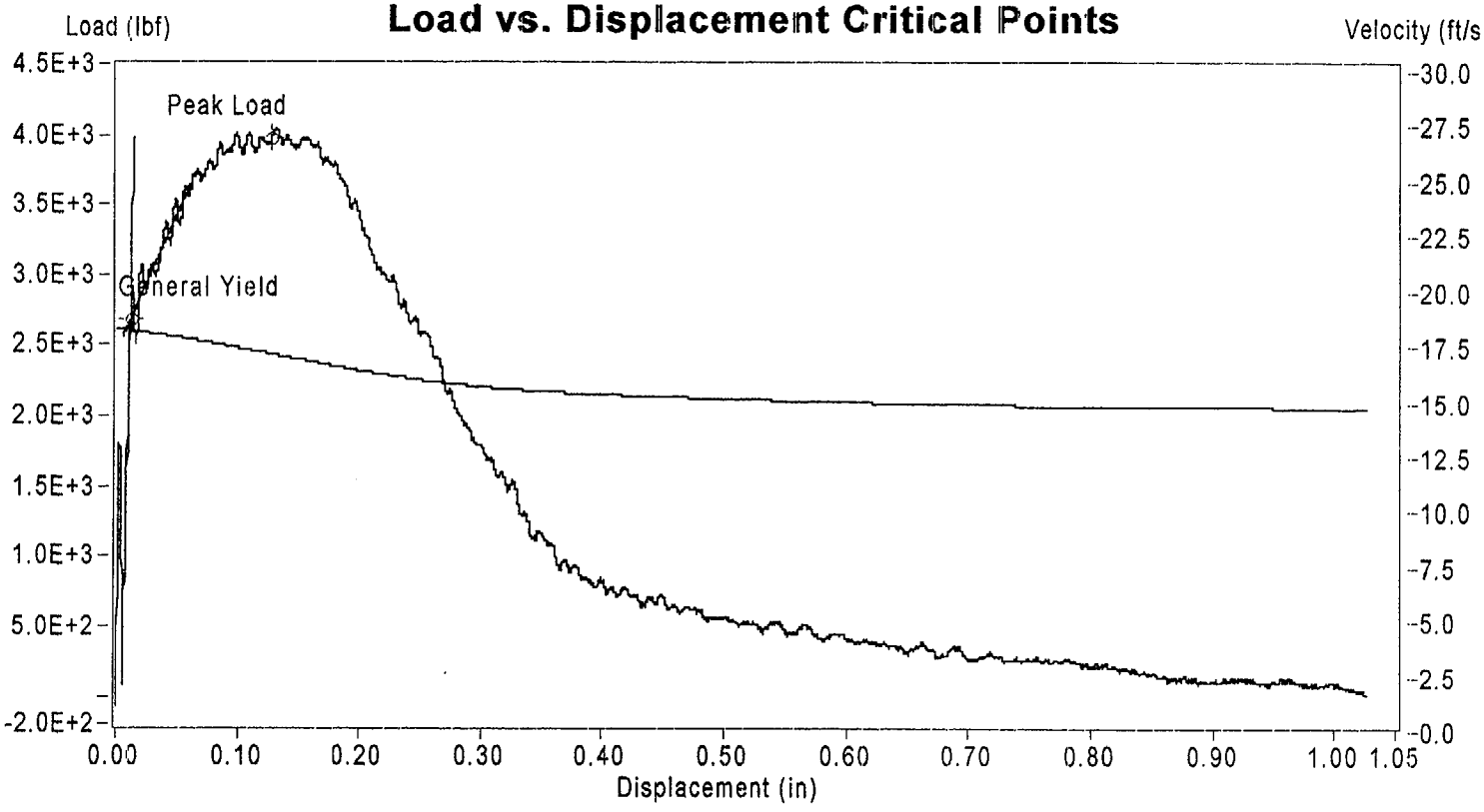

	Load (lbf)	Displacement (in)	Velocity (ft/s)	Time (s)	Energy (ft lbf)
General Yield	2.680E+3	1.133E-2	1.790E+1	4.786E-5	1.311E+0
Peak Load	3.972E+3	1.279E-1	1.684E+1	6.060E-4	3.595E+1
End of Signal	2.534E+0	1.025E+0	1.442E+1	5.614E-3	1.071E+2

Sample ID: Bf1-7

Impact V2.1

Summary Report

Sample ID

BF1-11

Material Description

NMP-2 3-Degree Surveillance Capsule - Base material

Test Parameter	Value
Operator	Dr. Michael P. Manahan, Sr.
Date Tested	11/28/00 10:03 AM
Temperature	63.00 °C
Oscilloscope	Model 441 Internal
Striker Name	8mm - Striker 16
Interpolation Method	Point-Point Linear
TO 892 Controller	Active Adjust
Sample Type	Metal
Sample Size	Type A
Orientation	TL
Notch Type	V Notch, no Side-Groove
Length	2.1654 in
Width	0.3937 in
Thickness	0.3937 in
Span	1.5748 in
Uncracked Ligament	0.3150 in
Notch Radius	0.0098 in
Velocity Determination	Potential Energy & Losses
Velocity	17.94 ft/s
Shear	100.00 %
Lateral Expansion	0.0675 in
Energy Adjustment	1.0245

Measured Data (V)

Oscilloscope Signal

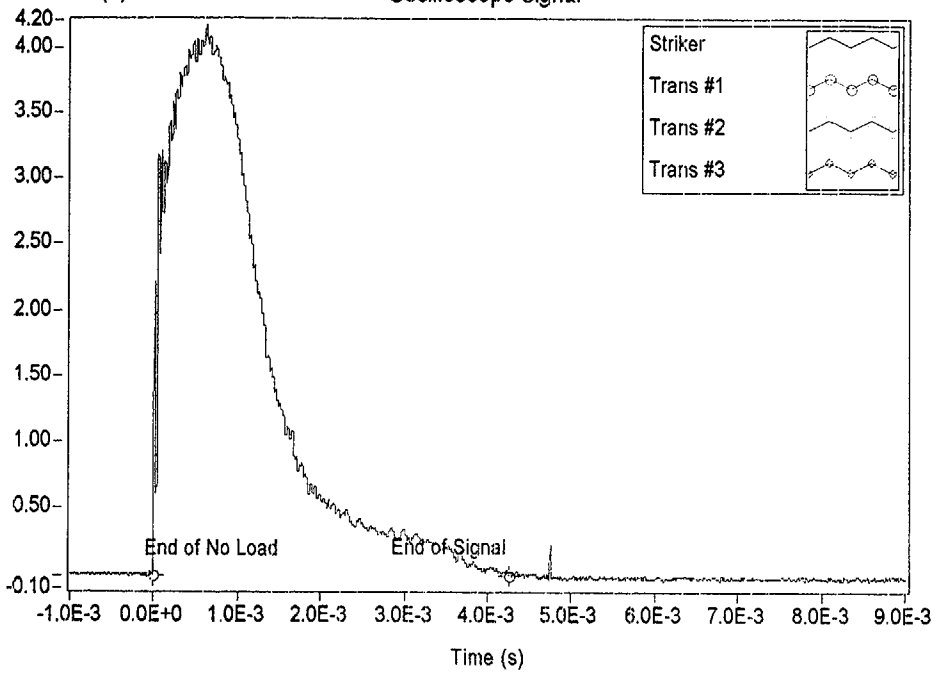

Result	Value
Optical Encoder Energy	97.020 ft lbf
Dial Gage Energy	96.80 ft lbf
Instrumented Striker Energy	97.020 ft lbf

Impact V2.1

Integration Report

Signal Source: 8mm - Striker 16 Striker

Load (lbf) vs. Time (s)

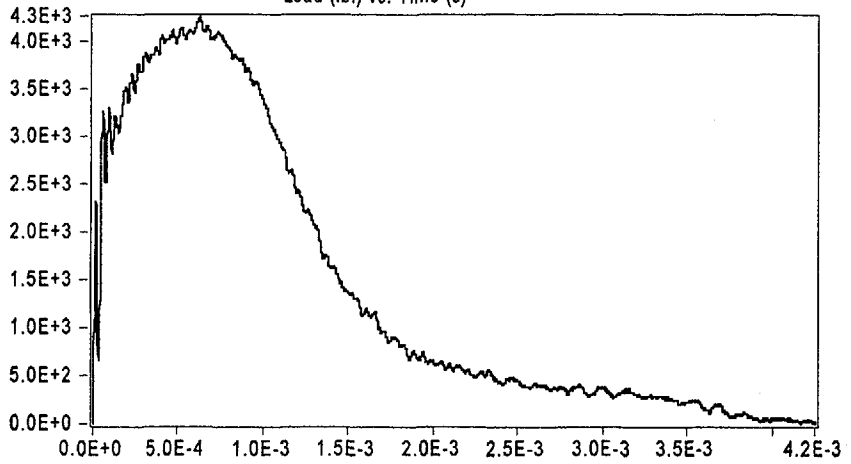

Velocity (ft/s) vs. Time (s)

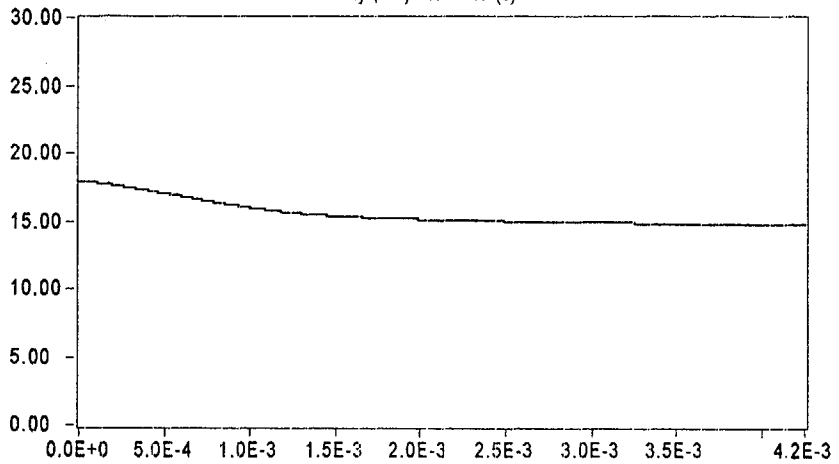

Displacement (in) vs. Time (s)

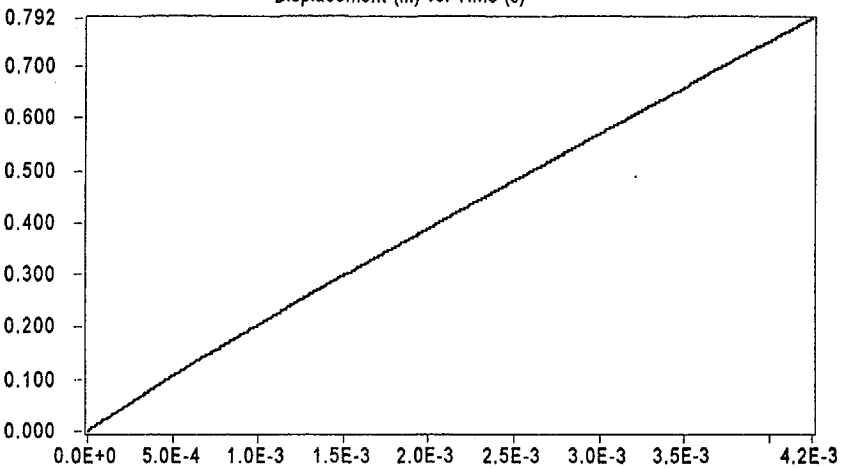

Load (lbf), Energy (ft lbf) vs. Displacement (in)

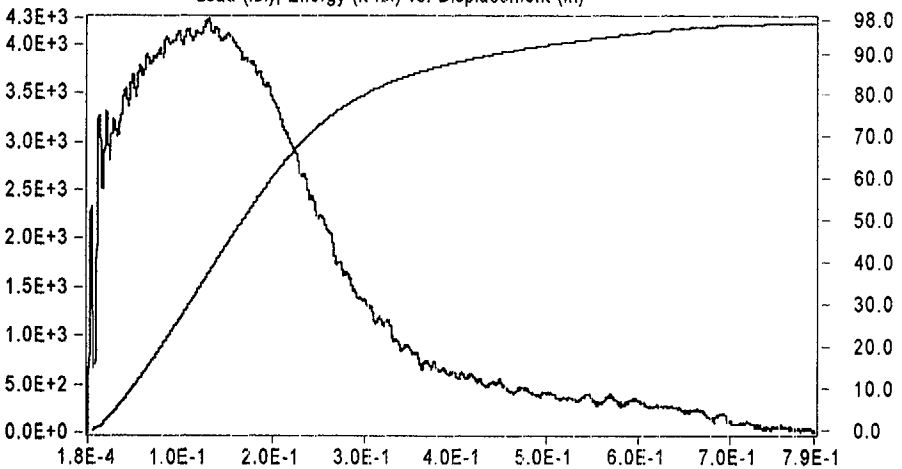

Sample Name: Bf1-11

Instrumented Striker Energy: 97.020 ft lbf

Impact V2.1

Load vs. Displacement Critical Points

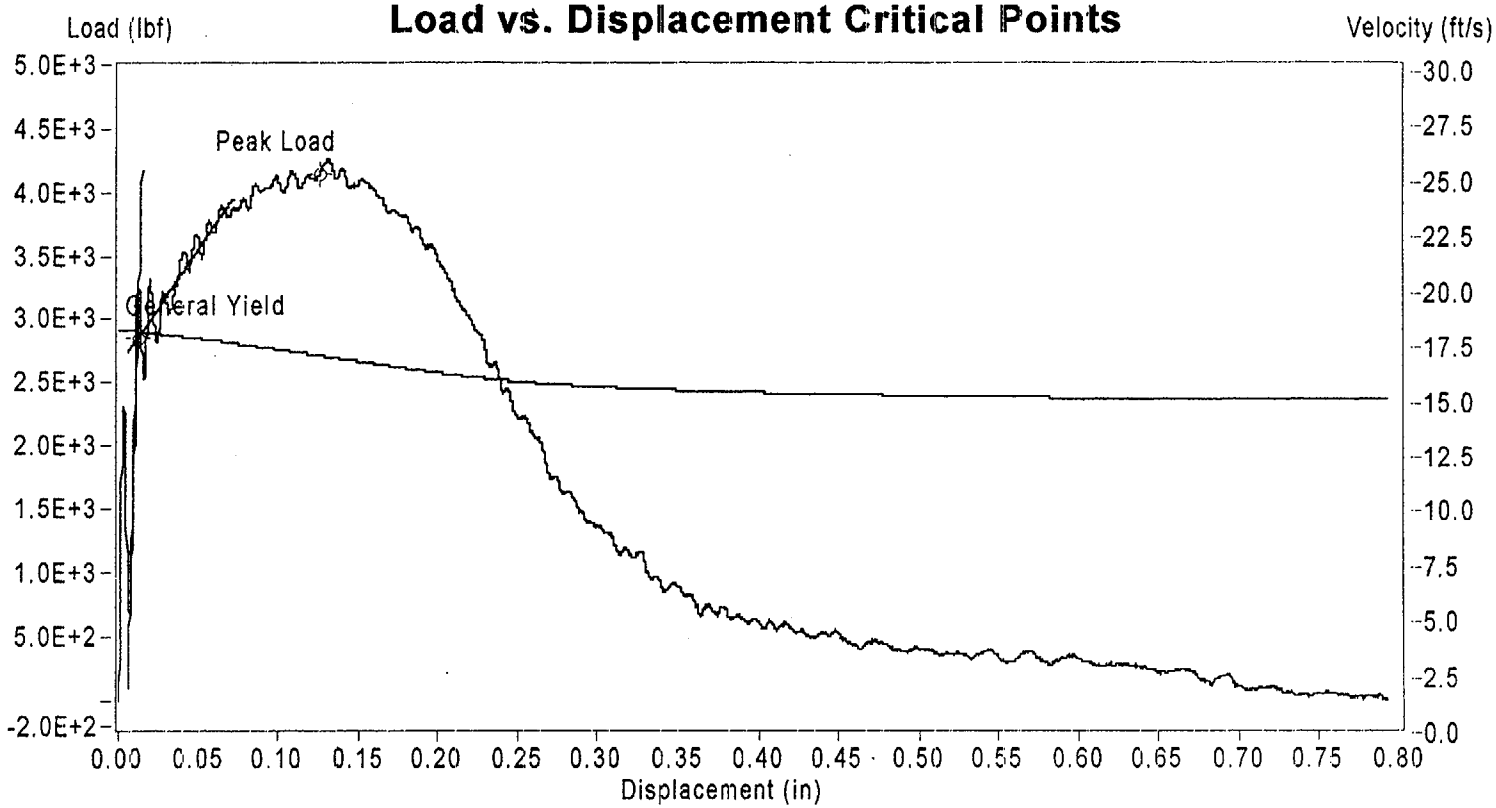

	Load (lbf)	Displacement (in)	Velocity (ft/s)	Time (s)	Energy (ft lbf)
General Yield	2.861E+3	1.198E-2	1.789E+1	4.987E-5	1.625E+0
Peak Load	4.143E+3	1.255E-1	1.682E+1	5.940E-4	3.662E+1
End of Signal	1.378E+0	7.917E-1	1.479E+1	4.243E-3	9.702E+1

Sample ID: Bf1-11

Impact V2.1

Summary Report

Sample ID

BF1-3

Material Description

NMP-2 3-Degree Surveillance Capsule - Base material

Test Parameter	Value
Operator	Dr. Michael P. Manahan, Sr.
Date Tested	11/28/00 10:49 AM
Temperature	122.00 °C
Oscilloscope	Model 441 Internal
Striker Name	8mm - Striker 16
Interpolation Method	Point-Point Linear
TO 892 Controller	Active Adjust
Sample Type	Metal
Sample Size	Type A
Orientation	TL
Notch Type	V Notch, no Side-Groove
Length	2.1654 in
Width	0.3937 in
Thickness	0.3937 in
Span	1.5748 in
Uncracked Ligament	0.3150 in
Notch Radius	0.0098 in
Velocity Determination	Potential Energy & Losses
Velocity	17.94 ft/s
Shear	100.00 %
Lateral Expansion	0.0675 in
Energy Adjustment	1.0186

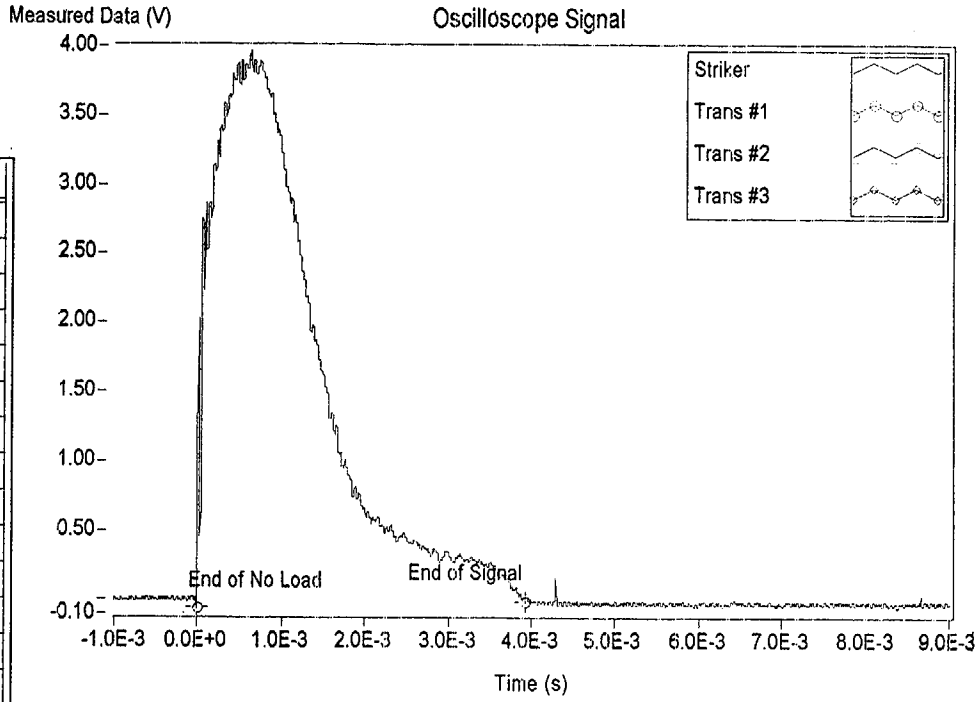

Result	Value
Optical Encoder Energy	**97.854 ft lbf**
Dial Gage Energy	**97.80 ft lbf**
Instrumented Striker Energy	**97.854 ft lbf**

Impact V2.1

Integration Report

Signal Source: 8mm - Striker 16 Striker

Load (lbf) vs. Time (s)

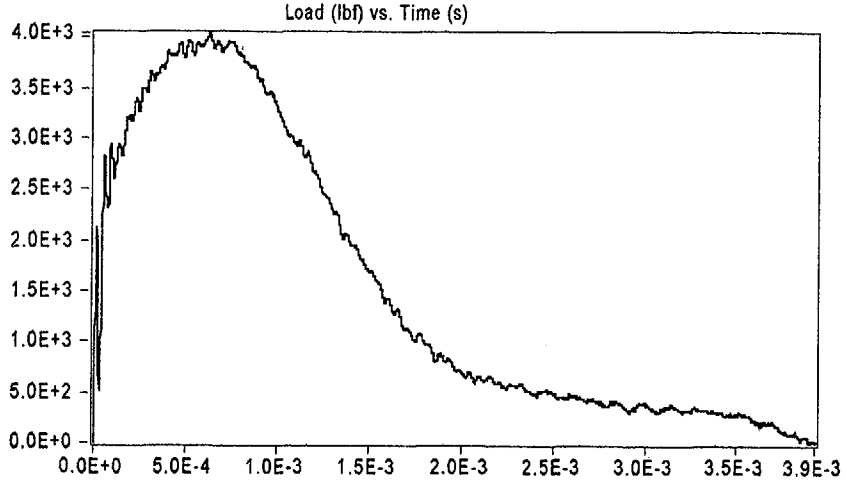

Velocity (ft/s) vs. Time (s)

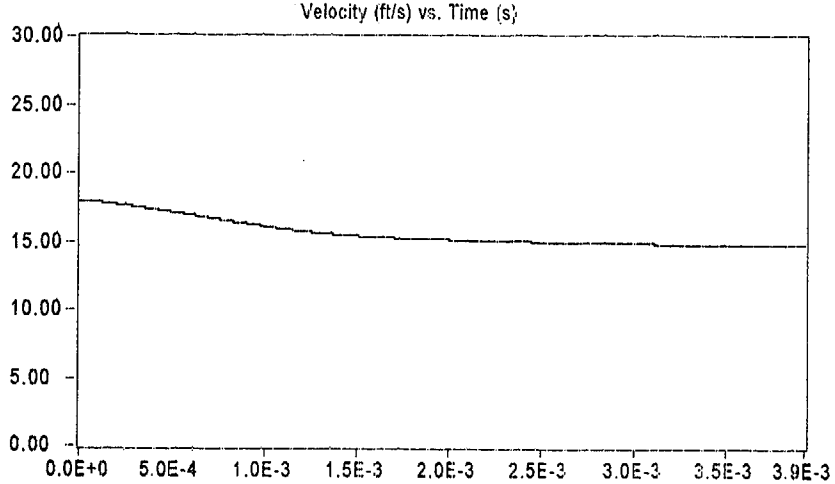

Displacement (in) vs. Time (s)

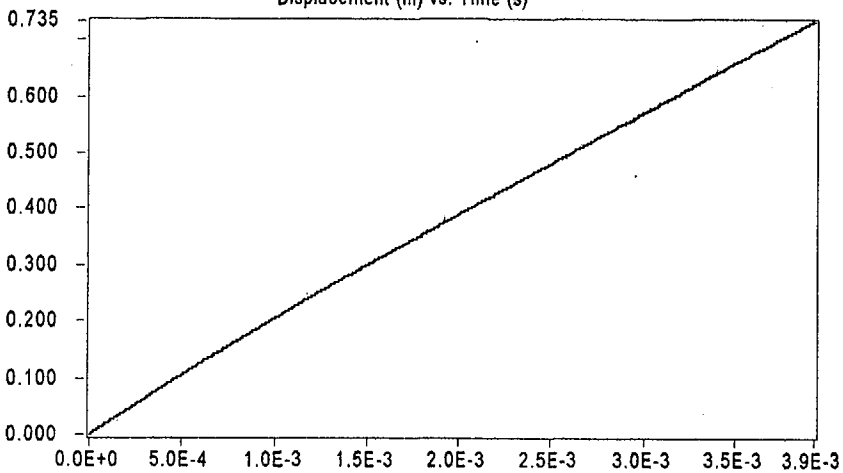

Load (lbf), Energy (ft lbf) vs. Displacement (in)

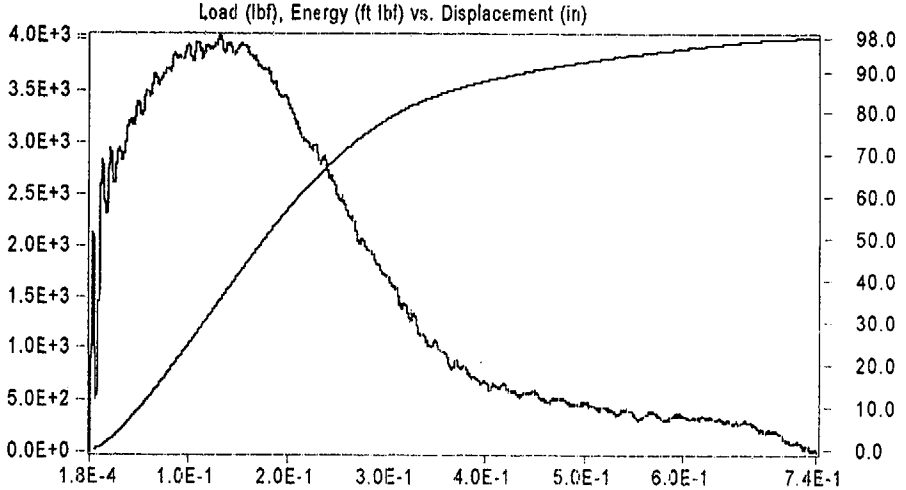

Sample Name: Bf1-3

Instrumented Striker Energy: 97.854 ft lbf

Impact V2.1

Load vs. Displacement Critical Points

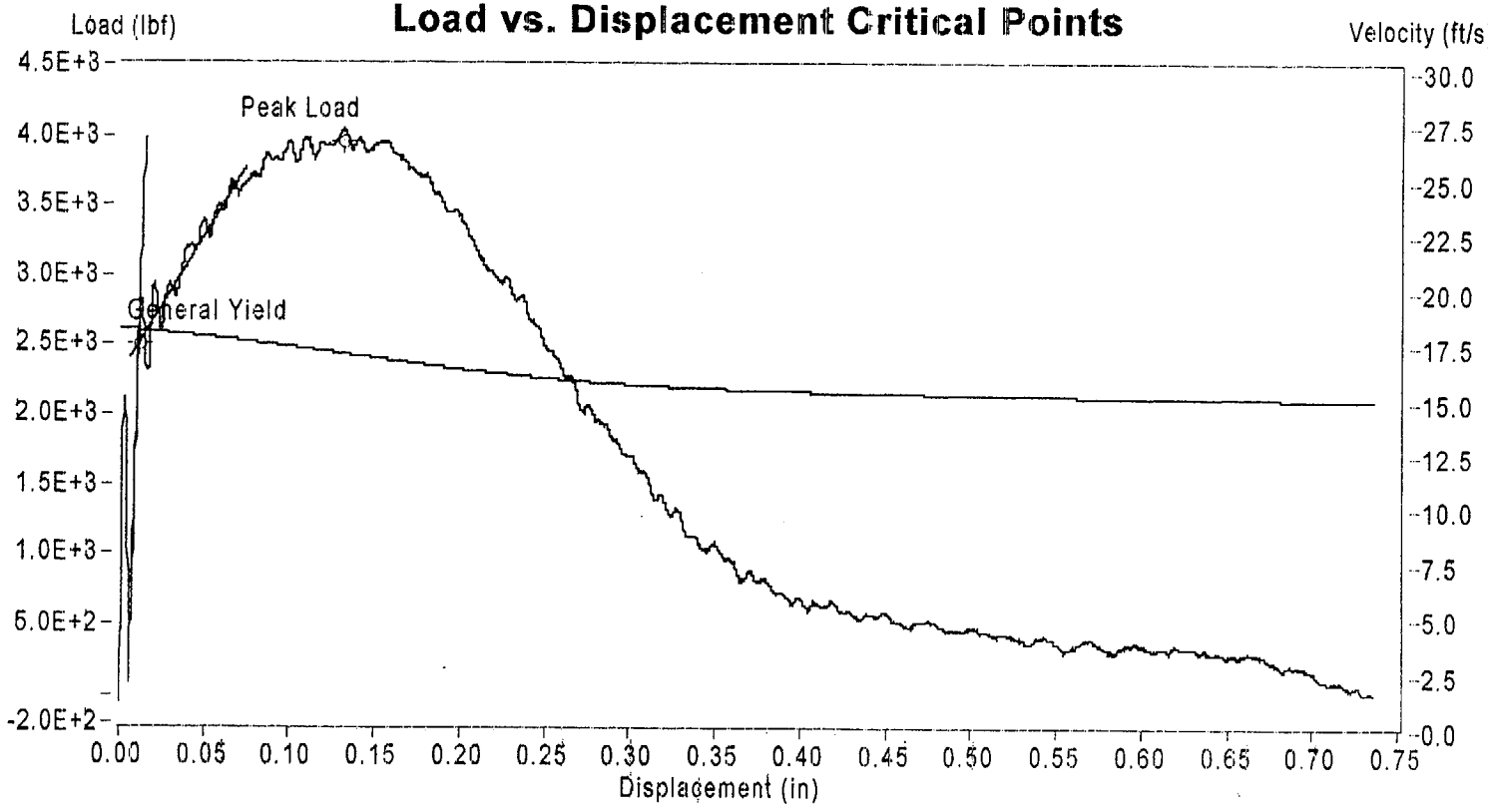

	Load (lbf)	Displacement (in)	Velocity (ft/s)	Time (s)	Energy (ft lbf)
General Yield	2.506E+3	1.090E-2	1.790E+1	4.586E-5	1.236E+0
Peak Load	3.950E+3	1.308E-1	1.684E+1	6.200E-4	3.610E+1
End of Signal	4.442E+0	7.350E-1	1.476E+1	3.920E-3	9.785E+1

Sample ID: Bf1-3

Impact V2.1

Summary Report

Sample ID

BF1-9

Material Description

NMP-2 3-Degree Surveillance Capsule - Base material

Test Parameter	Value
Operator	Dr. Michael P. Manahan, Sr.
Date Tested	11/28/00 11:54 AM
Temperature	127.00 °C
Oscilloscope	Model 441 Internal
Striker Name	8mm - Striker 16
Interpolation Method	Point-Point Linear
TO 892 Controller	Active Adjust
Sample Type	Metal
Sample Size	Type A
Orientation	TL
Notch Type	V Notch, no Side-Groove
Length	2.1654 in
Width	0.3937 in
Thickness	0.3937 in
Span	1.5748 in
Uncracked Ligament	0.3150 in
Notch Radius	0.0098 in
Velocity Determination	Potential Energy & Losses
Velocity	17.94 ft/s
Shear	100.00 %
Lateral Expansion	0.0690 in
Energy Adjustment	1.0245

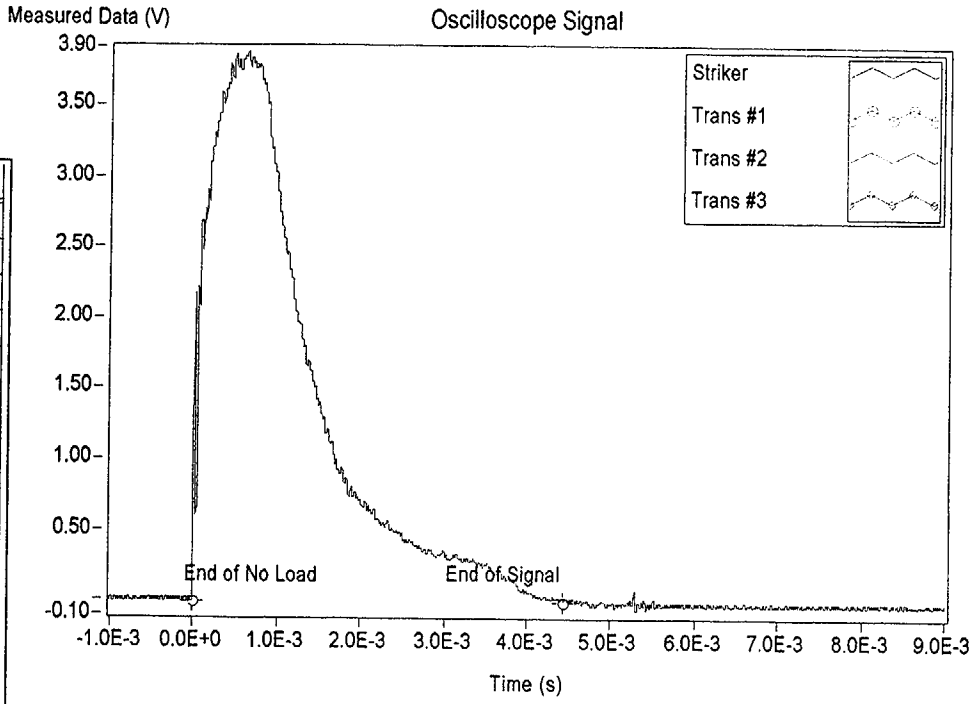

Result	Value
Optical Encoder Energy	95.213 ft lbf
Dial Gage Energy	95.00 ft lbf
Instrumented Striker Energy	95.213 ft lbf

Impact V2.1

Integration Report

Signal Source: 8mm - Striker 16 Striker

Load (lbf) vs. Time (s)

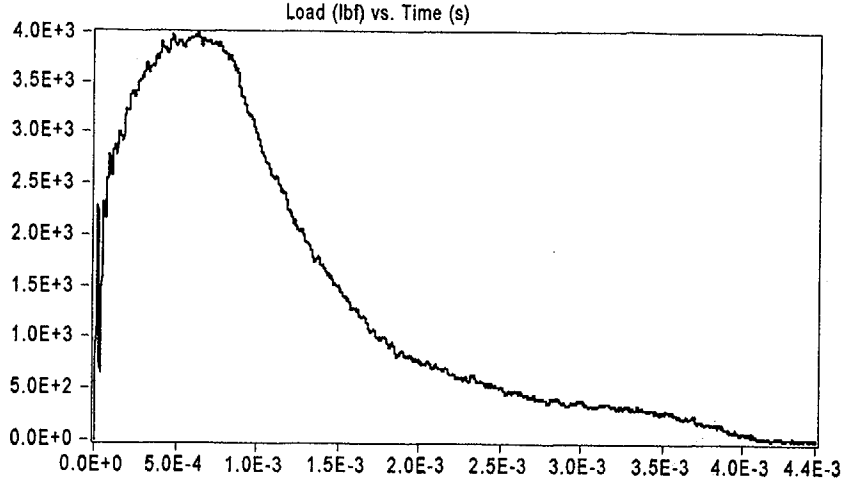

Velocity (ft/s) vs. Time (s)

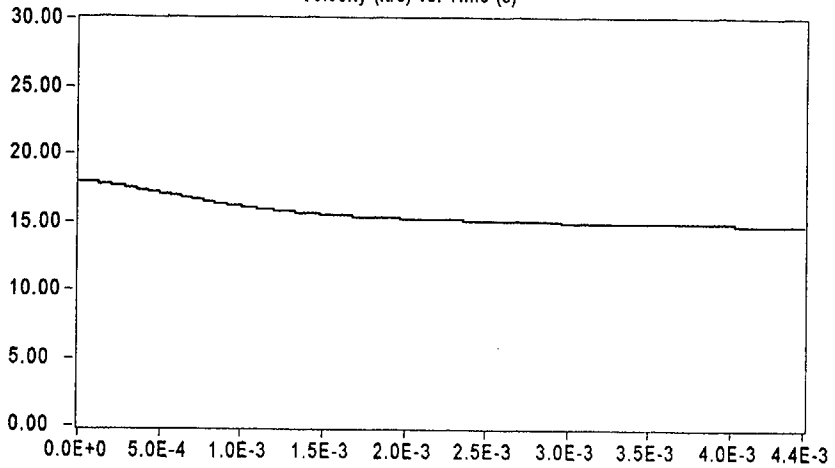

Displacement (in) vs. Time (s)

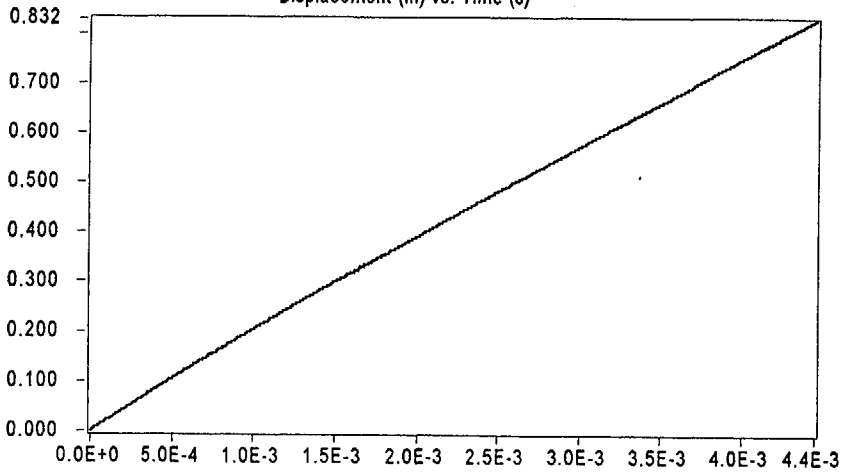

Sample Name: Bf1-9

Load (lbf), Energy (ft lbf) vs. Displacement (in)

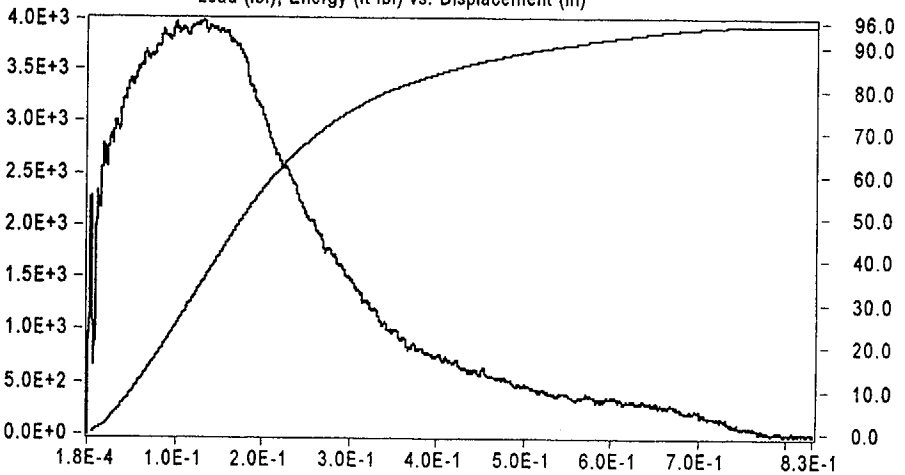

Instrumented Striker Energy: 95.213 ft lbf

Impact V2.1

Load vs. Displacement Critical Points

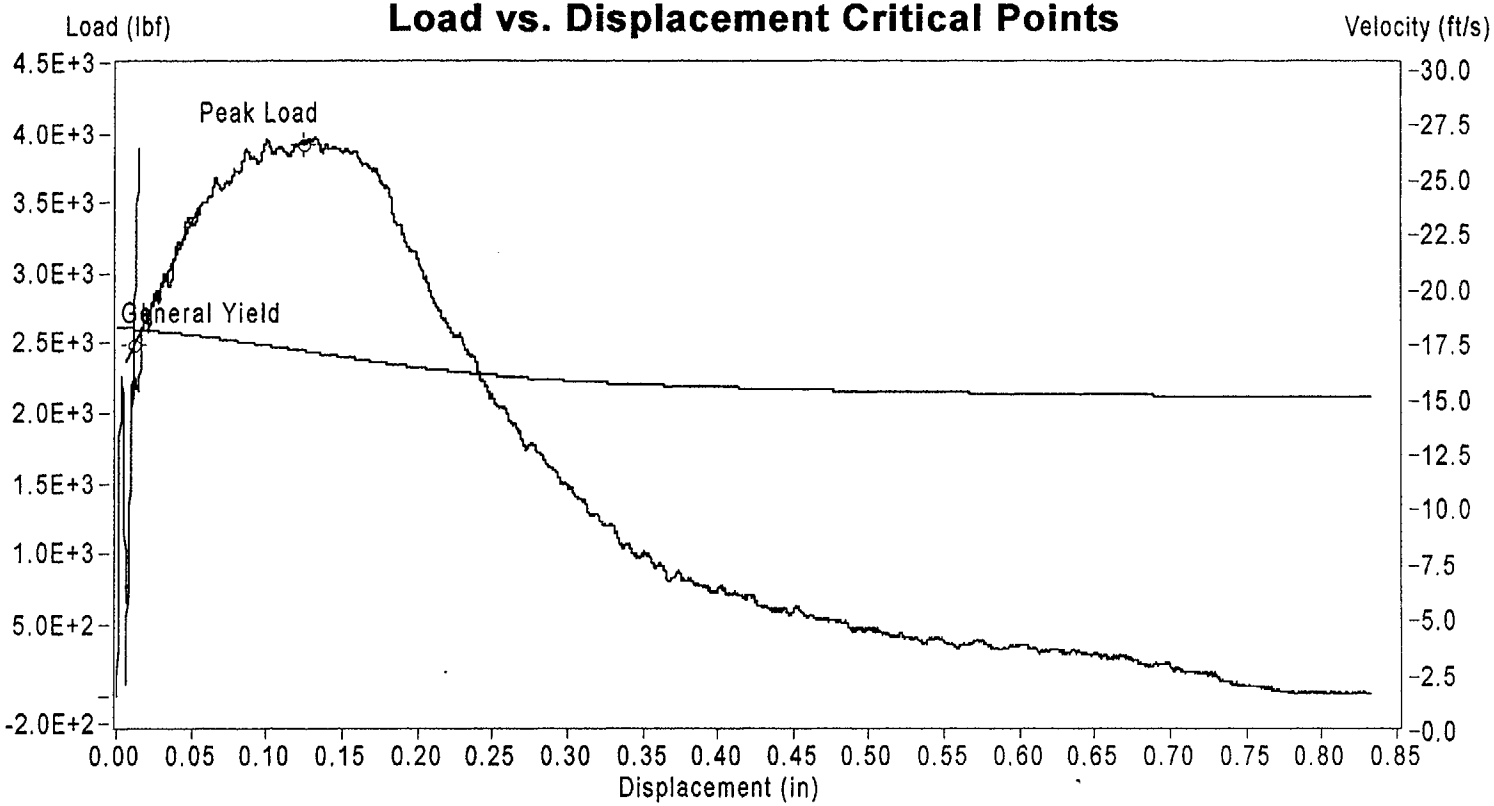

	Load (lbf)	Displacement (in)	Velocity (ft/s)	Time (s)	Energy (ft lbf)
General Yield	2.488E+3	1.155E-2	1.790E+1	4.786E-5	1.413E+0
Peak Load	3.922E+3	1.248E-1	1.690E+1	5.890E-4	3.402E+1
End of Signal	1.137E+0	8.316E-1	1.485E+1	4.439E-3	9.521E+1

Sample ID: Bf1-9

Appendix A-2 Weld Metal Data (heat 5P5657)

The weld metal Charpy data are summarized below. The instrumented data provided on the pages which follow are given in the order shown in the table. There are three instrumented data plots for each specimen tested.

Summary of Charpy V-Notch Impact Test Results for Irradiated Weld Metal Specimens (heat 5P5657) from the Nine Mile Point Unit 2 3-Degree Surveillance Capsule.

Specimen Identification	Test Temperature (°F)	Impact Energy (ft-lb)	Fracture Appearance (% Shear Area)	Lateral Expansion (mils)
WF2	-128.2	5.1	7.3	2.0
WF2-9	-115.6	5.7	19.9	4.0
WF2-12	-54.4	27.0	30.0	23.0
WF2-10	-50.8	26.8	29.3	25.0
WF2-2	-0.4	49.0	52.8	40.0
WF2-6	3.2	37.5	37.9	33.5
WF2-4	64.4	70.5	84.5	53.8
WF2-5	66.2	73.6	79.9	50.6
WF2-3	145.4	96.4	100.0	75.0
WF2-7	147.2	95.5	100.0	72.5
WF2-11	249.8	102.4	100.0	72.8
WF2-8	251.6	100.4	100.0	70.3

Impact V2.1

Summary Report

Sample ID

WF2

Material Description

NMP-2 3-Degree Surveillance Capsule - Weld material

Test Parameter	Value
Operator	Dr. Michael P. Manahan, Sr.
Date Tested	11/28/00 5:20 PM
Temperature	-89.00 °C
Oscilloscope	Model 441 Internal
Striker Name	8mm - Striker 16
Interpolation Method	Point-Point Linear
TO 892 Controller	Active Adjust
Sample Type	Metal
Sample Size	Type A
Orientation	TL
Notch Type	V Notch, no Side-Groove
Length	2.1654 in
Width	0.3937 in
Thickness	0.3937 in
Span	1.5748 in
Uncracked Ligament	0.3150 in
Notch Radius	0.0098 in
Velocity Determination	Potential Energy & Losses
Velocity	17.94 ft/s
Shear	7.30 %
Lateral Expansion	0.0020 in
Energy Adjustment	0.9992

Measured Data (V)

Oscilloscope Signal

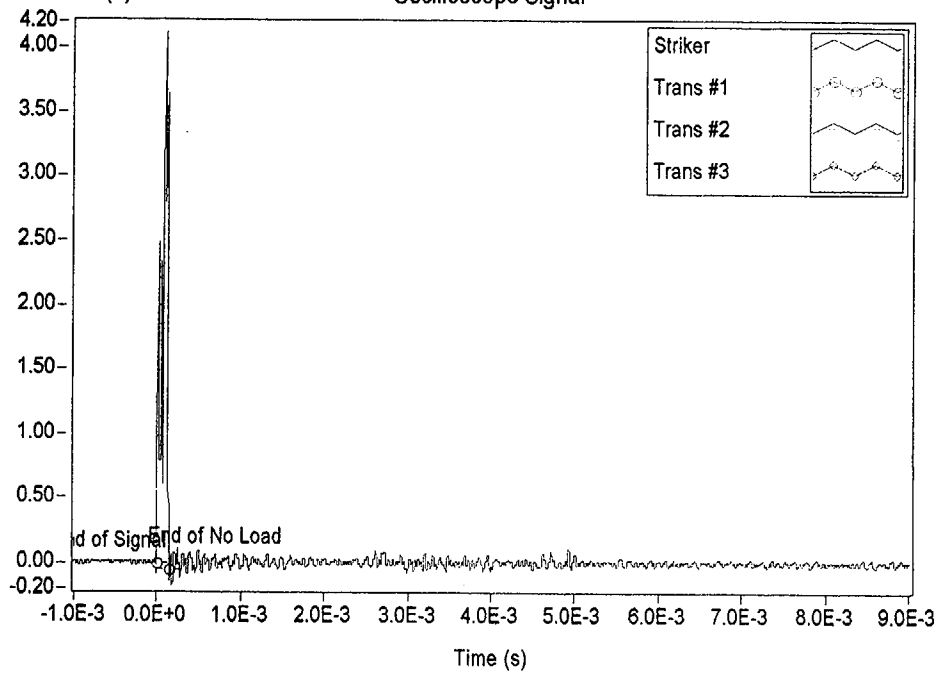

Result	Value
Optical Encoder Energy	5.1423 ft lbf
Dial Gage Energy	5.400 ft lbf
Instrumented Striker Energy	5.1423 ft lbf

Impact V2.1

Integration Report

Signal Source: 8mm - Striker 16 Striker

Load (lbf) vs. Time (s)

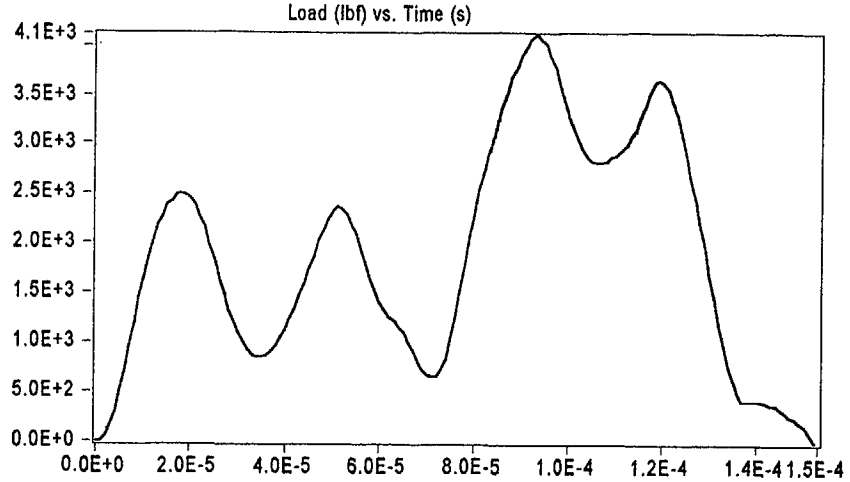

Velocity (ft/s) vs. Time (s)

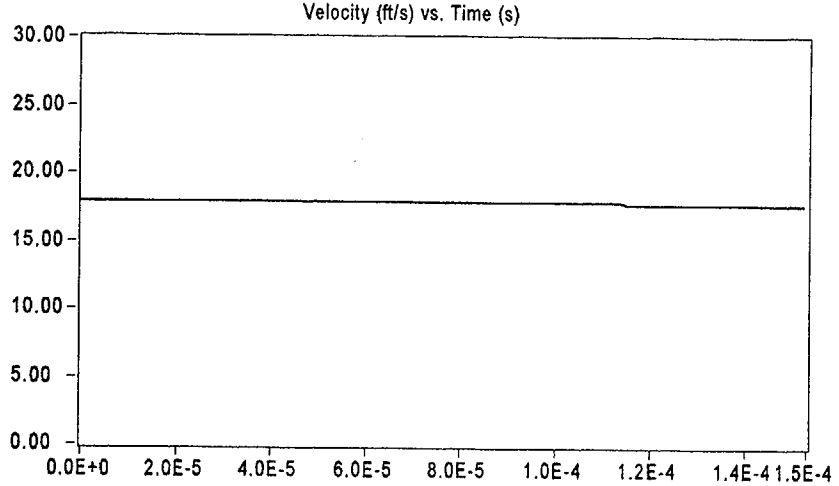

Displacement (in) vs. Time (s)

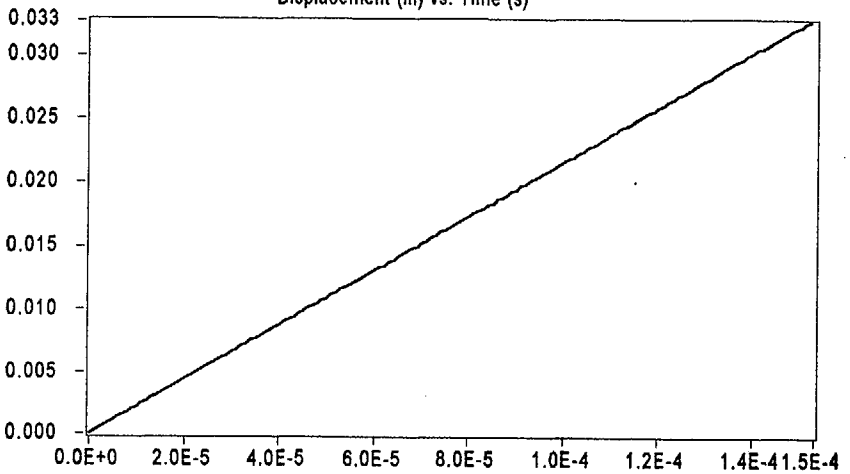

Load (lbf), Energy (ft lbf) vs. Displacement (in)

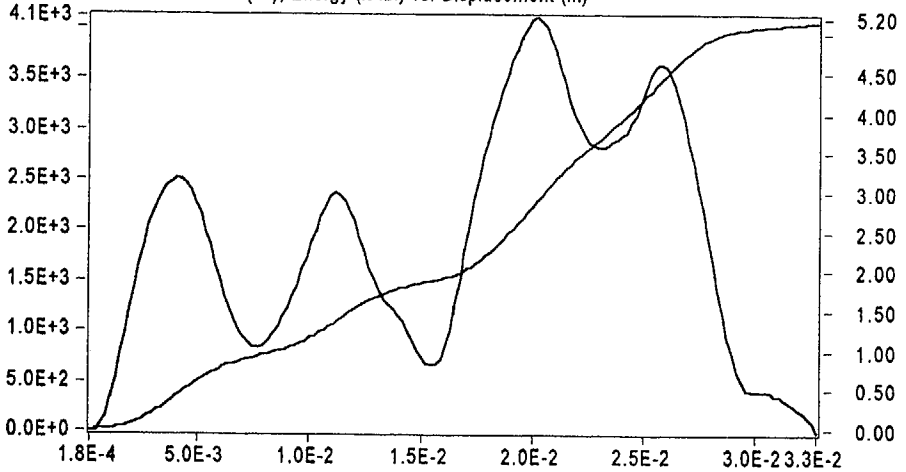

Sample Name: Wf2

Instrumented Striker Energy: 5.1423 ft lbf

Impact V2.1

Load vs. Displacement Critical Points

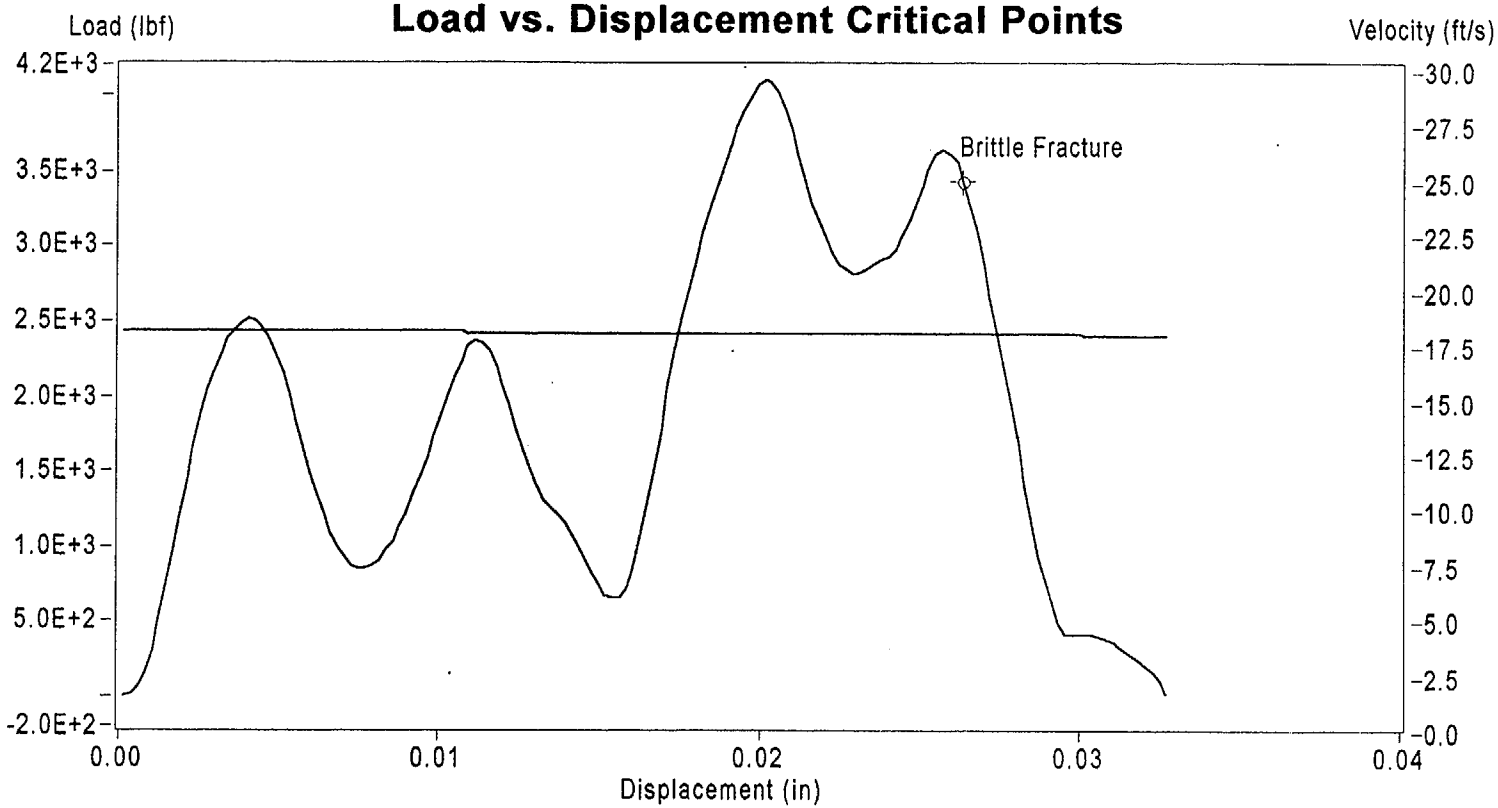

	Load (lbf)	Displacement (in)	Velocity (ft/s)	Time (s)	Energy (ft lbf)
Brittle Fracture	3.431E+3	2.636E-2	1.780E+1	1.160E-4	4.604E+0
End of Signal	4.955E+0	3.273E-2	1.779E+1	1.460E-4	5.142E+0

Sample ID: Wf2

Impact V2.1

Summary Report

Sample ID

WF2-9

Material Description

NMP-2 3-Degree Surveillance Capsule - Weld material

Test Parameter	Value
Operator	Dr. Michael P. Manahan, Sr.
Date Tested	11/28/00 5:41 PM
Temperature	-82.00 °C
Oscilloscope	Model 441 Internal
Striker Name	8mm - Striker 16
Interpolation Method	Point-Point Linear
TO 892 Controller	Active Adjust
Sample Type	Metal
Sample Size	Type A
Orientation	TL
Notch Type	V Notch, no Side-Groove
Length	2.1654 in
Width	0.3937 in
Thickness	0.3937 in
Span	1.5748 in
Uncracked Ligament	0.3150 in
Notch Radius	0.0098 in
Velocity Determination	Potential Energy & Losses
Velocity	17.94 ft/s
Shear	19.90 %
Lateral Expansion	0.0040 in
Energy Adjustment	1.4442

Measured Data (V)

Oscilloscope Signal

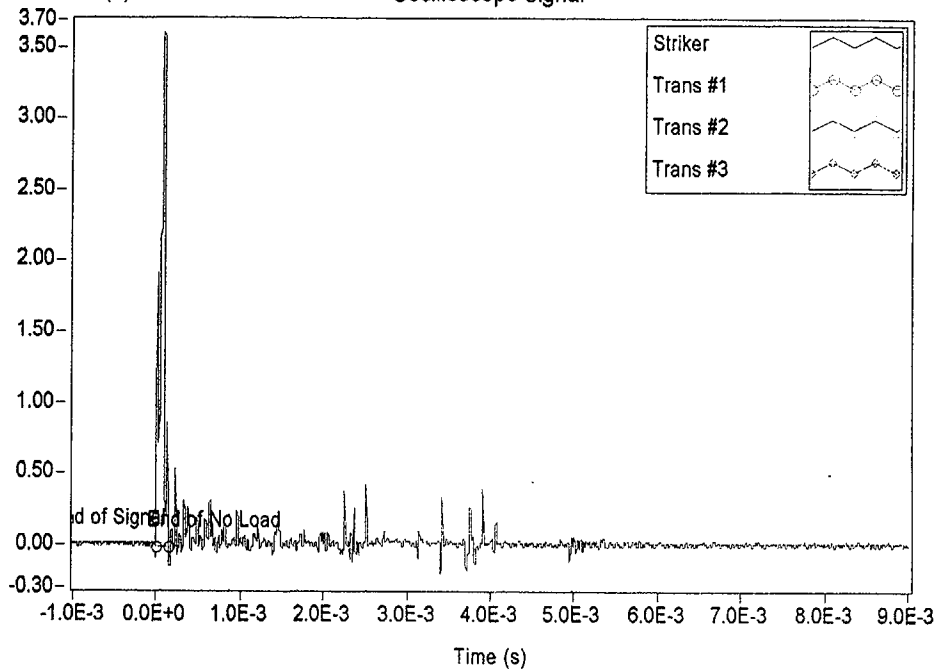

Result	Value
Optical Encoder Energy	5.7248 ft lbf
Dial Gage Energy	5.900 ft lbf
Instrumented Striker Energy	5.7248 ft lbf

Impact V2.1

Integration Report

Signal Source: 8mm - Striker 16 Striker

Load (lbf) vs. Time (s)

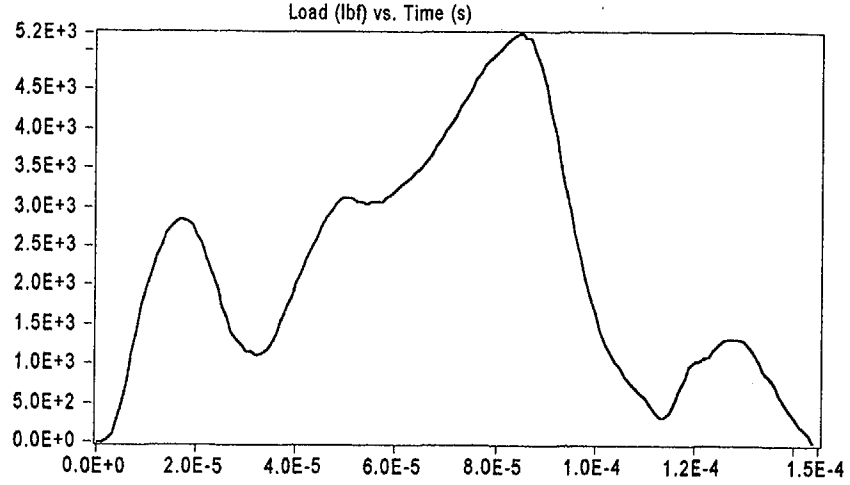

Velocity (ft/s) vs. Time (s)

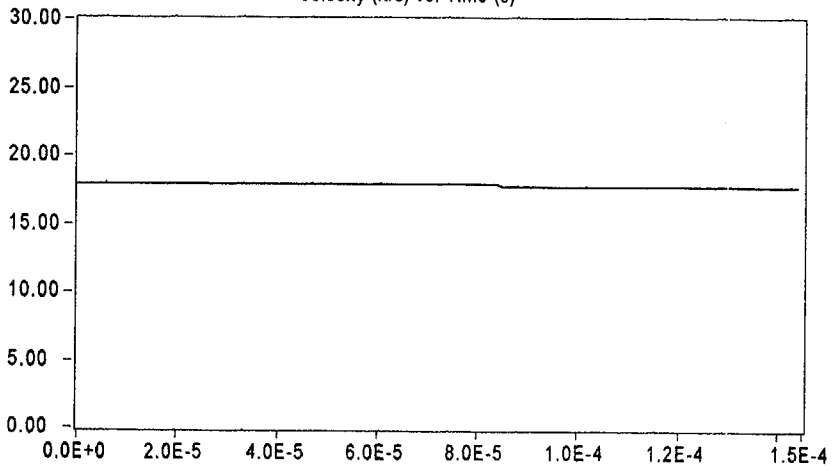

Displacement (in) vs. Time (s)

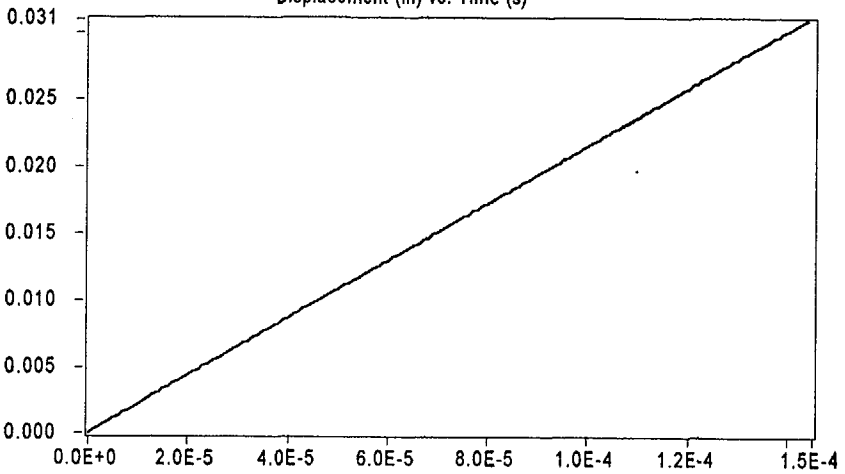

Load (lbf), Energy (ft lbf) vs. Displacement (in)

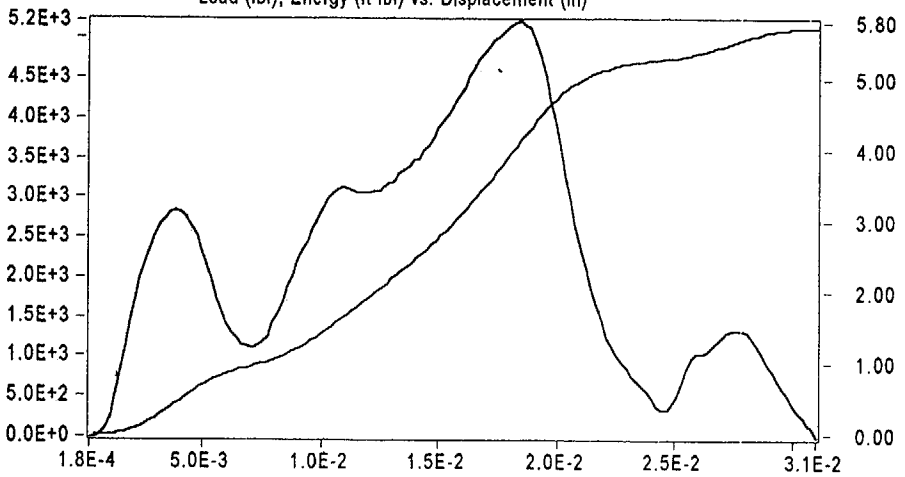

Sample Name: Wf2-9

Instrumented Striker Energy: 5.7248 ft lbf

Impact V2.1

Load vs. Displacement Critical Points

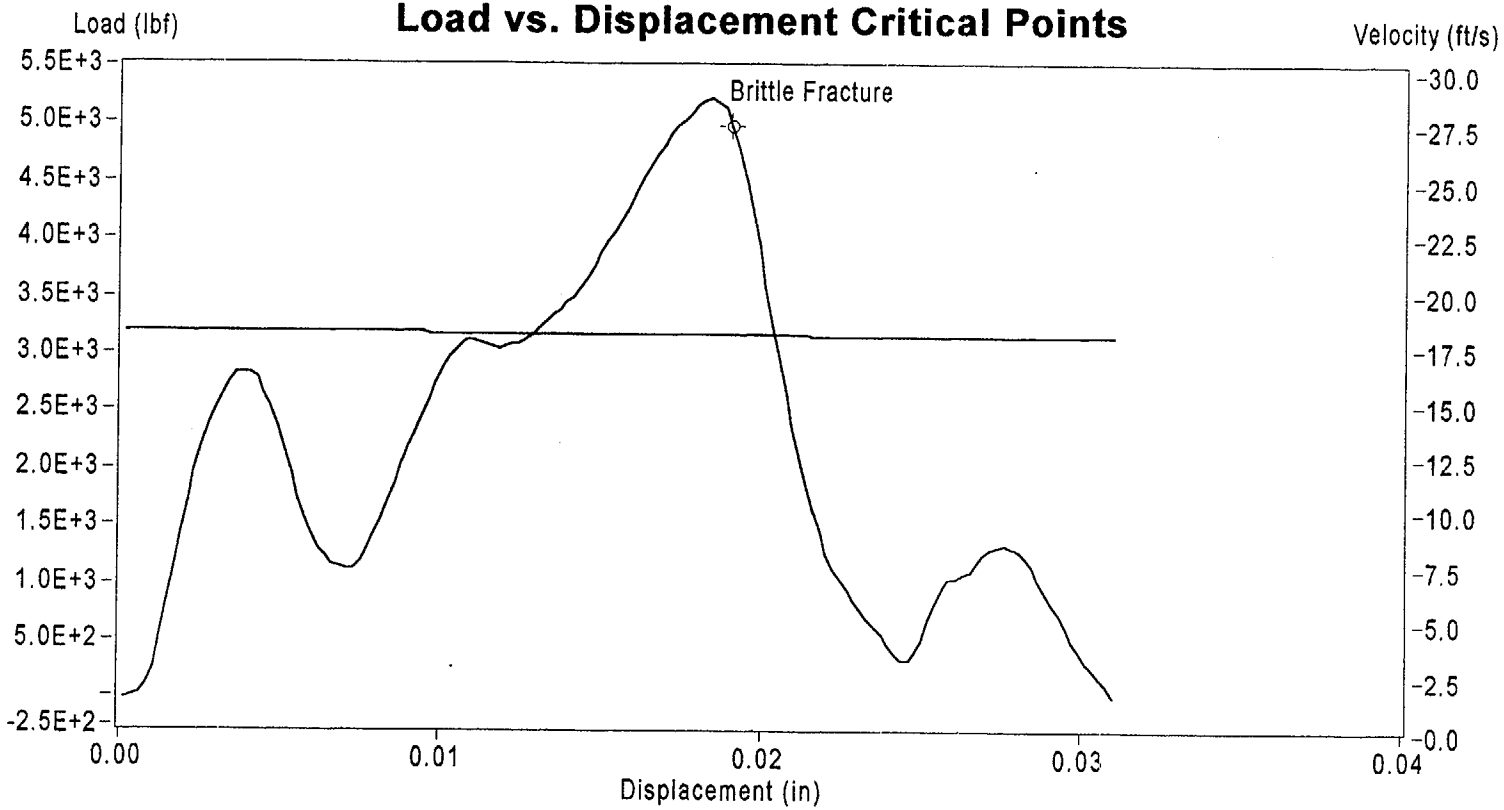

	Load (lbf)	Displacement (in)	Velocity (ft/s)	Time (s)	Energy (ft lbf)
Brittle Fracture	4.996E+3	1.907E-2	1.781E+1	8.100E-5	4.414E+0
End of Signal	8.326E+0	3.098E-2	1.777E+1	1.370E-4	5.725E+0

Sample ID: Wf2-9

Impact V2.1

Summary Report

Sample ID

WF2-12

Material Description

NMP-2 3-Degree Surveillance Capsule - Weld material

Test Parameter	Value
Operator	Dr. Michael P. Manahan, Sr.
Date Tested	11/29/00 5:35 PM
Temperature	-48.00 °C
Oscilloscope	Model 441 Internal
Striker Name	8mm - Striker 16
Interpolation Method	Point-Point Linear
TO 892 Controller	Active Adjust
Sample Type	Metal
Sample Size	Type A
Orientation	TL
Notch Type	V Notch, no Side-Groove
Length	2.1654 in
Width	0.3937 in
Thickness	0.3937 in
Span	1.5748 in
Uncracked Ligament	0.3150 in
Notch Radius	0.0098 in
Velocity Determination	Potential Energy & Losses
Velocity	17.94 ft/s
Shear	30.00 %
Lateral Expansion	0.0230 in
Energy Adjustment	1.0524

Measured Data (V)

Oscilloscope Signal

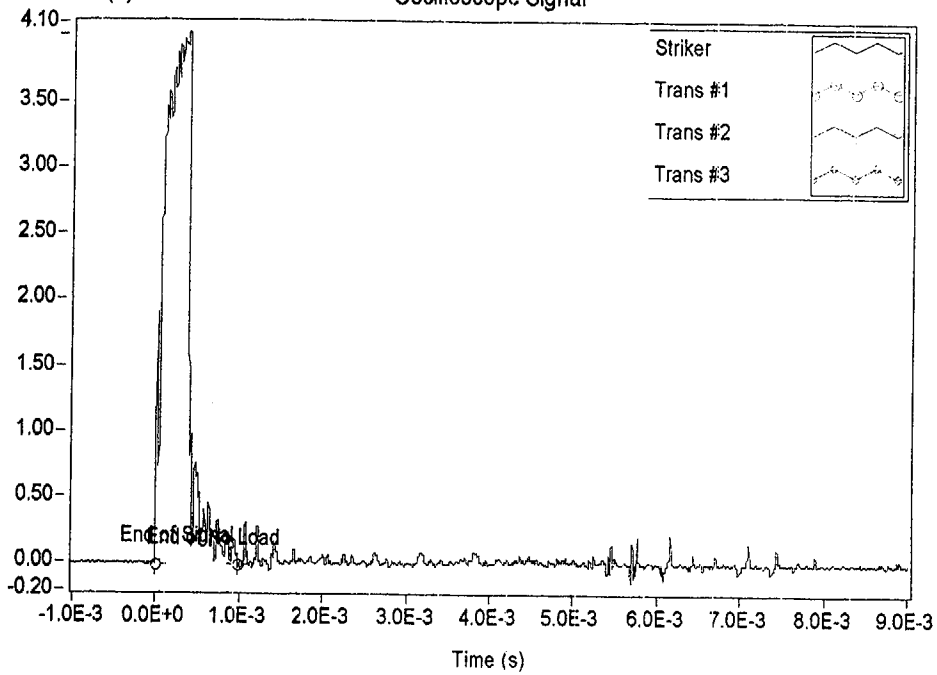

Result	Value
Optical Encoder Energy	26.986 ft lbf
Dial Gage Energy	26.80 ft lbf
Instrumented Striker Energy	26.986 ft lbf

Impact V2.1

Integration Report

Signal Source: 8mm - Striker 16 Striker

Load (lbf) vs. Time (s)

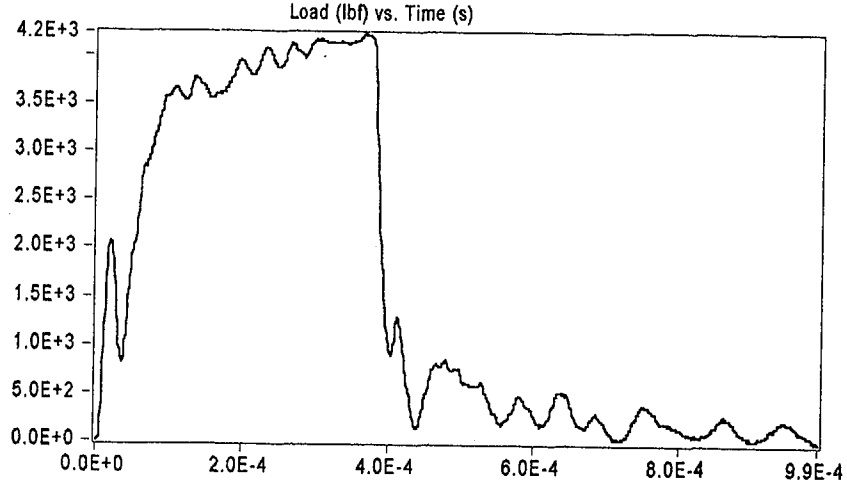

Velocity (ft/s) vs. Time (s)

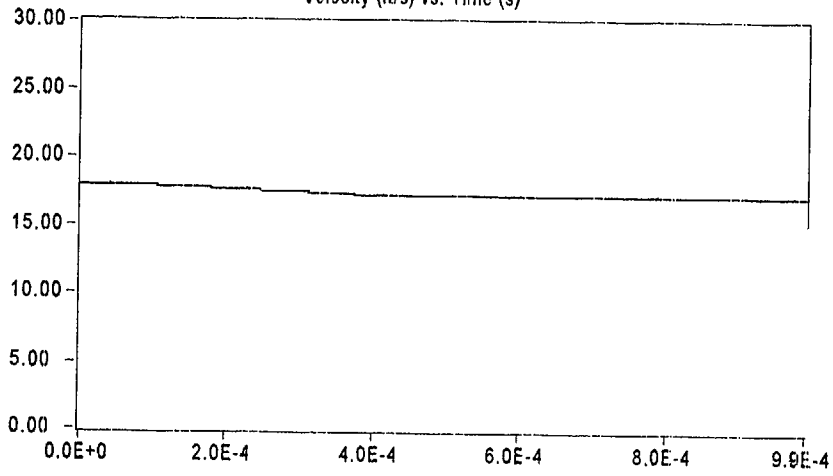

Displacement (in) vs. Time (s)

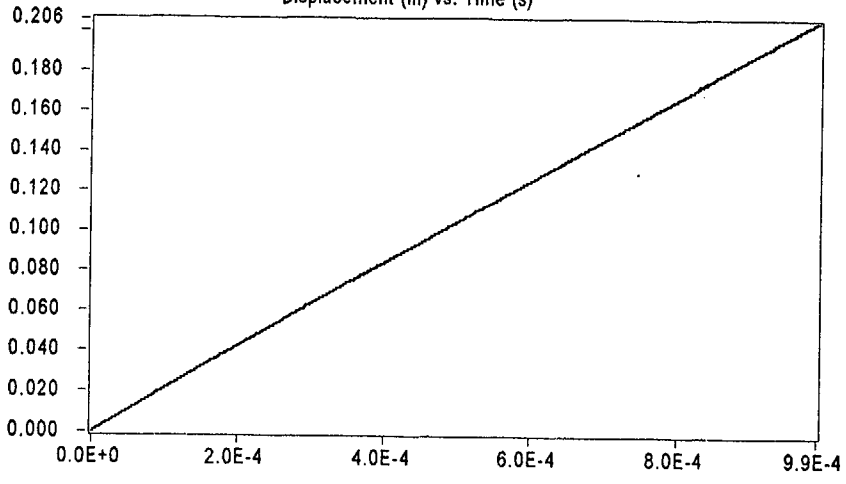

Load (lbf), Energy (ft lbf) vs. Displacement (in)

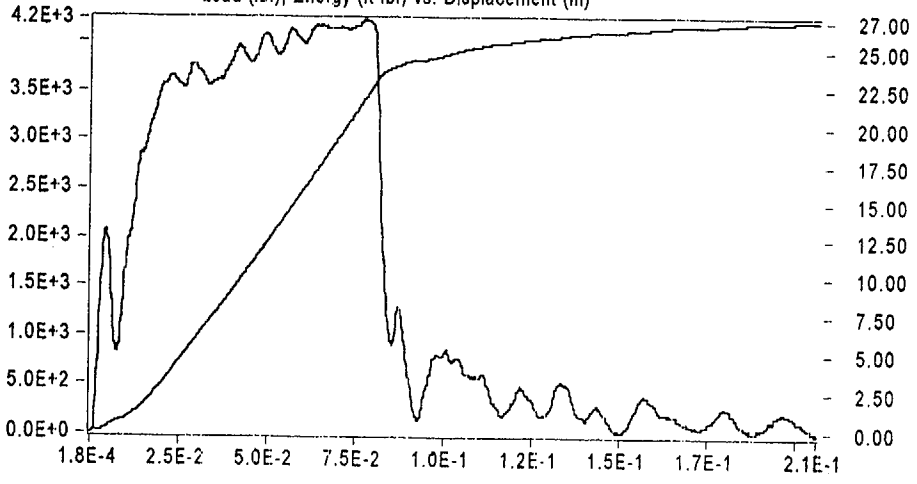

Sample Name: Wf2-12

Instrumented Striker Energy: 26.986 ft lbf

Impact V2.1

Load vs. Displacement Critical Points

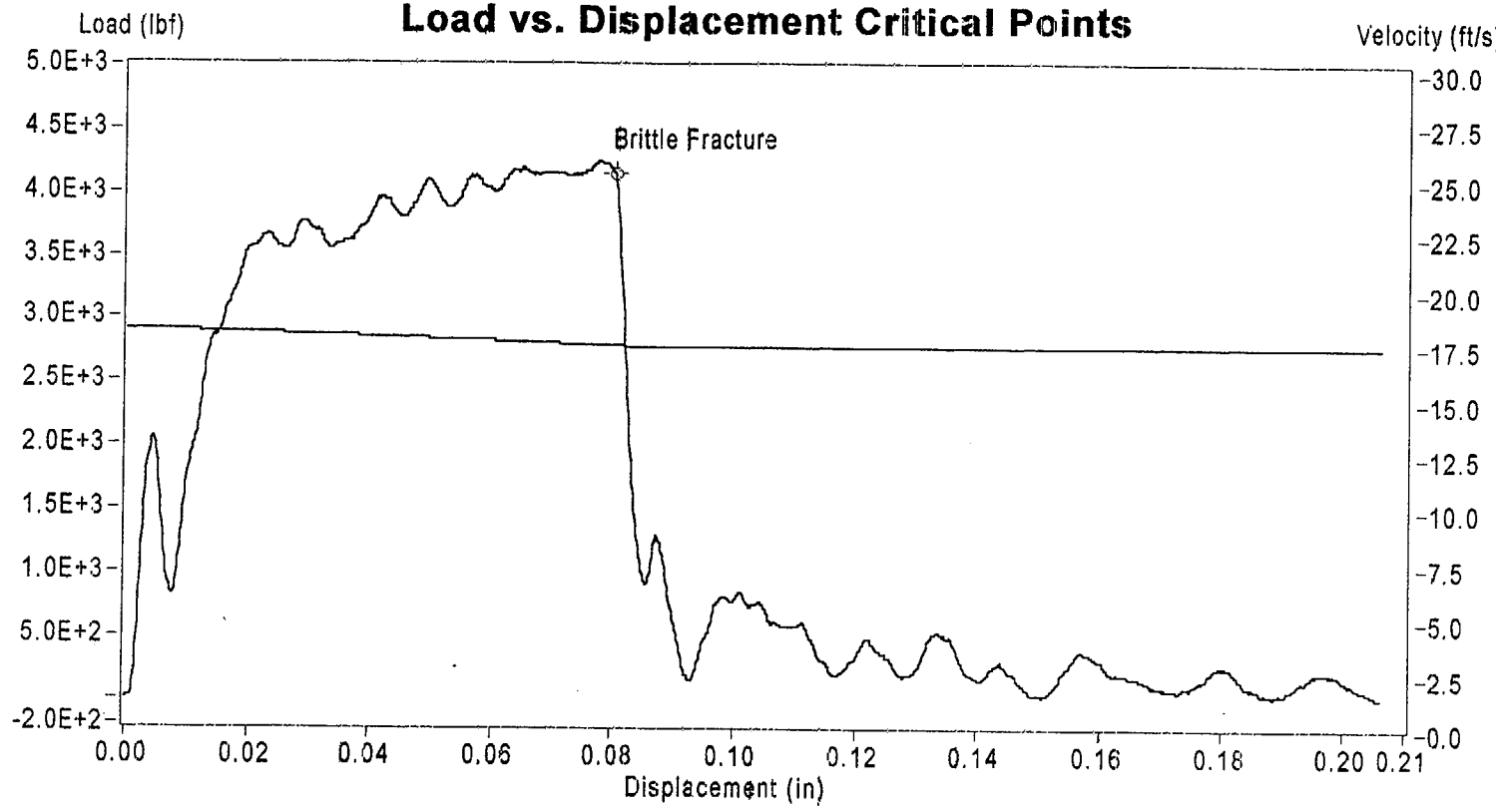

	Load (lbf)	Displacement (in)	Velocity (ft/s)	Time (s)	Energy (ft lbf)
Brittle Fracture	4.145E+3	8.018E-2	1.725E+1	3.690E-4	2.298E+1
End of Signal	3.791E+0	2.061E-1	1.712E+1	9.810E-4	2.699E+1

Sample ID: Wf2-12

Impact V2.1

Summary Report

Sample ID

WF2-10

Material Description

NMP-2 3-Degree Surveillance Capsule - Weld material

Test Parameter	Value
Operator	Dr. Michael P. Manahan, Sr.
Date Tested	11/29/00 5:55 PM
Temperature	-46.00 °C
Oscilloscope	Model 441 Internal
Striker Name	8mm - Striker 16
Interpolation Method	Point-Point Linear
TO 892 Controller	Active Adjust
Sample Type	Metal
Sample Size	Type A
Orientation	TL
Notch Type	V Notch, no Side-Groove
Length	2.1654 in
Width	0.3937 in
Thickness	0.3937 in
Span	1.5748 in
Uncracked Ligament	0.3150 in
Notch Radius	0.0098 in
Velocity Determination	Potential Energy & Losses
Velocity	17.94 ft/s
Shear	29.30 %
Lateral Expansion	0.0250 in
Energy Adjustment	1.1371

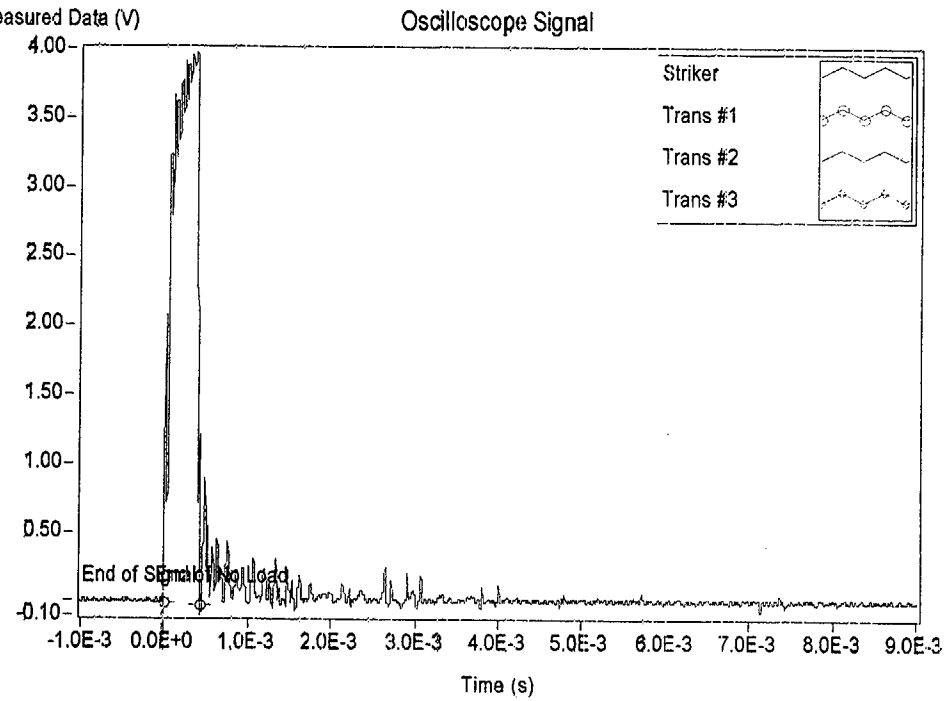

Result	Value
Optical Encoder Energy	26.749 ft lbf
Dial Gage Energy	26.90 ft lbf
Instrumented Striker Energy	26.749 ft lbf

Impact V2.1

Integration Report

Signal Source: 8mm - Striker 16 Striker

Load (lbf) vs. Time (s)

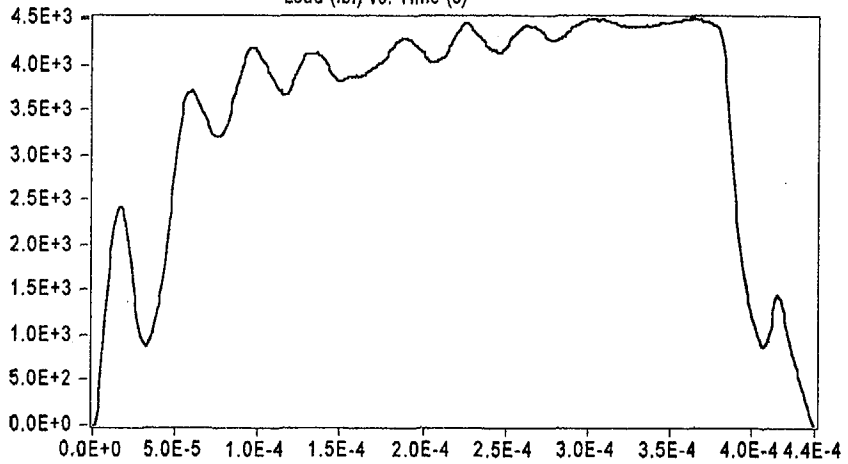

Velocity (ft/s) vs. Time (s)

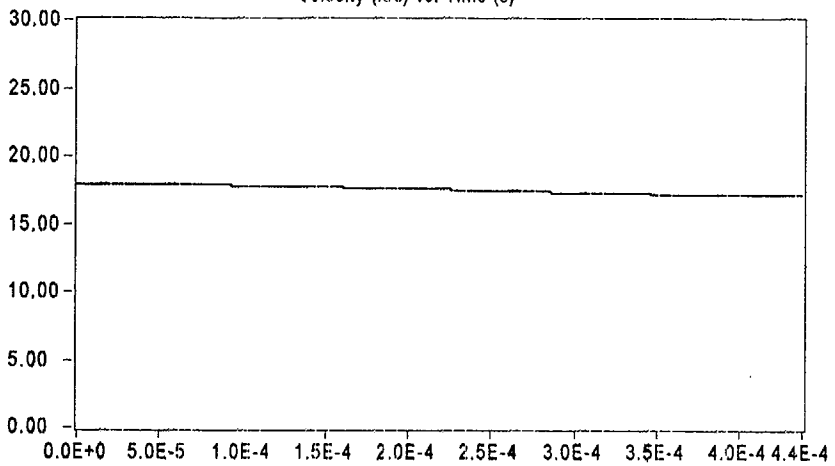

Displacement (in) vs. Time (s)

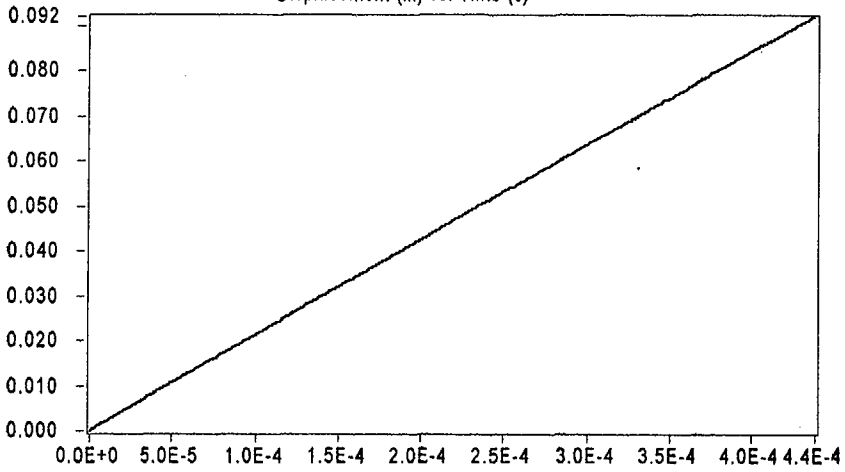

Load (lbf), Energy (ft lbf) vs. Displacement (in)

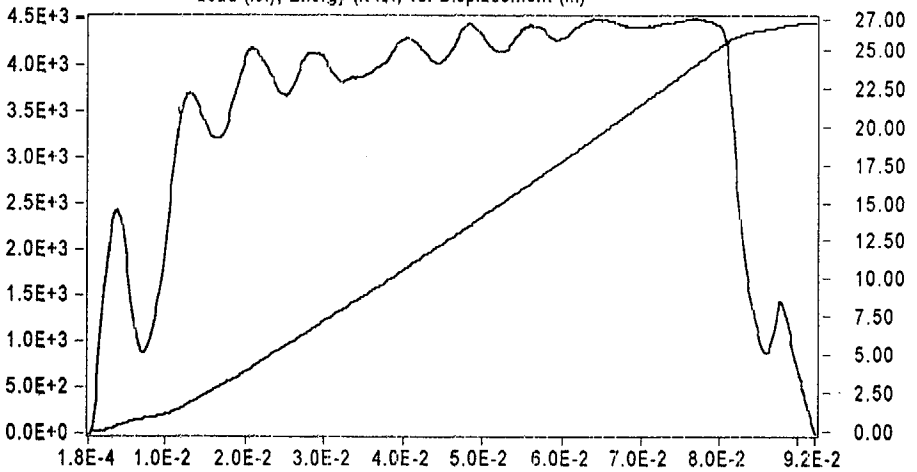

Sample Name: Wf2-10

Instrumented Striker Energy: 26.749 ft lbf

Impact V2.1

Load vs. Displacement Critical Points

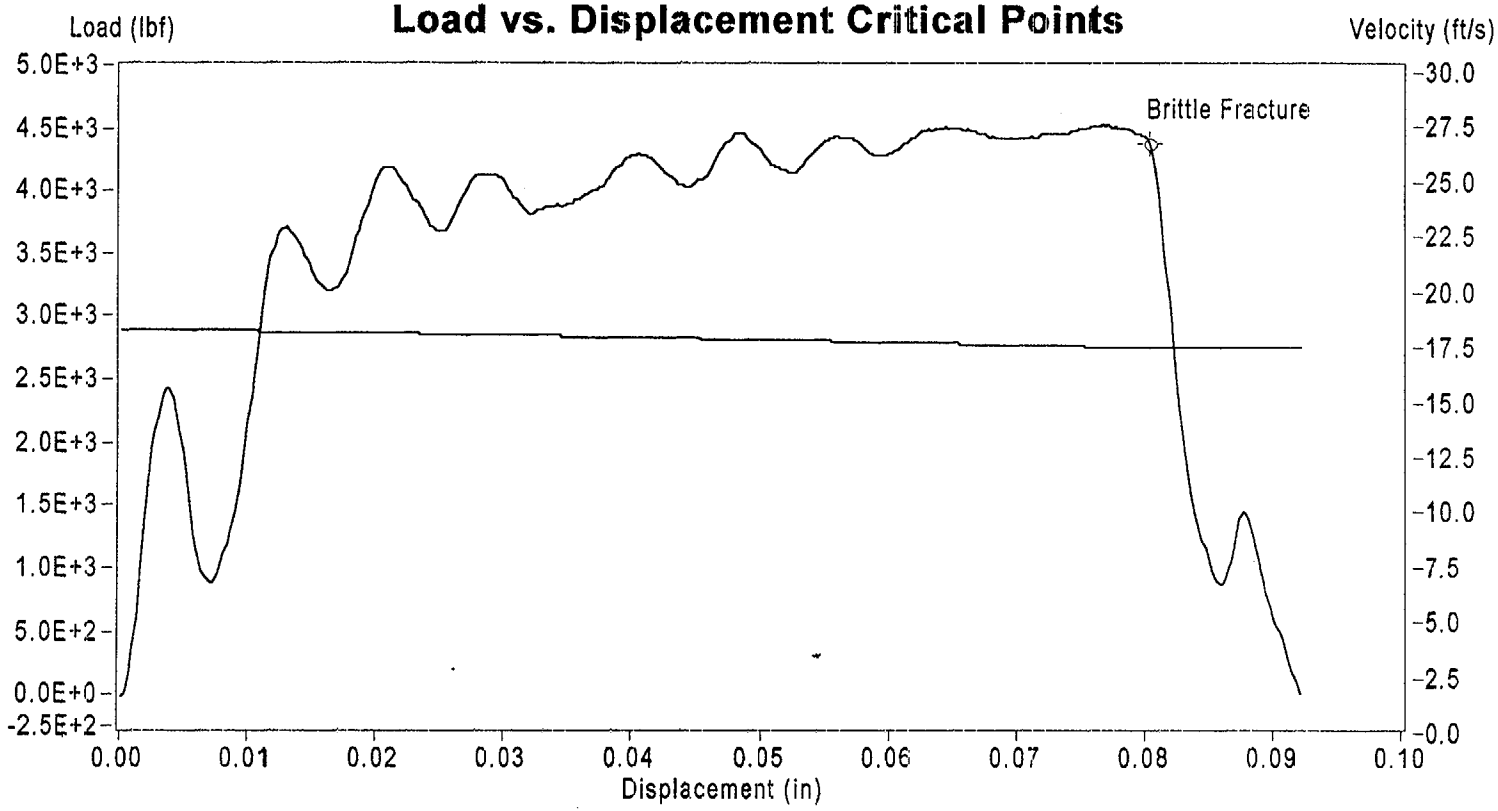

	Load (lbf)	Displacement (in)	Velocity (ft/s)	Time (s)	Energy (ft lbf)
Brittle Fracture	4.377E+3	8.043E-2	1.717E+1	3.740E-4	2.534E+1
End of Signal	7.236E+0	9.212E-2	1.713E+1	4.310E-4	2.675E+1

Sample ID: Wf2-10

Impact V2.1

Summary Report

Sample ID

WF2-2

Material Description

NMP-2 3-Degree Surveillance Capsule - Weld material

Test Parameter	Value
Operator	Dr. Michael P. Manahan, Sr.
Date Tested	11/29/00 5:04 PM
Temperature	-18.00 °C
Oscilloscope	Model 441 Internal
Striker Name	8mm - Striker 16
Interpolation Method	Point-Point Linear
TO 892 Controller	Active Adjust
Sample Type	Metal
Sample Size	Type A
Orientation	TL
Notch Type	V Notch, no Side-Groove
Length	2.1654 in
Width	0.3937 in
Thickness	0.3937 in
Span	1.5748 in
Uncracked Ligament	0.3150 in
Notch Radius	0.0098 in
Velocity Determination	Potential Energy & Losses
Velocity	17.94 ft/s
Shear	52.80 %
Lateral Expansion	0.0400 in
Energy Adjustment	1.0139

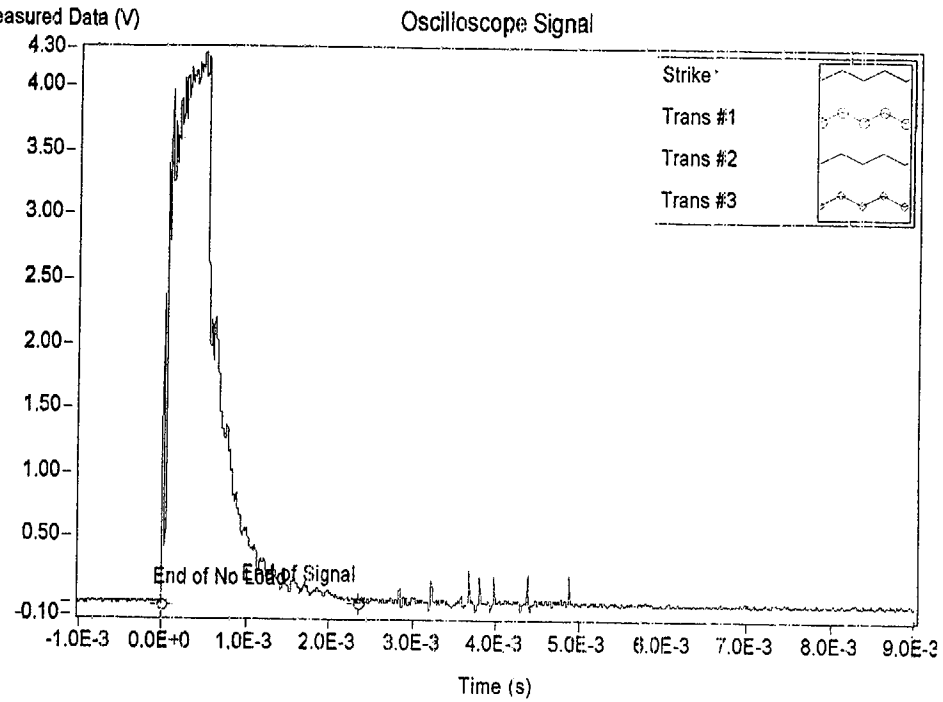

Result	Value
Optical Encoder Energy	48.956 ft lbf
Dial Gage Energy	49.10 ft lbf
Instrumented Striker Energy	48.956 ft lbf

Impact V2.1

Integration Report

Signal Source: 8mm - Striker 16 Striker

Load (lbf) vs. Time (s)

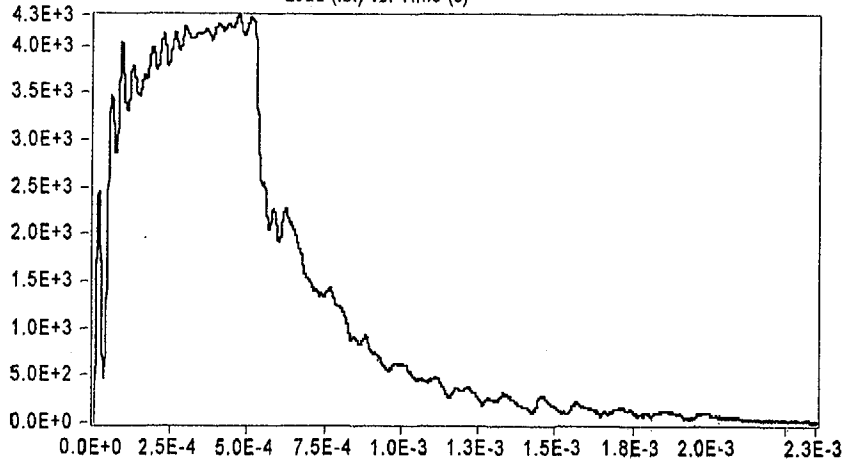

Velocity (ft/s) vs. Time (s)

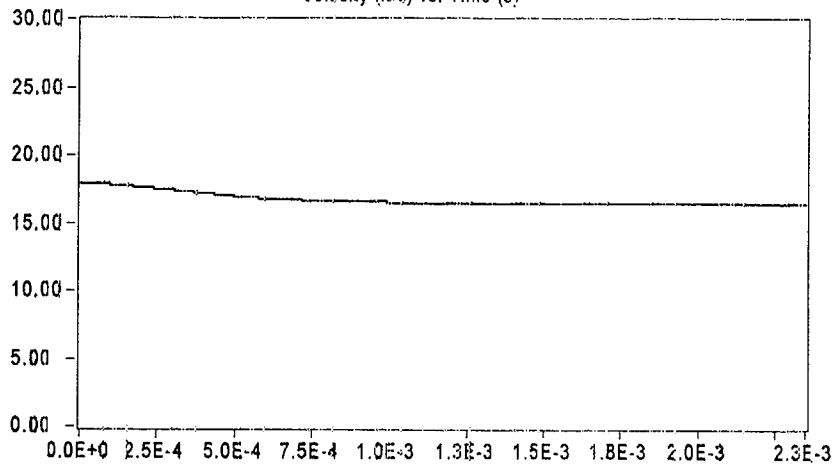

Displacement (in) vs. Time (s)

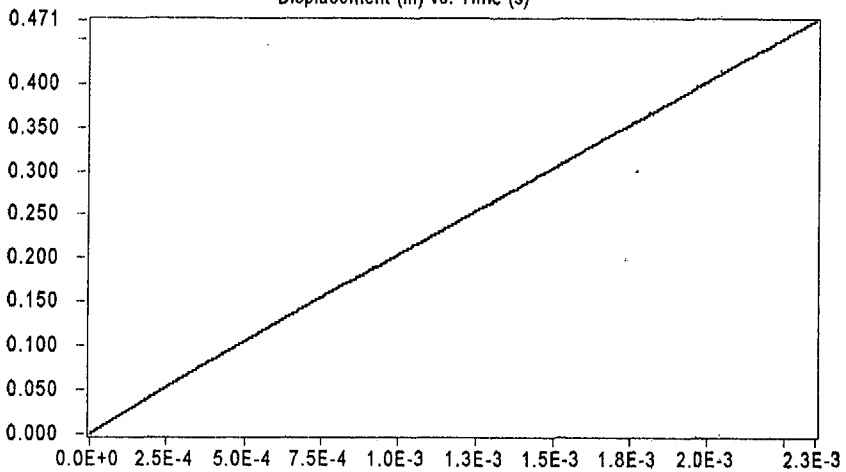

Load (lbf), Energy (ft lbf) vs. Displacement (in)

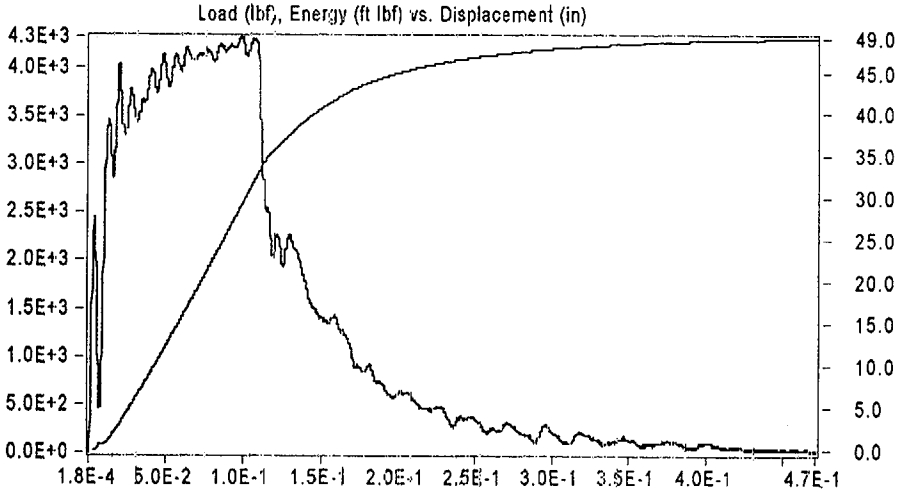

Sample Name: WF2-2-b

Instrumented Striker Energy: 48.956 ft lbf

Impact V2.1

Load vs. Displacement Critical Points

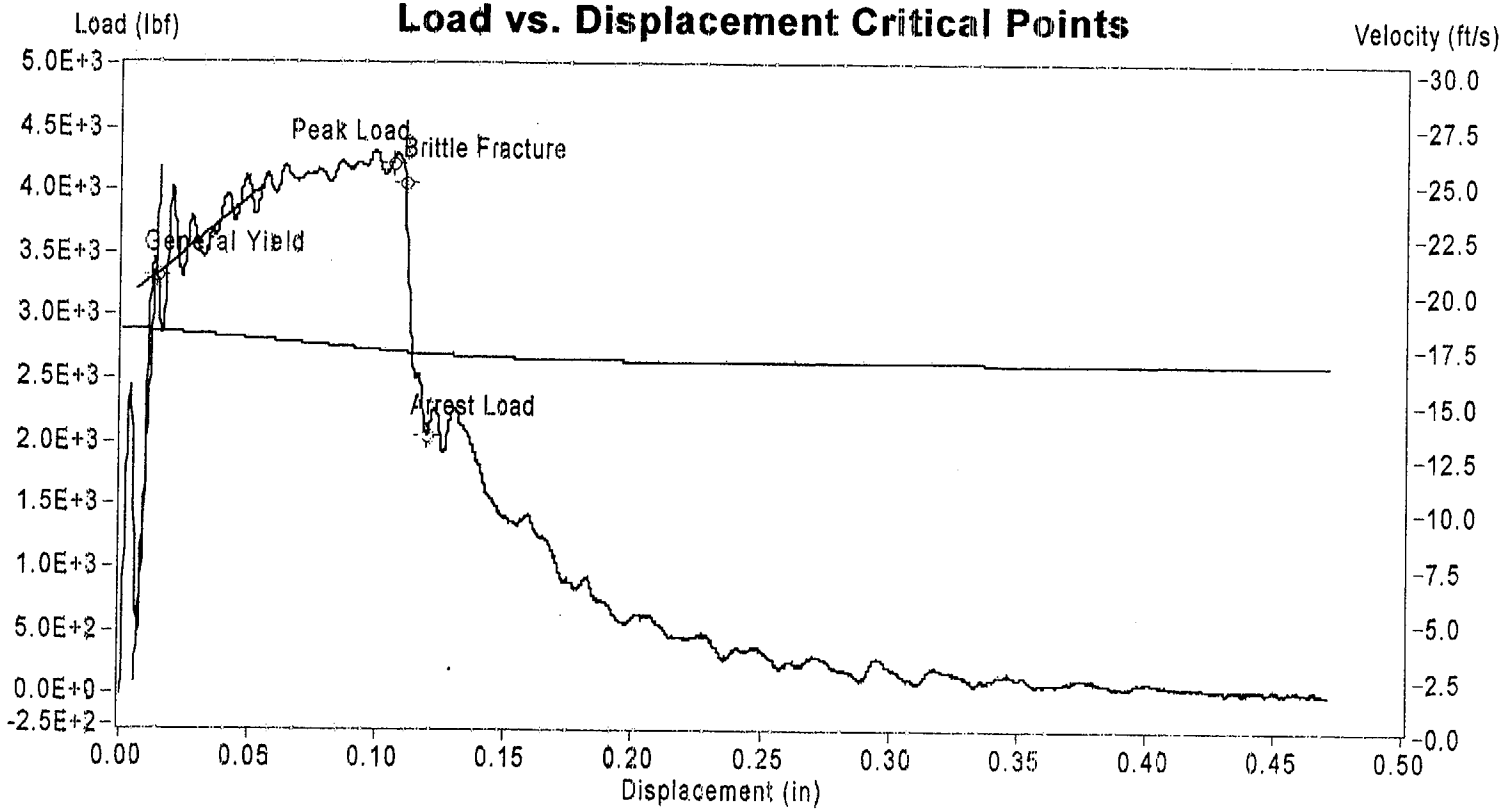

	Load (lbf)	Displacement (in)	Velocity (ft/s)	Time (s)	Energy (ft lbf)
General Yield	3.327E+3	1.305E-2	1.788E+1	5.487E-5	1.924E+0
Peak Load	4.224E+3	1.054E-1	1.696E+1	4.960E-4	3.221E+1
Brittle Fracture	4.060E+3	1.102E-1	1.690E+1	5.200E-4	3.394E+1
Arrest Load	2.044E+3	1.187E-1	1.684E+1	5.620E-4	3.586E+1
End of Signal	2.134E+0	4.713E-1	1.643E+1	2.342E-3	4.896E+1

Sample ID: WF2-2-b

Impact V2.1

Summary Report

Sample ID

WF2-6

Material Description

NMP-2 3-Degree Surveillance Capsule - Weld material

Test Parameter	Value
Operator	Dr. Michael P. Manahan, Sr.
Date Tested	11/29/00 5:18 PM
Temperature	-16.00 °C
Oscilloscope	Model 441 Internal
Striker Name	8mm - Striker 16
Interpolation Method	Point-Point Linear
TO 892 Controller	Active Adjust
Sample Type	Metal
Sample Size	Type A
Orientation	TL
Notch Type	V Notch, no Side-Groove
Length	2.1654 in
Width	0.3937 in
Thickness	0.3937 in
Span	1.5748 in
Uncracked Ligament	0.3150 in
Notch Radius	0.0098 in
Velocity Determination	Potential Energy & Losses
Velocity	17.94 ft/s
Shear	37.90 %
Lateral Expansion	0.0335 in
Energy Adjustment	1.0093

Measured Data (V)

Oscilloscope Signal

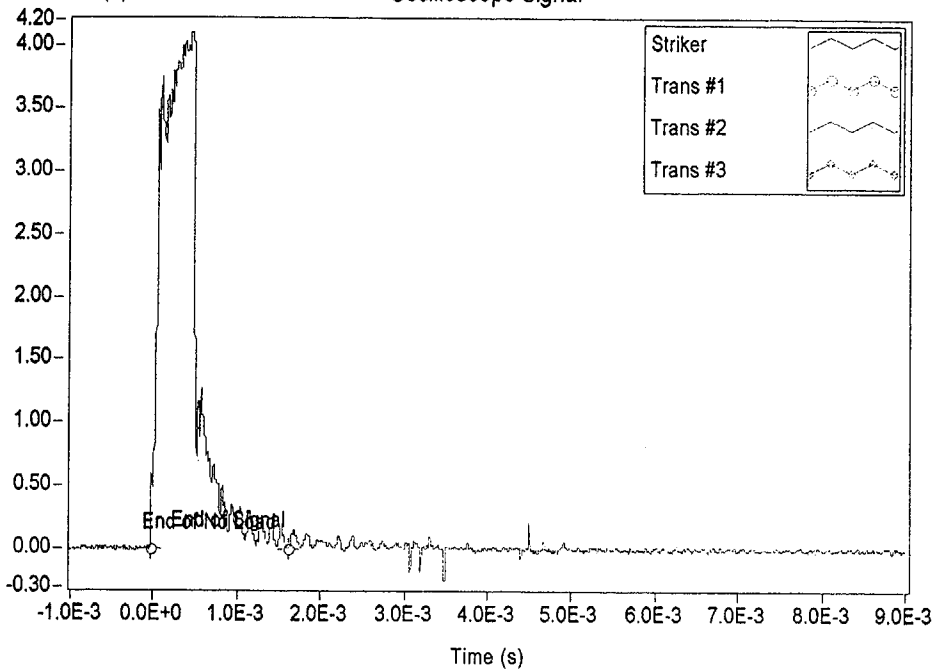

Result	Value
Optical Encoder Energy	37.516 ft lbf
Dial Gage Energy	37.40 ft lbf
Instrumented Striker Energy	37.516 ft lbf

Impact V2.1

Integration Report

Signal Source: 8mm - Striker 16 Striker

Load (lbf) vs. Time (s)

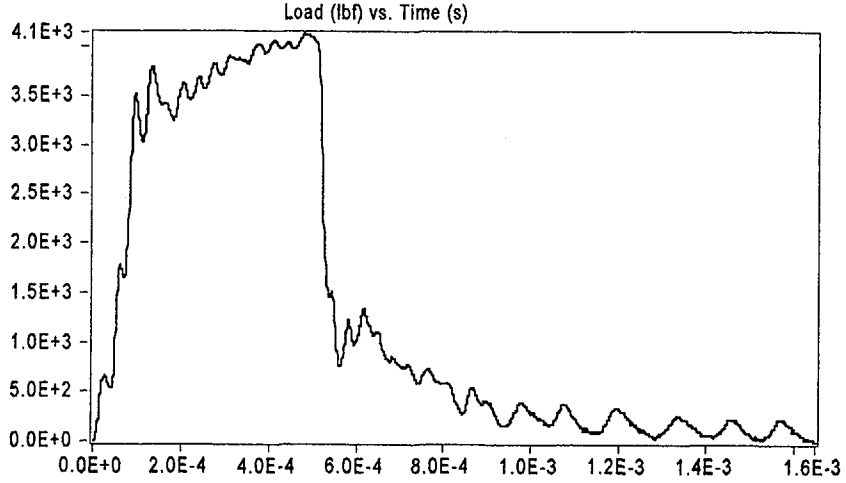

Velocity (ft/s) vs. Time (s)

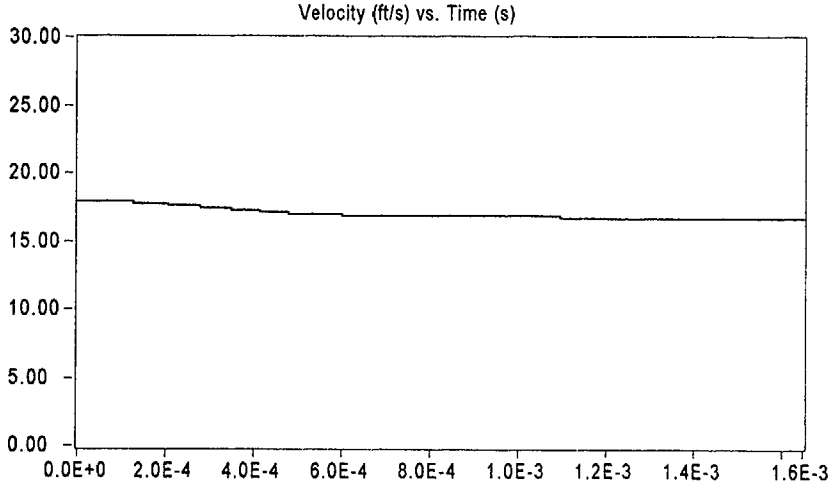

Displacement (in) vs. Time (s)

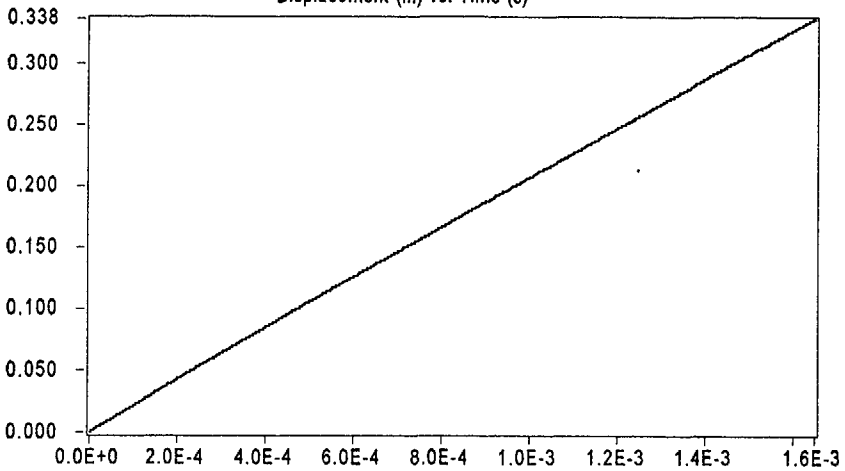

Load (lbf), Energy (ft lbf) vs. Displacement (in)

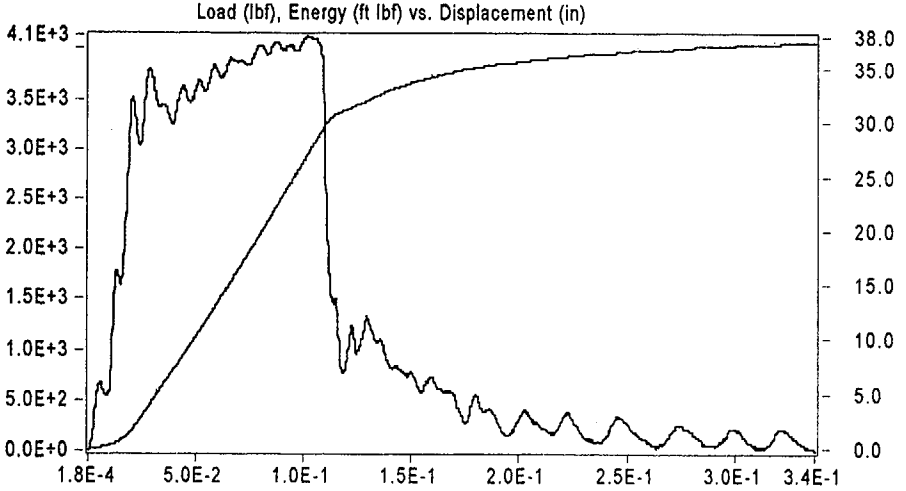

Sample Name: Wf2-6

Instrumented Striker Energy: 37.516 ft lbf

Impact V2.1

Load vs. Displacement Critical Points

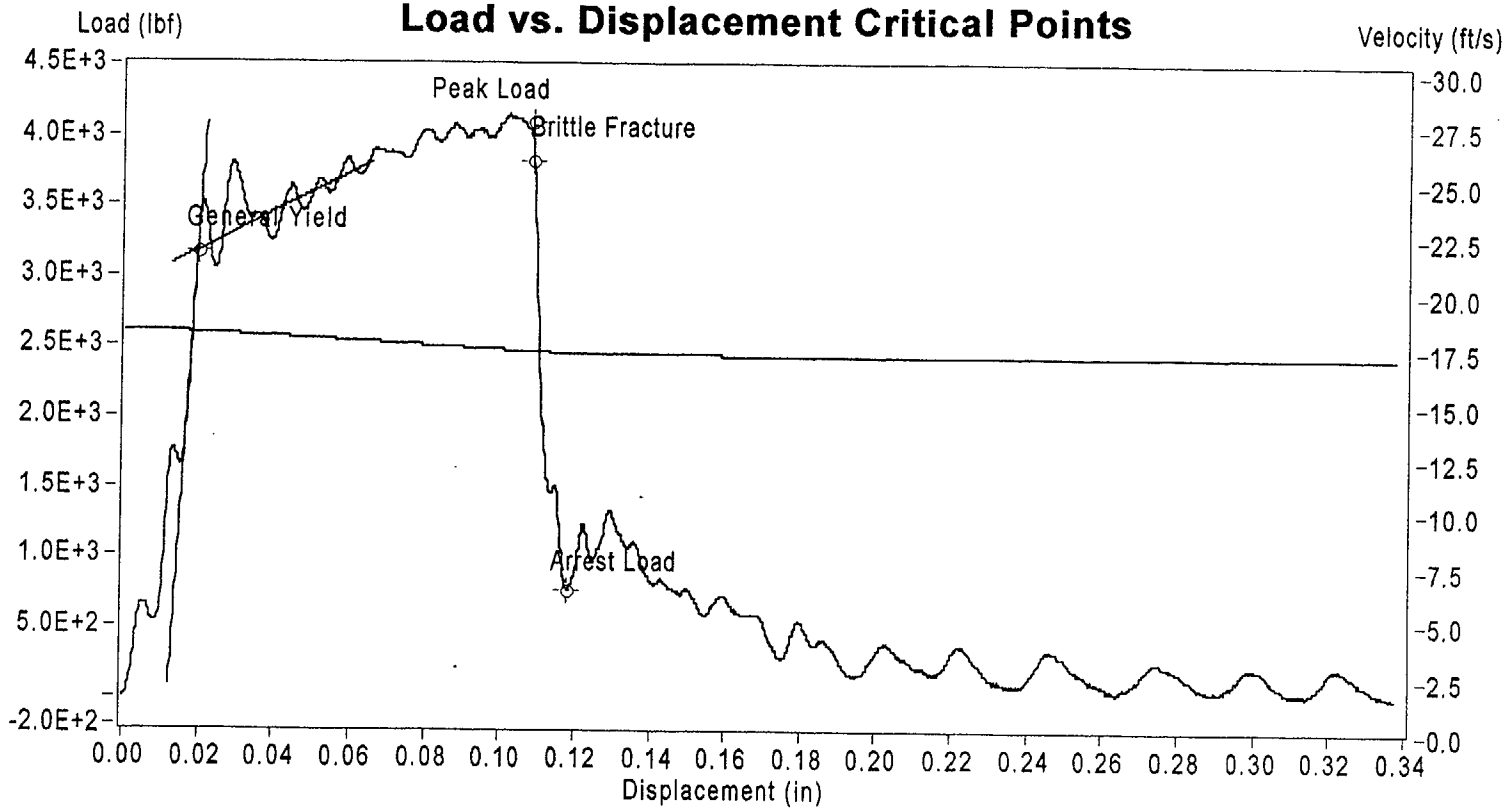

	Load (lbf)	Displacement (in)	Velocity (ft/s)	Time (s)	Energy (ft lbf)
General Yield	3.179E+3	1.930E-2	1.789E+1	4.289E-5	1.814E+0
Peak Load	4.091E+3	1.080E-1	1.704E+1	4.660E-4	2.959E+1
Brittle Fracture	3.825E+3	1.087E-1	1.703E+1	4.690E-4	2.979E+1
Arrest Load	7.653E+2	1.180E-1	1.699E+1	5.150E-4	3.114E+1
End of Signal	5.305E+0	3.376E-1	1.679E+1	1.601E-3	3.752E+1

Sample ID: **Wf2-6**

Impact V2.1

Summary Report

Sample ID

WF2-4

Material Description

NMP-2 3-Degree Surveillance Capsule - Weld material

Test Parameter	Value
Operator	Dr. Michael P. Manahan, Sr.
Date Tested	11/29/00 11:44 AM
Temperature	18.00 °C
Oscilloscope	Model 441 Internal
Striker Name	8mm - Striker 16
Interpolation Method	Point-Point Linear
TO 892 Controller	Active Adjust
Sample Type	Metal
Sample Size	Type A
Orientation	TL
Notch Type	V Notch, no Side-Groove
Length	2.1654 in
Width	0.3937 in
Thickness	0.3937 in
Span	1.5748 in
Uncracked Ligament	0.3150 in
Notch Radius	0.0098 in
Velocity Determination	Potential Energy & Losses
Velocity	17.94 ft/s
Shear	84.50 %
Lateral Expansion	0.0538 in
Energy Adjustment	1.0044

Measured Data (V)

Oscilloscope Signal

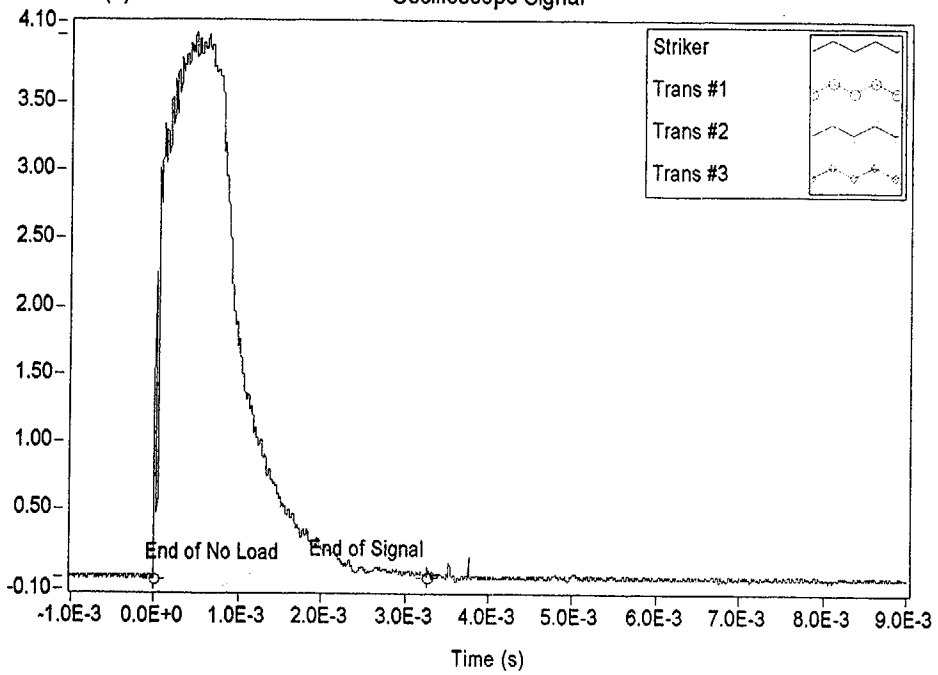

Result	Value
Optical Encoder Energy	70.491 ft lbf
Dial Gage Energy	70.30 ft lbf
Instrumented Striker Energy	70.491 ft lbf

Impact V2.1

Integration Report

Signal Source: 8mm - Striker 16 Striker

Load (lbf) vs. Time (s)

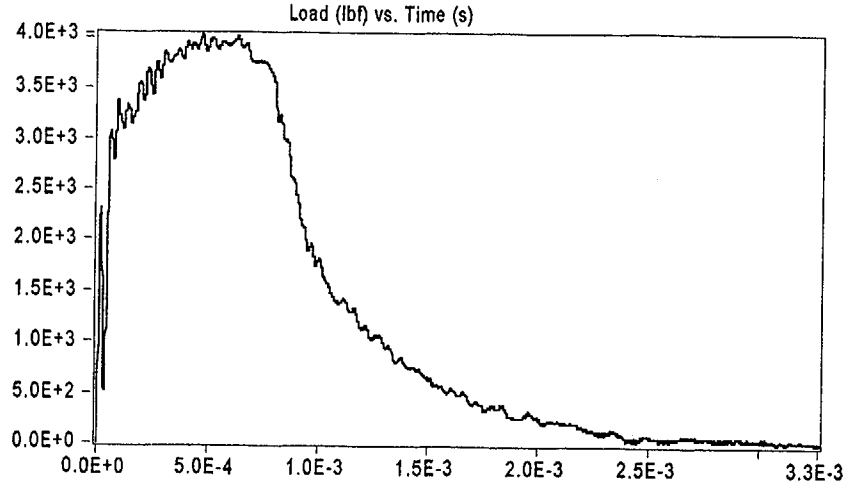

Velocity (ft/s) vs. Time (s)

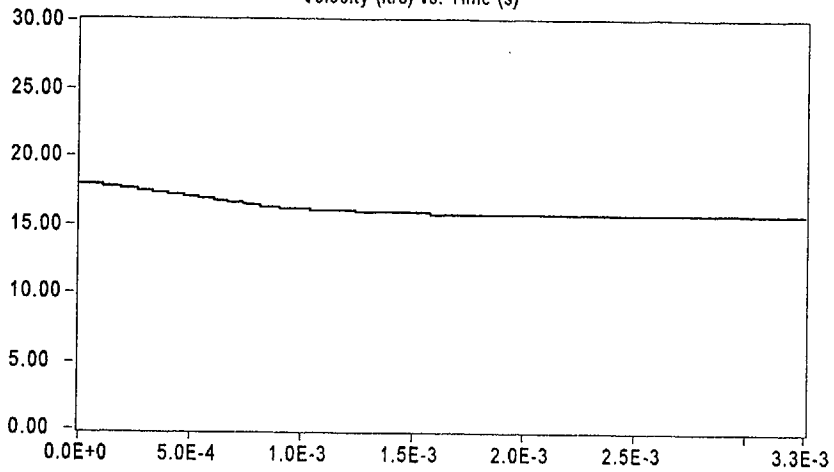

Displacement (in) vs. Time (s)

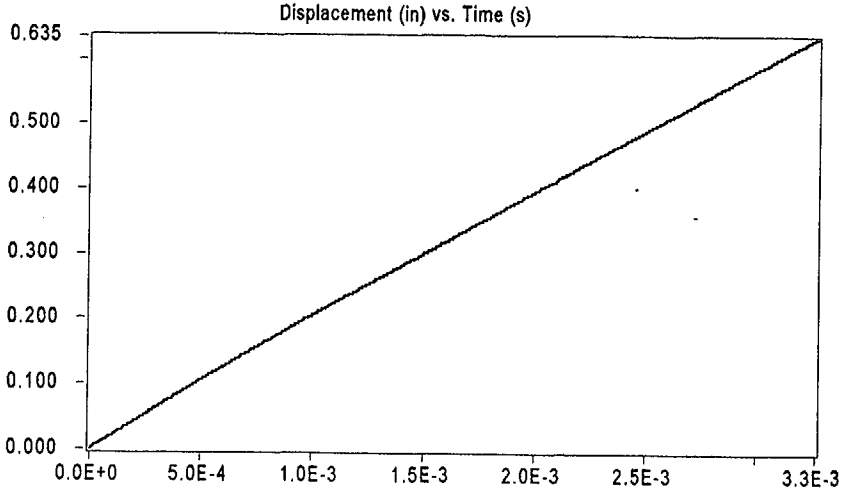

Load (lbf), Energy (ft lbf) vs. Displacement (in)

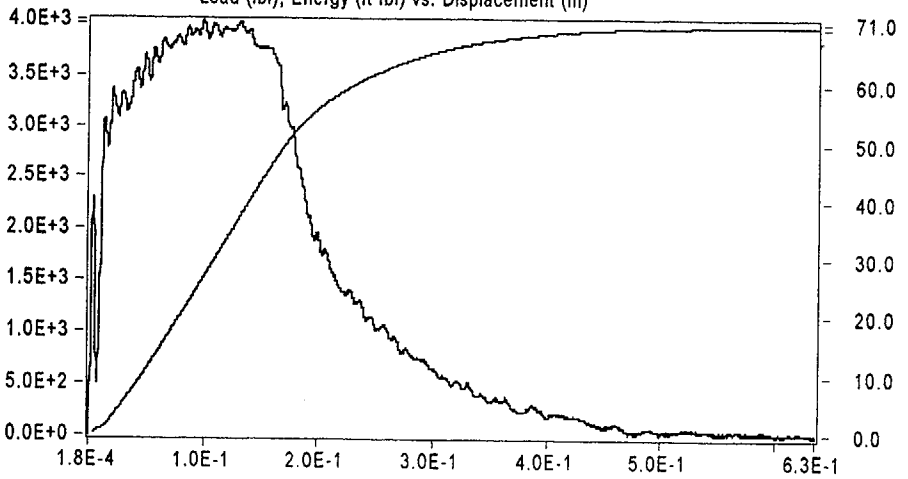

Sample Name: Wf2-4

Instrumented Striker Energy: 70.491 ft lbf

Impact V2.1

Load vs. Displacement Critical Points

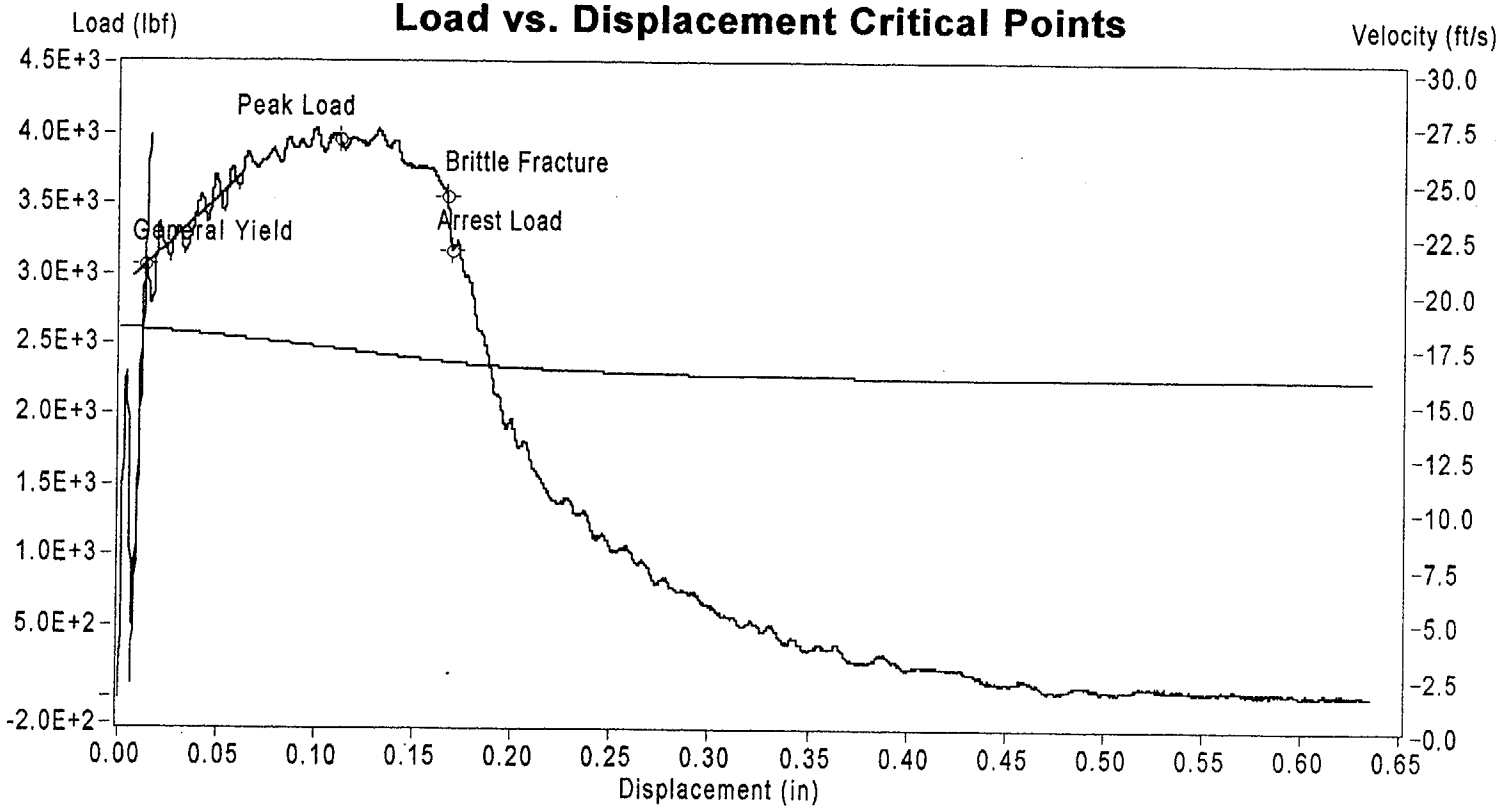

	Load (lbf)	Displacement (in)	Velocity (ft/s)	Time (s)	Energy (ft lbf)
General Yield	3.061E+3	1.284E-2	1.789E+1	5.387E-5	1.743E+0
Peak Load	3.963E+3	1.109E-1	1.699E+1	5.220E-4	3.137E+1
Brittle Fracture	3.559E+3	1.658E-1	1.643E+1	7.960E-4	4.897E+1
Arrest Load	3.165E+3	1.684E-1	1.640E+1	8.090E-4	4.968E+1
End of Signal	5.241E+0	6.350E-1	1.571E+1	3.264E-3	7.049E+1

Sample ID: Wf2-4

Impact V2.1

Summary Report

Sample ID

WF2-5

Material Description

NMP-2 3-Degree Surveillance Capsule - Weld material

Test Parameter	Value
Operator	Dr. Michael P. Manahan, Sr.
Date Tested	11/29/00 11:51 AM
Temperature	19.00 °C
Oscilloscope	Model 441 Internal
Striker Name	8mm - Striker 16
Interpolation Method	Point-Point Linear
TO 892 Controller	Active Adjust
Sample Type	Metal
Sample Size	Type A
Orientation	TL
Notch Type	V Notch, no Side-Groove
Length	2.1654 in
Width	0.3937 in
Thickness	0.3937 in
Span	1.5748 in
Uncracked Ligament	0.3150 in
Notch Radius	0.0098 in
Velocity Determination	Potential Energy & Losses
Velocity	17.94 ft/s
Shear	79.90 %
Lateral Expansion	0.0506 in
Energy Adjustment	1.0078

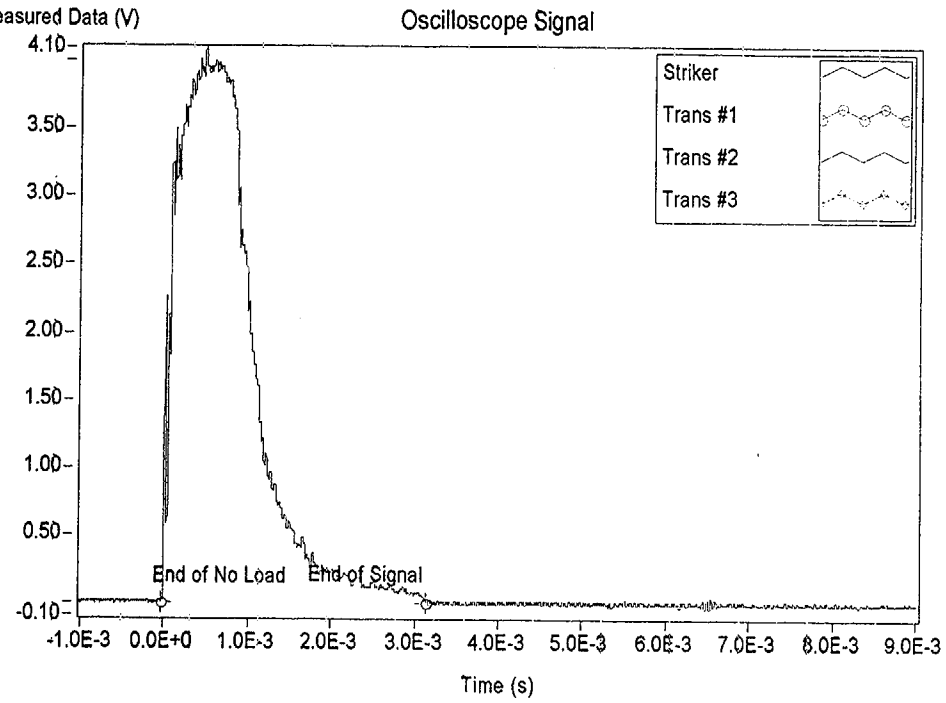

Result	Value
Optical Encoder Energy	73.589 ft lbf
Dial Gage Energy	73.40 ft lbf
Instrumented Striker Energy	73.589 ft lbf

Impact V2.1

Integration Report

Signal Source: 8mm - Striker 16 Striker

Load (lbf) vs. Time (s)

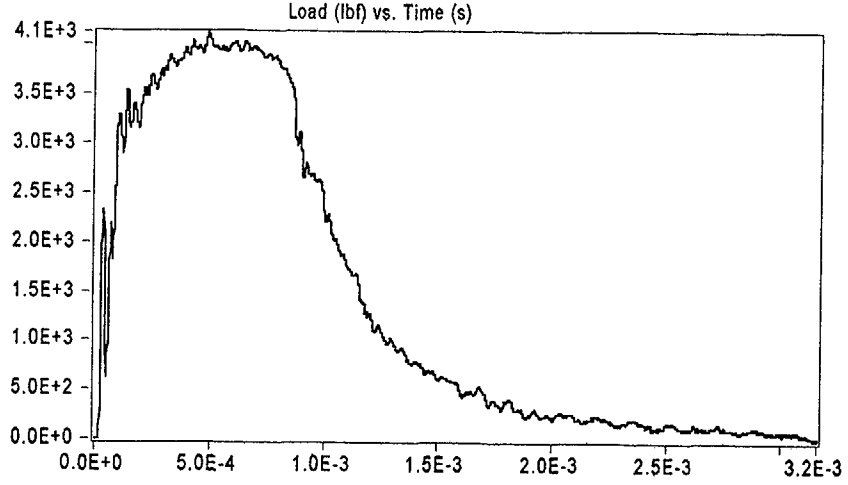

Velocity (ft/s) vs. Time (s)

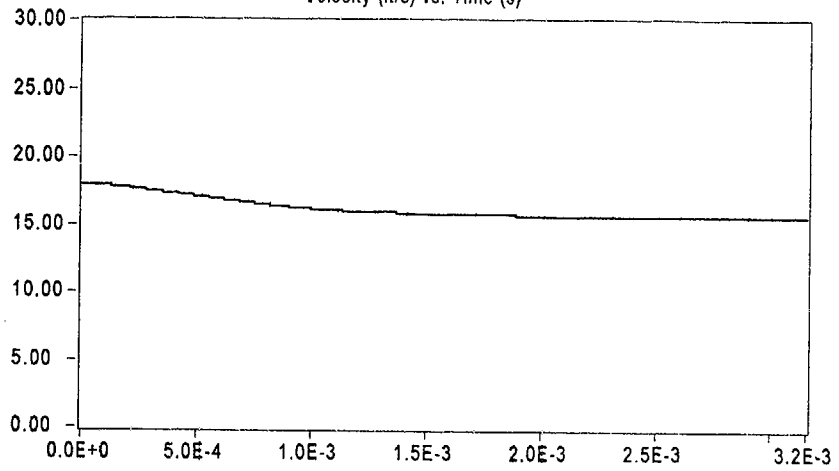

Displacement (in) vs. Time (s)

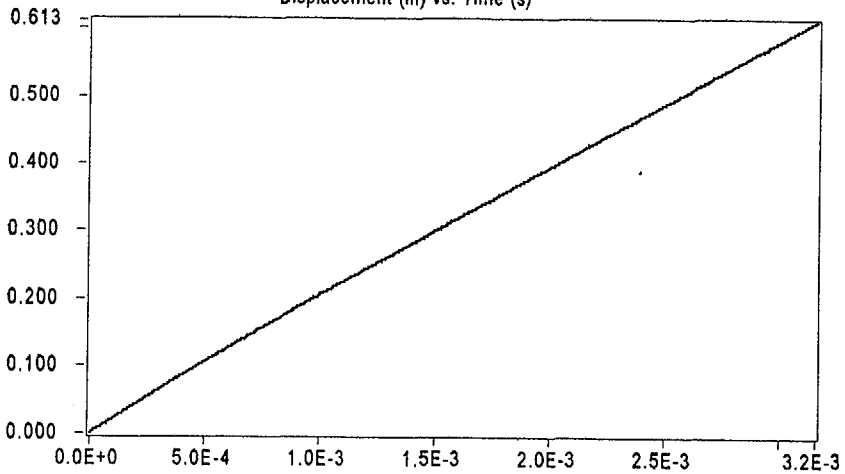

Load (lbf), Energy (ft lbf) vs. Displacement (in)

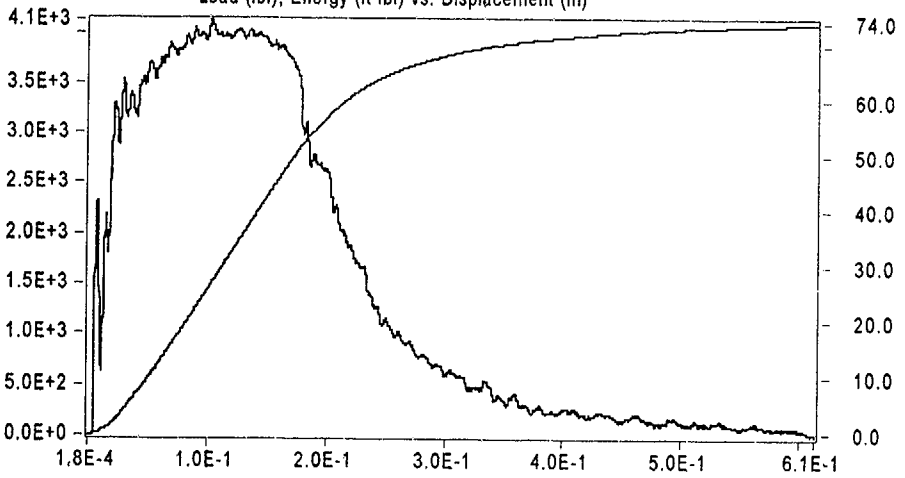

Sample Name: Wf2-5

Instrumented Striker Energy: 73.589 ft lbf

Impact V2.1

Load vs. Displacement Critical Points

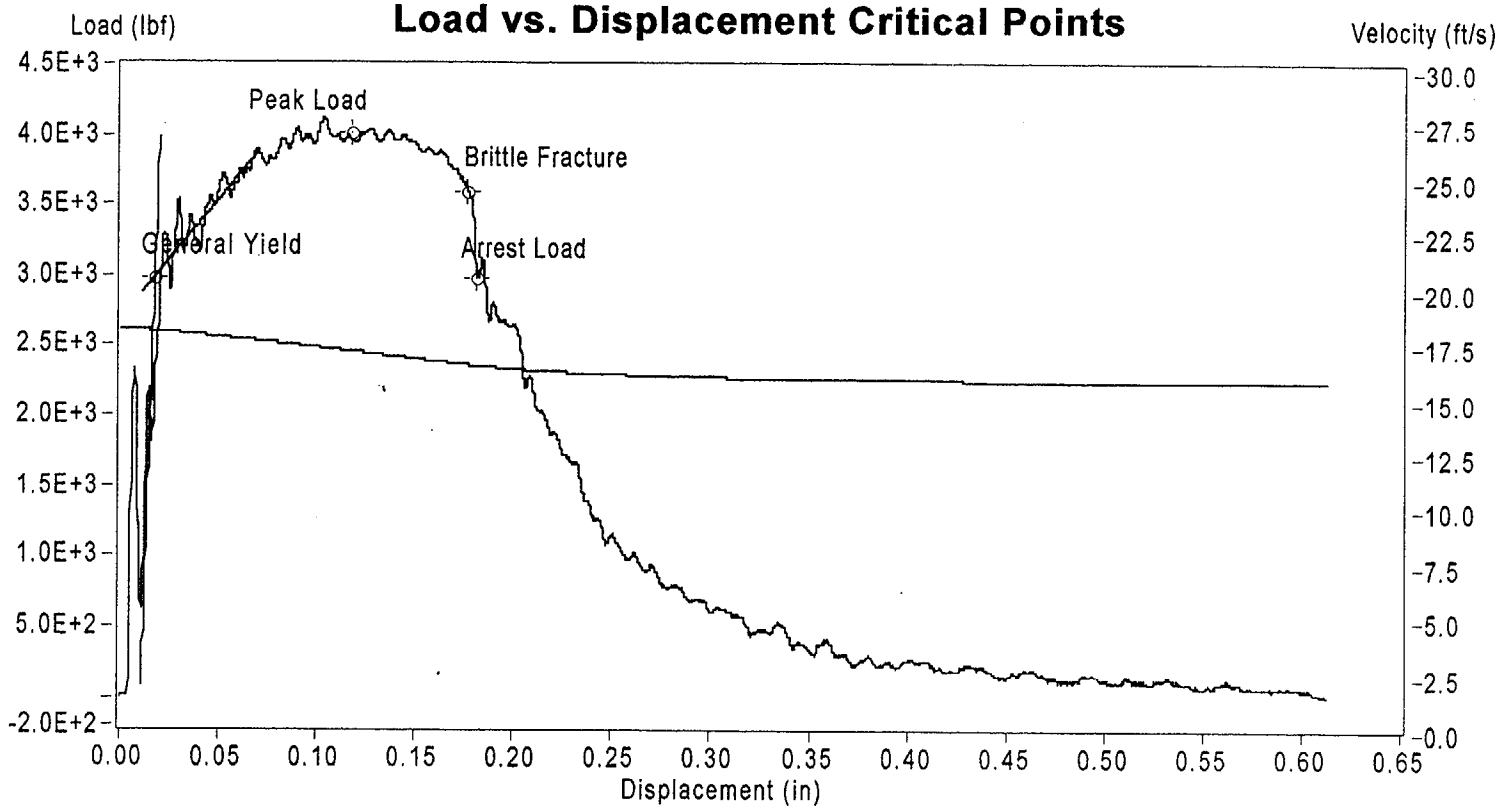

	Load (lbf)	Displacement (in)	Velocity (ft/s)	Time (s)	Energy (ft lbf)
General Yield	2.983E+3	1.758E-2	1.789E+1	5.789E-5	1.733E+0
Peak Load	4.004E+3	1.179E-1	1.695E+1	5.370E-4	3.246E+1
Brittle Fracture	3.598E+3	1.764E-1	1.634E+1	8.300E-4	5.148E+1
Arrest Load	2.976E+3	1.811E-1	1.630E+1	8.540E-4	5.280E+1
End of Signal	2.230E+0	6.126E-1	1.561E+1	3.137E-3	7.359E+1

Sample ID: Wf2-5

Impact V2.1

Summary Report

Sample ID

WF2-3

Material Description

NMP-2 3-Degree Surveillance Capsule - Weld material

Test Parameter	Value
Operator	Dr. Michael P. Manahan, Sr.
Date Tested	11/29/00 12:55 PM
Temperature	63.00 °C
Oscilloscope	Model 441 Internal
Striker Name	8mm - Striker 16
Interpolation Method	Point-Point Linear
TO 892 Controller	Active Adjust
Sample Type	Metal
Sample Size	Type A
Orientation	TL
Notch Type	V Notch, no Side-Groove
Length	2.1654 in
Width	0.3937 in
Thickness	0.3937 in
Span	1.5748 in
Uncracked Ligament	0.3150 in
Notch Radius	0.0098 in
Velocity Determination	Potential Energy & Losses
Velocity	17.94 ft/s
Shear	100.00 %
Lateral Expansion	0.0750 in
Energy Adjustment	1.0166

Measured Data (V)

Oscilloscope Signal

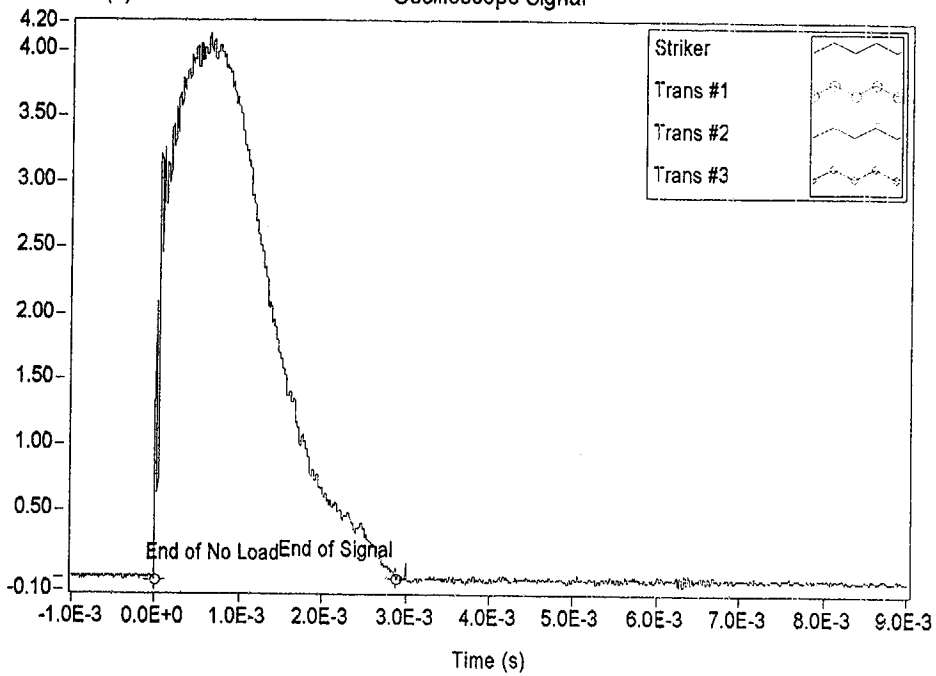

Result	Value
Optical Encoder Energy	96.438 ft lbf
Dial Gage Energy	96.20 ft lbf
Instrumented Striker Energy	96.438 ft lbf

Impact V2.1

Integration Report

Signal Source: 8mm - Striker 16 Striker

Load (lbf) vs. Time (s)

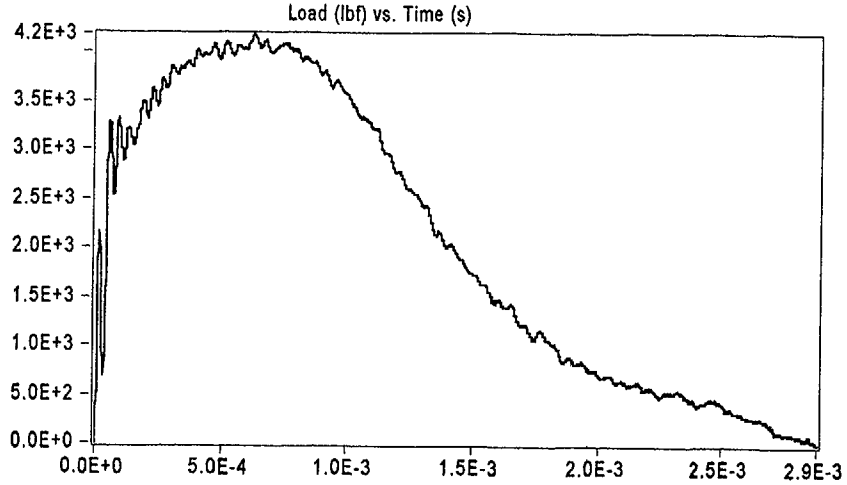

Velocity (ft/s) vs. Time (s)

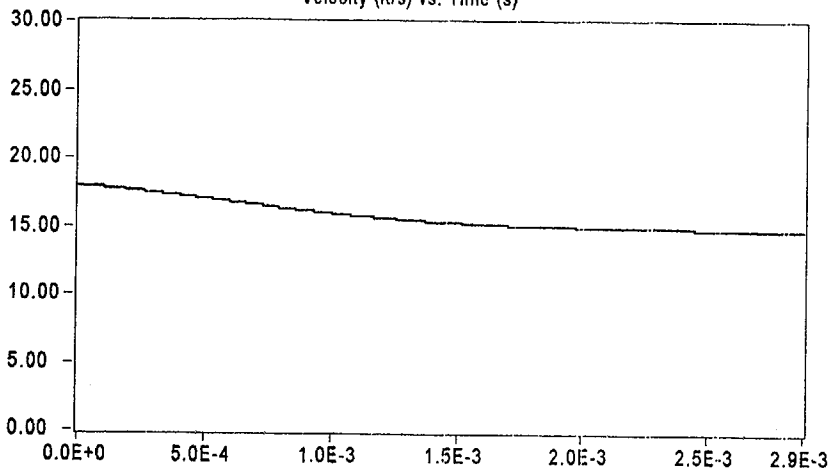

Displacement (in) vs. Time (s)

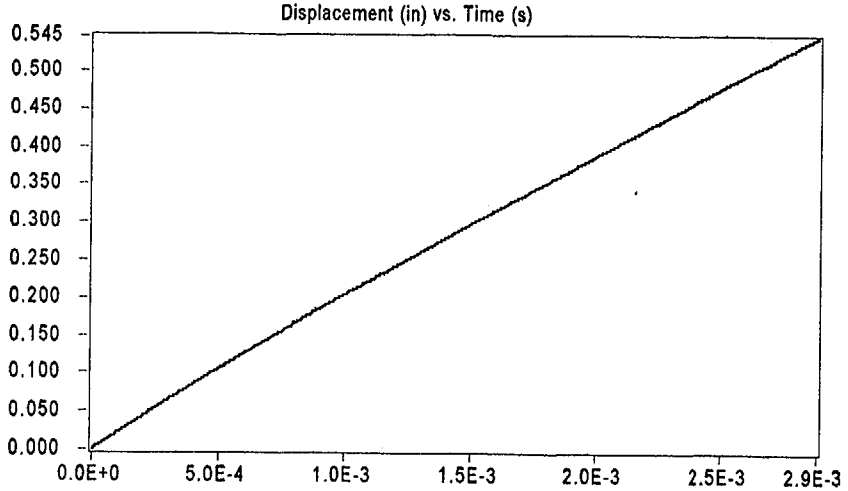

Load (lbf), Energy (ft lbf) vs. Displacement (in)

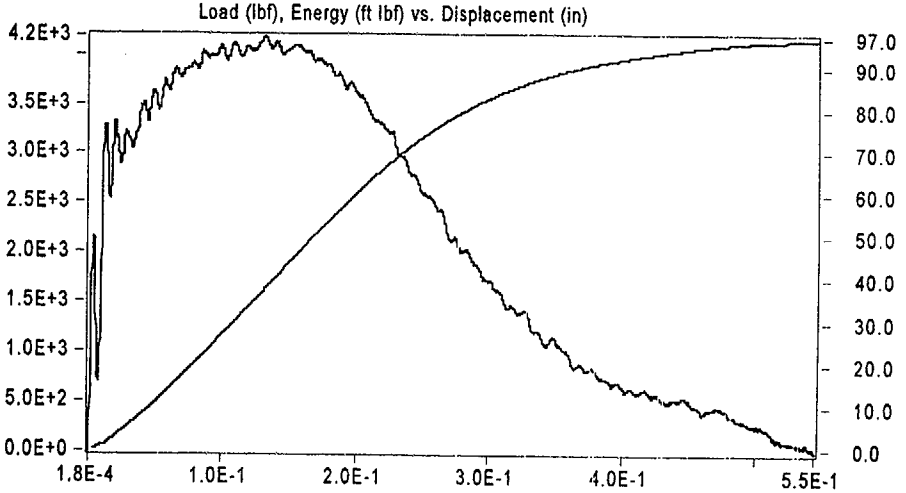

Sample Name: Wf2-3

Instrumented Striker Energy: 96.438 ft lbf

Impact V2.1

Load vs. Displacement Critical Points

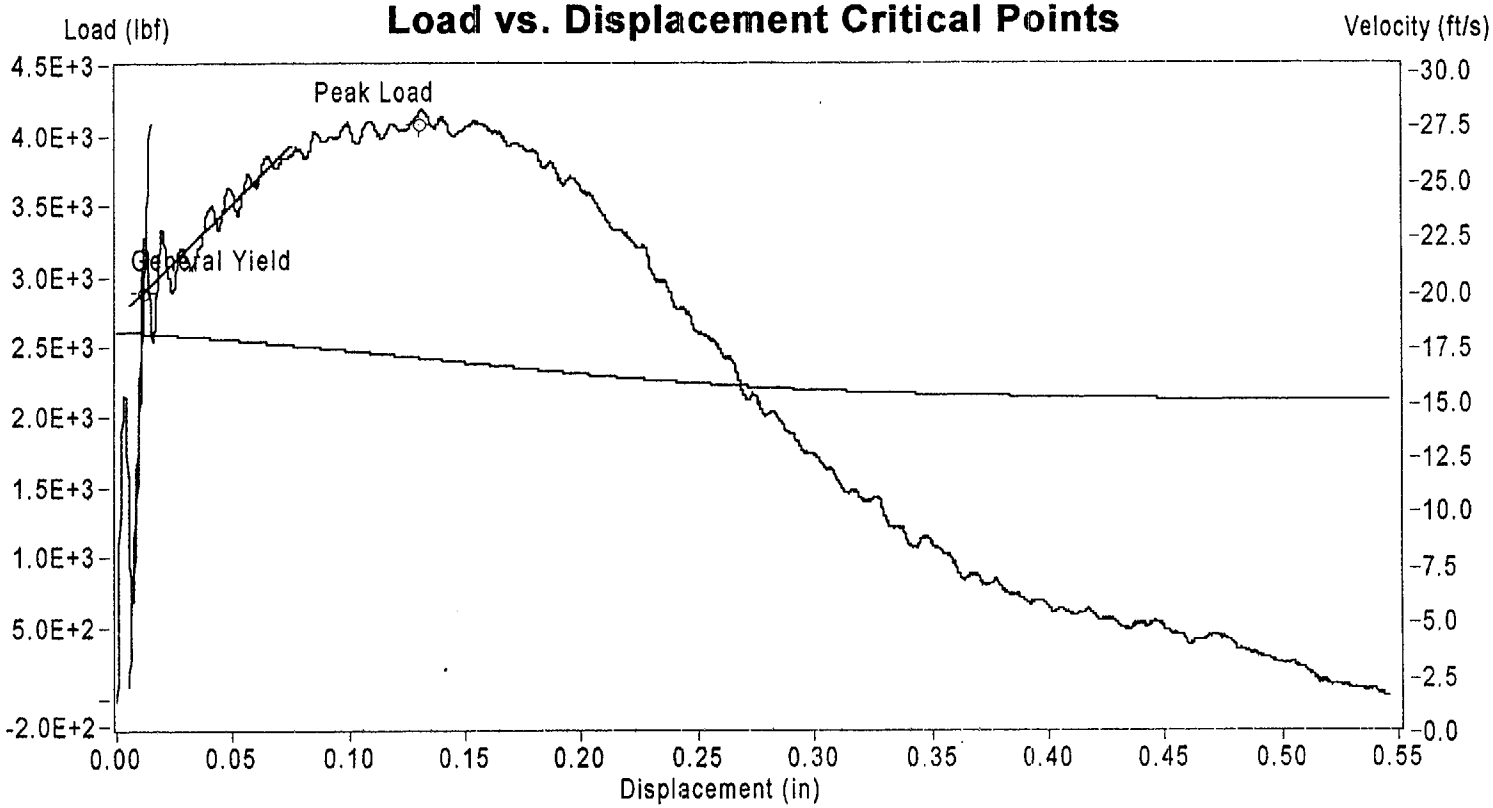

	Load (lbf)	Displacement (in)	Velocity (ft/s)	Time (s)	Energy (ft lbf)
General Yield	2.899E+3	1.176E-2	1.789E+1	4.886E-5	1.548E+0
Peak Load	4.085E+3	1.294E-1	1.679E+1	6.130E-4	3.764E+1
End of Signal	2.438E+0	5.453E-1	1.481E+1	2.872E-3	9.644E+1

Sample ID: Wf2-3

Impact V2.1

Summary Report

Sample ID

WF2-7

Material Description

NMP-2 3-Degree Surveillance Capsule - Weld material

Test Parameter	Value
Operator	Dr. Michael P. Manahan, Sr.
Date Tested	11/29/00 12:34 PM
Temperature	64.00 °C
Oscilloscope	Model 441 Internal
Striker Name	8mm - Striker 16
Interpolation Method	Point-Point Linear
TO 892 Controller	Active Adjust
Sample Type	Metal
Sample Size	Type A
Orientation	TL
Notch Type	V Notch, no Side-Groove
Length	2.1654 in
Width	0.3937 in
Thickness	0.3937 in
Span	1.5748 in
Uncracked Ligament	0.3150 in
Notch Radius	0.0098 in
Velocity Determination	Potential Energy & Losses
Velocity	17.94 ft/s
Shear	100.00 %
Lateral Expansion	0.0725 in
Energy Adjustment	1.0322

Measured Data (V)

Oscilloscope Signal

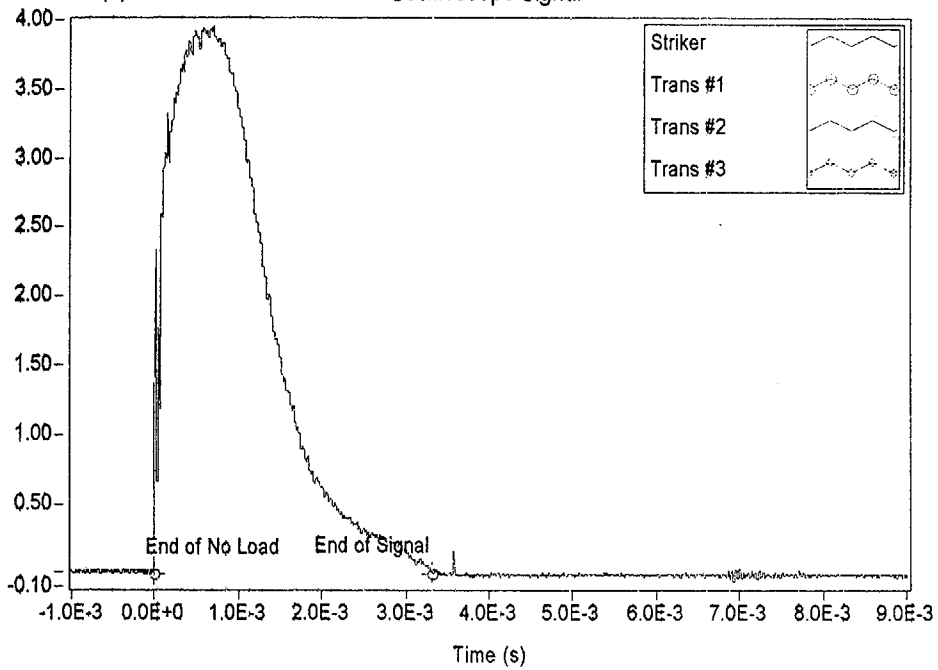

Result	Value
Optical Encoder Energy	95.535 ft lbf
Dial Gage Energy	95.40 ft lbf
Instrumented Striker Energy	95.535 ft lbf

Impact V2.1

Integration Report

Signal Source: 8mm - Striker 16 Striker

Load (lbf) vs. Time (s)

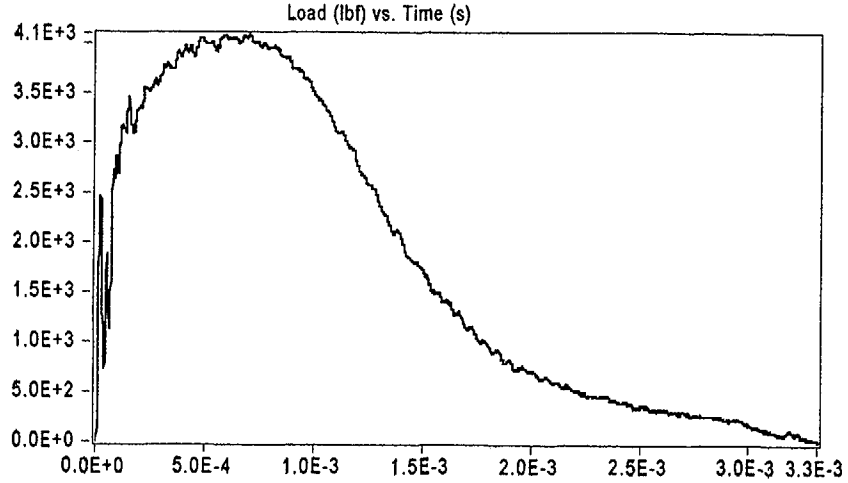

Velocity (ft/s) vs. Time (s)

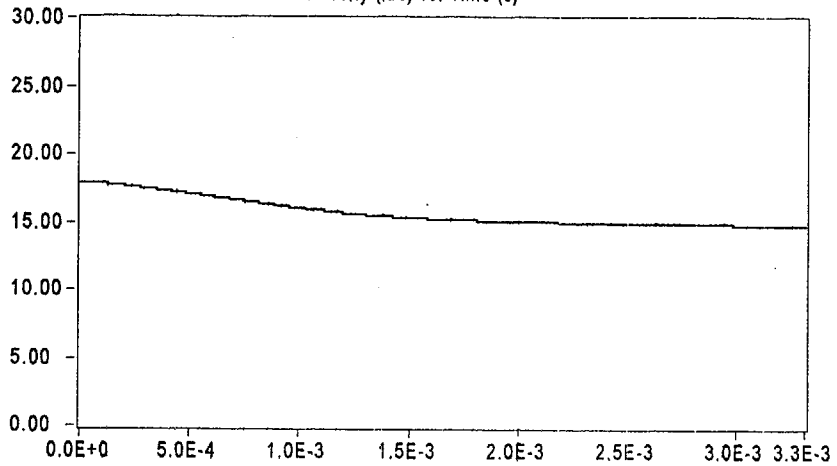

Displacement (in) vs. Time (s)

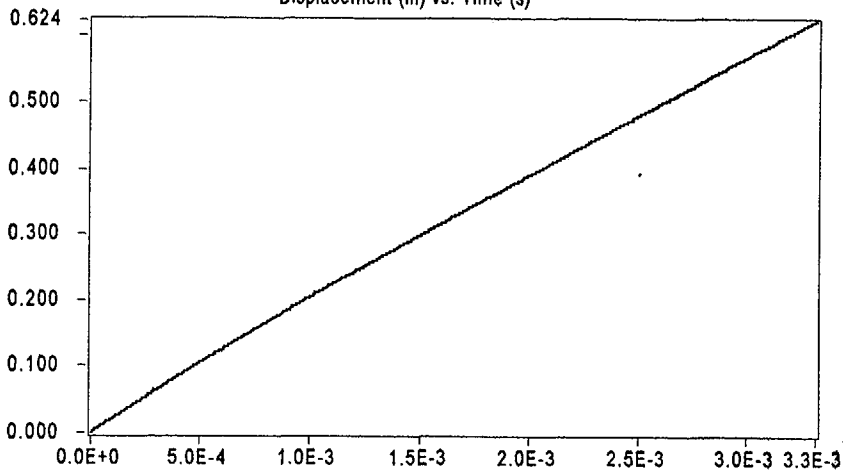

Load (lbf), Energy (ft lbf) vs. Displacement (in)

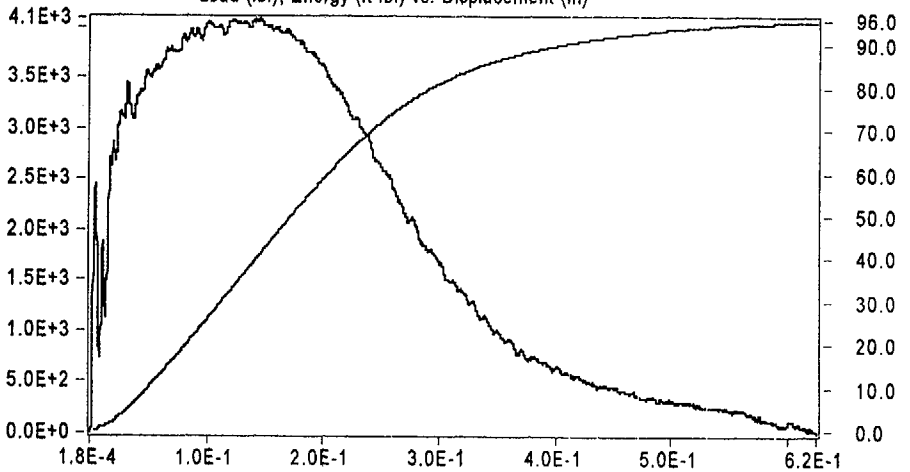

Sample Name: WF2-7-b

Instrumented Striker Energy: 95.535 ft lbf

Impact V2.1

Load vs. Displacement Critical Points

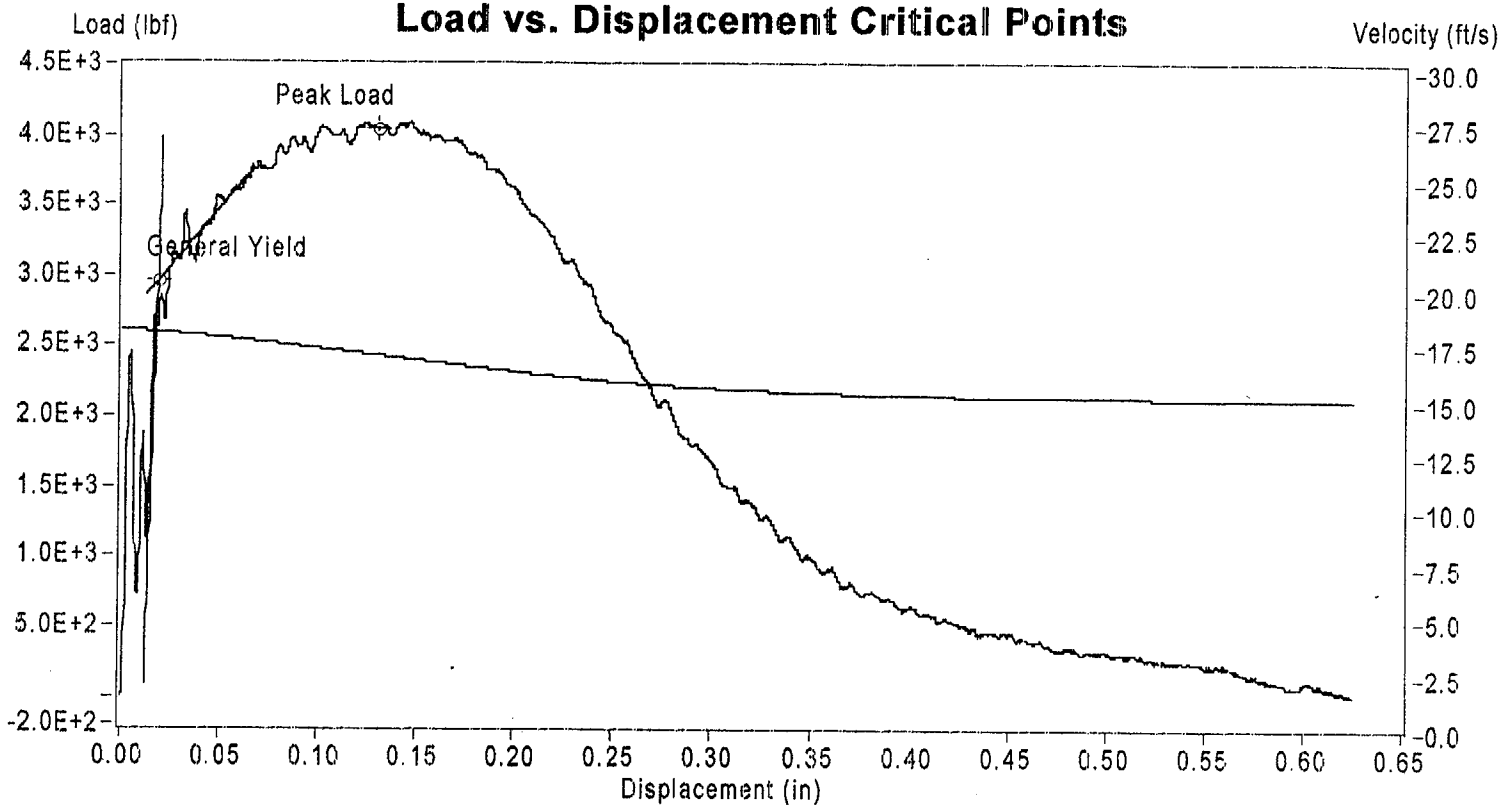

	Load (lbf)	Displacement (in)	Velocity (ft/s)	Time (s)	Energy (ft lbf)
General Yield	2.956E+3	1.843E-2	1.787E+1	7.591E-5	2.425E+0
Peak Load	4.043E+3	1.296E-1	1.682E+1	6.090E-4	3.651E+1
End of Signal	2.028E+0	6.244E-1	1.484E+1	3.302E-3	9.554E+1

Sample ID: WF2-7-b

Impact V2.1

Summary Report

Sample ID

WF2-11

Material Description

NMP-2 3-Degree Surveillance Capsule - Weld material

Test Parameter	Value
Operator	Dr. Michael P. Manahan, Sr.
Date Tested	11/29/00 2:32 PM
Temperature	121.00 °C
Oscilloscope	Model 441 Internal
Striker Name	8mm - Striker 16
Interpolation Method	Point-Point Linear
TO 892 Controller	Active Adjust
Sample Type	Metal
Sample Size	Type A
Orientation	TL
Notch Type	V Notch, no Side-Groove
Length	2.1654 in
Width	0.3937 in
Thickness	0.3937 in
Span	1.5748 in
Uncracked Ligament	0.3150 in
Notch Radius	0.0098 in
Velocity Determination	Potential Energy & Losses
Velocity	17.94 ft/s
Shear	100.00 %
Lateral Expansion	0.0728 in
Energy Adjustment	1.0162

Measured Data (V)

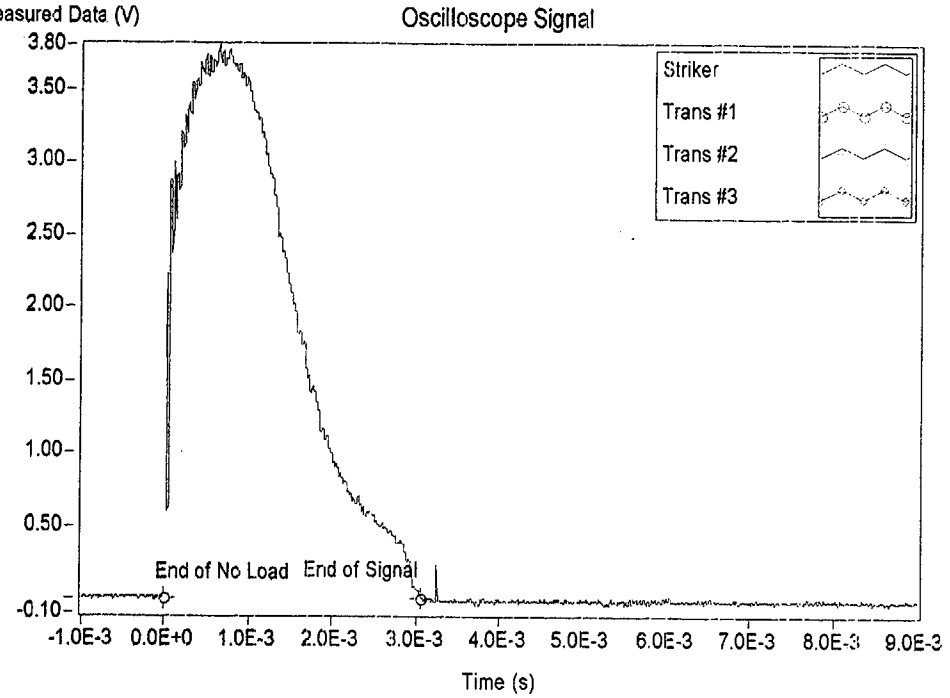

Result	Value
Optical Encoder Energy	102.36 ft lbf
Dial Gage Energy	102.1 ft lbf
Instrumented Striker Energy	102.36 ft lbf

Impact V2.1

Integration Report

Signal Source: 8mm - Striker 16 Striker

Load (lbf) vs. Time (s)

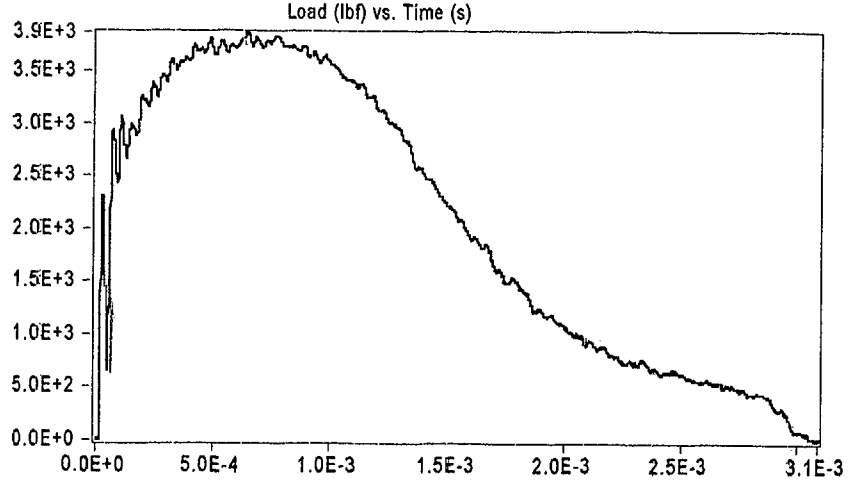

Velocity (ft/s) vs. Time (s)

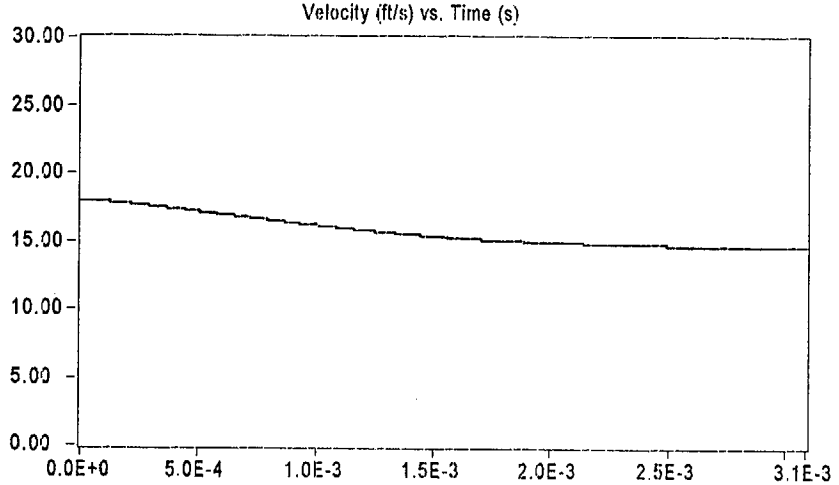

Displacement (in) vs. Time (s)

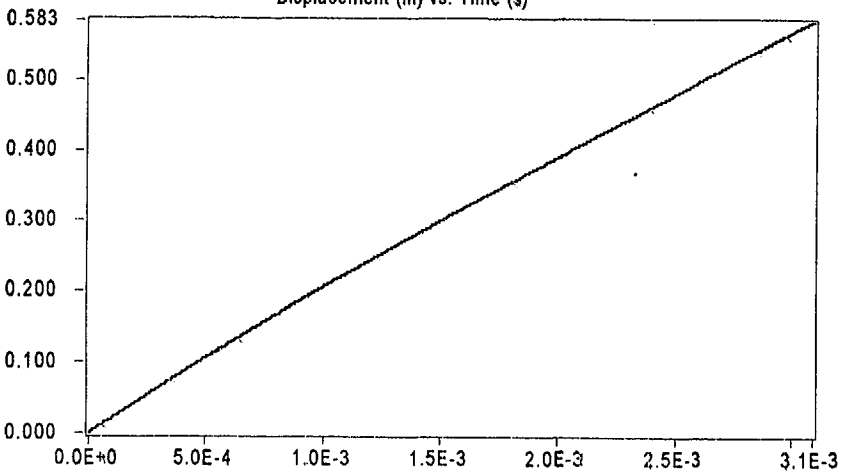

Load (lbf), Energy (ft lbf) vs. Displacement (in)

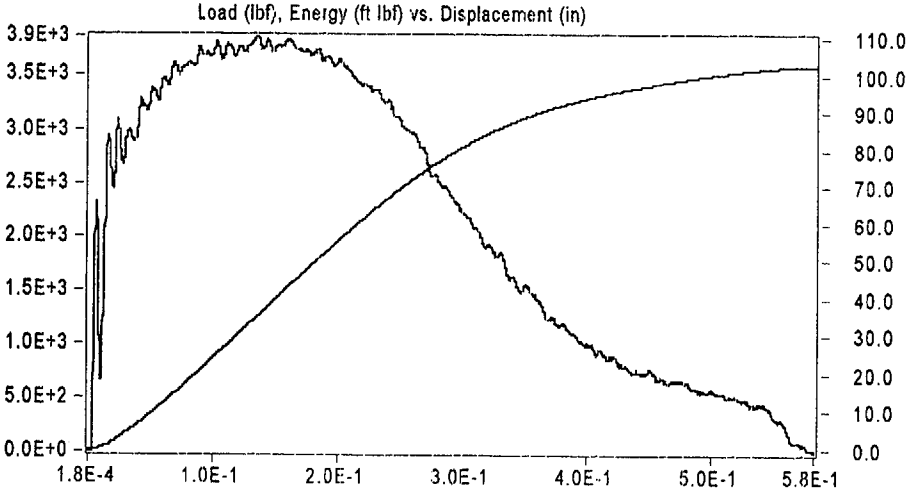

Sample Name: Wf2-11

Instrumented Striker Energy: 102.36 ft lbf

Impact V2.1

Load vs. Displacement Critical Points

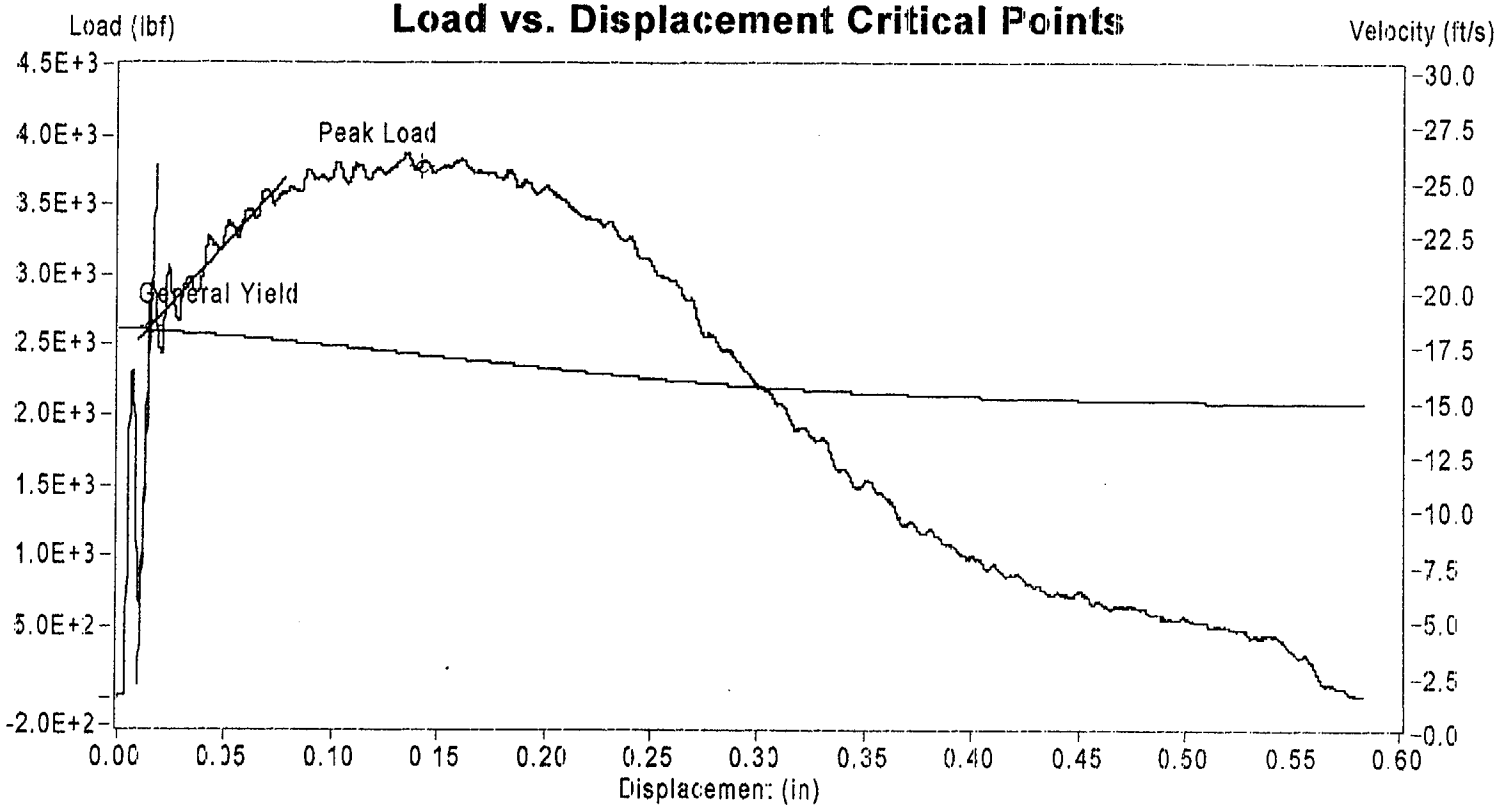

	Load (lbf)	Displacement (in)	Velocity (ft/s)	Time (s)	Energy (ft lbf)
General Yield	2.632E+3	1.499E-2	1.789E+1	5.088E-5	1.582E+0
Peak Load	3.783E+3	1.415E-1	1.678E+1	6.580E-4	3.795E+1
End of Signal	2.411E+0	5.828E-1	1.460E+1	3.070E-3	1.024E+2

Sample ID: Wf2-11

Impact V2.1

Summary Report

Sample ID

WF2-8

Material Description

NMP-2 3-Degree Surveillance Capsule - Weld material

Test Parameter	Value
Operator	Dr. Michael P. Manahan, Sr.
Date Tested	11/29/00 2:44 PM
Temperature	122.00 °C
Oscilloscope	Model 441 Internal
Striker Name	8mm - Striker 16
Interpolation Method	Point-Point Linear
TO 892 Controller	Active Adjust
Sample Type	Metal
Sample Size	Type A
Orientation	TL
Notch Type	V Notch, no Side-Groove
Length	2.1654 in
Width	0.3937 in
Thickness	0.3937 in
Span	1.5748 in
Uncracked Ligament	0.3150 in
Notch Radius	0.0098 in
Velocity Determination	Potential Energy & Losses
Velocity	17.94 ft/s
Shear	100.00 %
Lateral Expansion	0.0703 in
Energy Adjustment	1.0306

Measured Data (V)

Oscilloscope Signal

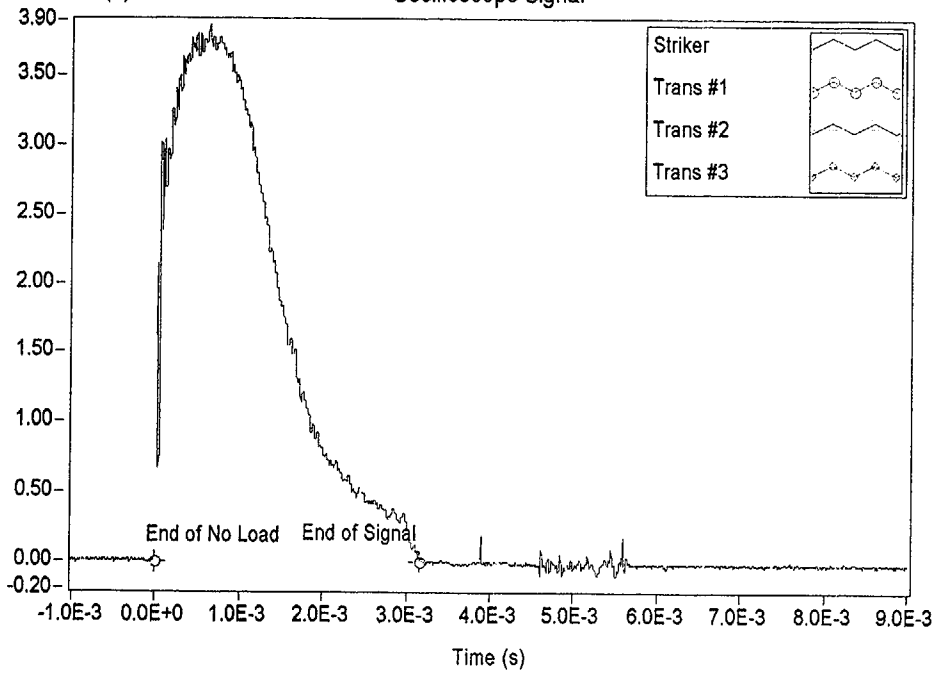

Result	Value
Optical Encoder Energy	100.41 ft lbf
Dial Gage Energy	100.1 ft lbf
Instrumented Striker Energy	100.41 ft lbf

Impact V2.1

Integration Report

Signal Source: 8mm - Striker 16 Striker

Load (lbf) vs. Time (s)

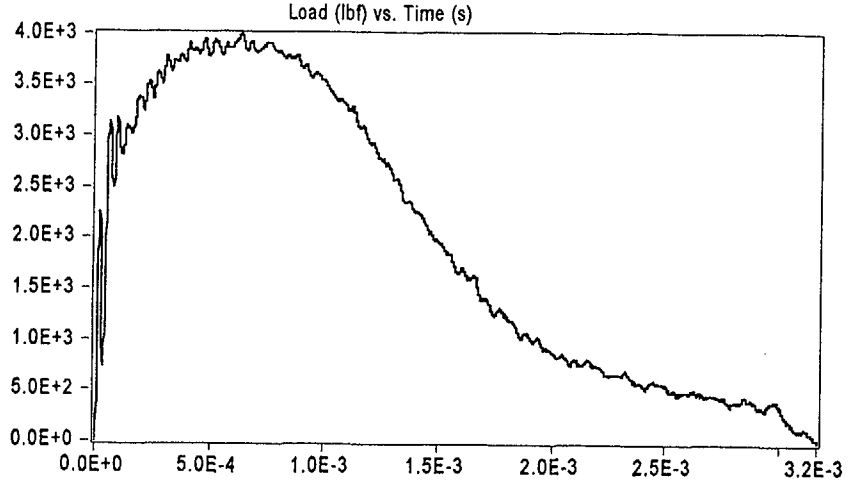

Velocity (ft/s) vs. Time (s)

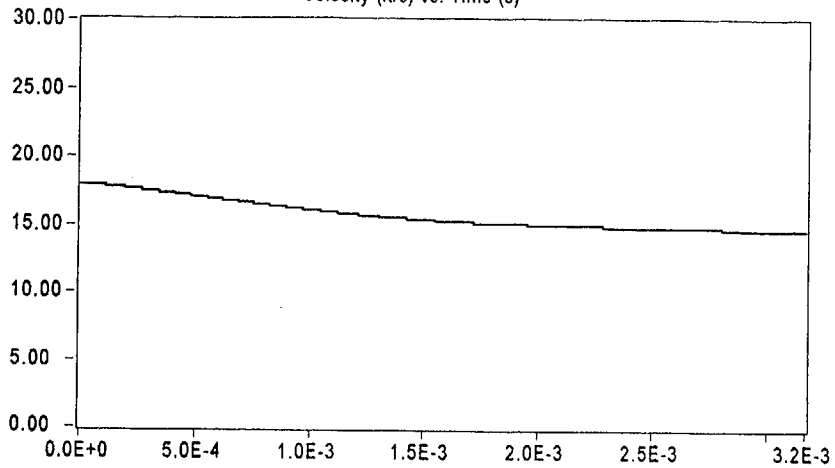

Displacement (in) vs. Time (s)

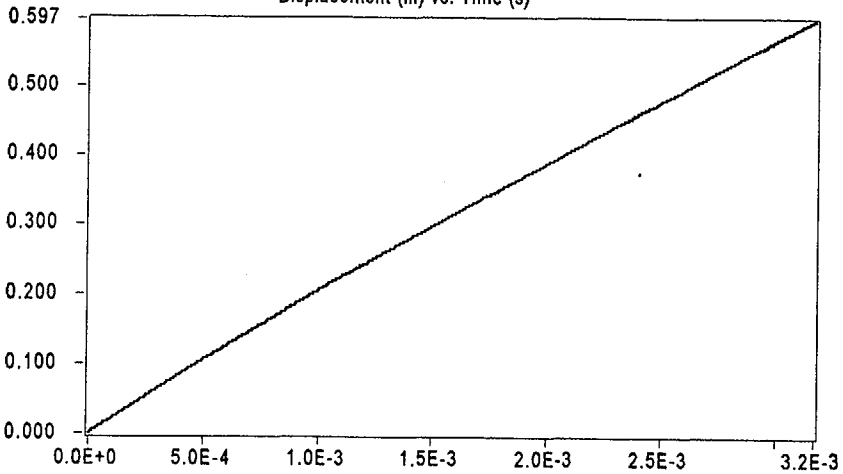

Load (lbf), Energy (ft lbf) vs. Displacement (in)

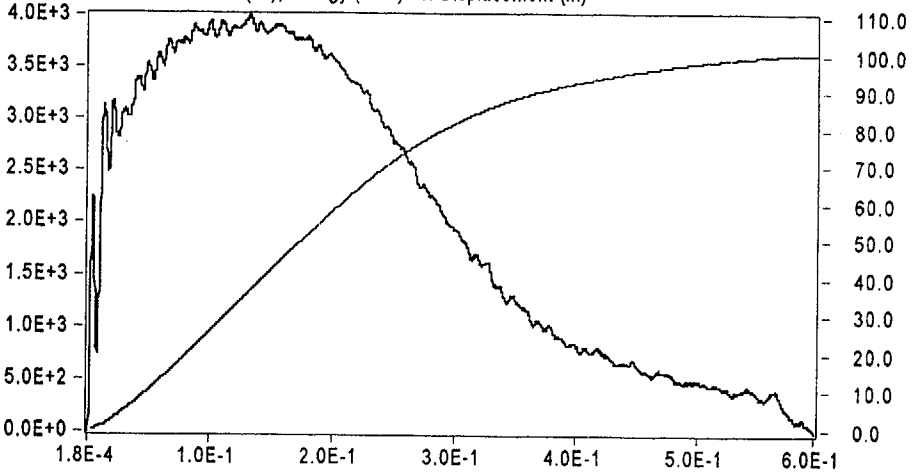

Sample Name: Wf2-8

Instrumented Striker Energy: 100.41 ft lbf

Impact V2.1

Load vs. Displacement Critical Points

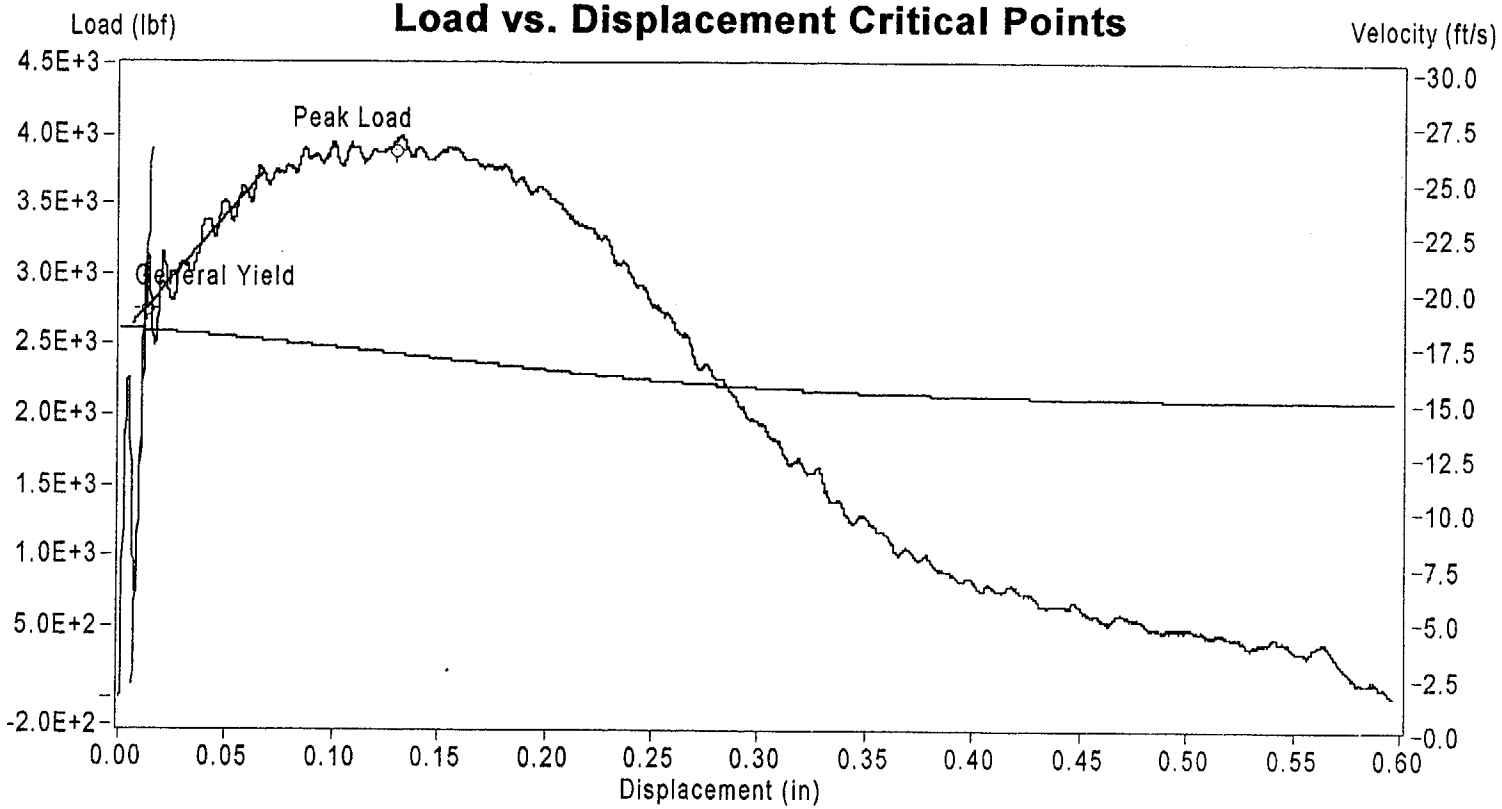

	Load (lbf)	Displacement (in)	Velocity (ft/s)	Time (s)	Energy (ft lbf)
General Yield	2.760E+3	1.219E-2	1.789E+1	4.887E-5	1.564E+0
Peak Load	3.895E+3	1.285E-1	1.684E+1	6.060E-4	3.595E+1
End of Signal	1.736E+0	5.966E-1	1.467E+1	3.160E-3	1.004E+2

Sample ID: Wf2-8

Appendix A-3 HAZ Data

The HAZ Charpy data are summarized below. The instrumented data provided on the pages which follow are given in the order shown in the table. There are three instrumented data plots for each specimen tested.

Summary of Charpy V-Notch Impact Test Results for Irradiated HAZ Metal Specimens from the Nine Mile Point Unit 2 3-Degree Surveillance Capsule.

Specimen Identification	Test Temperature (°F)	Impact Energy (ft-lb)	Fracture Appearance (% Shear Area)	Lateral Expansion (mils)
HF3-11	-99.4	16.3	12.3	10.5
HF3-10	-92.2	9.9	14.0	6.0
HF3-6	-56.2	18.5	21.3	12.5
HF3	-54.4	39.8	24.2	30.5
HF3-5	-29.2	47.3	55.8	a
HF3-7	-29.2	64.7	42.6	43.0
HF3-2	-0.4	36.2	53.0	30.0
HF3-9	1.4	103.6	78.7	a
HF3-4	59.0	109.9	100.0	73.2
HF3-8	66.2	117.7	100.0	73.5
HF3-12	206.6	94.8	100.0	73.0
HF3-3	212.0	96.2	100.0	74.0

a In accordance with ASTM E23, these values are not reported due to limitations on the partial break.

Impact V2.1

Summary Report

Sample ID

HF3-11

Material Description

NMP-2 3-Degree Surveillance Capsule - HAZ material

Test Parameter	Value
Operator	Dr. Michael P. Manahan, Sr.
Date Tested	11/27/00 2:59 PM
Temperature	-73.00 °C
Oscilloscope	Model 441 Internal
Striker Name	8mm - Striker 16
Interpolation Method	Point-Point Linear
TO 892 Controller	Active Adjust
Sample Type	Metal
Sample Size	Type A
Orientation	TL
Notch Type	V Notch, no Side-Groove
Length	2.1654 in
Width	0.3937 in
Thickness	0.3937 in
Span	1.5748 in
Uncracked Ligament	0.3150 in
Notch Radius	0.0098 in
Velocity Determination	Potential Energy & Losses
Velocity	17.94 ft/s
Shear	12.30 %
Lateral Expansion	0.0105 in
Energy Adjustment	1.0158

Measured Data (V)

Oscilloscope Signal

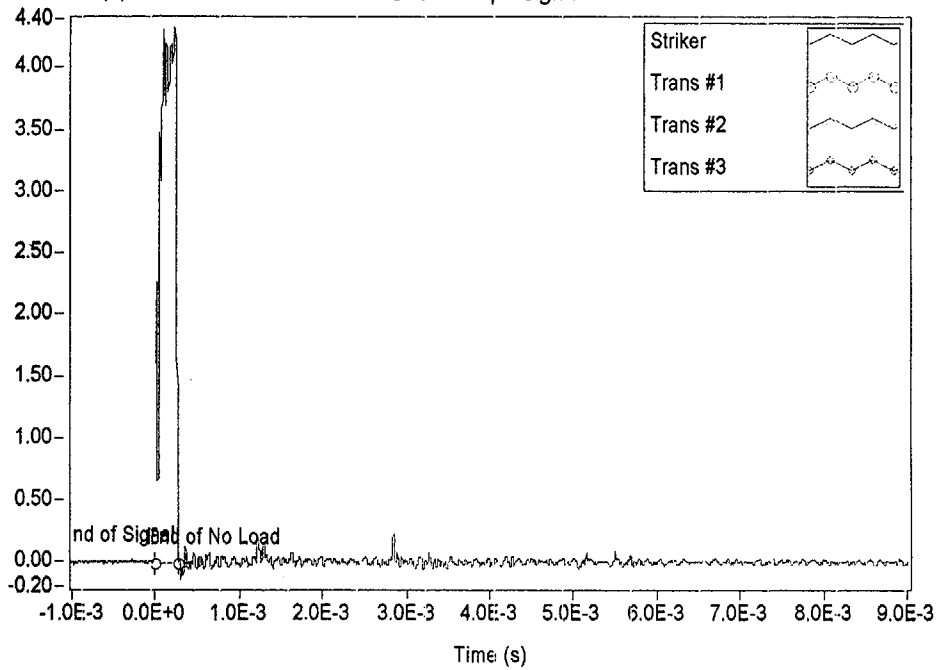

Result	Value
Optical Encoder Energy	16.341 ft lbf
Dial Gage Energy	16.00 ft lbf
Instrumented Striker Energy	16.341 ft lbf

Impact V2.1

Integration Report

Signal Source: 8mm - Striker 16 Striker

Load (lbf) vs. Time (s)

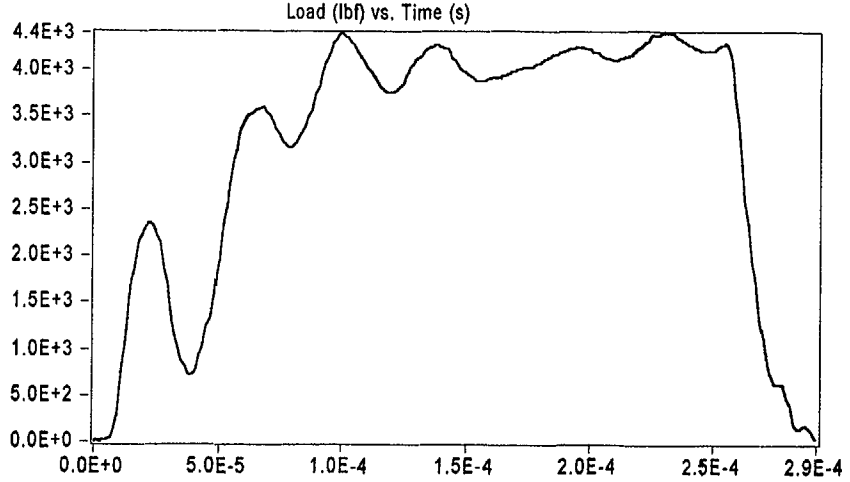

Velocity (ft/s) vs. Time (s)

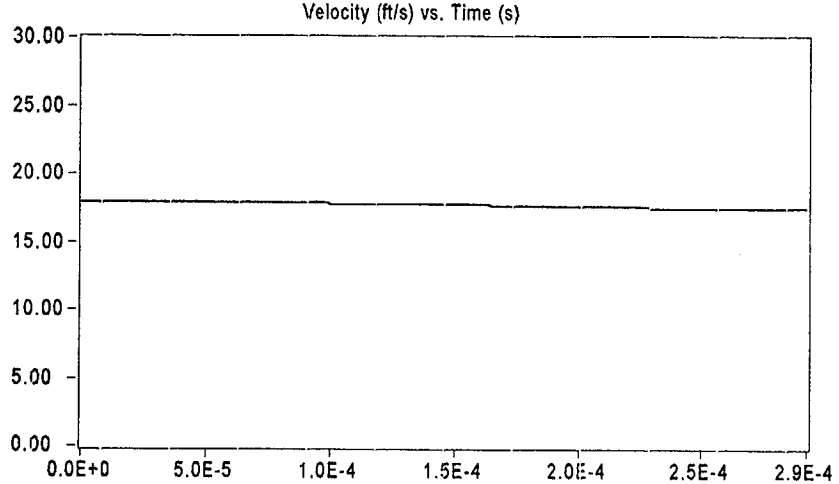

Displacement (in) vs. Time (s)

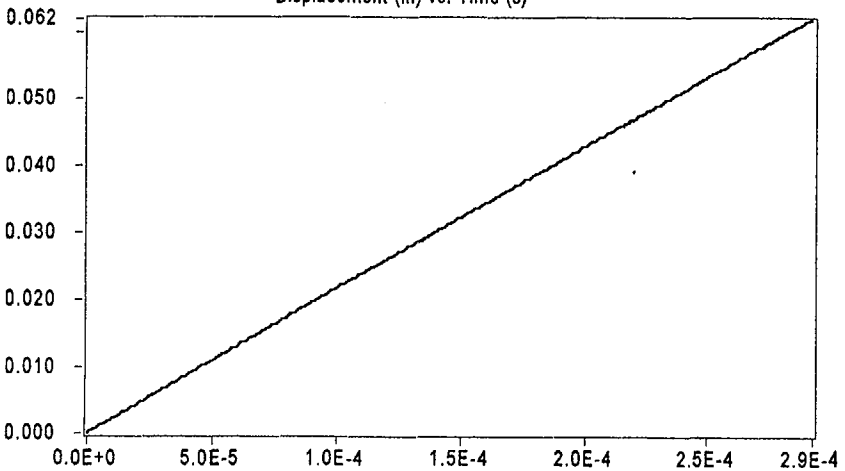

Load (lbf), Energy (ft lbf) vs. Displacement (in)

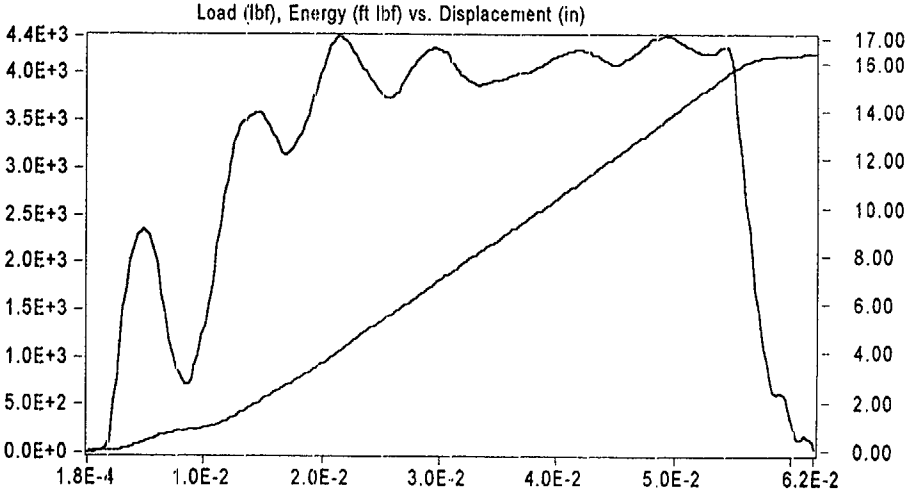

Sample Name: Hf3-11

Instrumented Striker Energy: 16.341 ft lbf

Impact V2.1

Load vs. Displacement Critical Points

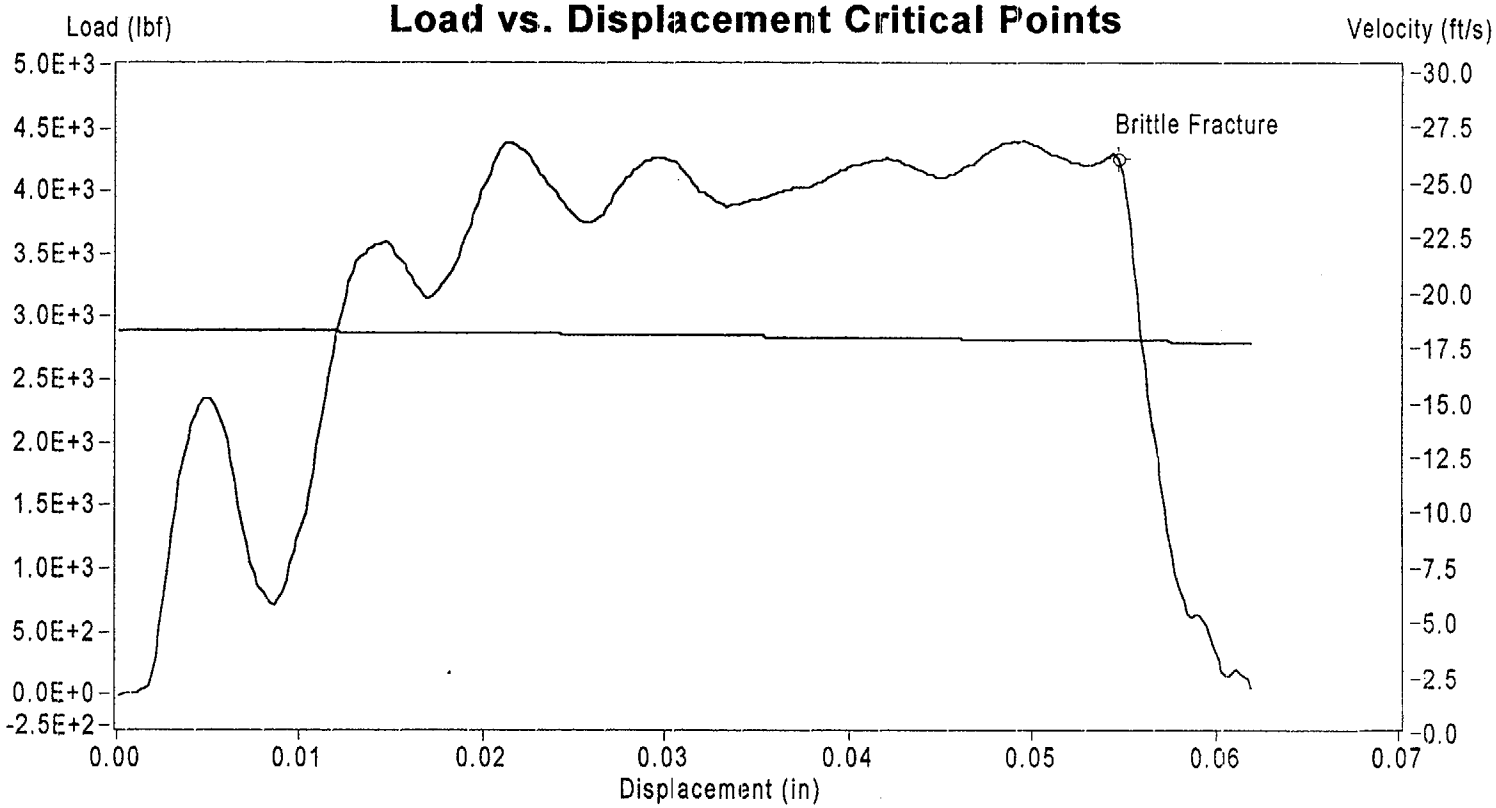

	Load (lbf)	Displacement (in)	Velocity (ft/s)	Time (s)	Energy (ft lbf)
Brittle Fracture	4.265E+3	5.468E-2	1.747E+1	2.450E-4	1.556E+1
End of Signal	4.689E+1	6.198E-2	1.745E+1	2.800E-4	1.634E+1

Sample ID: Hf3-11

Impact V2.1

Summary Report

Sample ID

HF3-10

Material Description

NMP-2 3-Degree Surveillance Capsule - HAZ material

Test Parameter	Value
Operator	Dr. Michael P. Manahan, Sr.
Date Tested	11/27/00 4:50 PM
Temperature	-69.00 °C
Oscilloscope	Model 441 Internal
Striker Name	8mm - Striker 16
Interpolation Method	Point-Point Linear
TO 892 Controller	Active Adjust
Sample Type	Metal
Sample Size	Type A
Orientation	TL
Notch Type	V Notch, no Side-Groove
Length	2.1654 in
Width	0.3937 in
Thickness	0.3937 in
Span	1.5748 in
Uncracked Ligament	0.3150 in
Notch Radius	0.0098 in
Velocity Determination	Potential Energy & Losses
Velocity	17.94 ft/s
Shear	14.00 %
Lateral Expansion	0.0060 in
Energy Adjustment	1.1216

Measured Data (V)

Oscilloscope Signal

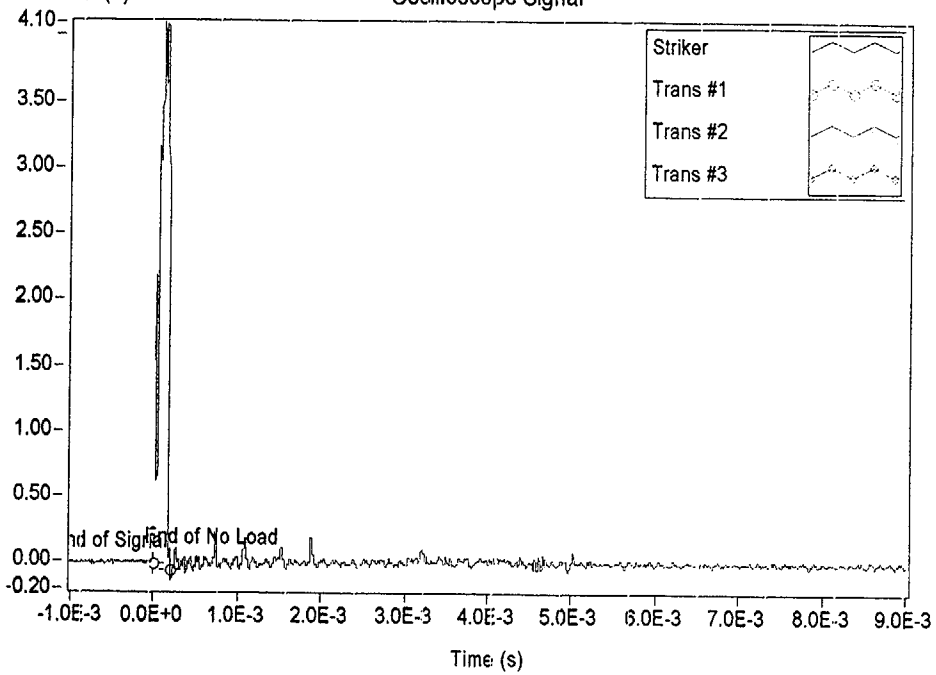

Result	Value
Optical Encoder Energy	9.8589 ft lbf
Dial Gage Energy	10.000 ft lbf
Instrumented Striker Energy	9.8589 ft lbf

Impact V2.1

Integration Report

Signal Source: 8mm - Striker 16 Striker

Load (lbf) vs. Time (s)

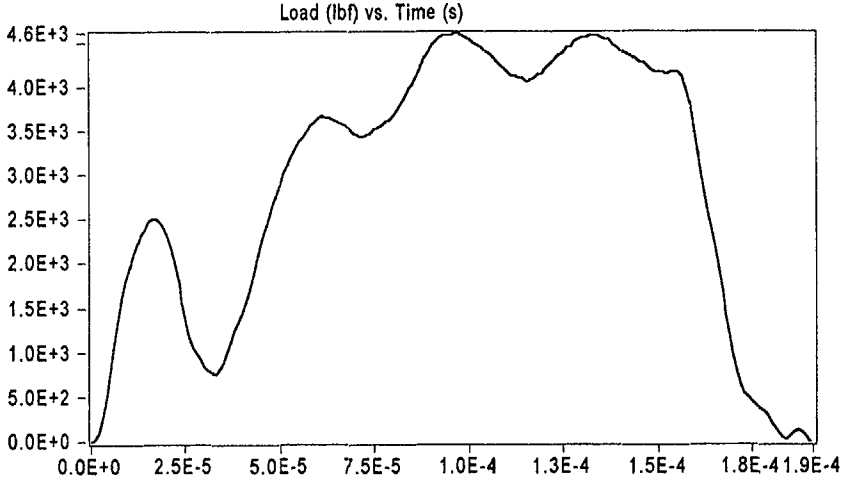

Velocity (ft/s) vs. Time (s)

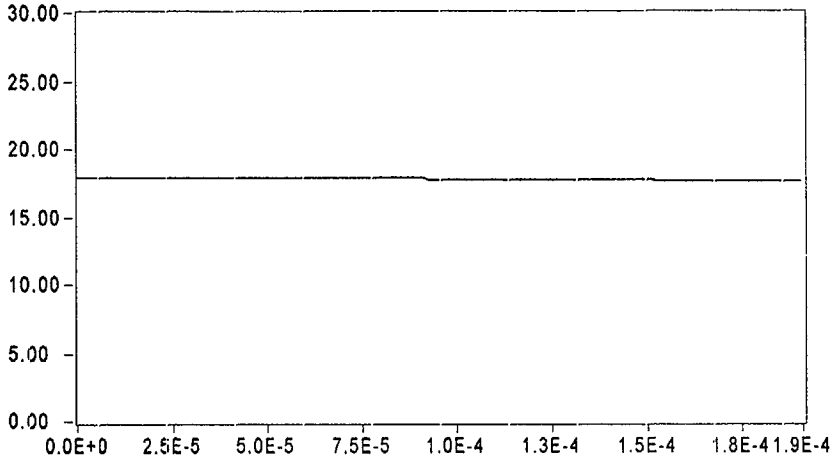

Displacement (in) vs. Time (s)

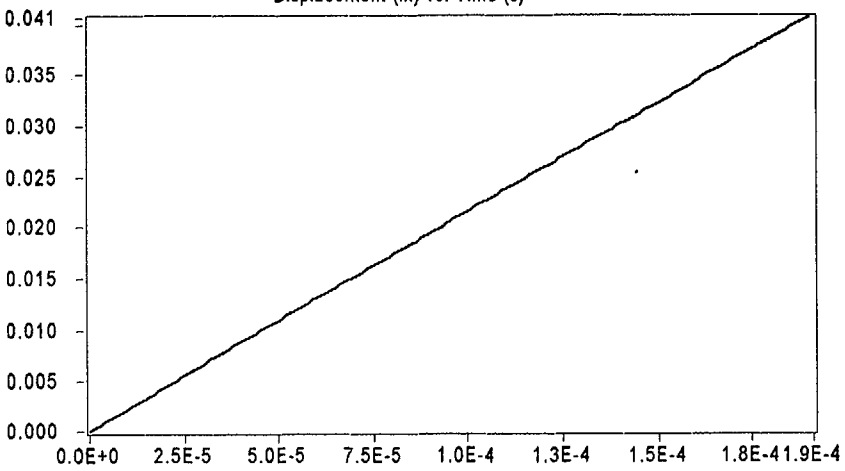

Load (lbf), Energy (ft lbf) vs. Displacement (in)

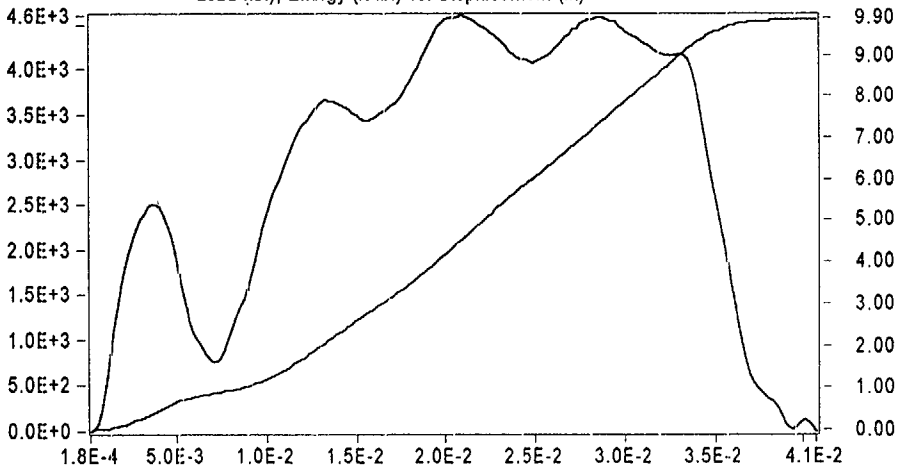

Sample Name: Hf3-10

Instrumented Striker Energy: 9.8589 ft lbf

Impact V2.1

Load vs. Displacement Critical Points

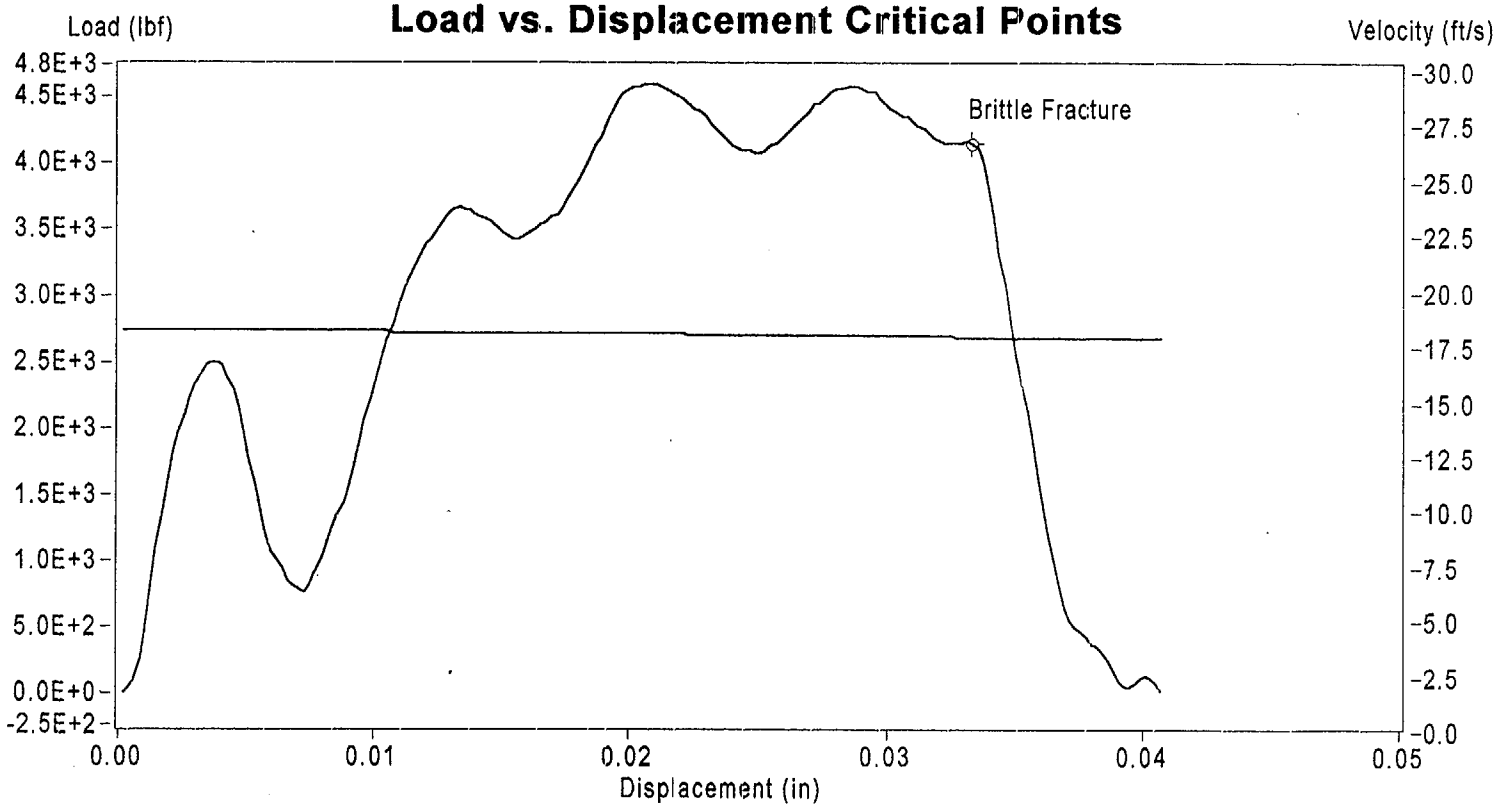

	Load (lbf)	Displacement (in)	Velocity (ft/s)	Time (s)	Energy (ft lbf)
Brittle Fracture	4.163E+3	3.334E-2	1.767E+1	1.500E-4	9.075E+0
End of Signal	4.085E+0	4.072E-2	1.765E+1	1.850E-4	9.859E+0

Sample ID: Hf3-10

Impact V2.1

Summary Report

Sample ID

HF3-6

Material Description

NMP-2 3-Degree Surveillance Capsule - HAZ material

Test Parameter	Value
Operator	Dr. Michael P. Manahan, Sr.
Date Tested	11/27/00 2:18 PM
Temperature	-49.00 °C
Oscilloscope	Model 441 Internal
Striker Name	8mm - Striker 16
Interpolation Method	Point-Point Linear
TO 892 Controller	Active Adjust
Sample Type	Metal
Sample Size	Type A
Orientation	TL
Notch Type	V Notch, no Side-Groove
Length	2.1654 in
Width	0.3937 in
Thickness	0.3937 in
Span	1.5748 in
Uncracked Ligament	0.3150 in
Notch Radius	0.0098 in
Velocity Determination	Potential Energy & Losses
Velocity	17.94 ft/s
Shear	21.30 %
Lateral Expansion	0.0125 in
Energy Adjustment	1.2051

Measured Data (V)

Oscilloscope Signal

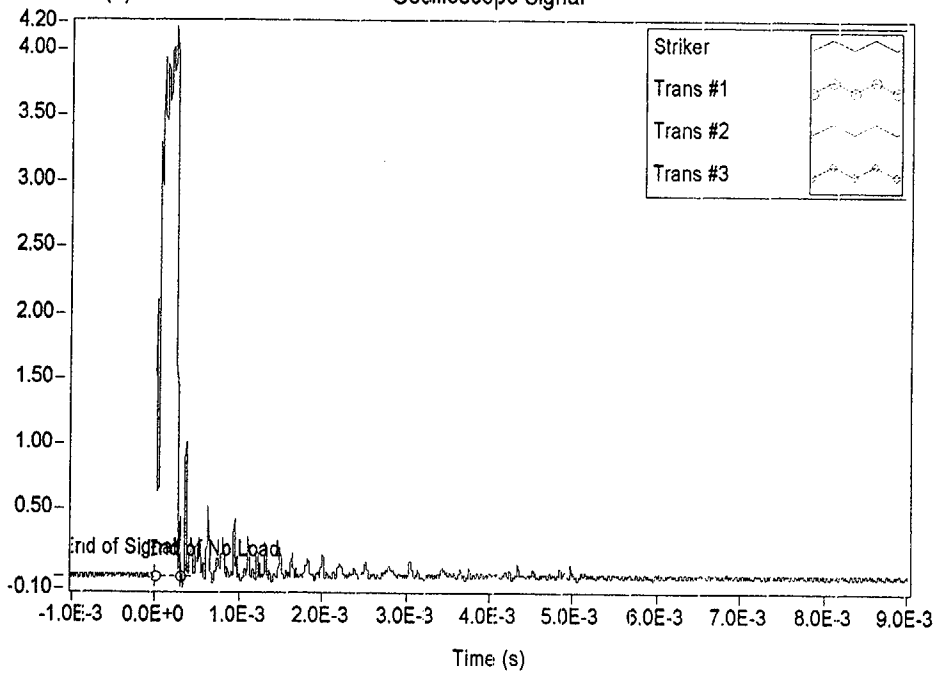

Result	Value
Optical Encoder Energy	**18.496 ft lbf**
Dial Gage Energy	**18.30 ft lbf**
Instrumented Striker Energy	**18.496 ft lbf**

Impact V2.1

Integration Report

Signal Source: 8mm - Striker 16 Striker

Load (lbf) vs. Time (s)

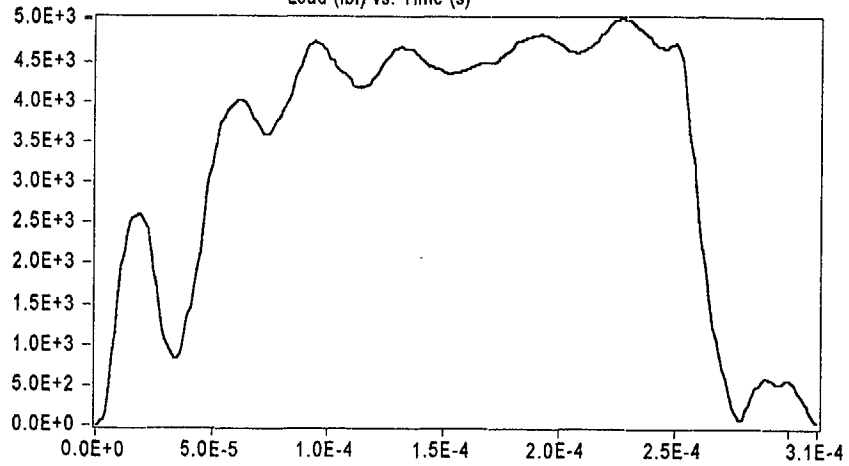

Velocity (ft/s) vs. Time (s)

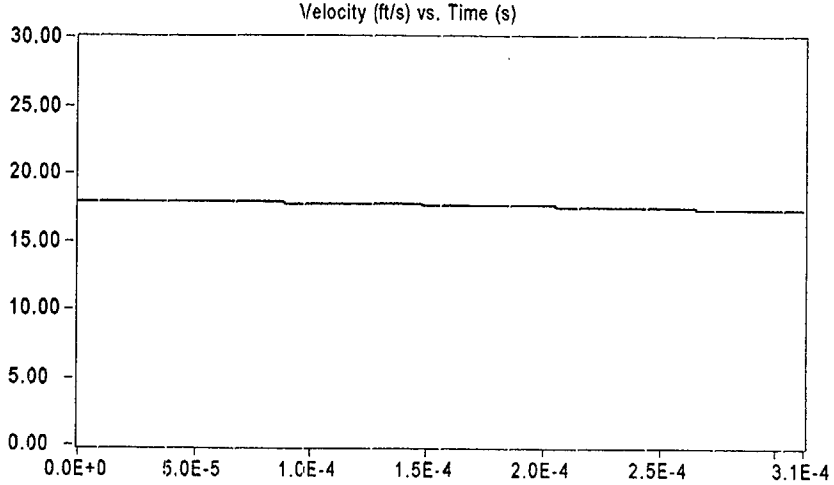

Displacement (in) vs. Time (s)

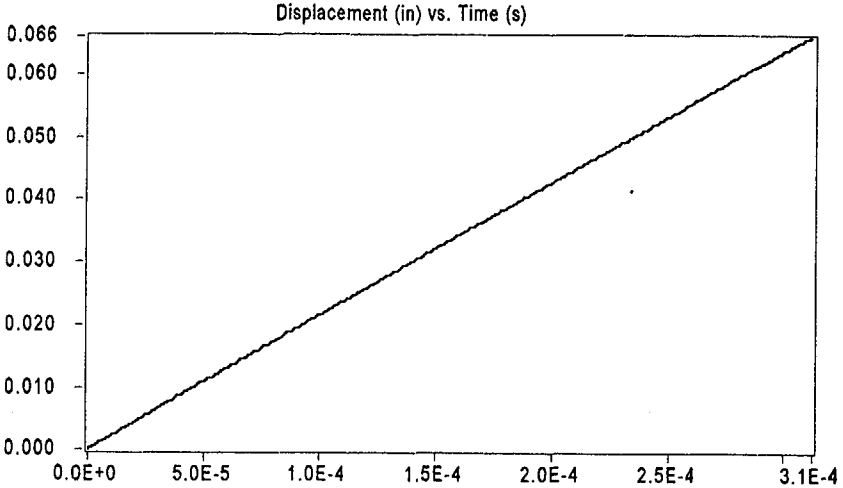

Load (lbf), Energy (ft lbf) vs. Displacement (in)

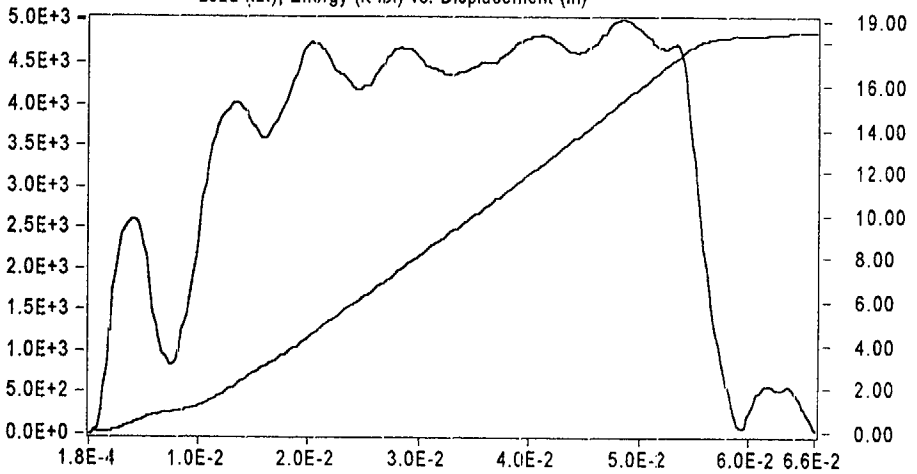

Sample Name: Hf3-6

Instrumented Striker Energy: 18.496 ft lbf

Impact V2.1

Load vs. Displacement Critical Points

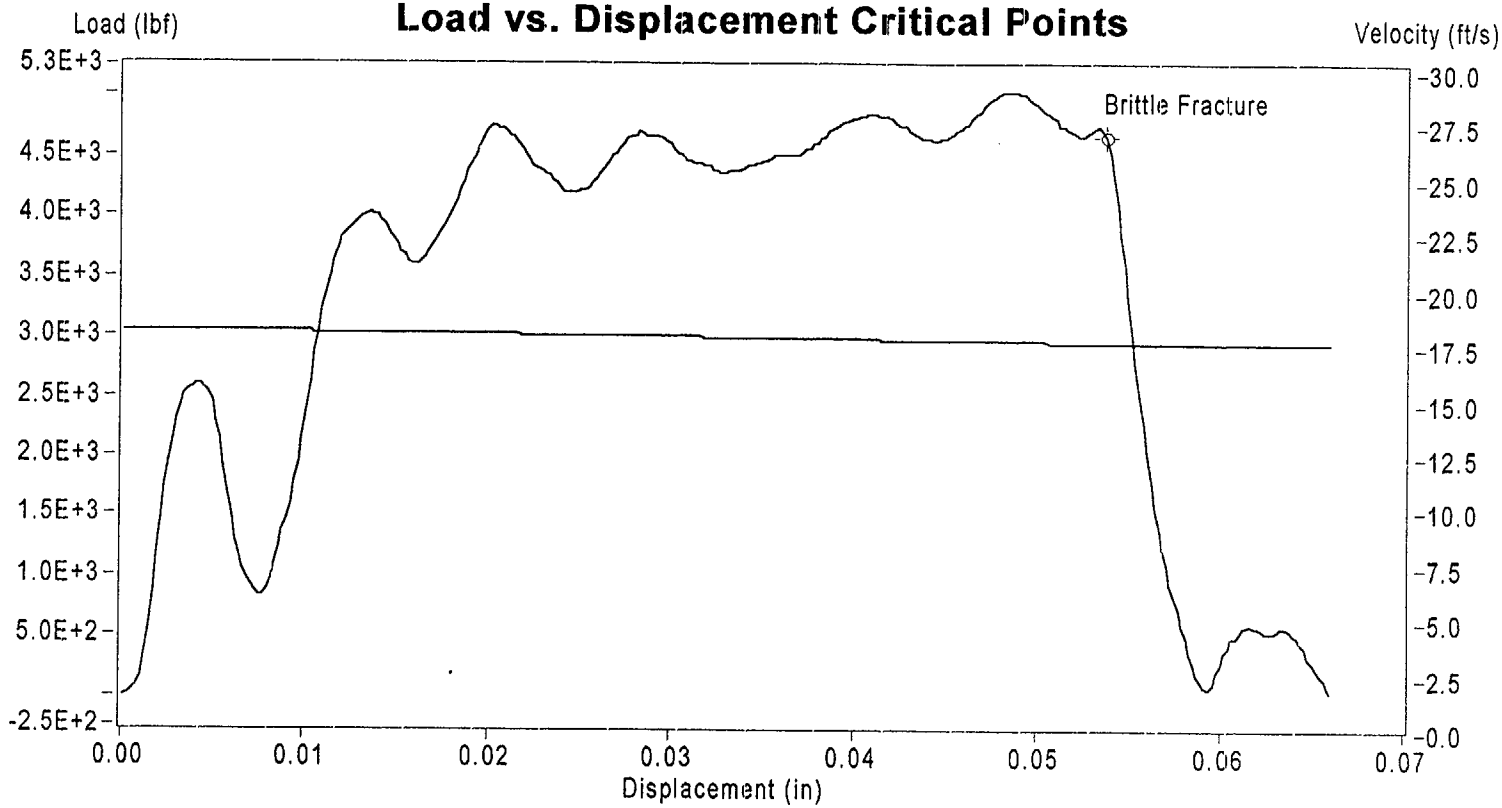

	Load (lbf)	Displacement (in)	Velocity (ft/s)	Time (s)	Energy (ft lbf)
Brittle Fracture	4.653E+3	5.375E-2	1.742E+1	2.450E-4	1.743E+1
End of Signal	3.743E+1	6.603E-2	1.733E+1	3.040E-4	1.850E+1

Sample ID: Hf3-6

Impact V2.1

Summary Report

Sample ID

HF3

Material Description

NMP-2 3-Degree Surveillance Capsule - HAZ material

Test Parameter	Value
Operator	Dr. Michael P. Manahan, Sr.
Date Tested	11/27/00 4:18 PM
Temperature	-48.00 °C
Oscilloscope	Model 441 Internal
Striker Name	8mm - Striker 16
Interpolation Method	Point-Point Linear
TO 892 Controller	Active Adjust
Sample Type	Metal
Sample Size	Type A
Orientation	TL
Notch Type	V Notch, no Side-Groove
Length	2.1654 in
Width	0.3937 in
Thickness	0.3937 in
Span	1.5748 in
Uncracked Ligament	0.3150 in
Notch Radius	0.0098 in
Velocity Determination	Potential Energy & Losses
Velocity	17.94 ft/s
Shear	24.20 %
Lateral Expansion	0.0305 in
Energy Adjustment	1.0249

Measured Data (V)

Oscilloscope Signal

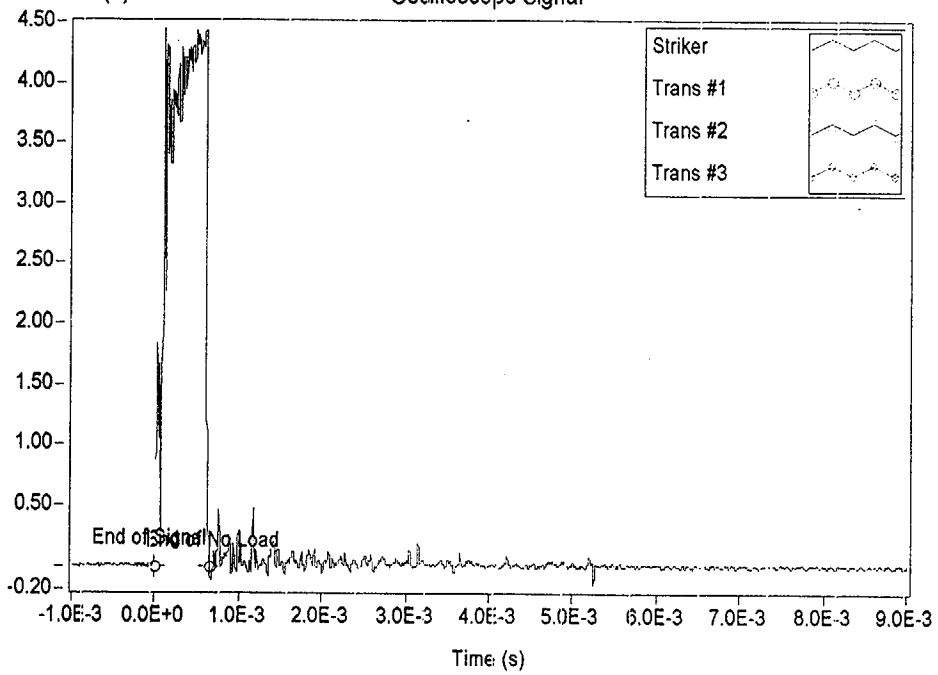

Result	Value
Optical Encoder Energy	39.808 ft lbf
Dial Gage Energy	39.90 ft lbf
Instrumented Striker Energy	39.808 ft lbf

Impact V2.1

Integration Report

Signal Source: 8mm - Striker 16 Striker

Load (lbf) vs. Time (s)

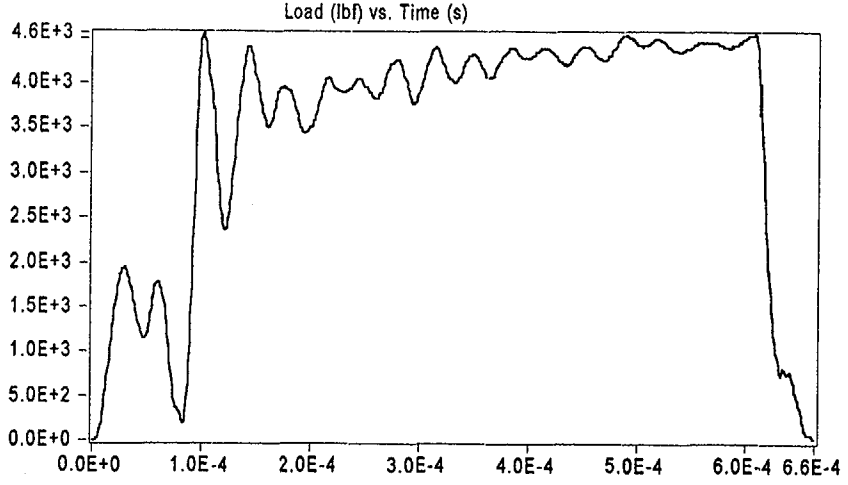

Velocity (ft/s) vs. Time (s)

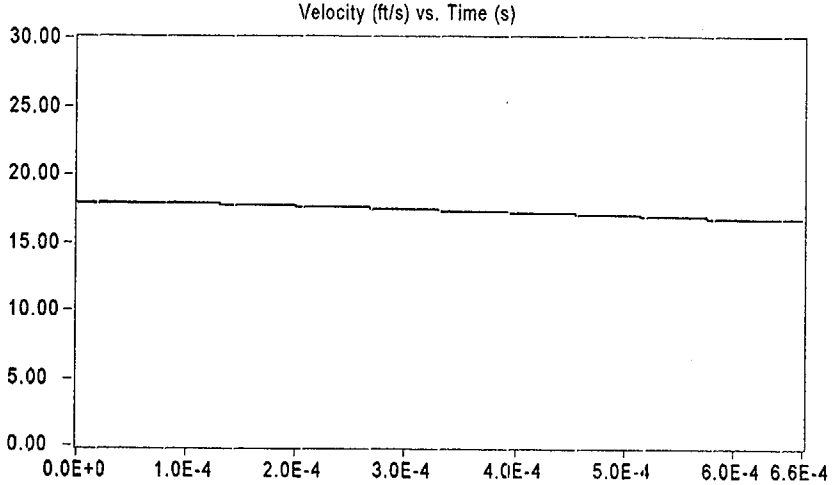

Displacement (in) vs. Time (s)

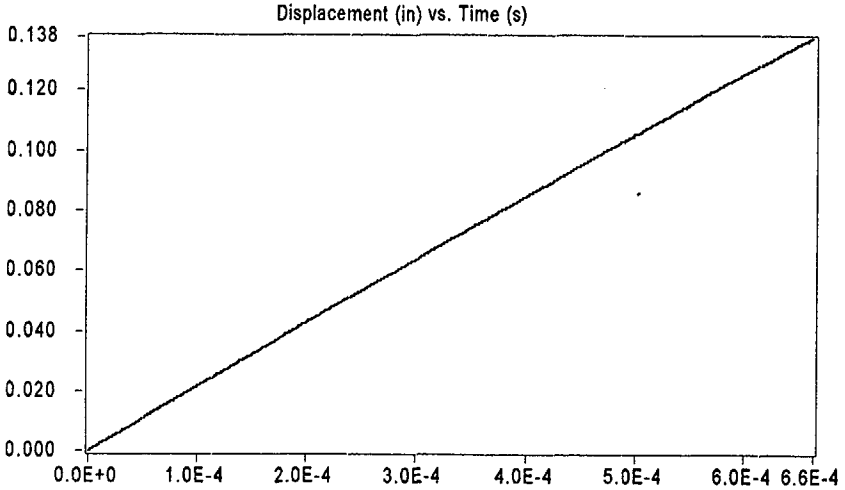

Load (lbf), Energy (ft lbf) vs. Displacement (in)

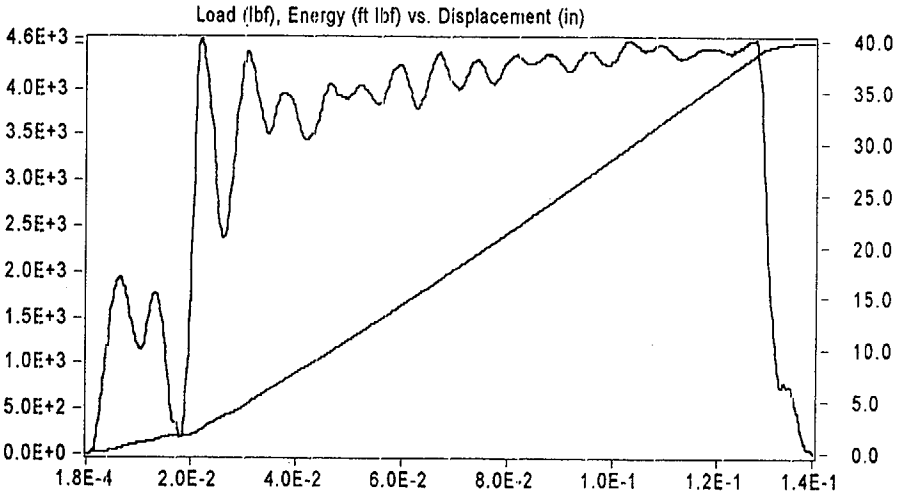

Sample Name: Hf3

Instrumented Striker Energy: 39.808 ft lbf

Impact V2.1

Load vs. Displacement Critical Points

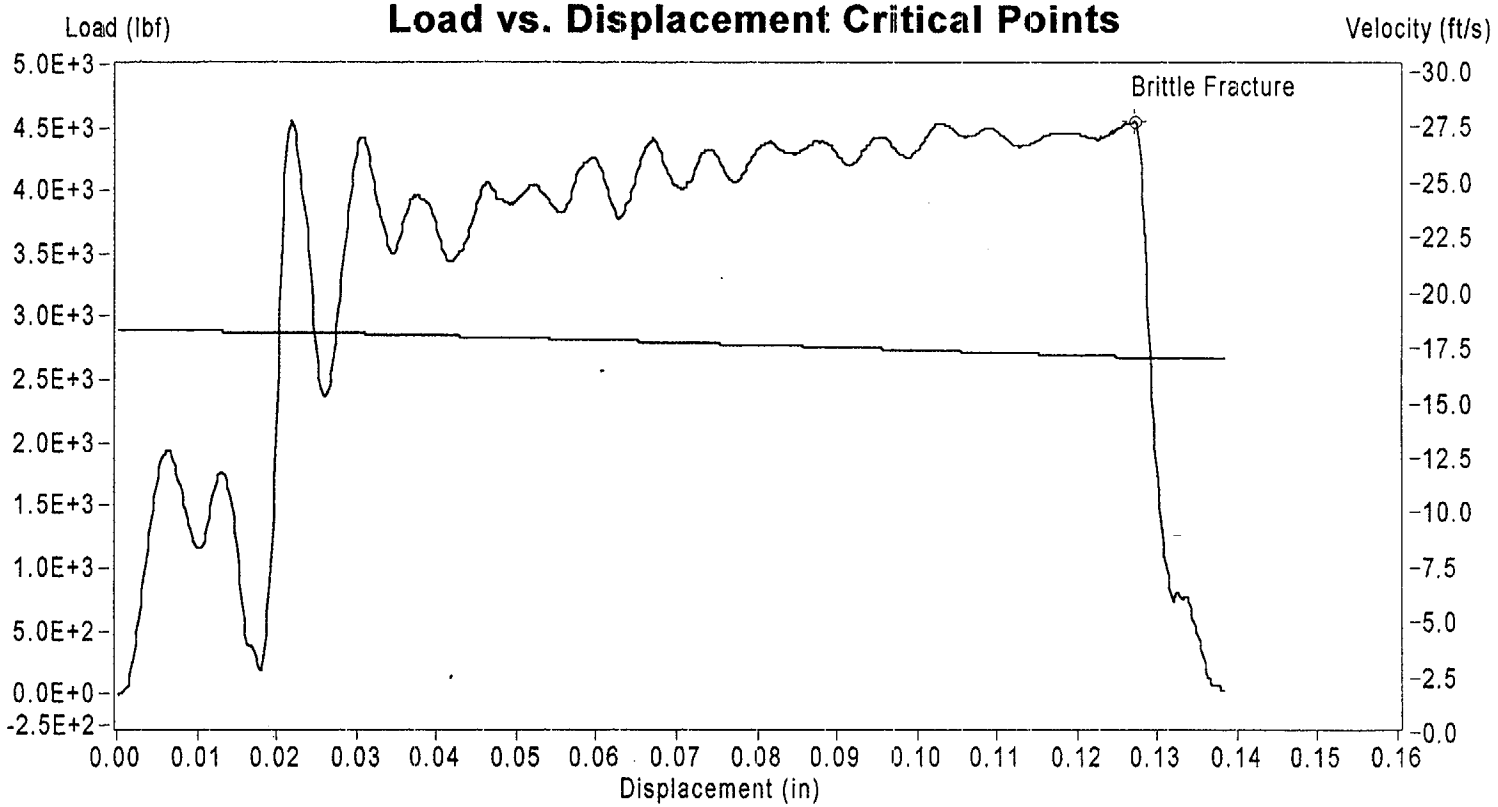

	Load (lbf)	Displacement (in)	Velocity (ft/s)	Time (s)	Energy (ft lbf)
Brittle Fracture	4.549E+3	1.271E-1	1.676E+1	5.940E-4	3.864E+1
End of Signal	1.532E+1	1.381E-1	1.672E+1	6.490E-4	3.981E+1

Sample ID: Hf3

Impact V2.1

Summary Report

Sample ID

HF3-5

Material Description

NMP-2 3-Degree Surveillance Capsule - HAZ material

Test Parameter	Value
Operator	Dr. Michael P. Manahan, Sr.
Date Tested	11/27/00 3:38 PM
Temperature	-34.00 °C
Oscilloscope	Model 441 Internal
Striker Name	8mm - Striker 16
Interpolation Method	Point-Point Linear
TO 892 Controller	Active Adjust
Sample Type	Metal
Sample Size	Type A
Orientation	TL
Notch Type	V Notch, no Side-Groove
Length	2.1654 in
Width	0.3937 in
Thickness	0.3937 in
Span	1.5748 in
Uncracked Ligament	0.3150 in
Notch Radius	0.0098 in
Velocity Determination	Potential Energy & Losses
Velocity	17.94 ft/s
Shear	55.80 %
Lateral Expansion	NaN in
Energy Adjustment	1.0242

Measured Data (V)

Oscilloscope Signal

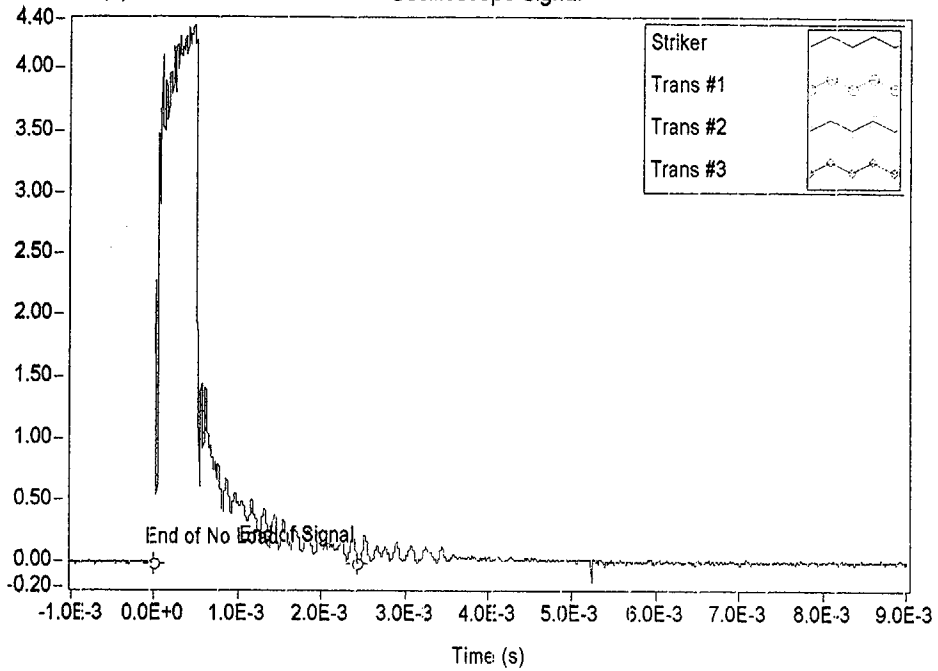

Result	Value
Optical Encoder Energy	47.297 ft lbf
Dial Gage Energy	47.20 ft lbf
Instrumented Striker Energy	47.297 ft lbf

Impact V2.1

Integration Report

Signal Source: 8mm - Striker 16 Striker

Load (lbf) vs. Time (s)

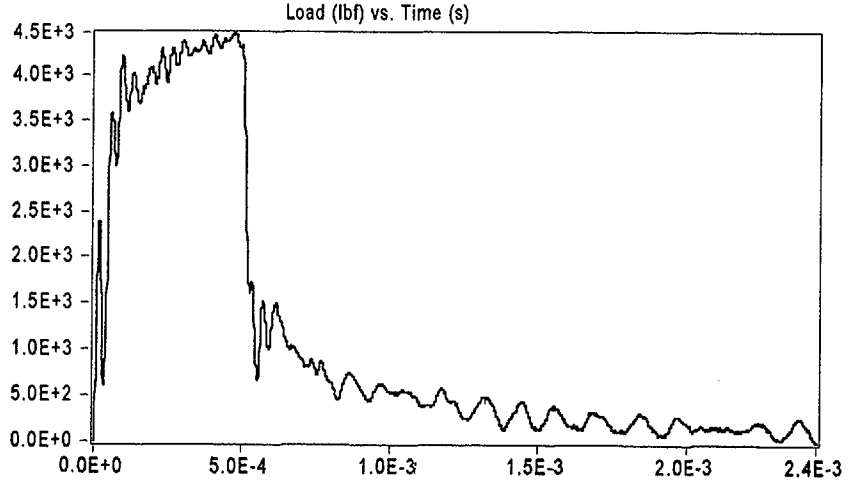

Velocity (ft/s) vs. Time (s)

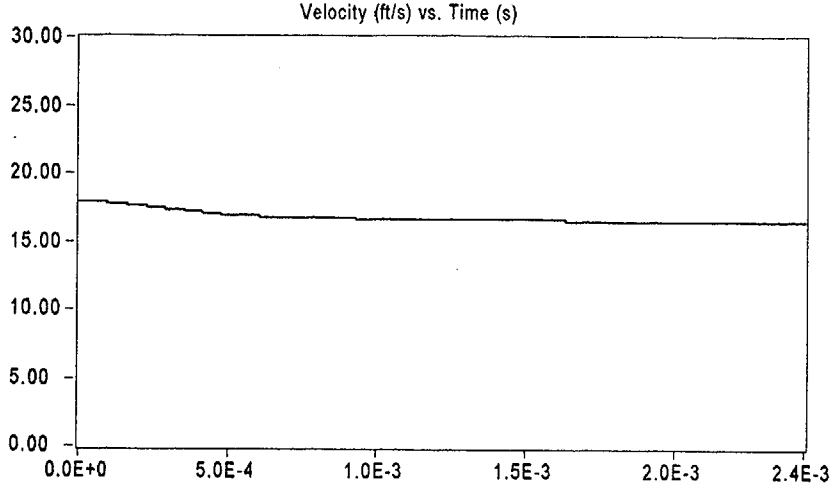

Displacement (in) vs. Time (s)

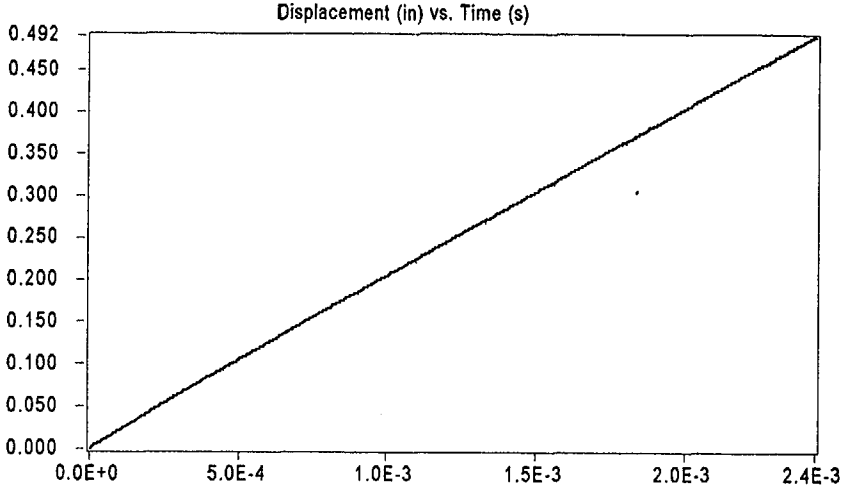

Load (lbf), Energy (ft lbf) vs. Displacement (in)

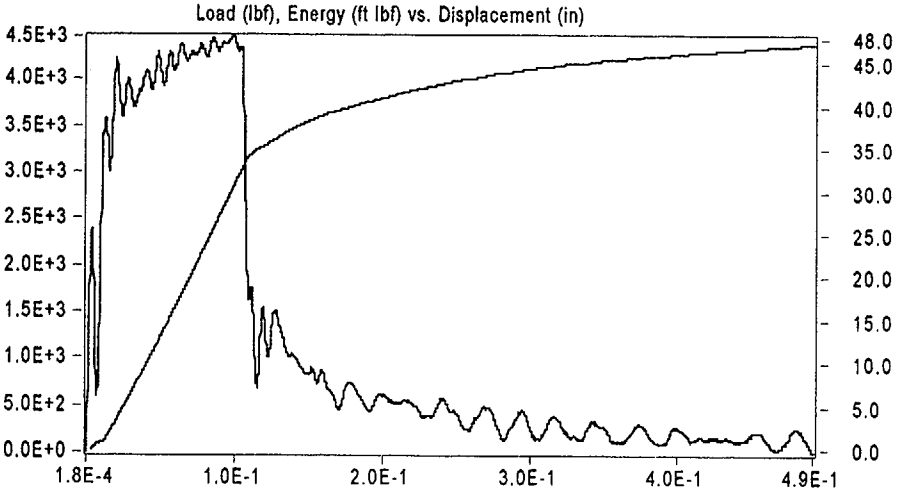

Sample Name: Hf3-5

Instrumented Striker Energy: 47.297 ft lbf

Impact V2.1

Load vs. Displacement Critical Points

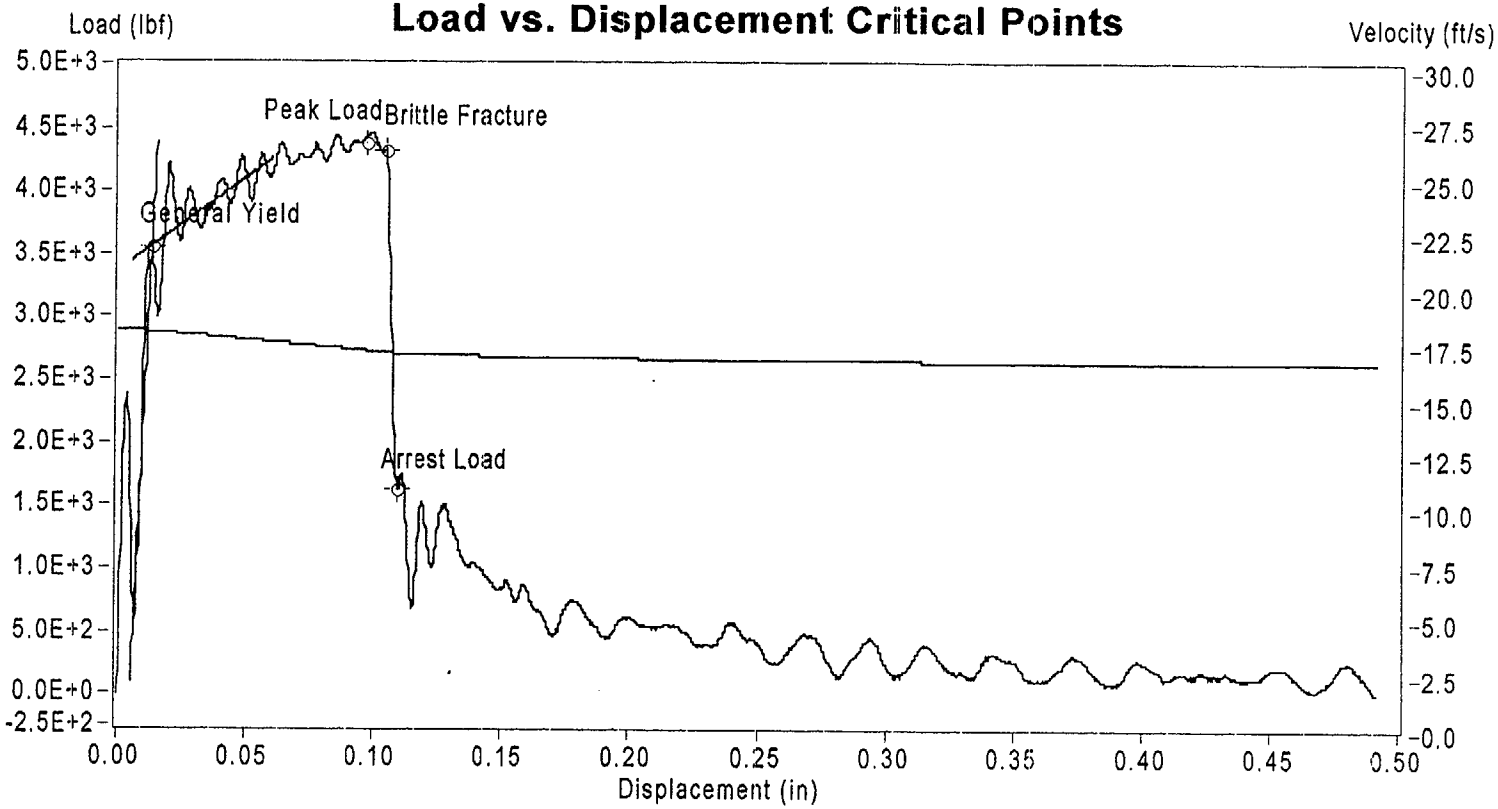

	Load (lbf)	Displacement (in)	Velocity (ft/s)	Time (s)	Energy (ft lbf)
General Yield	3.562E+3	1.327E-2	1.788E+1	5.588E-5	2.106E+0
Peak Load	4.377E+3	9.708E-2	1.701E+1	4.560E-4	3.065E+1
Brittle Fracture	4.326E+3	1.042E-1	1.693E+1	4.910E-4	3.325E+1
Arrest Load	1.626E+3	1.097E-1	1.688E+1	5.180E-4	3.456E+1
End of Signal	4.213E+0	4.916E-1	1.648E+1	2.435E-3	4.730E+1

Sample ID: Hf3-5

Impact V2.1

Summary Report

Sample ID

HF3-7

Material Description

NMP-2 3-Degree Surveillance Capsule - HAZ material

Test Parameter	Value
Operator	Dr. Michael P. Manahan, Sr.
Date Tested	11/27/00 3:51 PM
Temperature	-34.00 °C
Oscilloscope	Model 441 Internal
Striker Name	8mm - Striker 16
Interpolation Method	Point-Point Linear
TO 892 Controller	Active Adjust
Sample Type	Metal
Sample Size	Type A
Orientation	TL
Notch Type	V Notch, no Side-Groove
Length	2.1654 in
Width	0.3937 in
Thickness	0.3937 in
Span	1.5748 in
Uncracked Ligament	0.3150 in
Notch Radius	0.0098 in
Velocity Determination	Potential Energy & Losses
Velocity	17.94 ft/s
Shear	42.60 %
Lateral Expansion	0.0430 in
Energy Adjustment	1.0178

Measured Data (V)

Oscilloscope Signal

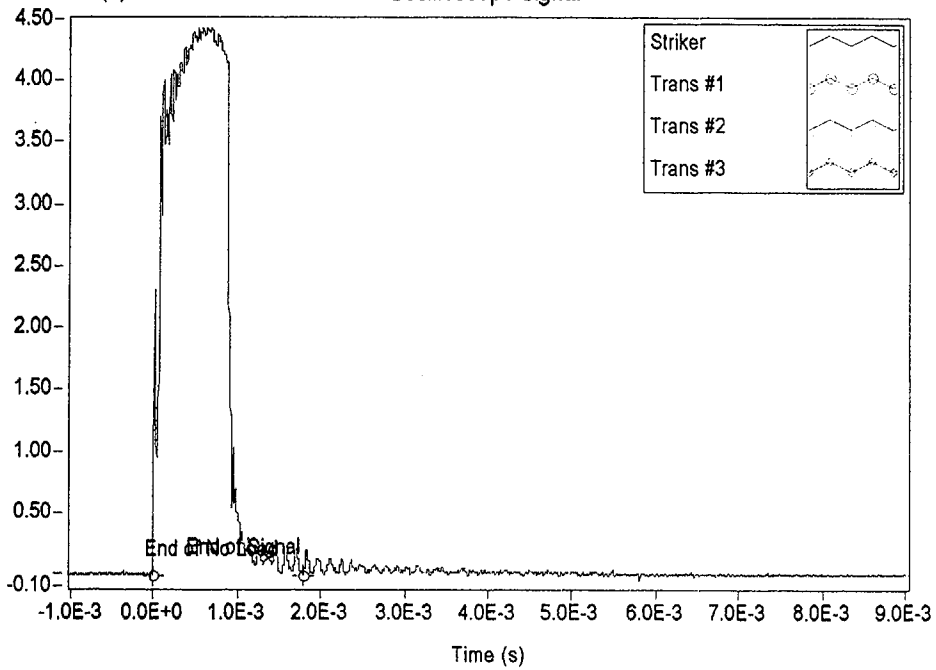

Result	Value
Optical Encoder Energy	64.745 ft lbf
Dial Gage Energy	64.90 ft lbf
Instrumented Striker Energy	64.745 ft lbf

Impact V2.1

Integration Report

Signal Source: 8mm - Striker 16 Striker

Load (lbf) vs. Time (s)

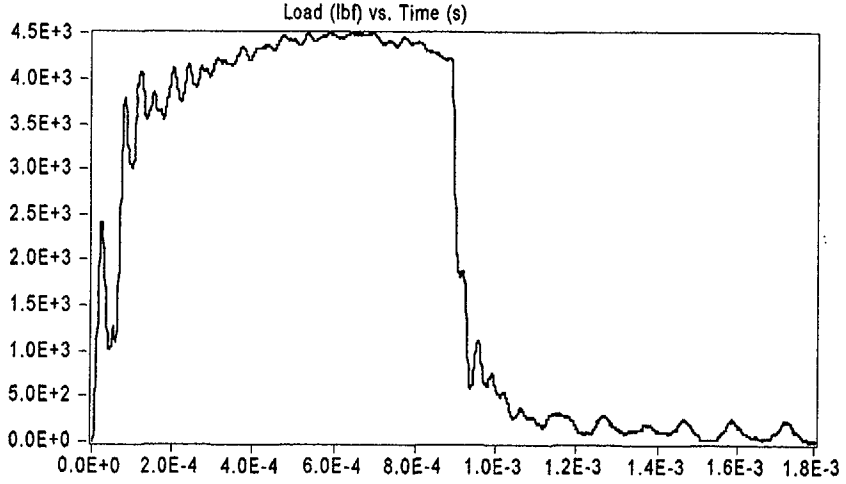

Velocity (ft/s) vs. Time (s)

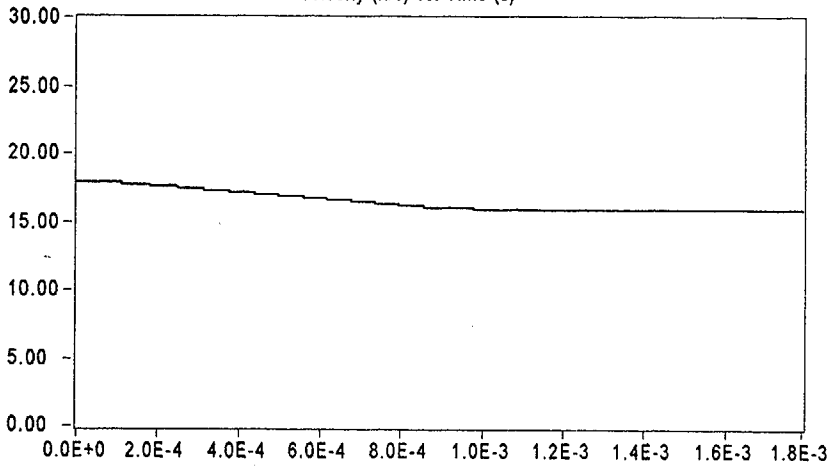

Displacement (in) vs. Time (s)

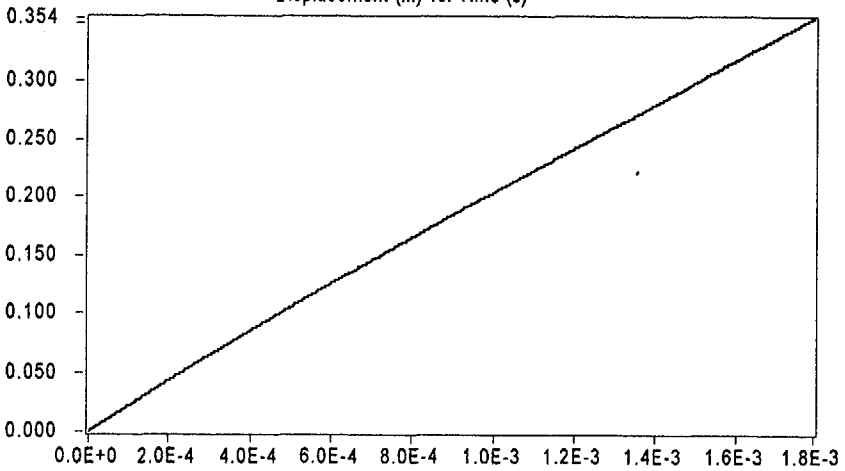

Load (lbf), Energy (ft lbf) vs. Displacement (in)

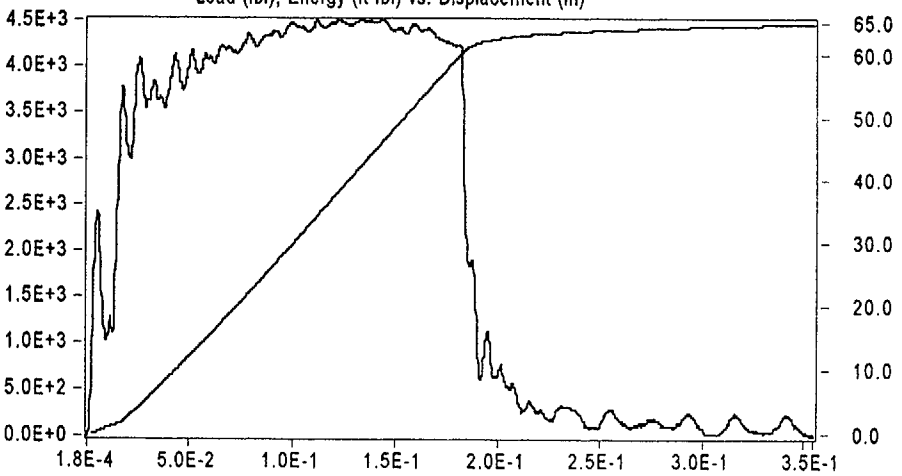

Sample Name: Hf3-7

Instrumented Striker Energy: 64.745 ft lbf

Impact V2.1

Load vs. Displacement Critical Points

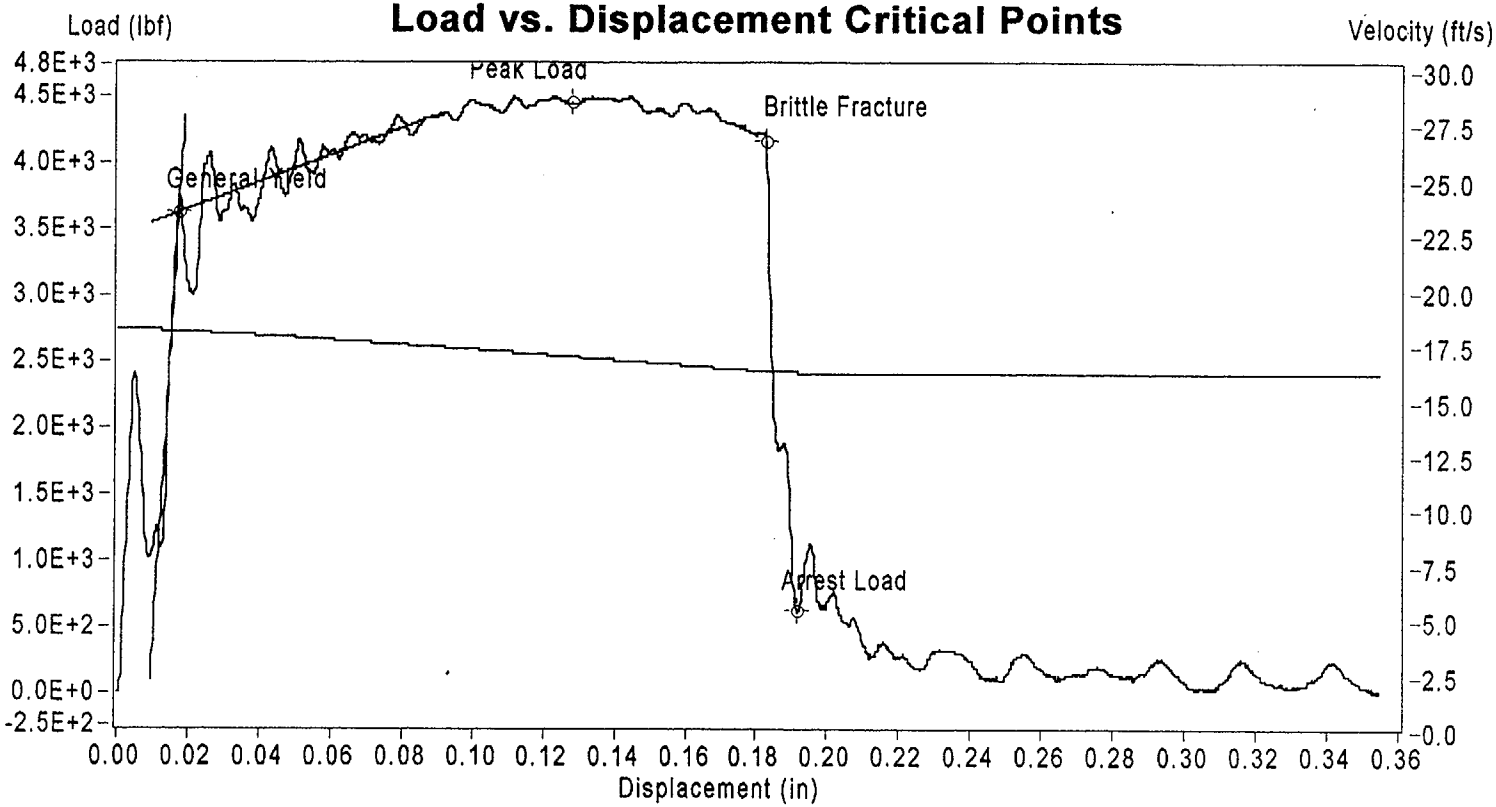

	Load (lbf)	Displacement (in)	Velocity (ft/s)	Time (s)	Energy (ft lbf)
General Yield	3.629E+3	1.735E-2	1.787E+1	7.091E-5	2.408E+0
Peak Load	4.479E+3	1.277E-1	1.670E+1	6.020E-4	4.034E+1
Brittle Fracture	4.176E+3	1.823E-1	1.605E+1	8.800E-4	6.036E+1
Arrest Load	6.215E+2	1.911E-1	1.600E+1	9.260E-4	6.182E+1
End of Signal	7.500E-1	3.544E-1	1.591E+1	1.780E-3	6.475E+1

Sample ID: Hf3-7

Impact V2.1

Summary Report

Sample ID

HF3-2

Material Description

NMP-2 3-Degree Surveillance Capsule - HAZ material

Test Parameter	Value
Operator	Dr. Michael P. Manahan, Sr.
Date Tested	11/27/00 5:17 PM
Temperature	-18.00 °C
Oscilloscope	Model 441 Internal
Striker Name	8mm - Striker 16
Interpolation Method	Point-Point Linear
TO 892 Controller	Active Adjust
Sample Type	Metal
Sample Size	Type A
Orientation	TL
Notch Type	V Notch, no Side-Groove
Length	2.1654 in
Width	0.3937 in
Thickness	0.3937 in
Span	1.5748 in
Uncracked Ligament	0.3150 in
Notch Radius	0.0098 in
Velocity Determination	Potential Energy & Losses
Velocity	17.94 ft/s
Shear	53.00 %
Lateral Expansion	0.0300 in
Energy Adjustment	0.9787

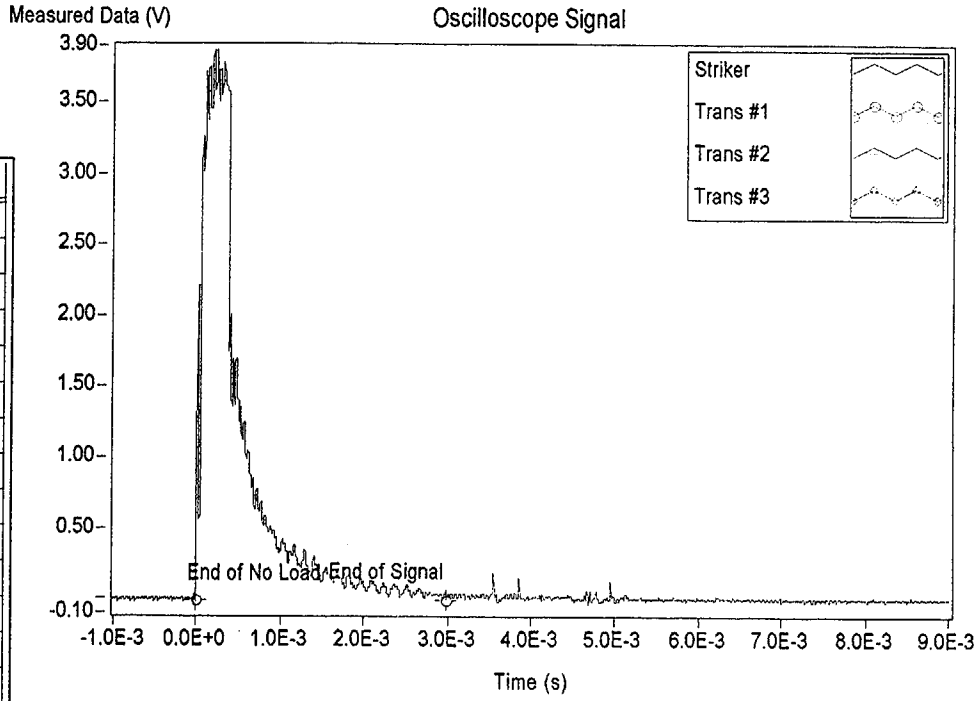

Result	Value
Optical Encoder Energy	36.223 ft lbf
Dial Gage Energy	36.30 ft lbf
Instrumented Striker Energy	36.223 ft lbf

Impact V2.1

Integration Report

Signal Source: 8mm - Striker 16 Striker

Load (lbf) vs. Time (s)

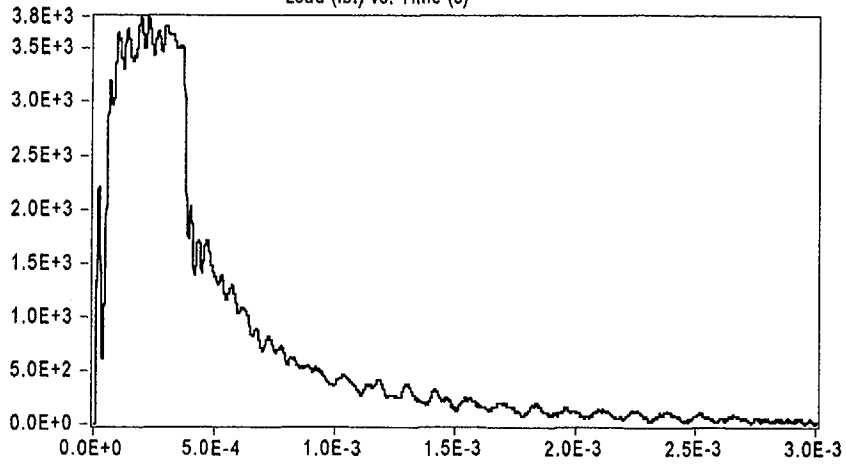

Velocity (ft/s) vs. Time (s)

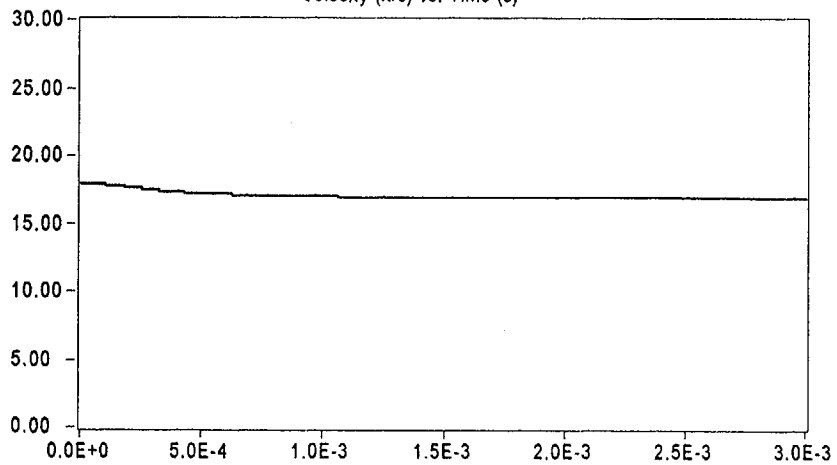

Displacement (in) vs. Time (s)

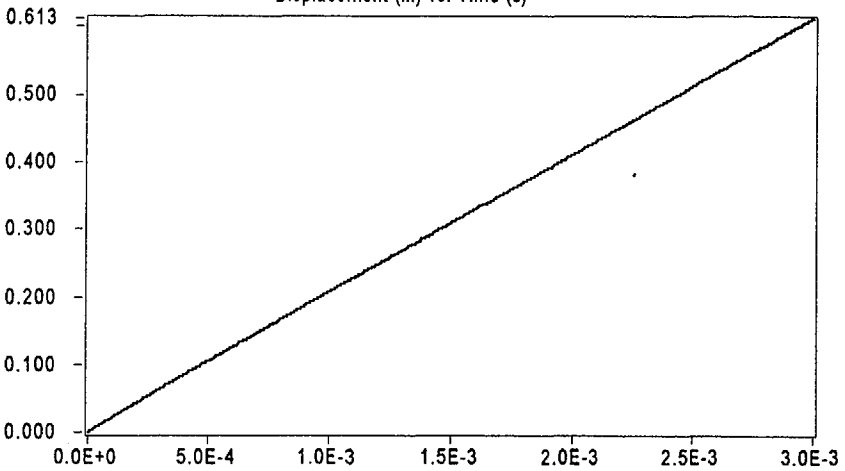

Load (lbf), Energy (ft lbf) vs. Displacement (in)

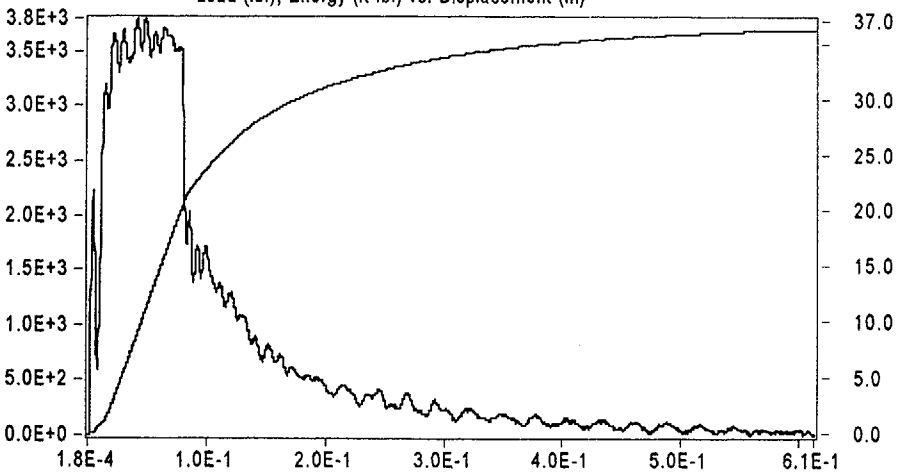

Sample Name: Hf3-2

Instrumented Striker Energy: 36.223 ft lbf

Impact V2.1

Load vs. Displacement Critical Points

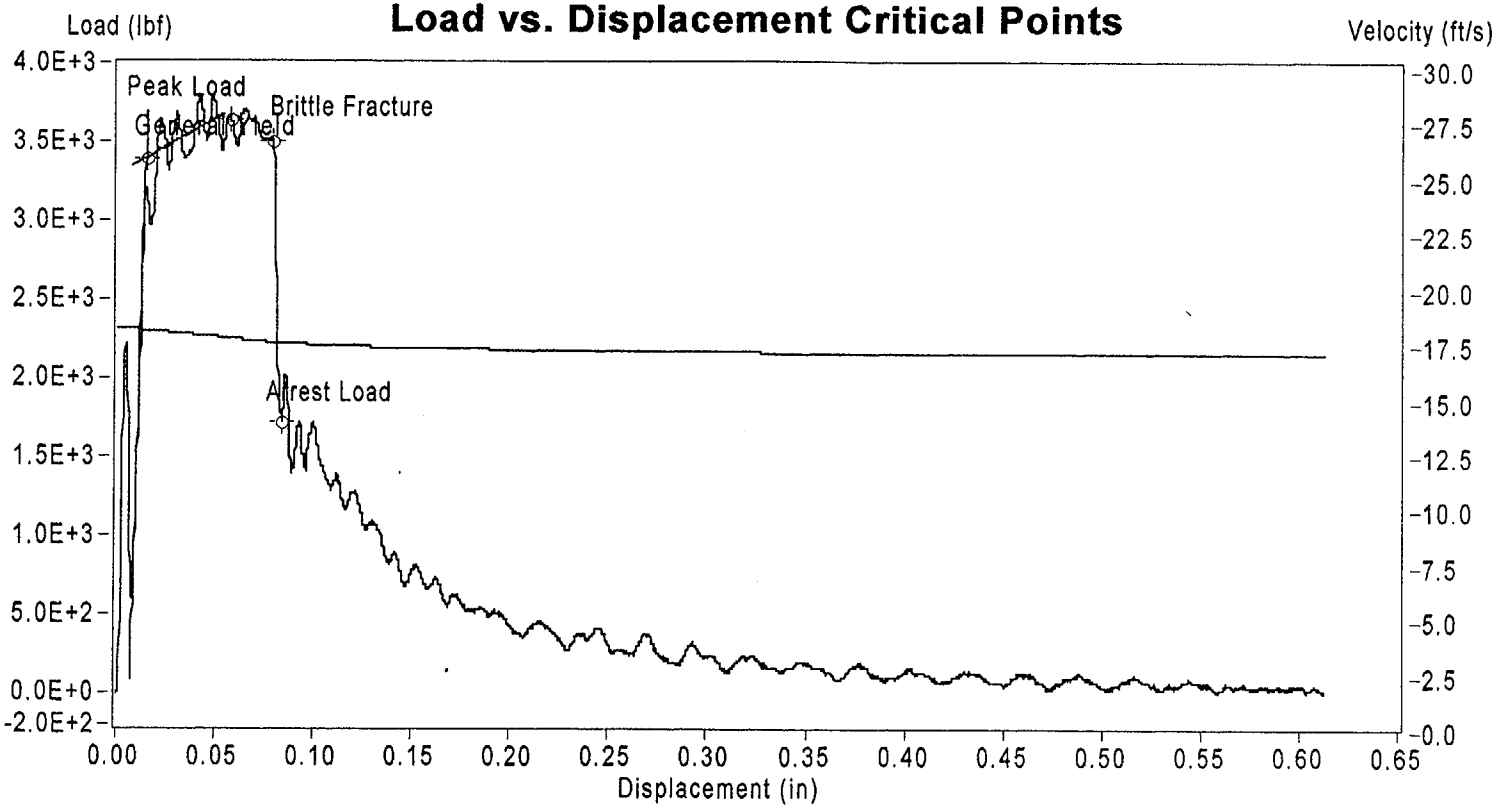

	Load (lbf)	Displacement (in)	Velocity (ft/s)	Time (s)	Energy (ft lbf)
General Yield	3.398E+3	1.477E-2	1.788E+1	5.888E-5	1.940E+0
Peak Load	3.635E+3	5.728E-2	1.751E+1	2.590E-4	1.437E+1
Brittle Fracture	3.502E+3	7.900E-2	1.731E+1	3.630E-4	2.085E+1
Arrest Load	1.724E+3	8.357E-2	1.728E+1	3.850E-4	2.176E+1
End of Signal	4.048E+0	6.125E-1	1.683E+1	2.989E-3	3.622E+1

Sample ID: Hf3-2

Impact V2.1

Summary Report

Sample ID

HF3-9

Material Description

NMP-2 3-Degree Surveillance Capsule - HAZ material

Test Parameter	Value
Operator	Dr. Michael P. Manahan, Sr.
Date Tested	11/27/00 1:38 PM
Temperature	-17.00 °C
Oscilloscope	Model 441 Internal
Striker Name	8mm - Striker 16
Interpolation Method	Point-Point Linear
TO 892 Controller	Active Adjust
Sample Type	Metal
Sample Size	Type A
Orientation	TL
Notch Type	V Notch, no Side-Groove
Length	2.1654 in
Width	0.3937 in
Thickness	0.3937 in
Span	1.5748 in
Uncracked Ligament	0.3150 in
Notch Radius	0.0098 in
Velocity Determination	Potential Energy & Losses
Velocity	17.94 ft/s
Shear	78.70 %
Lateral Expansion	NaN in
Energy Adjustment	1.0266

Measured Data (V)

Oscilloscope Signal

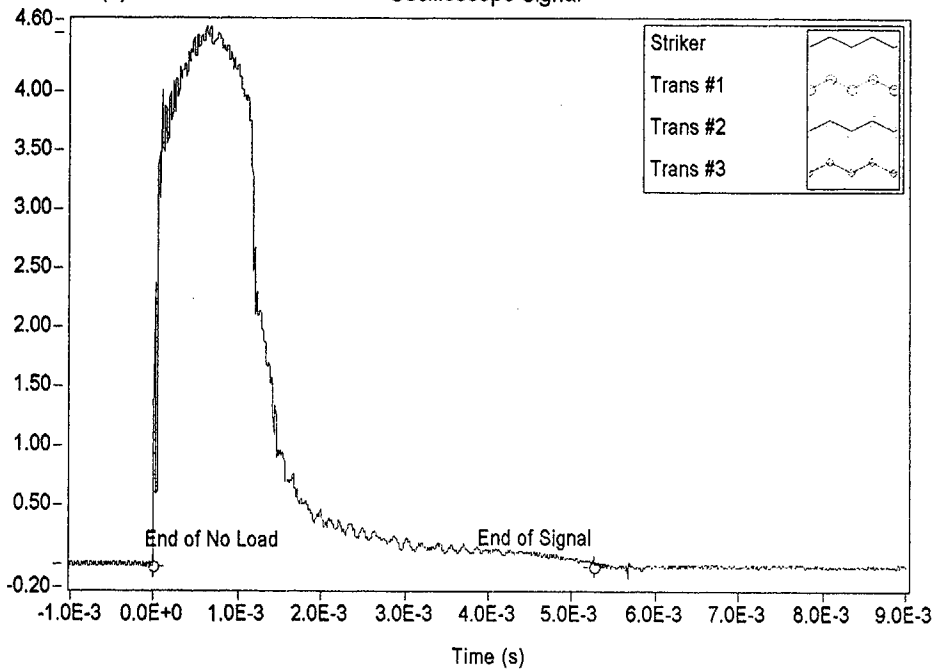

Result	Value
Optical Encoder Energy	103.62 ft lbf
Dial Gage Energy	103.4 ft lbf
Instrumented Striker Energy	103.62 ft lbf

Impact V2.1

Integration Report

Signal Source: 8mm - Striker 16 Striker

Load (lbf) vs. Time (s)

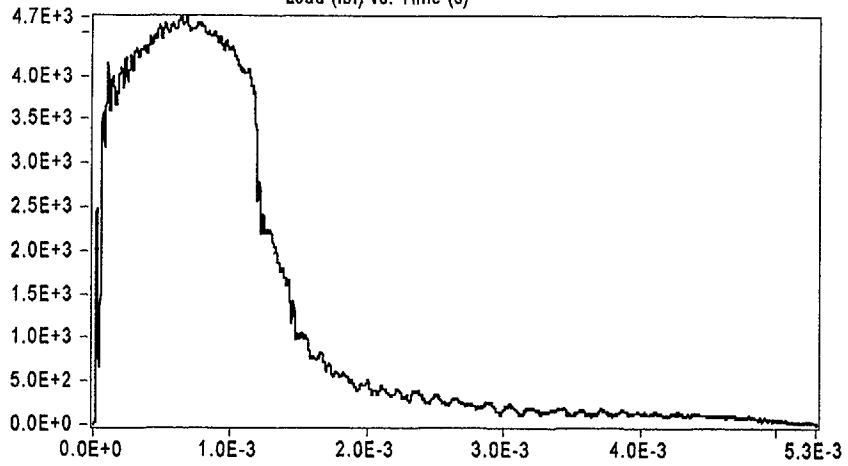

Velocity (ft/s) vs. Time (s)

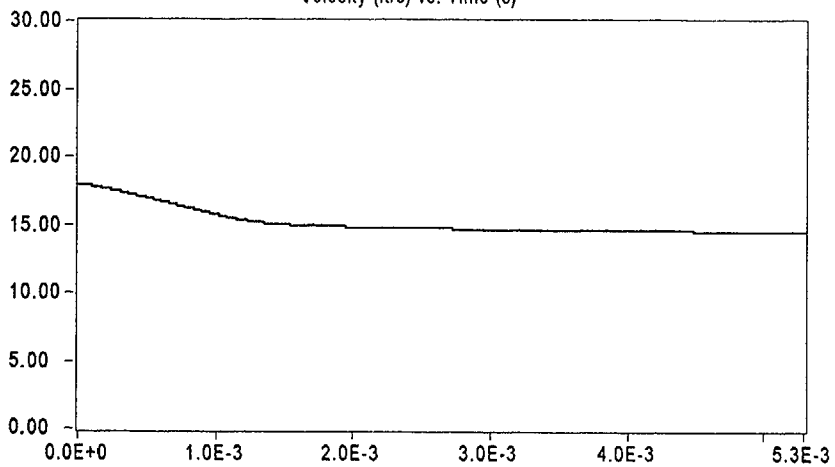

Displacement (in) vs. Time (s)

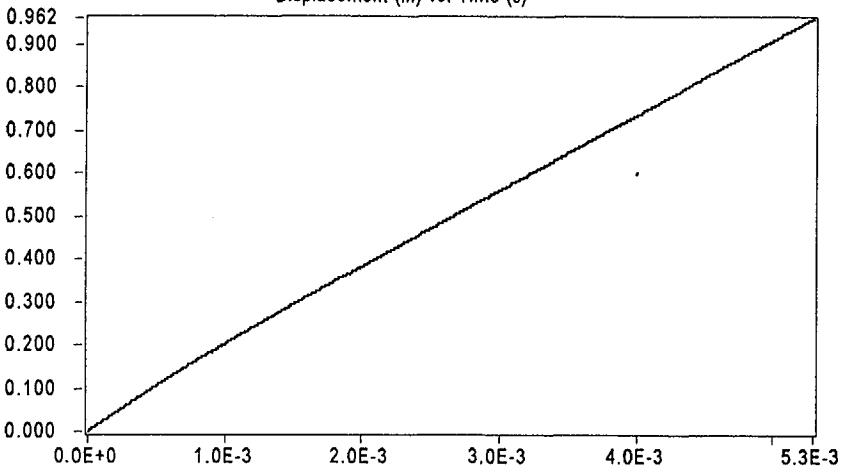

Load (lbf), Energy (ft lbf) vs. Displacement (in)

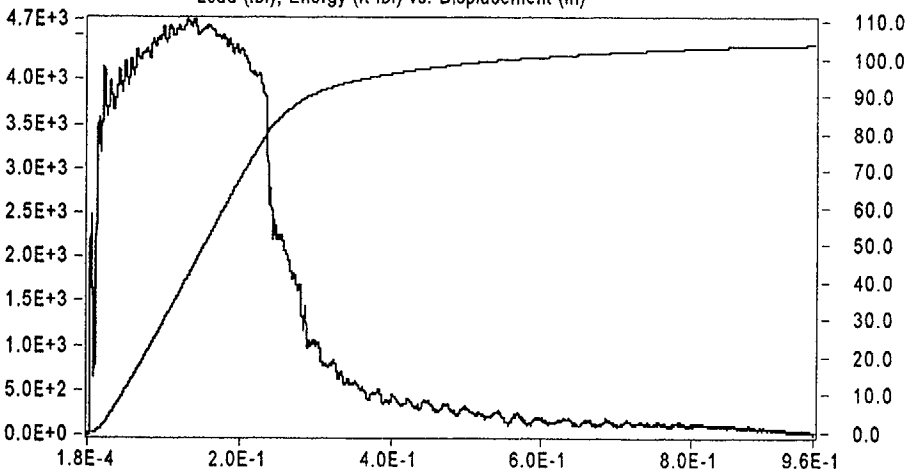

Sample Name: Hf3-9

Instrumented Striker Energy: 103.62 ft lbf

Impact V2.1

Load vs. Displacement Critical Points

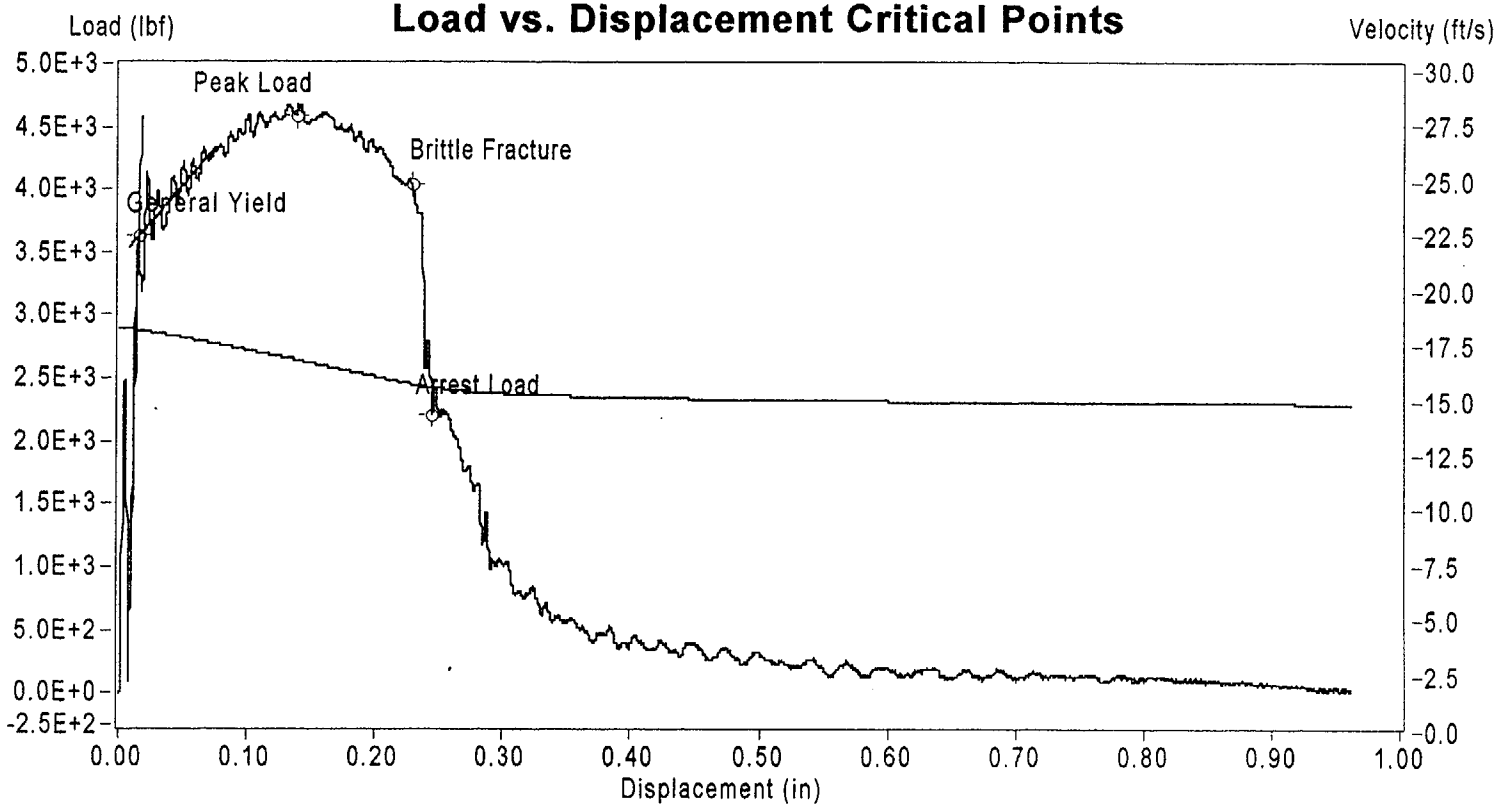

	Load (lbf)	Displacement (in)	Velocity (ft/s)	Time (s)	Energy (ft lbf)
General Yield	3.624E+3	1.521E-2	1.787E+1	5.889E-5	2.192E+0
Peak Load	4.600E+3	1.374E-1	1.654E+1	6.500E-4	4.539E+1
Brittle Fracture	4.048E+3	2.276E-1	1.544E+1	1.120E-3	7.840E+1
Arrest Load	2.205E+3	2.442E-1	1.528E+1	1.210E-3	8.300E+1
End of Signal	1.163E+1	9.620E-1	1.455E+1	5.275E-3	1.036E+2

Sample ID: Hf3-9

Impact V2.1

Summary Report

Sample ID

HF3-4

Material Description

NMP-2 3-Degree Surveillance Capsule - HAZ material

Test Parameter	Value
Operator	Dr. Michael P. Manahan, Sr.
Date Tested	11/27/00 5:39 PM
Temperature	15.00 °C
Oscilloscope	Model 441 Internal
Striker Name	8mm - Striker 16
Interpolation Method	Point-Point Linear
TO 892 Controller	Active Adjust
Sample Type	Metal
Sample Size	Type A
Orientation	TL
Notch Type	V Notch, no Side-Groove
Length	2.1654 in
Width	0.3937 in
Thickness	0.3937 in
Span	1.5748 in
Uncracked Ligament	0.3150 in
Notch Radius	0.0098 in
Velocity Determination	Potential Energy & Losses
Velocity	17.94 ft/s
Shear	100.00 %
Lateral Expansion	0.0732 in
Energy Adjustment	1.0264

Measured Data (V)

Oscilloscope Signal

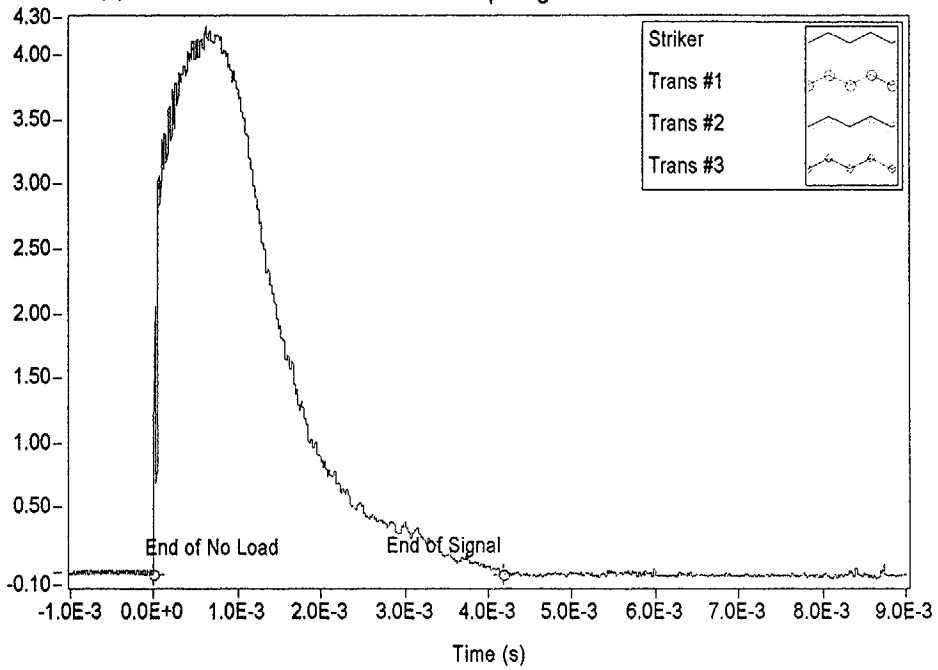

Result	Value
Optical Encoder Energy	109.92 ft lbf
Dial Gage Energy	109.8 ft lbf
Instrumented Striker Energy	109.92 ft lbf

Impact V2.1

Integration Report

Signal Source: 8mm - Striker 16 Striker

Load (lbf) vs. Time (s)

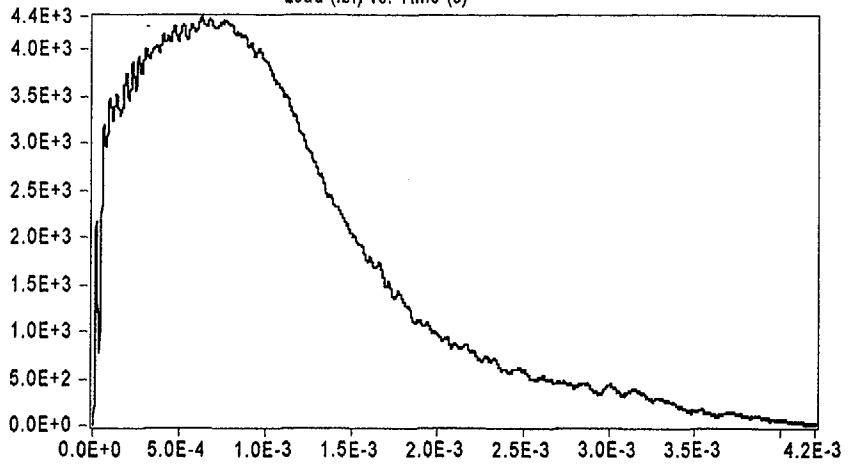

Velocity (ft/s) vs. Time (s)

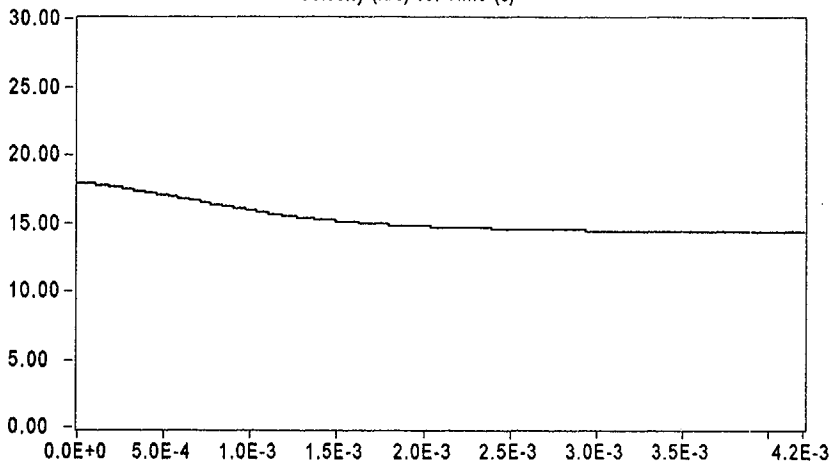

Displacement (in) vs. Time (s)

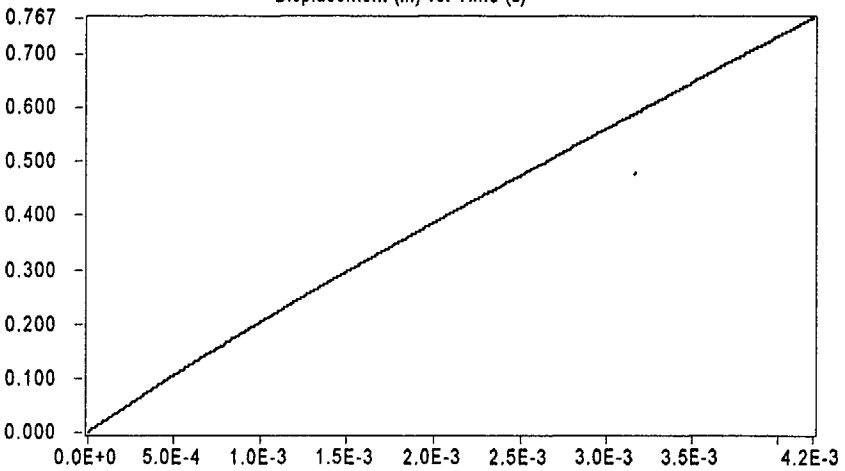

Load (lbf), Energy (ft lbf) vs. Displacement (in)

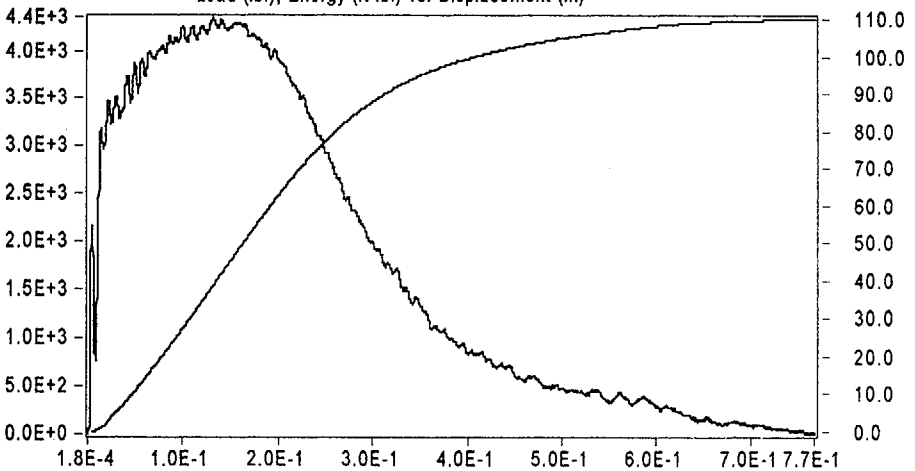

Sample Name: Hf3-4

Instrumented Striker Energy: 109.92 ft lbf

Impact V2.1

Load vs. Displacement Critical Points

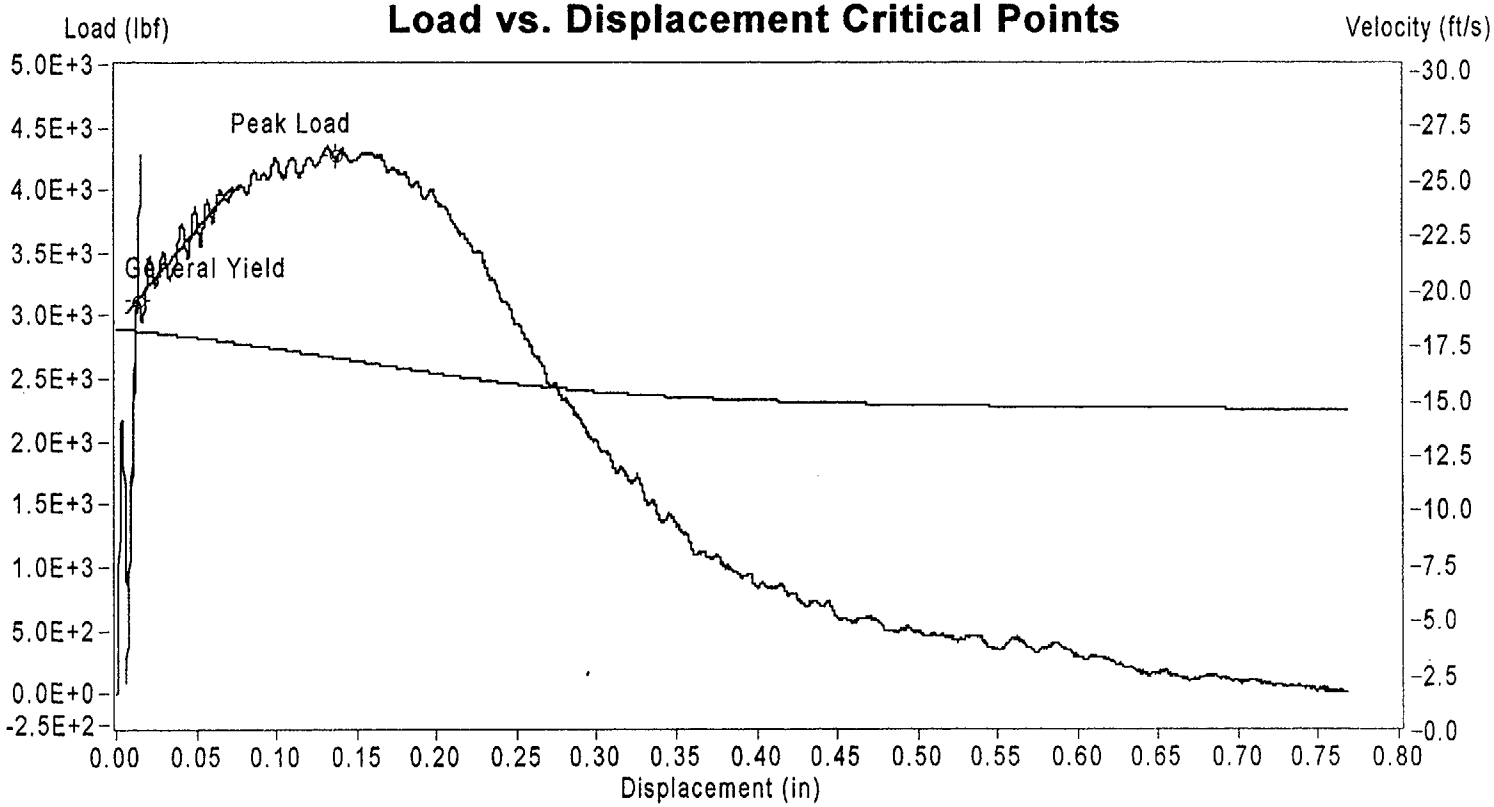

	Load (lbf)	Displacement (in)	Velocity (ft/s)	Time (s)	Energy (ft lbf)
General Yield	3.128E+3	1.327E-2	1.789E+1	5.287E-5	1.733E+0
Peak Load	4.271E+3	1.370E-1	1.666E+1	6.490E-4	4.176E+1
End of Signal	1.171E+0	7.670E-1	1.432E+1	4.189E-3	1.099E+2

Sample ID: Hf3-4

Impact V2.1

Summary Report

Sample ID

HF3-8

Material Description

NMP-2 3-Degree Surveillance Capsule - HAZ material

Test Parameter	Value
Operator	Dr. Michael P. Manahan, Sr.
Date Tested	11/27/00 10:44 AM
Temperature	19.00 °C
Oscilloscope	Model 441 Internal
Striker Name	8mm - Striker 16
Interpolation Method	Point-Point Linear
TO 892 Controller	Active Adjust
Sample Type	Metal
Sample Size	Type A
Orientation	TL
Notch Type	V Notch, no Side-Groove
Length	2.1654 in
Width	0.3937 in
Thickness	0.3937 in
Span	1.5748 in
Uncracked Ligament	0.3150 in
Notch Radius	0.0098 in
Velocity Determination	Potential Energy & Losses
Velocity	17.94 ft/s
Shear	100.00 %
Lateral Expansion	0.0735 in
Energy Adjustment	1.0198

Measured Data (V)

Oscilloscope Signal

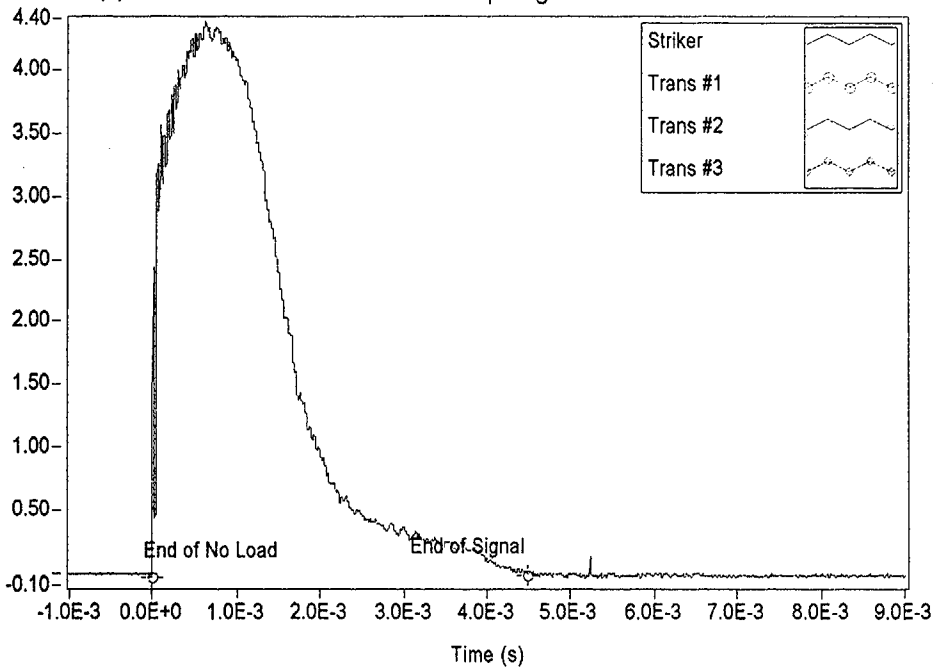

Result	Value
Optical Encoder Energy	117.71 ft lbf
Dial Gage Energy	117.3 ft lbf
Instrumented Striker Energy	117.71 ft lbf

Impact V2.1

Integration Report

Signal Source: 8mm - Striker 16 Striker

Load (lbf) vs. Time (s)

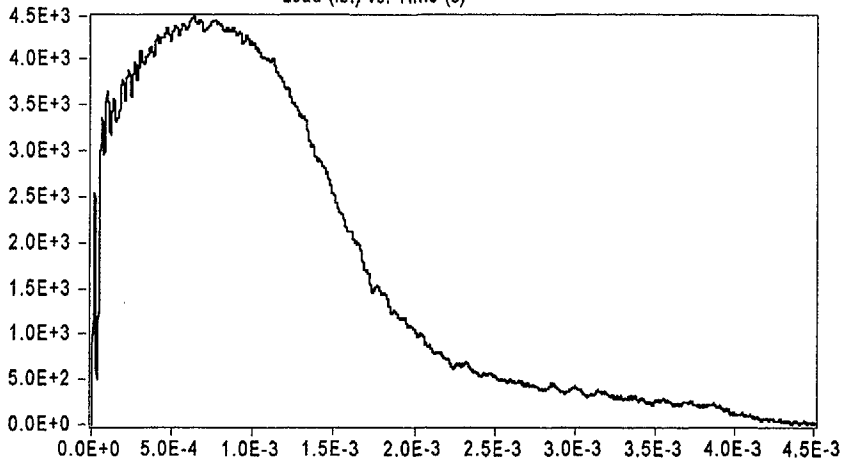

Velocity (ft/s) vs. Time (s)

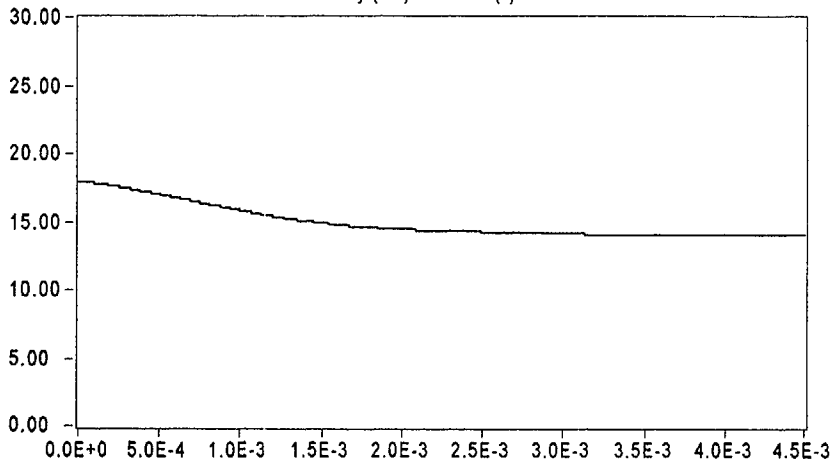

Displacement (in) vs. Time (s)

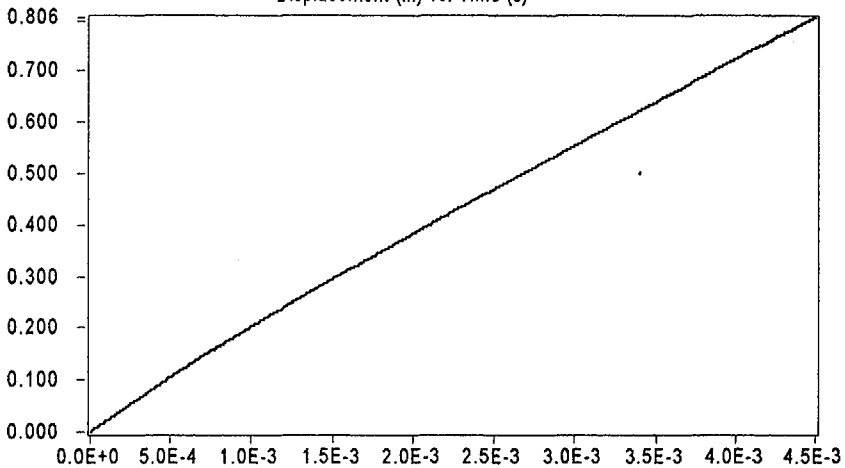

Load (lbf), Energy (ft lbf) vs. Displacement (in)

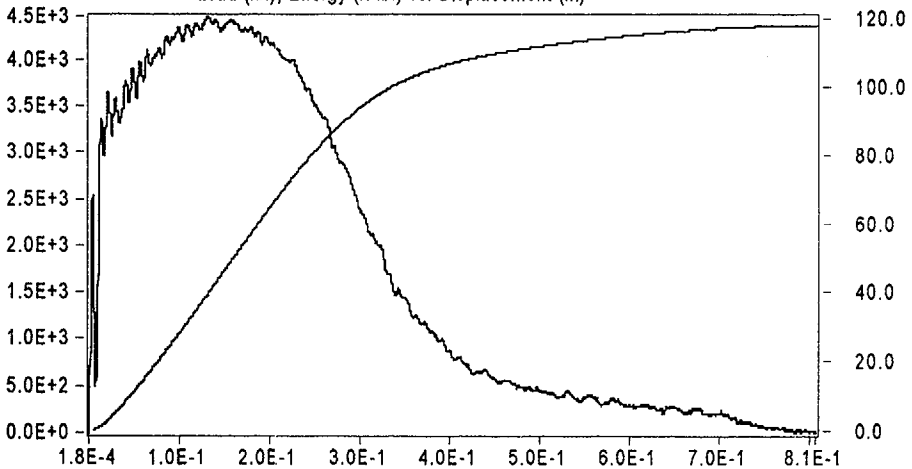

Sample Name: Hf3-8

Instrumented Striker Energy: 117.71 ft lbf

Impact V2.1

Load vs. Displacement Critical Points

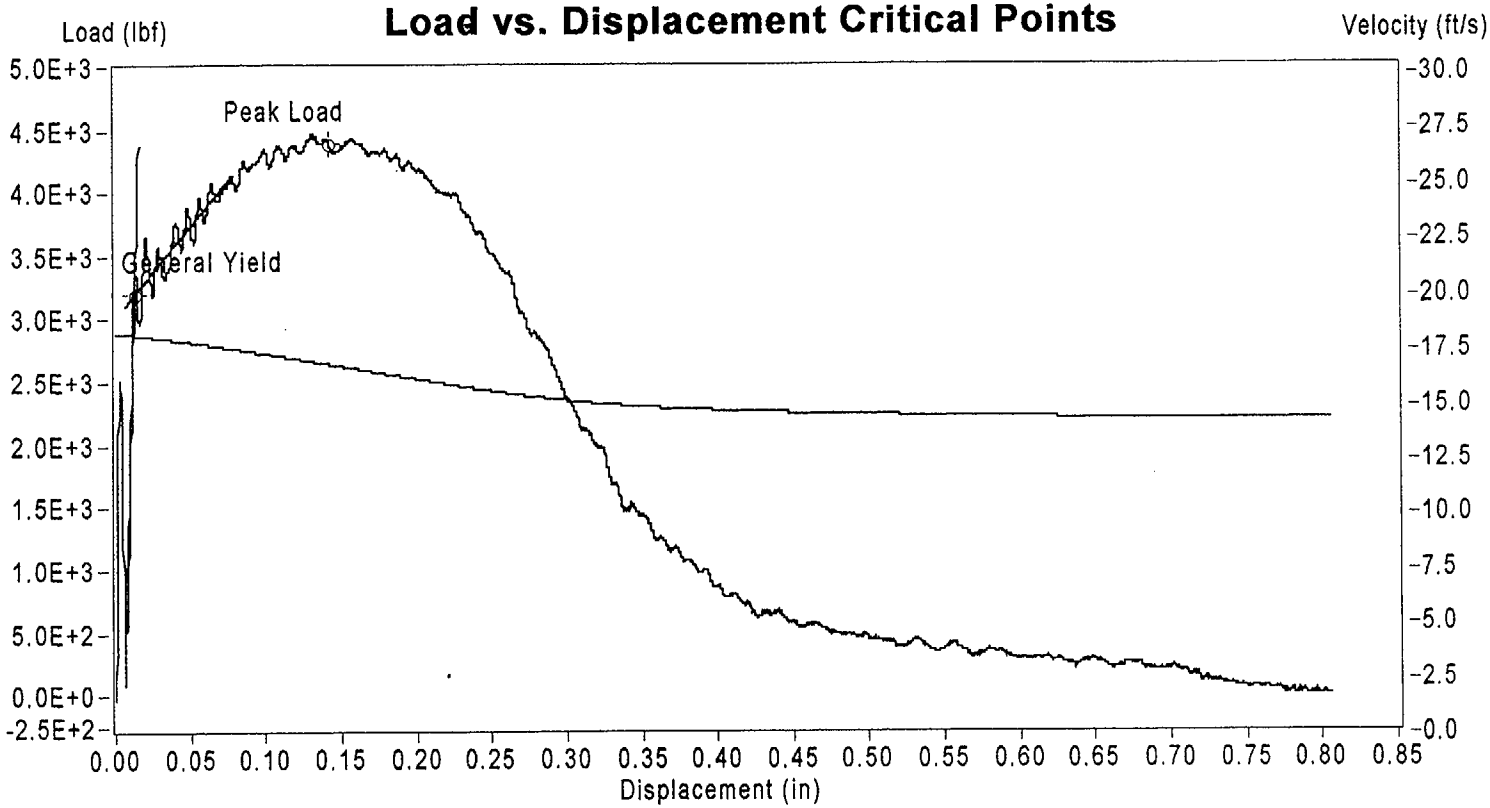

	Load (lbf)	Displacement (in)	Velocity (ft/s)	Time (s)	Energy (ft lbf)
General Yield	3.203E+3	1.327E-2	1.788E+1	5.587E-5	1.895E+0
Peak Load	4.396E+3	1.423E-1	1.656E+1	6.790E-4	4.479E+1
End of Signal	1.188E+0	8.062E-1	1.403E+1	4.480E-3	1.177E+2

Sample ID: Hf3-8

Impact V2.1

Summary Report

Sample ID

HF3-12

Material Description

NMP-2 3-Degree Surveillance Capsule - HAZ material

Test Parameter	Value
Operator	Dr. Michael P. Manahan, Sr.
Date Tested	11/27/00 6:22 PM
Temperature	97.00 °C
Oscilloscope	Model 441 Internal
Striker Name	8mm - Striker 16
Interpolation Method	Point-Point Linear
TO 892 Controller	Active Adjust
Sample Type	Metal
Sample Size	Type A
Orientation	TL
Notch Type	V Notch, no Side-Groove
Length	2.1654 in
Width	0.3937 in
Thickness	0.3937 in
Span	1.5748 in
Uncracked Ligament	0.3150 in
Notch Radius	0.0098 in
Velocity Determination	Potential Energy & Losses
Velocity	17.94 ft/s
Shear	100.00 %
Lateral Expansion	0.0730 in
Energy Adjustment	1.0175

Measured Data (V)

Oscilloscope Signal

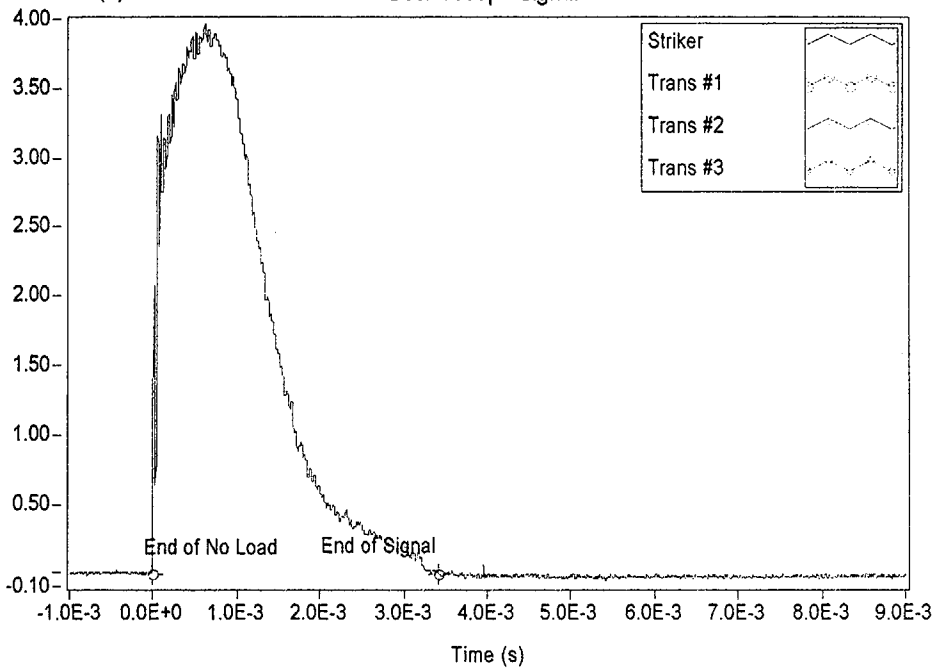

Result	Value
Optical Encoder Energy	94.841 ft lbf
Dial Gage Energy	94.50 ft lbf
Instrumented Striker Energy	94.841 ft lbf

Impact V2.1

Integration Report

Signal Source: 8mm - Striker 16 Striker

Load (lbf) vs. Time (s)

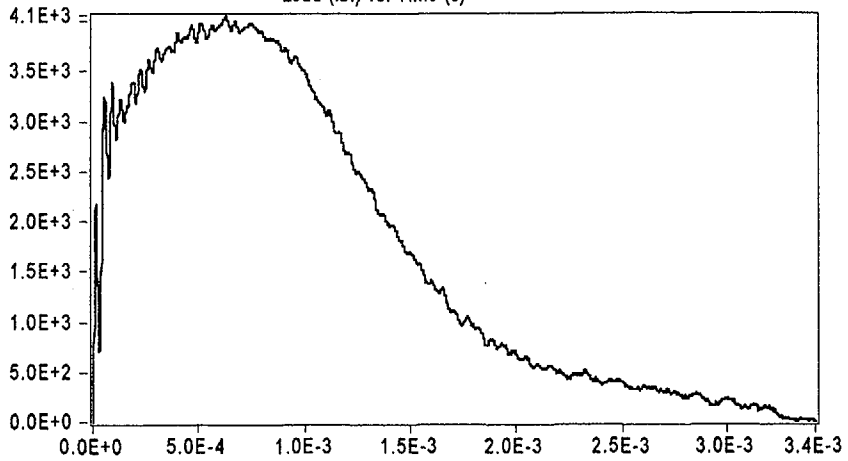

Velocity (ft/s) vs. Time (s)

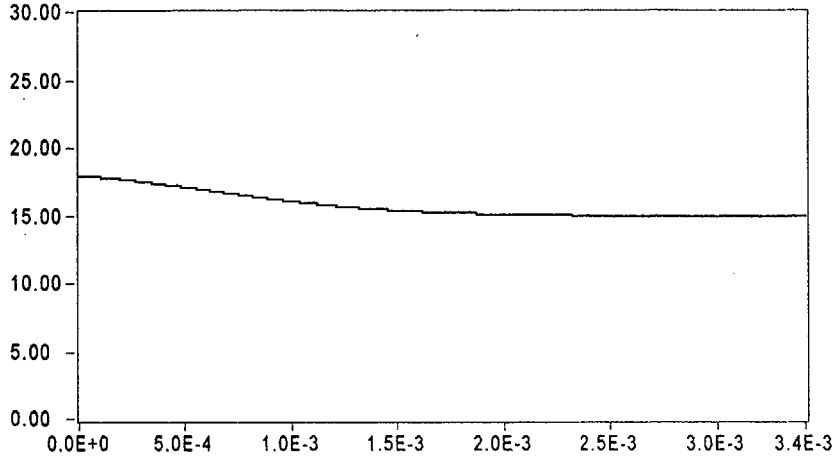

Displacement (in) vs. Time (s)

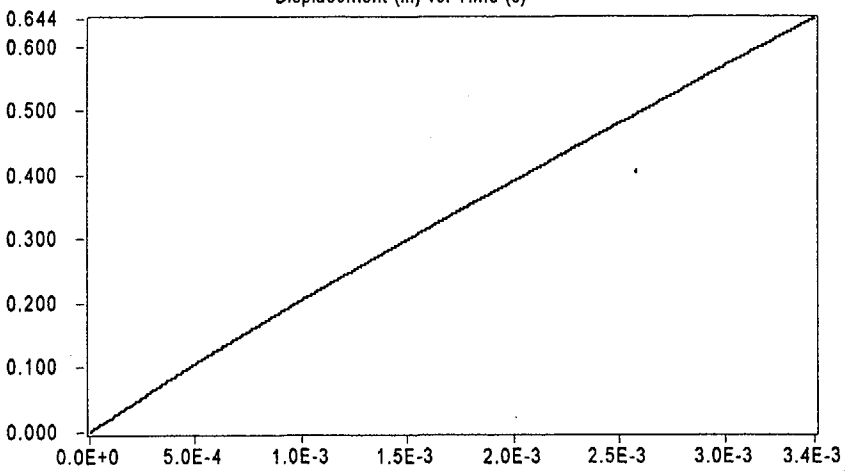

Load (lbf), Energy (ft lbf) vs. Displacement (in)

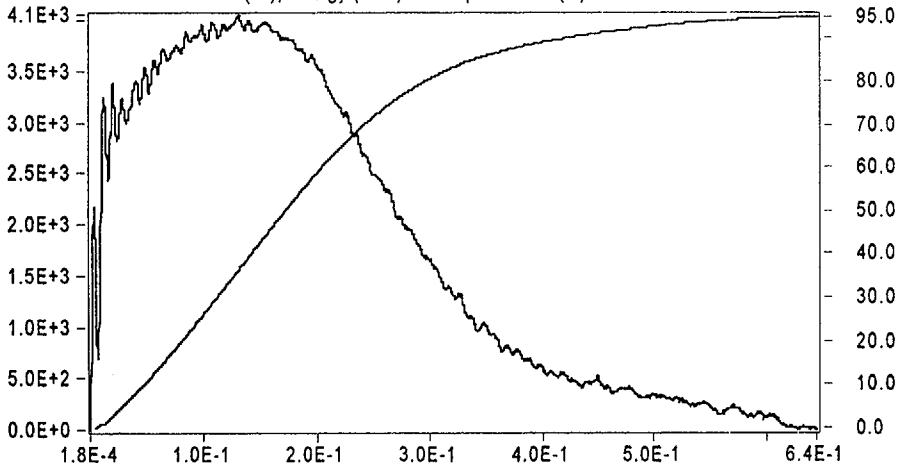

Sample Name: Hf3-12

Instrumented Striker Energy: 94.841 ft lbf

Impact V2.1

Load vs. Displacement Critical Points

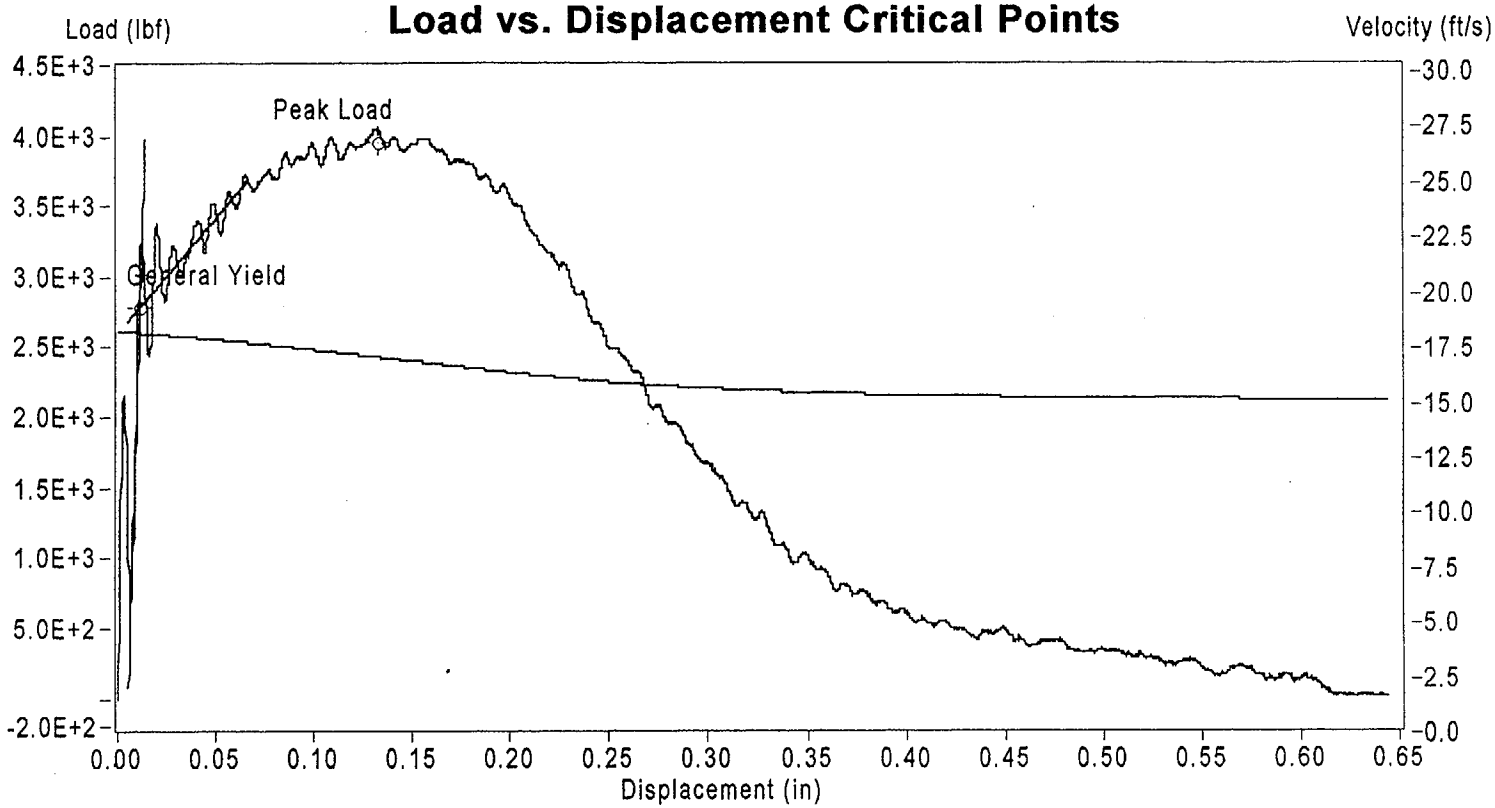

	Load (lbf)	Displacement (in)	Velocity (ft/s)	Time (s)	Energy (ft lbf)
General Yield	2.788E+3	1.155E-2	1.789E+1	4.786E-5	1.513E+0
Peak Load	3.960E+3	1.325E-1	1.679E+1	6.280E-4	3.757E+1
End of Signal	1.467E+0	6.435E-1	1.487E+1	3.409E-3	9.484E+1

Sample ID: Hf3-12

Impact V2.1

Summary Report

Sample ID

HF3-3

Material Description

NMP-2 3-Degree Surveillance Capsule - HAZ material

Test Parameter	Value
Operator	Dr. Michael P. Manahan, Sr.
Date Tested	11/27/00 11:31 AM
Temperature	100.00 °C
Oscilloscope	Model 441 Internal
Striker Name	8mm - Striker 16
Interpolation Method	Point-Point Linear
TO 892 Controller	Active Adjust
Sample Type	Metal
Sample Size	Type A
Orientation	TL
Notch Type	V Notch, no Side-Groove
Length	2.1654 in
Width	0.3937 in
Thickness	0.3937 in
Span	1.5748 in
Uncracked Ligament	0.3150 in
Notch Radius	0.0098 in
Velocity Determination	Potential Energy & Losses
Velocity	17.94 ft/s
Shear	100.00 %
Lateral Expansion	0.0740 in
Energy Adjustment	1.0173

Measured Data (V)

Oscilloscope Signal

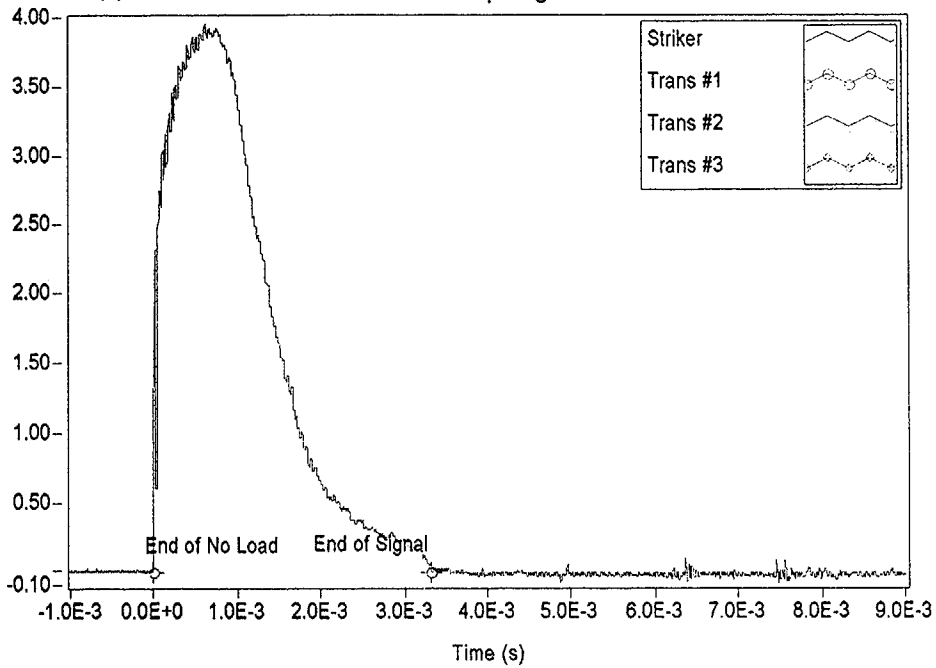

Result	Value
Optical Encoder Energy	96.160 ft lbf
Dial Gage Energy	96.00 ft lbf
Instrumented Striker Energy	96.160 ft lbf

Impact V2.1

Integration Report

Signal Source: 8mm - Striker 16 Striker

Load (lbf) vs. Time (s)

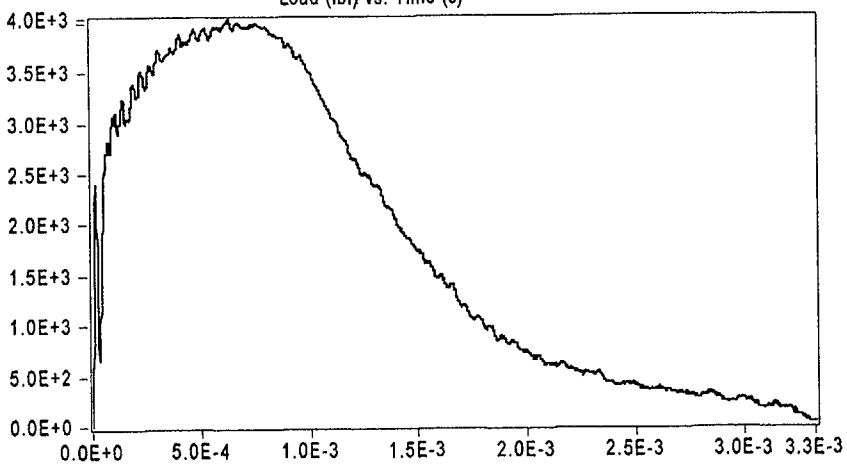

Velocity (ft/s) vs. Time (s)

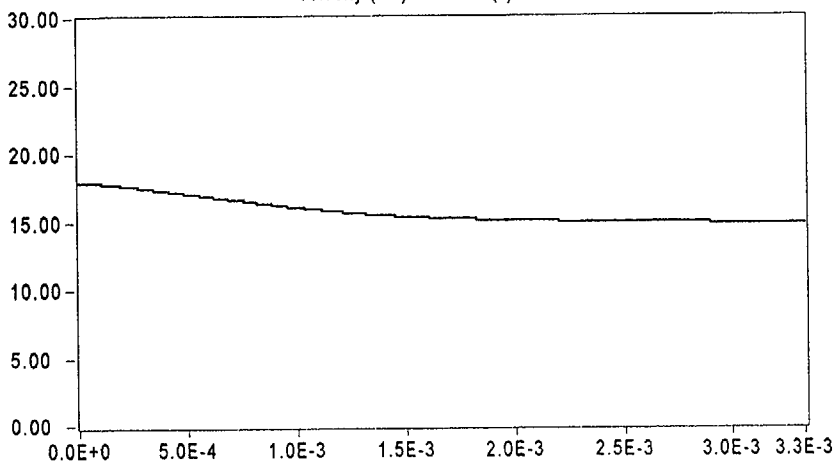

Displacement (in) vs. Time (s)

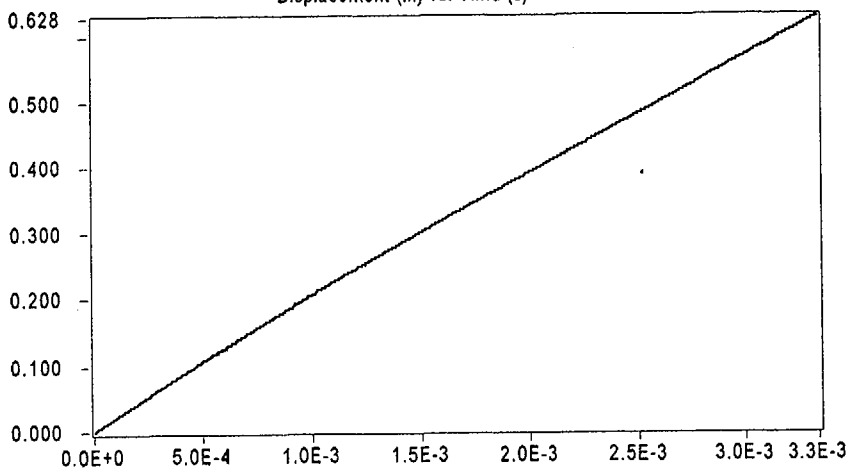

Load (lbf), Energy (ft lbf) vs. Displacement (in)

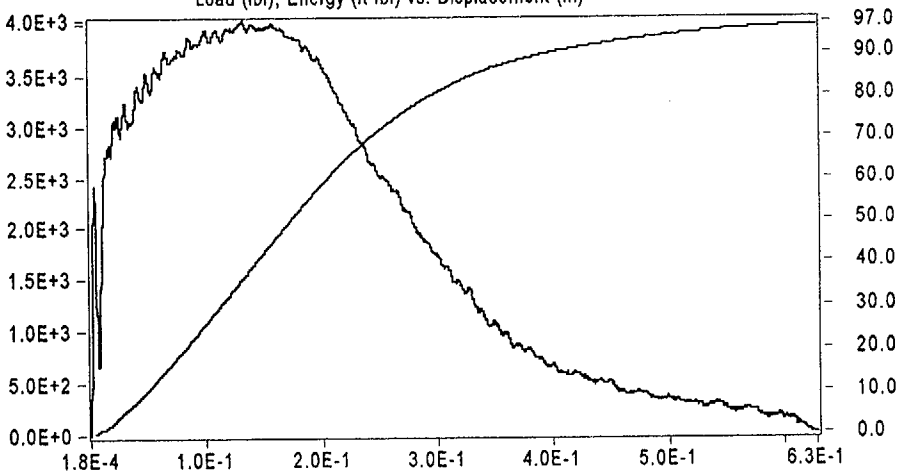

Sample Name: Hf3-3

Instrumented Striker Energy: 96.160 ft lbf

Impact V2.1

Load vs. Displacement Critical Points

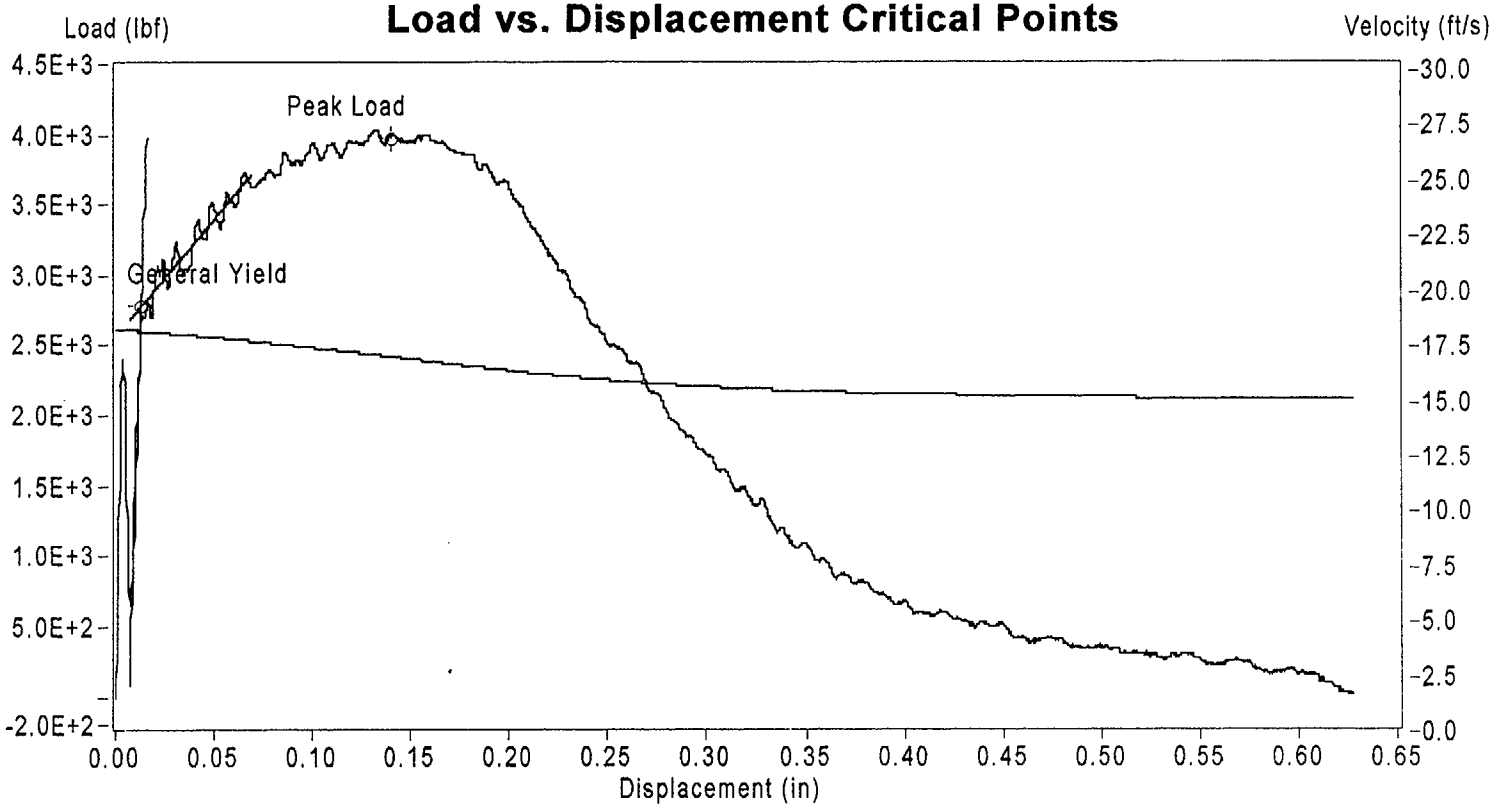

	Load (lbf)	Displacement (in)	Velocity (ft/s)	Time (s)	Energy (ft lbf)
General Yield	2.783E+3	1.305E-2	1.789E+1	5.487E-5	1.700E+0
Peak Load	3.971E+3	1.394E-1	1.673E+1	6.620E-4	3.947E+1
End of Signal	1.101E+1	6.278E-1	1.482E+1	3.324E-3	9.616E+1

Sample ID: Hf3-3

2161 Sandy Drive

Office (814) 234-8860

State College, PA 16803-2283

Fax (814) 234-0248

U S A